UNIVERSITÀ DEGLI STUDI DI PADOVA

Dipartimento di Geoscienze
Direttore Prof. Fabrizio Nestola
Tesi di Laurea Magistrale in
Geologia e Geologia Tecnica

PETROLOGY AND MELT INCLUSIONS STUDY OF LOWER CRUSTAL XENOLITHS FROM MERCADERES – RIO MAYO, COLOMBIA

Relatore: ***Prof. Bernardo Cesare***

Correlatore***: Dott. Omar Gianola***

Laureanda: ***Benedetta Costa***
Numero di Matricola: ***1202373***

ANNO ACCADEMICO 2019/2020

"… I remember daddy told me, fairy tales can come true,
You gotta make 'em happen, it all depends on you
So I work real hard each and every day
Now things for sure are going my way…
There's been trials and tribulations
You know I've had my share
But I've climbed the mountain, I've crossed the river
And I'm almost there."

For you, M & G.

Index

Abstract

The study of melt inclusions (MI) inside minerals from crustal xenoliths represents a powerful access key to study the deep processes of the Earth.

This research is a petrological study of the rocks and a detailed characterization of their glassy inclusions performed on a suite of lower crustal xenoliths, occurring within the Granatifera Tuff, in Colombia. The aim of the work is to understand the petrological significance of the inclusions and the genetic link between them and their host rocks.

The Granatifera Tuff formation, exposed in a tuff ring, is situated in the Mercaderes - Rio Mayo region which is located in the south-west of Colombian Republic, in the Cauca Department.

Mercaderes – Rio Mayo has a peculiar geological setting, and belongs at the North Volcanic Zone (NVZ) in the Andean Cordillera. Its evolution is actually linked with a subduction setting where the Nazca Plate underlies to the South American Plate. Therefore, the NVZ represents a continental arc system, in which an important seismic and volcanic activity is ongoing. The evidences of these geodynamic processes and of the architecture of the subduction zone are enclosed inside these xenoliths, which directly come from the lower arc crust or mantle wedge overlying the subducting plate.

Most of the studied xenoliths come from to 60 – 80 km depths, but some derive from greater depths of about 150 km (Bloch et al., 2017).

Several samples have been collected from Mercaderes - Rio Mayo, during the fieldwork activity conducted by Dr. Fabio Ferri, and twenty thin sections have been obtained from the crustal xenoliths. A preliminary investigation of each sample has been done under the optical microscope in order to identify the samples which contain the MI. This has led to the choice of six samples for further characterization and more detailed analyses, which were conducted using the scanning electron microscope (SEM-EDS).

The SEM has permitted to identify the three most promising samples (18XC1, 18XC10 and 18XC20) which contain melt inclusions in several mineral hosts and, in some cases, also intergranular melt (18XC20). In some cases, xenoliths also preserved some remains of the lava of the Granatifera Tuff itself (18XC10).

The sample 18XC10 which is classified as granulite, is composed of Grt - Cpx - Pl - Amp (in very low quantity). 18XC10 exhibits the most different mineral assemblage with respect to sample 18XC1 (Grt - Pl- Amp - Cpx - Scap) and 18XC20 (Amp - Grt - Cpx - Pl), which tend to be quite similar.

All six samples were investigated by microprobe (EMPA) at the Department of Earth Science of Milan University, which permitted to measure the chemical composition of the minerals, of the MI and of the intergranular melt.

A specific study of the MI was conducted on the three selected samples mentioned above, which contain fairly large (10 to 70 μm) glassy inclusions, especially inside the garnet.

Among all observed MI, some of these are primary, indicating that their entrapment took place in the presence of a melt phase during the growth of their host mineral.

The studied MI present different features, indeed some are perfectly homogeneous, whereas others contain white nanocrystals, probably consisting of ilmenite or magnetite, which can be interpreted as an early stage of crystallization of the glass. MI often display multiple shrinkage bubbles.

EMPA characterization of these MI shows that the chemical composition of MI varies in terms of silica content among different samples: from andesitic–trachyandesitic (18XC1), to rhyolitic (18XC10), with an intermediate composition (dacitic-trachydacitic) exhibited by 18XC20.

Based on the petrographic features of the xenoliths, on the composition of minerals in the assemblage and on the chemical and microstructural information provided by MI, an origin for two of the studied xenoliths is proposed.

Sample 18XC10 is interpreted as the Grt-Cpx-Pl residue after an event of partial melting that produced a rhyolitic melt starting from a Qz-bearing mafic (amphibolitic) precursor.

Sample 18XC20 is interpreted as a high-pressure cumulate deriving from the magmatic differentiation of a basaltic – andesitic melt, typical of a volcanic arc setting.

Considering a pressure value of 1,5 GPa, which approximately corresponds to the pressure conditions at the base of a volcanic arc, it was possible to calculate that sample 18XC1 has been equilibrated between 1229 and 1291 °C, the sample 18XC10 between 974 – 1035 °C and the sample 18XC20 records temperature of about 1089 – 1099 °C.

Introduction

Melt inclusions (MI) are small droplets of silicate melt entrapped in different minerals (defined as hosts) during or after their growth (Sorby, 1858; Vogelsang, 1867; Deicha, 1955). For this reason, they provide a unique possibility of reconstructing the chemical composition of the melt (silicate melt + volatiles) at a specific stage of its evolution, from its formation at lower crust or mantle depths through its ascent and extrusion at the surface (Frezzotti, 2001).

The MI inside a host can appear in several ways, from totally crystallized to glassy (as in this thesis work). In general, the preservation of glass in MI is related to rapid cooling, typical of volcanic environments such as in lava and xenoliths. More rarely glassy MI have been observed also in slowly cooled regional metamorphic rocks (Cesare et al., 2009).

There are two principal types of MI: the primary, trapped during the growth of the host, and the secondary, trapped after the growth of the host. The primary MI represent the most important petrological tool, because their composition can be linked to the time of formation of a particular mineral or mineral assemblage (Roedder, 1984).

The study of MI can provide a multitude of information regarding both magmatic and metamorphic settings. Indeed, for the entrapment of MI the presence of a melt phase is required, and the entrapment can occur both during a melt-consuming process or during a melt-producing process (Cesare et al., 2009).

The first case refers to crystallization in an igneous setting, and MI trap an evolved melt; in the second case the MI is trapped during an incongruent melting process which occurs in an anatectic context. This means that the composition of MI reflects the composition of primitive melts.

The MI studied in this work are contained in lower crustal xenoliths, that can be defined as fragments of rocks that are carried rapidly to the Earth's surface by fast erupting volcanoes (Rudnick, 1992). The study of xenoliths is a powerful tool which allows to constrain the composition of the lower continental crust which is an inaccessible region of the Earth. Through their mineral assemblage it is possible to understand and determine the bulk composition of the lower crust and the processes which are responsible for its formation and modification (Rudnick & Taylor, 1987).

The melt inclusions inside these xenoliths have not been much investigated before, because the Mercaderes – Rio Mayo area, despite its high scientific potential, has so far received limited attention. This is due to several factors such as the difficulty to access the studied area combined with the complex social and political context of Colombia which makes fieldwork potentially unsafe.

The principal aims of this thesis are:

1. To study in detail the petrography of the lower crustal xenoliths, occurring in the Cenozoic Granatifera Tuff (whose age is still uncertain) from Mercaderes - Rio Mayo. The study area is located in the southwestern part of the Colombian Republic.
2. To characterize these xenoliths, which contain the MI, with the aim to obtain some information about their mineral chemistry and their P-T conditions of equilibrations.

In order to do this, geothermometry provides a useful tool to constrain the temperature that these xenoliths have experienced in the lower crustal setting.

3. To characterize petrologically and chemically the MI which are contained in them and try to reconstruct their entrapment processes using the magmatic or metamorphic features that some xenoliths exhibit.
4. Finally, to discuss the data focused on understanding the relationship between xenoliths and MI, trying to explain their origin and provenance in the crust beneath Mercaderes.

Chapter 1 – FLUID AND MELT INCLUSIONS

1.1 Introduction

"The geologist works as a detective in attempting to reconstruct the events of the remote past from the evidence of the present. Unlike the detective, however, the geologist works with events that took place millions or even billions of years ago, and the clues he has to piece together are unusually meager in view of the long history."

In this way Edwin Roedder, who is considered the modern father of modern fluid inclusion studies, describes the work and the role of geologist, and he considers the fluid inclusions (FI) as a useful and precious tool to reconstruct and understand the history of rocks.

Indeed, the FI represents a minuscule and fragmentary but reliable record of the past geological processes, thereby FI could be considered as an actual and direct access key for the past. Through the study of FI it is possible to obtain temperature, pressure, density and composition of the fluids that formed or traversed the rock (Roedder, 1984).

It is important to keep in mind that FI do not tell about one specific episode of the rock forming processes, but generally about different stages of its evolution, and in particular give important information of the role of fluid during different metamorphic, sedimentary or magmatic processes (Van Den Kerkhof & Hein, 2001).

1.1.1 Fluid inclusions

From a compositional point of view, the greater part of fluid inclusions is composed at room temperature by two phases, the liquid and the gas which is contained in the shrinkage bubble. The liquid phase is composed predominantly of an H_2O solution with ions of Na, K, Ca, Mg, Cl and SO_4 where Na and Cl represent the principal ones. The bubble, instead could be formed of H_2O vapor, CO_2 or less frequently from CH_4, which have exsolved from the trapped fluid.

In the fluid inclusions group, are also considered the melt inclusions (MI) often constituted of silicate glass, which form when a rapid cooling occurs in igneous rock (Roedder, 1984).

Inside the host minerals, a FI appears as small droplet with size ranging from 1 μm to more than 1 cm, where most FI fall in the dimensional range 5 to 20 μm (Viti & Frezzotti, 2001). Their shape is extremely variable from elongated, irregular, rounded or negative crystal, the latter reflecting the crystallographic forms of the host crystal. This particular shape achieved through a process which is meant to minimize the shape energy of FI giving more thermodynamic stability (Fig. 1.1). The negative crystal shape results from post entrapment readjustment of the inclusion shape, by a process of dissolution-reprecipitation that is argued not to change the volume of the inclusion or its composition (Frezzotti, 2001; Manley, 1996).

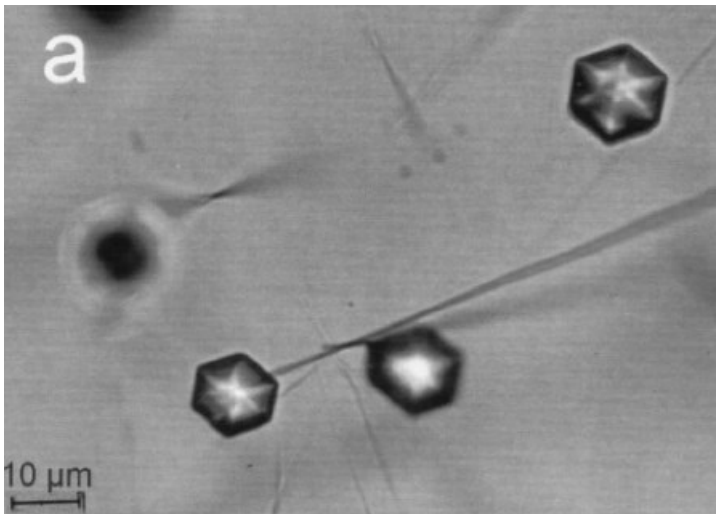

Figure 1.1 *Fluid inclusions which show negative crystal shape in quartz* (Van Den Kerkhof & Hein, 2001).

At room temperature, FI usually are not homogeneous but may display different phases along with the liquid one. These could be represented by vapor (V), potentially together with one or more solid phases (S) (Fig. 1.2a) (Van Den Kerkhof & Hein, 2001).

When in the FI a liquid phase coexists with a vapor bubble, this one appears quite dark compared to the liquid, due to the different refractive index (Fig. 1.2b). If more than one phase is present, the density is the key factor which controls their distribution: the lower density phase is surrounded by a higher density fluid (Fig. 1.2a) (Goldstein, 2003).

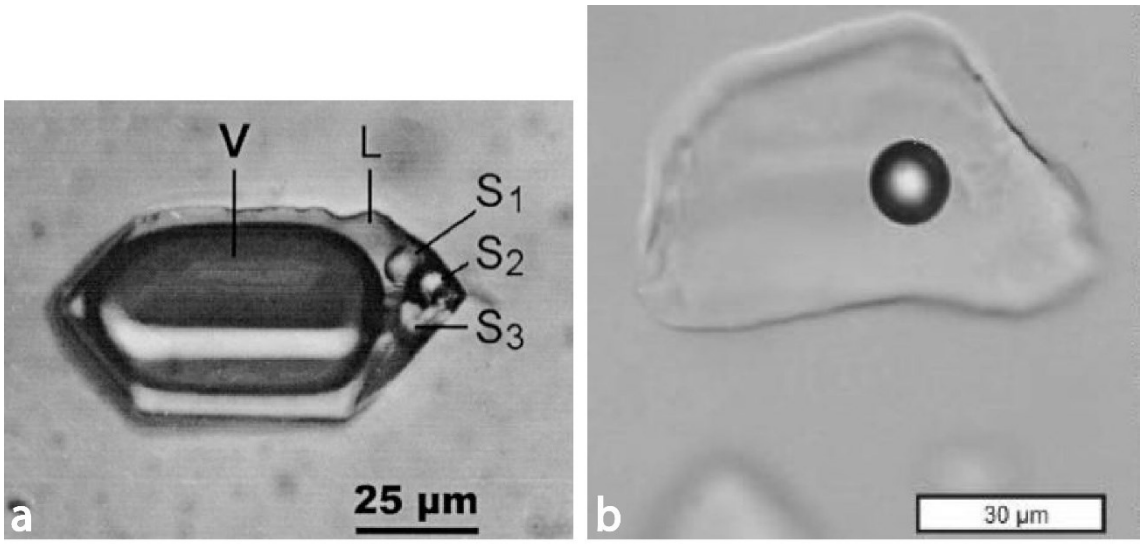

Figure 1.2 (a) *Multi-phase fluid inclusion in smoky quartz* (Van Den Kerkhof & Hein, 2001); ***(b)*** *Large aqueous fluid inclusion in fluorite* (Goldstein, 2003).

For a correct interpretation of all parameters that can be obtained from FI, as P – V – T – X, it is fundamental to know and understand how the FI was trapped. Generally, the greater part of fluid inclusions is entrapped through the same process, even if they present different nature of the fluid. In many cases, the starting point of the trapping process is represented by a

homogeneous fluid, but there are also some exceptions, and a minor quantity of FI is entrapped starting from a heterogeneous system, formed by two or more immiscible fluids (Roedder, 1984).

In these terms, FI could be classified in this way:

Primary fluid inclusions are trapped during the host crystal growth process, especially when this one presents some imperfections (e.g. a crack in the growing surface) which promotes the development of FI. Many inclusions are the result of the non-uniform supply of nutrients in time and space of the host, and could be defined as accidents in the normal process of crystal growth. The primary inclusions have some characteristic features which make them recognizable among the others: they are isolated and randomly located in the host, or arranged in small clusters near the core. In other cases they exhibit a *zonal arrangement* which reflects the progressive growth of the host (Fig. 1.3) (Roedder, 1984).

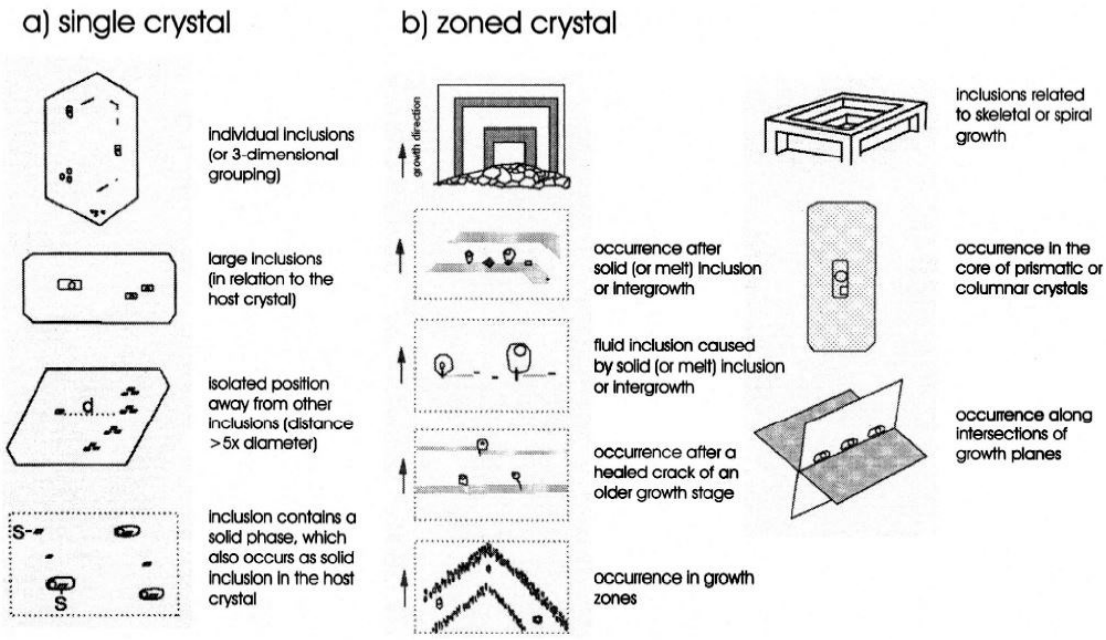

Figure 1.3 (a) *Diagnostic criteria for classifying fluid inclusions as primary;* ***(b)*** *Relationship between primary inclusions and zonal arrangements* (Van Den Kerkhof & Hein, 2001).

Secondary fluid inclusions are trapped at any time after the growth of the host crystal, which is entirely developed. This occurs when a fluid is channelized into the fractures of the host mineral, which is able to trap small droplets of fluid after a rearrangement of its crystal structure. The secondary fluid inclusions are easily recognized when they are located in planes or trails.

Generally, secondary inclusions are quite distinguishable from the primary ones, by the tendency of secondary inclusions to form planes which cross each other (Fig. 1.4) and the tendency of primary fluid inclusion to mimic the crystal terminations.

Determining the time of entrapment of every single plane could be extremely complex, but at the same time it is very important because also secondary inclusions record different stages of the geological history in terms of P – T – X. The technique employed to establish relative timing

is a basic cross cutting relationship, based on the fact that each planar array presents inclusions with distinctive features (Goldstein, 2003).

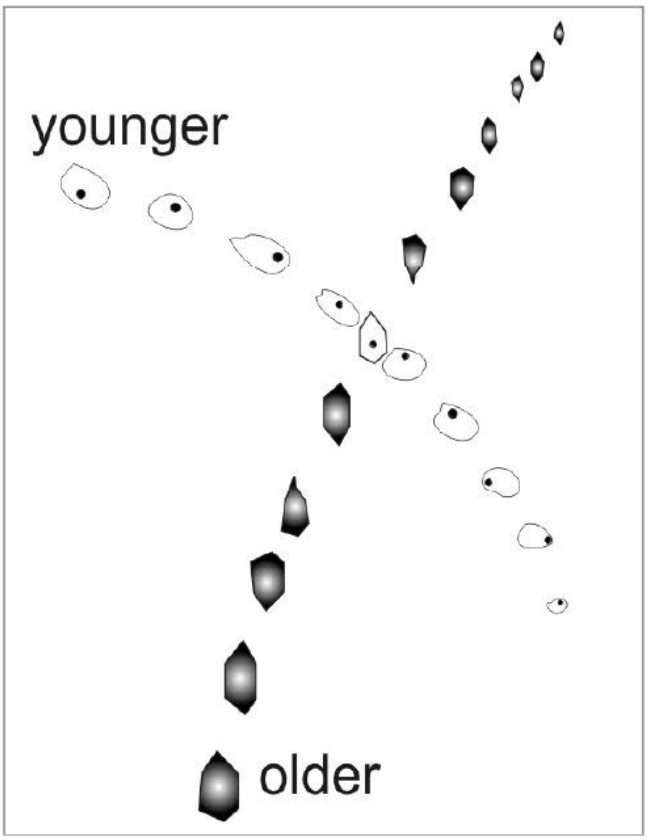

Figure 1.4 *Several planes of secondary inclusions which cross each other* (Goldstein, 2003).

Pseudosecondary fluid inclusions are entrapped before the crystal growth process is complete, but not necessarily as direct result of crystal growth. They are similar in origin to secondary FI one, because there are located along microfractures, but for pseudosecondary inclusions, the entrapment is followed by further crystal growth. The recognition of pseudosecondary inclusions requires multiple planar arrays of inclusions which terminate against a growth zone (Goldstein, 2003).

Despite every category of inclusions mentioned above presents a few diagnostic features for their recognition, in some cases it is not easy to classify every FI, because the petrographic criteria could be absent or ambiguous. Below is reported a summary image (Fig. 1.5) which shows all types of FI that could be present inside a host mineral and their relative location.

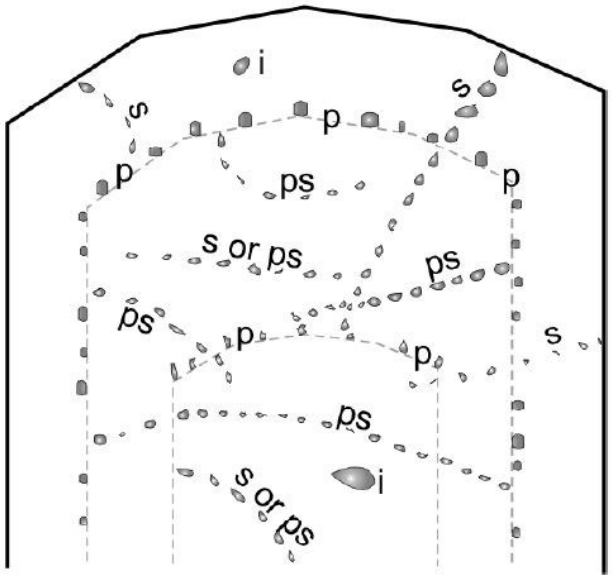

Figure 1.5 *Composite sketch showing primary (p), secondary (s), pseudosecondary (ps) and inclusions of indeterminable origin (i) in a host mineral* (Goldstein, 2003).

As mentioned above, the fluid phase in FI could be associated with solid phases which can have two different origins, a trapped crystal or a daughter mineral. The solid phase that can be defined as a trapped crystal, is a solid constituted by a contaminant or a settled phase which was already present on the surface of a growing crystal and then was accidentally incorporated as part of a fluid inclusion when host grew around it.

On the other hand, a daughter mineral represents a phase which is directly precipitated from the fluid and constitutes part of the FI itself during cooling of the host rock.

A useful technique to distinguish these two types of solid inclusions, is through heating stage experiments in laboratory.

When a small droplet was enclosed inside the host crystal, many exchanges between host and FI itself may occur and this could provoke changes both in the phase assemblage and in the physical nature of the inclusion. Furthermore, when we observe and study a FI at room temperature, it generally looks different with respect to when it was trapped, since more than one phases, instead of a homogeneous supercritical fluid, coexist together. For what concerns physical changes, such as changes of shape, they are irreversible and difficult to prove also through laboratory experiments. These changes could cause several problems in the evaluations of P – T – X properties of the fluid.

About the change in shape, many inclusions do not present the actual shape that they assumed during the trapping, because at that moment they often have a large surface area.

In order to minimize large surface areas, the "necking down" process may take place (Fig. 1.6), that is a change in shape resulting in a reduction of the surface energy of the inclusions. Subsequent to necking down, there are a few smaller inclusions which have the same total volume as the original one but with minor surface energy.

It is important to say that through the necking down process, the chemical composition of the inclusion does not change, but the density may change (Fig 1.6).

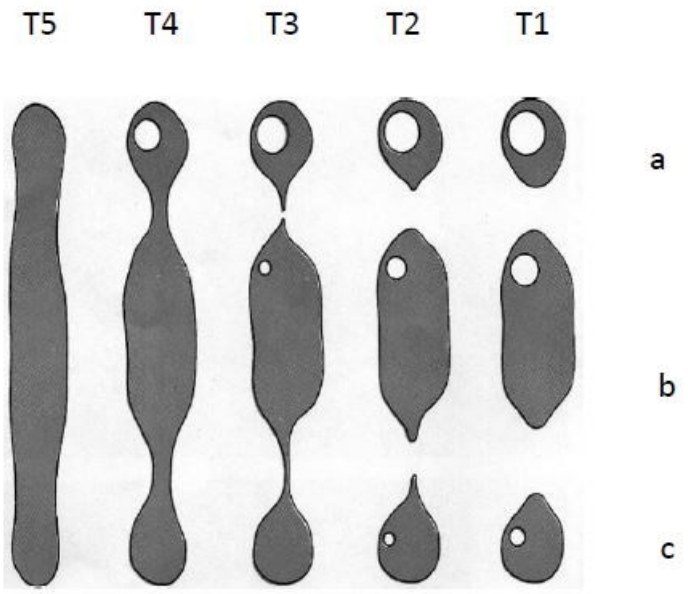

Figure 1.6 *Necking down process started form the tubular inclusion at temperature T5. At the end we obtain three different inclusions a – b – c. The total sum of their volume is the same of the previous inclusion during T5* (Roedder, 1984).

1.1.2 Silicate melt inclusions (MI)

Silicate-melt inclusions are small droplets of silicate melt entrapped in different minerals during their growth in the presence of a melt phase (Sorby, 1858; Frezzotti, 2001; Cesare et al., 2015). For this reason, they provide a unique possibility to reconstruct the chemical compositions of magma (silicate melt + volatiles) at a specific stage of its evolution, from its formation at crustal/mantle depth through its ascent and extrusion at the surface (Frezzotti, 2001).

MI are trapped in minerals called hosts and they could be quenched as glass or crystallized to polycrystalline aggregates upon the cooling of the system (Cesare et al., 2011).

The melt inclusions are extremely frequent in igneous and volcanic context, but they could be present also in metamorphic rocks when incongruent melting occurs during anatexis. As mentioned before, in most cases MI contain silicate phases, but may also display other more exotic compositions (e.g. carbonatite or metal liquids; (Cesare et al., 2015)).

Melt inclusion size ranges from a few to a few tens or, less frequently a few hundreds of micrometers, and like for FI their shape varies from irregular to a perfect negative crystals (Cesare et al., 2015).

Also MI can be distinguished into primary and secondary inclusions, and their trapping mechanism is the same as described above for FI.

From a petrological point of view, the primary inclusions are much more important than the secondary ones, because a particular type of melt can be directly linked to a particular mineral or assemblage (Cesare et al., 2011).

Following entrapment, some modifications of MI may take place depending on several factors as P-T conditions, deformation and melt compositions.

The most important changes that can occur are: the diffusional exchange between MI and the host; the complete crystallization of the melt or the nucleation of bubble during the contractional and cooling stage; the decrepitation of MI which takes place when the pressure inside the MI is much higher than the pressure on the host or the MI undergoes microfracturing, due to the application of strain on the host.

Since the entrapment process of MI necessarily takes place in presence of a melt phase, this means that the igneous system represents a major environment for MI entrapment. There is, however, another important context where entrapment occurs, that is during anatexis in a high-temperature metamorphic setting.

These two processes are extremely different because in an igneous context the MI is trapped during the cooling stages, when the host mineral crystallized directly from a melt which tends progressively to evolve changing its composition (magma differentiation processes). Thereby the droplets which will constitute the inclusions are an evidence of an evolved magma, and not of the primitive one.

On the contrary, during incongruent melting, when the temperature rises, anatexis takes place and MI may be trapped simultaneously with the growth of peritectic phases (Cesare et al., 2015).

The incongruent melting can be explained through this reaction:

A (+B) = C + M

where A, B and C are the solid phases and M the melt. The phase C grows together with the melt, thereby the fundamental condition of entrapment of MI is established.

A concrete example of incongruent melting is given by the reaction:

Bt + Pl + Qz + Sil (± fluid) = Grt + melt (± Kfs)

where Grt is produced via incongruent melting of Bt + Pl + Qz + Sil and grows together with the melt. This reaction is particularly important for metapelites, and explains many occurrences of MI in peritectic garnet.

A schematic representation of these two different processes it is reported below (Fig.1.7).

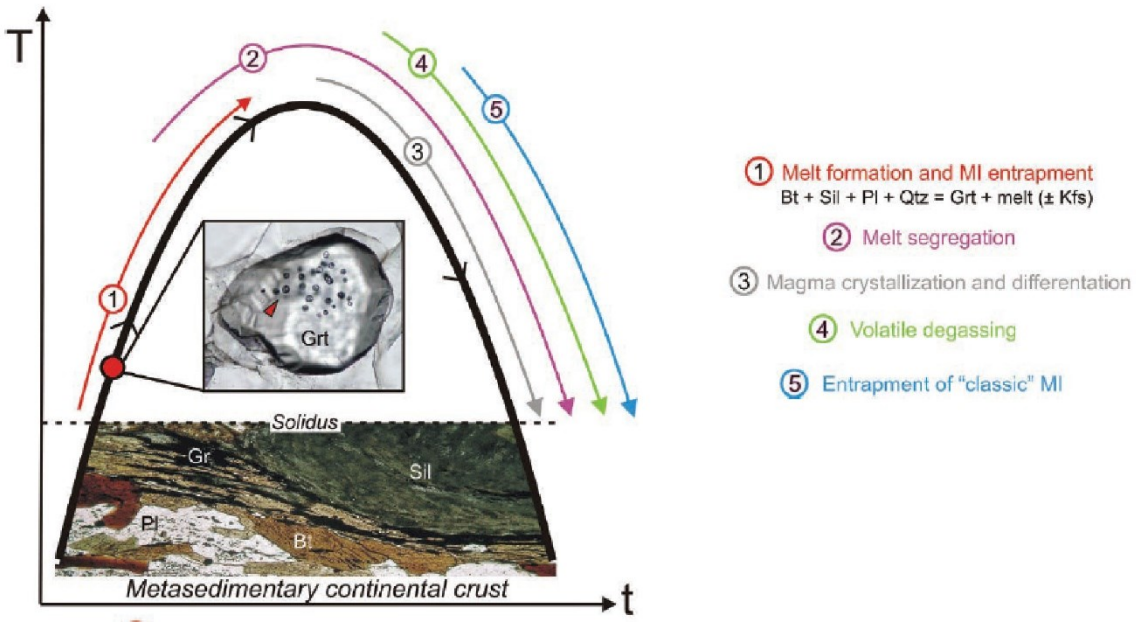

Figure 1.7 *Schematic T-t diagram showing the main processes occurring during melt production (heating or prograde path) and melt consumption (cooling or retrograde path) in the partially melted continental crust. MI can be trapped during incongruent melting (red arrow) and igneous crystallization (blue arrow). Ideal incongruent melting reaction from Vielzeuf and Holloway (1988)* - (Bartoli et al., 2016)

After the explanation of these two entrapment methods, it is clear how in the first case MI are trapped during melt-consuming processes, whereas in the second one they are trapped during melt-producing processes (Cesare et al., 2015).

Melt inclusions can have different degrees of crystallization, from glassy (as in the studied case) to fully crystallized (Fig. 1.8). The latter type is defined *nanogranites* after the work of Cesare et al (2009).

Nanogranite is a cryptocrystalline aggregate composed of Qz-Ab-Kfs-Bt-Ms, which recalls a granitoid composition, and is formed when a small droplet of anatectic melt gets trapped in the host. Nanogranites form in migmatites-granulite contexts where the cooling process is slow. Instead glassy inclusions are the result of rapid cooling, as commonly occurs in xenoliths in lavas, or of the inhibition by crystals nucleation (Cesare et al., 2015).

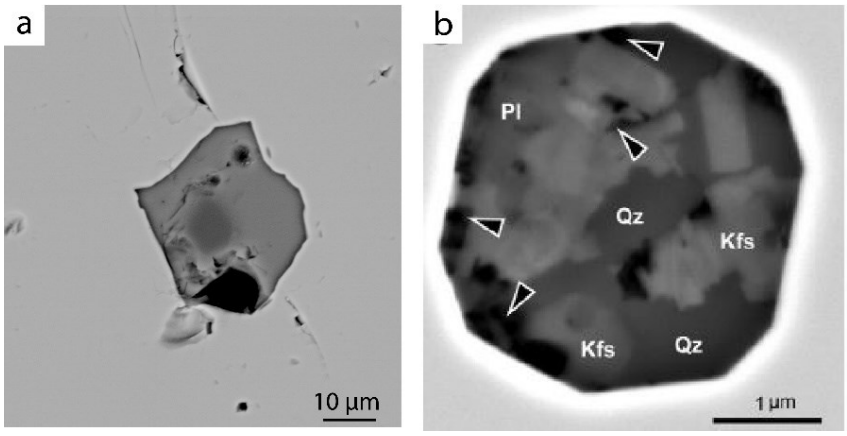

Figure 1.8 (a) *SEM-BSE image of a glassy inclusion in Grt from sample 18XC10;* ***(b)*** *SEM image of nanogranite from Ronda metatexites* (Cesare et al., 2015).

1.2 Geographical Setting

Mercaderes - Rio Mayo (1°48’32’’N, 77°09’45’’W) belongs to Cauca Department, and it is located in the south-west corner of the Colombian Republic, about 750 km from Bogotà, the capital of Colombia (Fig. 1.9).

Mercaderes is bordered on the east with Bolívar, on the north with Patía and Balboa, on the west with Levia and Rosario, both belong to Nariño Department, and on the south with Florencia and Nariño Department itself.

Fig. 1.9 *Location of the studied area. Satellite images from Google Earth.*

1.3 Geological Setting of The Andes

The Andean Cordillera is a continental volcanic arc that extends for about 10.000 km, and crosses the entire South America continent, from the Caribbean Sea to the Scotia Sea.

This important mountain chain results from the subduction of oceanic lithosphere (forming the floor of the Pacific Ocean Basin) under the South American continental margin. The Andean continental arc activity started during Middle-Late Triassic in the north and during Middle-Late Jurassic in the south (Dalziel, 1986), persisting until present day as testified by the presence of several Cenozoic active volcanoes (Marín-Cerón et al., 2019). Most of these active volcanoes are located preferentially along the axis of the Central Cordillera, approximately 150 km eastwards of the trench axis and 150 km above the Benioff zone (Marriner & Millward, 1984).

The Andean chain can be subdivided in three main segments that have different orientations and that are separated by two bends. The first segment is the Colombian– Ecuadorian segment, trending NNE-SSW, which is about 2000 km long and comprises the northernmost part of Perú and the easternmost part of Venezuela. It is divided from the Peruvian segment by the Huancabamba Bend. The Peruvian segment also develops for about 2000 km and shows a NW-SE orientation. It includes the northern part of Bolivia, and it is separated from the Chilean segment by the Arica Bend. The last segment, the Chilean one, is about 4000 km long with a N-S trend. Its orientation changes in its terminal part, assuming a E-W direction along the sinistral Scotia transform system (Jaillard et al., 2000).

Based on the geochemistry of the Cenozoic volcanic activity, the Andes can be further divided in four different portions. As reported in (Fig. 1.10), there are:

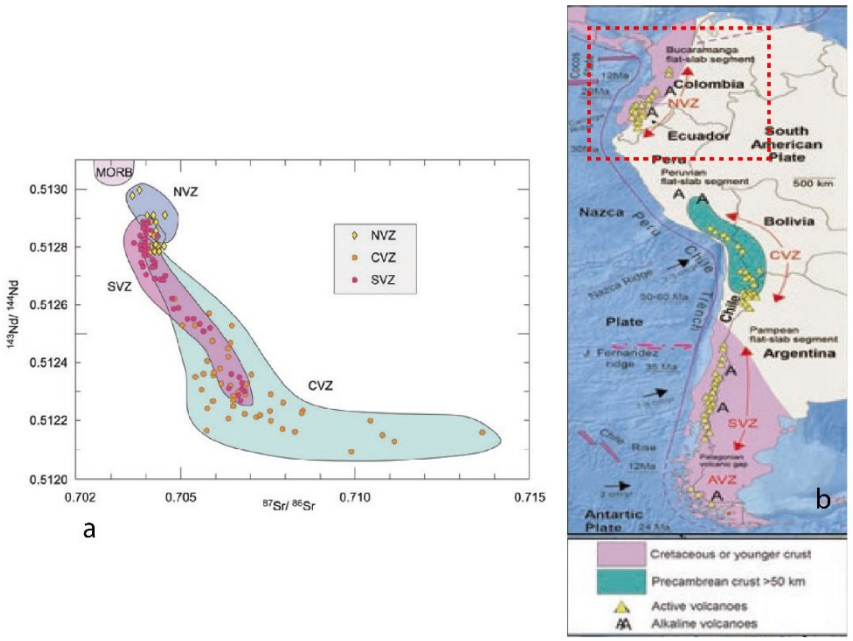

Fig. 1.10 ***(a)*** *Geochemical composition in terms of Sr vs. Nd for three of four portions of Andes* (Marín-Cerón et al., 2019). ***(b)*** *Subdivision of Andeans Cordillera in four principal portions: NVZ – CVZ – SVZ – AVZ. In the NVZ sector,, is located Mercaderes (red rectangle)* (Marín-Cerón et al., 2019).

1. **Northern Volcanic zone (NVZ, 5°N - 2°S)**

Its volcanic and seismic activity is intense. The NVZ represents an active arc system, bounded by the flat Peruvian slab to the south and the flat Colombian slab to the north, where a subduction process currently takes place. The development of a magmatic arc is allowed because fluids and melts liberated by dehydration of subducting oceanic crust recycle elements into the mantle wedge and trigger the production of volcanism in the arc of the subduction zone (Marín-Cerón et al., 2019). From a geochemical point of view, the magmatism in NVZ shows a calc-alkaline trend, indeed the dominant rocks type erupted are andesites and dacites (Stern, 2008). During the subduction process under the South American Plate, the Nazca Plate, which is covered by a thick layer of carbonate sediments, released abundant fluids rich in COH, causing melt and metasomatism of the mantle wedge. At the same time melt, which remains trapped under the arc crust, promoted the anatexis process and the differentiation of the continental crust.

In the NVZ arc zone the new continental crust comes from heterogeneous melting derived from two different sources: from the mantle wedge that has been metasomatized by the subduction fluids and from mantle magma which interacts with the crust that has undergone anatexis process. In this context, a delamination process takes place, and in particularity it could be explained in this manner: through the delamination occurs a lithospheric foundering because the lowermost lithosphere develops a stable assemblage composed in principal way of pyroxene and garnet. This means that the bulk density of the lower crust is greater than the asthenospheric mantle and consequently the resulting a gravitational instability provokes a breakdown of the lithospheric root, which sinks into the asthenosphere. The delamination process represents an important mechanism for lithospheric recycling materials into the upper mantle (Bloch et al., 2017).

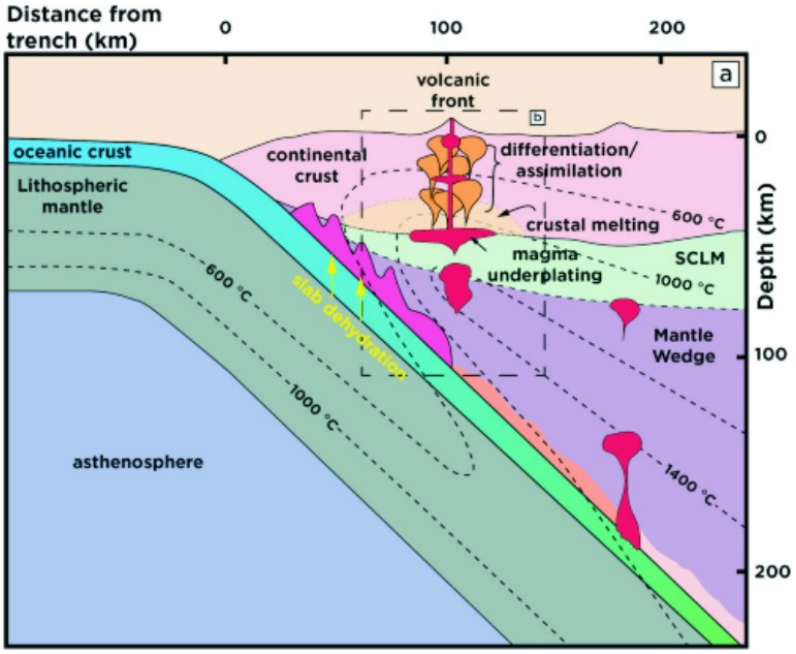

Fig. 1.11 *Schematic representation of a continental arc subduction zone system, showing the dehydration process of the subducting slab and the hydration and melting of mantle wedge from Winter (2014).*

2. Central Volcanic zone (CVZ, 16°S – 28°S)

The CVZ, reported in Fig 1.12, is composed by 44 active Quaternary stratovolcanoes and andesitic-rhyodacitic domes. It is assumed that in this zone crustal delamination processes have occurred (Bloch et al., 2017).

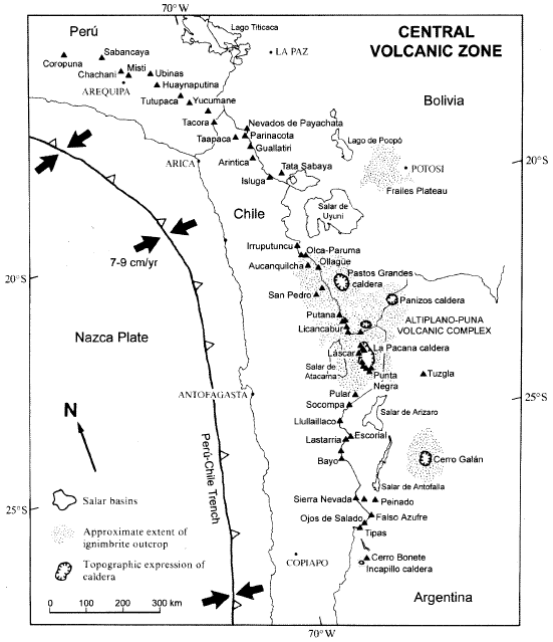

Fig 1.12 *Schematic map of the CVZ with its volcanic centres* (Stern, 2008).

3. Southern Volcanic zone (SVZ, 33°S – 46°S)

The SVZ, reported in Fig. 1.13, extends from the intersection of the Juan Fernandez ridge on the Chile trench to the Chile Rise triple junction. In this area two important episodes of volcanism occurred: the first one in Miocene and the second one in Quaternary (Sun, 2001). In the SVZ there are at least 60 historically and potentially active volcanic edifices, located between Chile and Argentina. In this zone, there are also three giant silicic caldera systems and numerous minor eruptive centres (Stern, 2008).

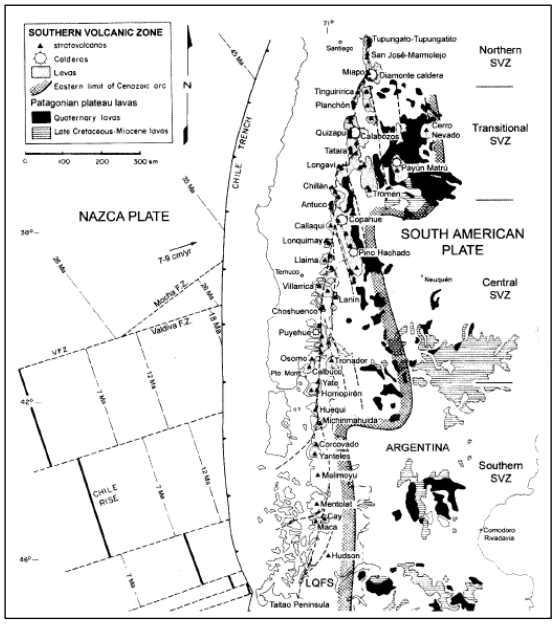

Figure 1.13 *Schematic map of SVZ zone with its volcanoes* (Stern, 2008)

4. Austral Volcanic zone (AVZ, 49°S – 55°S)

The AVZ is located in the southernmost portion of Patagonia (Fig 1.14). The AVZ zone is composed by six volcanic centres, which represent the southern portion of the active volcanic segment in the Andes. These volcanoes are connected to the relatively slow subduction of the young Antarctic Plate under the South American Plate (Stern, 2008).

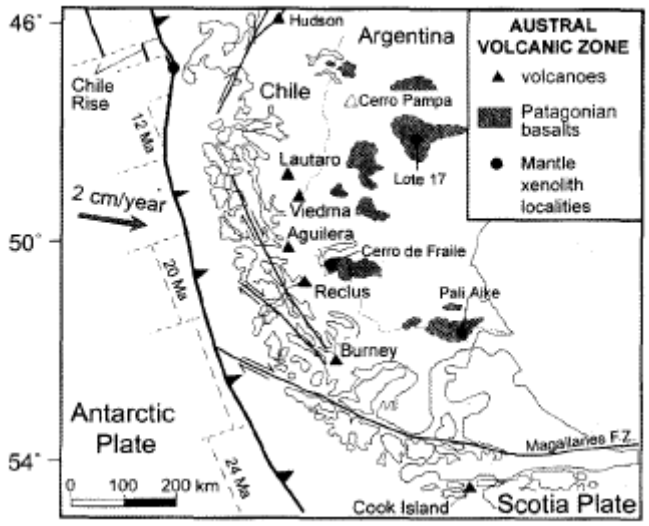

Figure 1.14 *Schematic map of AVZ and its volcanic centres* (Stern, 2008).

After this presentation of the four main zones, according to Barazangi and Isacks, (1976), the active volcanoes are located over the asthenospheric mantle zone, so it is possible that their evolution is closely related to the mantle wedge overlying the subducted slab. In this terms, the volcanic history of Colombian Andes recorded five major magmatic episodes, from Triassic to Neogene, and each of these were related to the subduction of Farallon Plate under the South American Plate (Marín-Cerón et al., 2019).

These four zones display some differences in terms of ages respect to the basement, which is Precambrian in the CVZ and Mesozoic-Cenozoic in the SVZ and NVZ. Moreover, differences in thickness and angle of the subducting slab can be observed.

1.3.1 Geodynamic evolution

In the NVZ, the Colombian section of the Andean Cordillera represents a complex geological setting due to the convergence of three lithospheric plates: the Nazca Plate, the South American Plate and the Caribbean Plate (Fig. 1.15).

About 23 Myr ago, the Farallon Plate split-up in two parts due to the oceanic Galapagos spreading centre, generating Cocos and Nazca plates (Meschede & Barckhausen, 2000). During this period, characterized by a strong tectonic rearrangement of the eastern Pacific, these two plates shifted in opposite directions: the Cocos Plate moved towards north-northeast, while the Nazca Plate moved towards east. This movement continues at present, producing an annual displacement in the directions mentioned before of 7.5 cm/yr for Cocos Plate and 3.7 cm/yr for the Nazca Plate (at 23°S) (Meschede & Barckhausen, 2000).

During the Cenozoic, the most important tectonic event that affected South America was the subduction of the Nazca oceanic plate, and many factors have played an important role in this process. For example:

1. The convergence velocity across the subduction zone:

The convergence velocity refers to the relative motion between the subducting Nazca Plate and the South American Plate. The convergence velocity vector shows a variation in terms of direction and rate in space and in time. Through some modelling it has been possible to define some pulses of very high convergence rate (204 ± 80 mm/yr between Middle to Late Eocene) and some pulses of deceleration with low convergence rate (44 ± 23 mm/yr between Oligocene and Early Miocene). Nowadays, a pulse with relatively high convergence rate in order to 125 ± 33mm/yr is recorded (Daly, 1989).

2. Age and composition of the subducting oceanic slab:

Molnar and Atwater (1978) suggested that the density of a slab is proportional to its age. When a slab is older and denser, it is also more gravitationally unstable and consequently easy to subduct. On the other hand, when a slab is younger a negative buoyancy takes place that provokes an increase of shear stress across the plate boundary. The age of the subducting slab (Nazca Plate) is difficult to determine and model because its nature is uncertain. However, according to Pilger (1984), the age of the subducted oceanic crust has been getting progressively younger throughout the Cenozoic (Daly, 1989).

3. The dip of subducting slab:

The slab dip has a controlling effect on the structure of active margins: if the dip is shallow the contact area with the upper plate is higher and the transmitted stress is huge. This situation promotes a compressive active margin, such as in the case of Andes slab (Daly, 1989).

Through the Cenozoic the geodynamic setting changed. Around 48 Ma, the subduction of the Farallon Plate (Nazca) under the South America Plate proceed oblique in the right side, while between 26-20 Ma the convergence between these two plates became more or less orthogonal (Cembrano et al., 2002).

Nowadays, if we consider the convergence of the South American Plate in relationship with the movement of the Nazca Plate, the total displacement is about 7.4 cm/yr in direction 78°N, because the South American Plate exhibits more or less the same amount of motion of the Nazca Plate. Also, the Chile Ridge, an active spreading centre, is currently subducting under the western margin of South America (Poveda et al., 2018).

The Caribbean Plate is a Cretaceous basaltic plateau derived from the Pacific Plate, which is subducting under the South American Plate, with a rate of ~ 1.9 cm/yr. This movement defines the Bucaramanga Segment and its associated seismic zone (Poveda et al., 2018).

Nowadays, the Andean Cordillera represents one of the most important environments of crustal growth in the world. This process could be studied and investigated through geophysics, petrology and volcanology. The Mercaderes context is particularly important because of the presence of numerous xenoliths, carried up to the surface through the volcanics. The xenoliths were derived from lower crust and upper mantle underlying the Mercaderes area, and represent a direct access key for studying crustal growth processes.

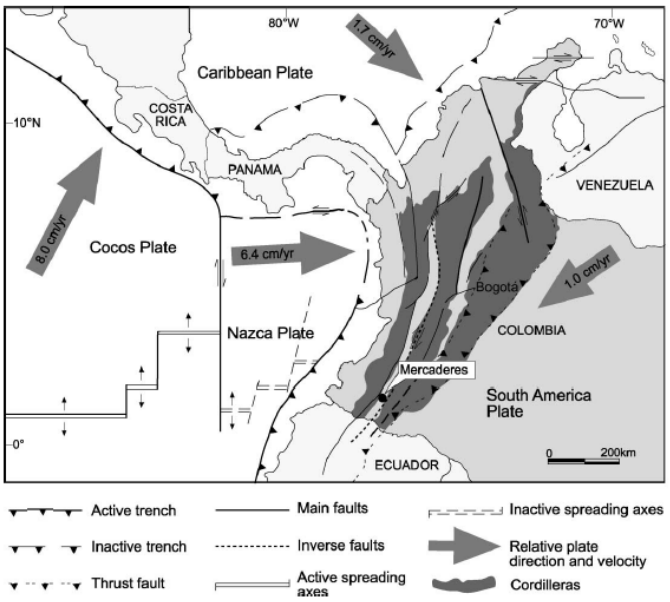

Figure 1.15 *Illustration of the three converging plates in Colombian Andes. (Weber et al 2002).*

1.4 The Studied Area: Mercaderes - Rio Mayo

The actual configuration of the Colombian sector of the Andean Cordillera is related to its previous evolution which took place during Early-Late Cretaceous and Middle Miocene. Besides the complex interaction between the three different plates mentioned before, some other important factors had contributed to produce the actual geodynamic setting: the collision of the Caribbean igneous province with the South American margin allowed to the formation of new crust that was added to the Pacific margin during Early-Late Cretaceous (Escalona & Mann, 2011) and also the emplacement of Panama arc in Western Colombia during Middle Miocene (Cediel et al., 2003; Restrepo & Toussaint, 1988; Taboada et al., 2000). These terranes were later involved and reworked in convergence processes that led to obtaining the actual configuration of the Colombian Sector (Poveda et al., 2018).

Nowadays, it is possible to subdivide this portion of Andean Cordillera in three geological provinces with particular features: the Eastern Province (ESAP) with the Guyana Shield rocks, the Western Province (WP) composed of basalts and Cenozoic volcanic rocks and the Central Province (CAP), made of a metamorphic core complex. Boundaries of CAP are defined by two important fault systems (Fig.1.16): the Cauca-Almaguer fault system in the western margin, which divides rocks with oceanic footprint from the continental ones, and the Borde Llanero Fault in the east. There are also two intervening valleys, the Middle Magdalena Valley and the Cauca-Patìa Valley, which separate these ranges. The Central Province is particularly relevant for this thesis because here is located the studied area.

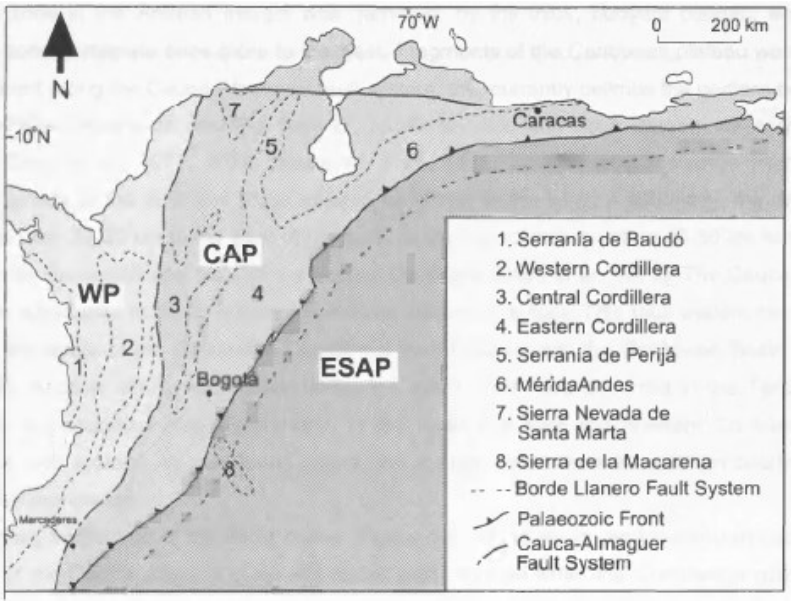

Figure 1.16 *Representation of the three main terranes provinces in the Colombian Andean Cordillera (Weber, 1998).*

The Mercaderes - Rio Mayo area is situated on the western flank of the Central Cordillera, at 1.5°N in the NVZ sector, near to the Dõna Juana Volcanic complex (Fig. 1.12). The Central sector is separated from the Western Cordillera by the Patía Valley, composed of Cenozoic sediments. Mercaderes is located between two important geological provinces, Cauca and Nariño, composed by Mesozoic – Cenozoic lithologies.

The Mercaderes - Rio Mayo area is characterized by the presence of xenolith-bearing volcanic rocks, which crop out in the Mercaderes plateau, 1000-2000 m above sea level. The Mercaderes tableland is composed of sediments and volcanic sediments that cover Cenozoic and Cretaceous rocks. Some of these are derived directly from the Dõna Juana volcano.

The most important area where it is possible to find abundant mantle and lower crustal xenoliths is situated to the south of the Mercaderes zone, precisely in the Granatifera Tuff outcrops (Fig. 1.17).

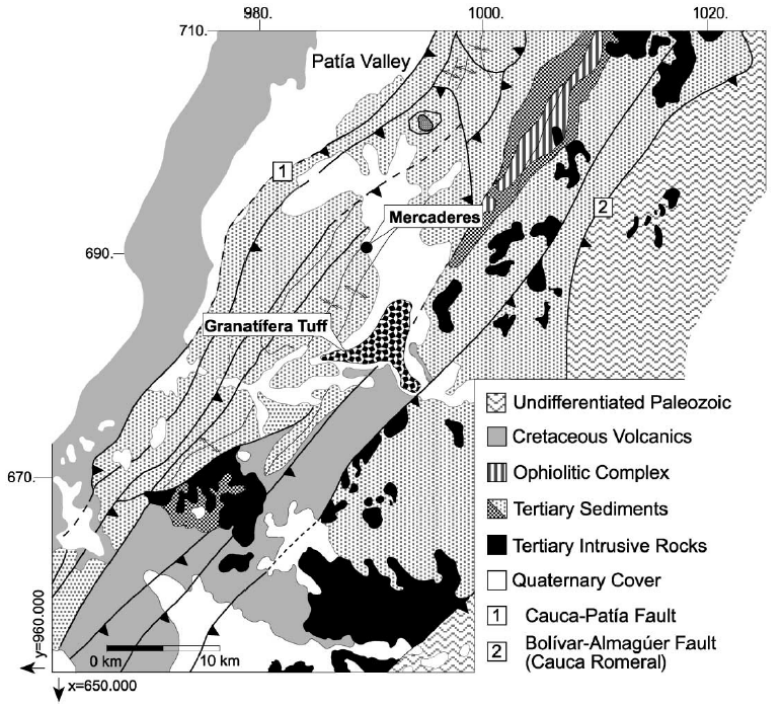

Figure 1.17 *Geological map of Mercaderes area with the Granatifera Tuff outcrops (Weber et al 2002).*

1.4.1 Lithologies of Mercaderes - Rio Mayo

In the Mercaderes area, different lithologies can be observed, whose ages span from Palaeozoic to Mesozoic and Cenozoic (Fig. 1.18). Below, a brief description of the main lithological units is provided:

Palaeozoic Rocks - These rocks are located predominantly in the east of Mercaderes village and they have been grouped into the Arquìa Complex, which includes metamorphic rocks of igneous and sedimentary origin.

The Arquìa Complex is composed by different types of rocks, mainly amphibolites, serpentinites, metagabbros, hornblendites and metadiorites, all metamorphosed between greenschist and amphibolite facies conditions.

In the southern zone of the Central Cordillera, precisely in the north of Mercaderes, blueschists and eclogites associated to serpentinized ultramafic bodies indicates an increase in metamorphic pressure conditions (Maya & González, 1995).

Some dating has been made in Arquìa Complex with the K/Ar method on hornblende, derived from amphibolites and metagabbros, and results indicate a Cretaceous age with two thermal events between 120 and 95 Myr. However, the age of the Arquìa Complex is not determined with certainty and it is still debated (McCourt et al., 1984).

Mesozoic Rocks - In the Central part of the Colombian Cordillera, Mesozoic rocks present a lithological variation from oceanic rocks, which are grouped in the Amaime Group, to volcanic rocks, that constitute the Volcánica Formation.

Both formations are interpreted as remnants of an obducted Cretaceous oceanic plateau (McCourt et al., 1984). Some rocks with similar composition of the Amaime Group like picrites, basalts and dolerites are present in the southern sector of Central Cordillera, but in this case they are younger than the previous one (Weber, 1998).

Eastwards of the Cali village, the Amaime Group is intruded by the Buga Batholith, which has been dated using several minerals and methods. Unfortunately, values show a large scatter but the youngest age, obtained by Rb–Sr dating on biotite, points towards a crystallization age of 99 $\pm$ 4 Ma. This indicates that the Amaime Group is certainly older, but due to the lack of any fossil records it is impossible to obtain a better time constraint (McCourt et al., 1984).

Another important formation located in the Central part is the Diabásico Group, which was defined by Nelson in 1962. Subsequently, the Diabásico Group has been subdivided in three separate lithological groups by Murcia and Cepeda (1991), who defined the Kiv, Kvs and Kvd units. The first represents the easternmost part of the Central Cordillera, whereas the other two units include some part of the Western Cordillera. The Diabásico Group is composed by basic rocks intercalated with different sediments and metasediments.

Both Amaime and Diabásico Group underwent very low-grade metamorphism in the zeolite and prehnite-pumpellyite facies, although in some cases they also display greenschist facies overprinting.

Cenozoic Rocks - The Amaime Group and the Palaeozoic basement are covered by folded Cenozoic sediments, that in the area are 850 m in thickness.

Cenozoic rocks are grouped in two principal formations, the Mosquera Formation and the Esmita Formation. The Mosquera Formation consists of conglomerates and sandstones intercalated with coal, which was probably deposited during a continental shallow water condition in the Middle Eocene or Lower Miocene. On the other hand, the Esmita Formation shows an inverse graded bedding, suggesting that the lithologies were deposited in a transitional environment, from saline shallow water to alluvial plains to alluvial fans. Alvarez (1983) and González (1988), through paleontological data, attribute to Esmita Formation an age between Middle-Upper Miocene.

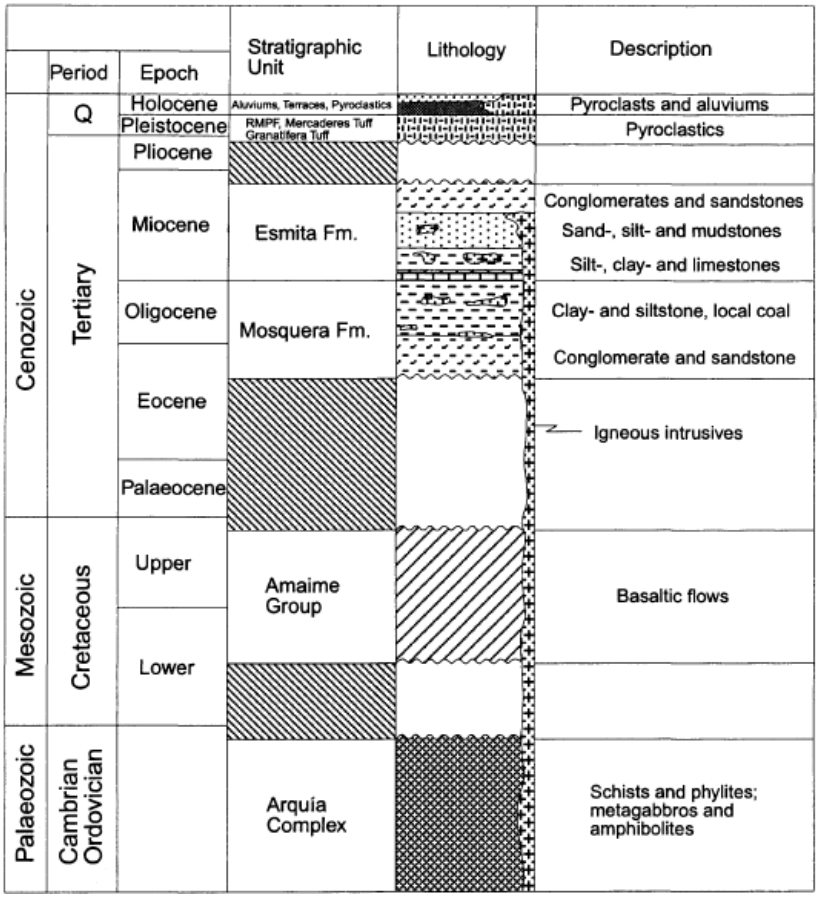

Figure 1.18 *Lithostratigraphic sequence of Mercaderes - Rio Mayo lithologies (Weber, 1998).*

A huge quantity of Cenozoic sediments occurs also in the Patía basin. These sediments were cut by numerous small sills, ranging from andesitic to dacitic composition. The Colombian volcanism is an important factor that affected the whole Cordillera in different periods of its evolution. Two main periods of volcanic activity have been individuated: the first syn-orogenic, from Lower to Middle Miocene, and the second post–orogenic, from Plio-Pleistocene to present days.

The origin of this magmatism is linked to the activity of the subduction zone, and the position of the igneous bodies is due to a strong tectonic control imposed by the Cauca- Almaguer fault system. The younger volcanogenic deposits in the area cover the Cenozoic sediments and the Amaime Group, and they come from different eruption centres included in the Dõna Juana Volcanic complex.

The most important volcanic deposits in this area are the folded sediments of the Esmita Formation and the Rio Mayo Pyroclastic Flow. The latter originally comprised all volcanic rocks outcropping in the Rio Mayo zone, also the Granatifera Tuff. More intensive studies of this zone have revealed the presence of many pyroclastic flows, not related to the Granatifera Tuff, and consequently a new type of Tuff, named Mercaderes Tuff, was introduced in the classification.

In the Cenozoic rocks context, pyroclastic rocks are very important, and they will be treated separately.

1.4.2 Pyroclastic rocks of Mercaderes - Rio Mayo

The Rio Mayo Pyroclastic Flow (RMPF) is the most important deposit in this area. It is composed by volcano-sedimentary rocks which covered the entire Mercaderes zone, and it includes also the Granatifera Tuff and the Mercaderes Tuff.

Granatifera Tuff - The Granatifera Tuff is located in the western flank of the NVZ, near the Dõna Juana Volcanic Complex which might represent the source of the Granatifera Tuff (Murcia and Cepeda, 1991). The importance of this tuff is marked by the presence of upper mantle and crustal xenoliths, which permitted to obtain many information about subduction and crustal growth processes under the Andean continental arc.

The tuff lies discordantly on Cretaceous basalts and on the folded Cenozoic sediments of the Esmita Formation.

The Granatifera Tuff is subdivided in two units, reported in Fig 1.19 as Unit A and Unit B, and briefly descripted below from the base to the top of the lithostratigraphic sequence.

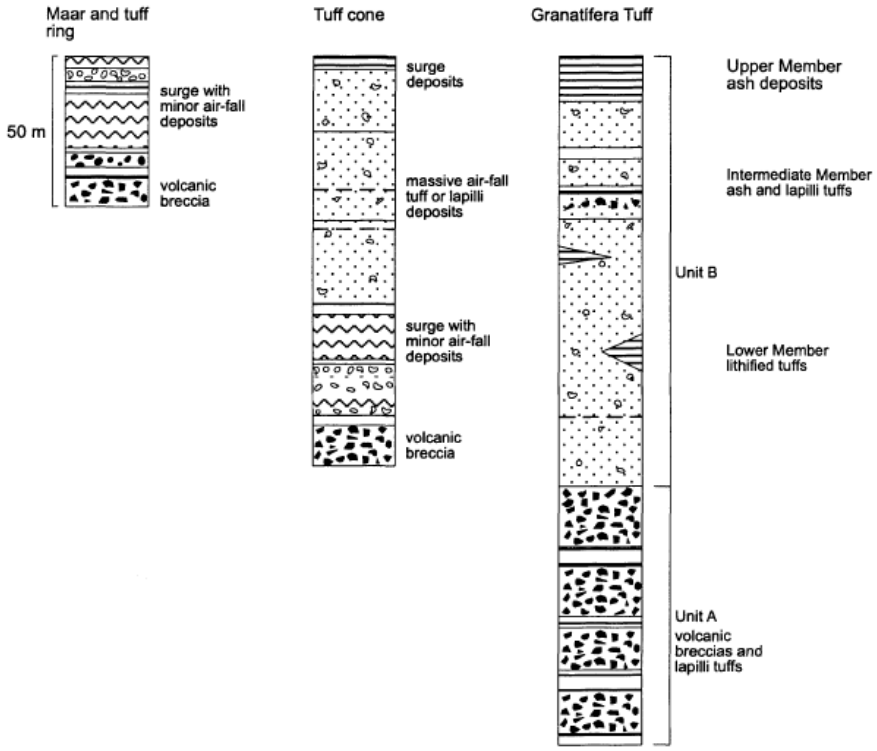

Figure 1.19 *Lithostratigraphic sequence of the Granatifera Tuff, subdivided in its two principal units A & B (Weber, 1998).*

Unit A

Its thickness of Unit A is about 200 m and it is mainly composed by an alternating sequence of breccias and lapilli tuffs.

Breccias: fragments are 30-70 cm in size and compositionally they are mainly represented by quartzites, schists and andesites. Additionally, it is clearly possible to see an increase in the dimensions and quantity of metamorphic fragments, from the base to the top of the sequence.

Lapilli tuffs: composed of andesite, diorite, pumice and a small fraction of fragments with different compositions, including schists, pyroxenites, peridotites and amphibolites. All these elements are mixed in an ash matrix. Within the sequence, the stratification appears plane parallel with a normal gradation (Martínenz and García, 1989).

Unit B

This unit is further divided into three members and it covers up the most portion of the entire Granatifera.

Lower member:

This member reaches maximum thickness of 90 m and it is composed of lithified tuffs, which show in their inner portion different fragments of various lithologies. Such fragments mainly consist of schists, phyllites, diorites, pyroxenites and peridotites, but other lithologies can also be observed (Weber, 1998). The size of the clasts is variable, ranging from millimetres to centimetres. The lateral thickness of the outcrop is irregular, often forming lenses.

Intermediate member:

This member comprises ash and lapilli tuffs with a thickness of 40 m. The lithification degrees between the different lithologies are not the same, suggesting that some sediments have been more subjected to erosional processes than others. The fragments observed in the intermediate member are similar in composition to those of the lower member but are notably larger (Weber, 1998).

Upper member:

It comprises a sequence of ash deposits that reach up to 15 m in thickness. The upper member is made of volcanic glass, biotite, plagioclase and metamorphic rocks, without ultramafic or mafic xenoliths (Weber, 1998).

Mercaderes tuff - The Mercaderes Tuff comprises unconsolidated arenaceous tuff and fragments composed of pumice, schist, basalt and andesite (Weber, 1998). Its stratification is strongly plane parallel, and fragments can reach up more than 50 cm in size.

The Mercaderes Tuff is deposited over the Granatifera Tuff. Moreover, the Mercaderes Tuff is not homogenously extended throughout the entire area, probably because it has undergone an intense erosion process.

The relationship with the Granatifera Tuff is not clear and different classifications have been proposed. Martìnez and Garcìa (1989) considered both tuffs as single formations, in which the Mercaderes Tuff represents the Unit C in the uppermost portion of the Granatifera Tuff. By contrast, Murcia and Cepeda (1991) suggested that both are part of Rio Mayo Pyroclastic Flow.

Pupo and Rodriguez (1992) highlighted the importance to split up these two formations because they present substantial differences in terms of lithology and nature of their fragments.

The contact between the Granatifera Tuff and the Mercaderes Tuff is erosional and characterized by the presence of a silt horizon rich in nodules and veins of Fe-oxides. This suggest that a period of soil formation occurred between the deposition of the two tuffs (Weber, 1998).

1.4.3 Origin and age of the Granatifera Tuff

The poor sorting and the coarse size of the fragments suggest that the Granatifera Tuff originated from a powerful eruption (Weber, 1998). Another evidence is the great amount of calcite, occurring in veins or in thick crusts formed after percolation, circulation and re-deposition of fluids inside the sediments. Syngenetic faults are common and often are filled with ash tuff and fragments.

Consequently, it is possible to assume that the Granatifera Tuff derives from an intense eruption that could have a phreatomagmatic origin. Typical features for phreatomagmatic eruptions, such as dune forms and cross stratifications, have not been recognized in the Granatifera Tuff and for this reason its origin is still ambiguous. However, due to the fact that such depositional indicators can be easily eroded and because of the rugged area on which the Granatifera Tuff is exposed, it might be that they have been overlooked. If the presence of dune and/or cross beds were confirmed, the Granatifera Tuff would be considered as a ring or a tuff cone (Weber, 1998).

There are not much and precise information about the age of Granatifera Tuff and most of them rely on stratigraphical relationships. Its sediments overlap the folded Cenozoic sediment of the Esmita Formation, dated to Upper Oligocene-Lower Miocene. Murcia and Pichler (1986) performed some dating with K-Ar method on biotite from the proximal Doña Juana Complex; the results indicate an age of 1.5 ± 0.1 Ma which is assumed to correspond to the minimum depositional age of the Granatifera Tuff.

1.5 Xenoliths

In order to understand the physical properties, compositions, age and growth processes of the lower continental crust and mantle, it is necessary to obtain samples that have resided at deep crustal levels or in the mantle for substantial periods of time (Rudnick, 1992). Sample that could be useful to know all of these features are xenoliths. Xenoliths are extremely important because they represent an access key to study subduction process and crustal growth that take place in NVZ area. Using xenoliths, it is possible to know the chemical change and composition of some inner portions of the Earth, such as lower crust and mantle, that otherwise would be inaccessible. It is possible to define xenoliths such as fragments that are carried rapidly to the Earth's surface by fast erupting volcanics (Rudnick, 1992).

In the studied area, there are both mantle and lower crustal xenoliths. It is possible to distinguish between these two categories on the basis of several factors.

Characteristic features of lower crust xenoliths

On the base of the previous work by Rudnick (1992), it is possible to assume:

1. Generally, lower crustal xenoliths exhibit a typical mineral assemblage of granulite facies, but in some cases, they can show also a typical assemblage of amphibolite facies, especially when the water content tends to be high, such as in subduction zone.
2. Lower crust xenoliths exhibit a mineral assemblage that should be equilibrated an appropriate lower crustal depth, in terms of pressure about 0.6 to 1.4 GPa.

3. The presence of decompression features, for example cracks in garnets, which are interpreted such as result of rapid ascent of the xenolith from deep crustal levels.

Characteristic features of mantle xenoliths

1. Generally, mantle xenoliths present an alkaline nature (Pearson et al., 2003).
2. Xenoliths through the rapidly eruption and quenching from the upper mantle record temperature, pressure and oxygen fugacity of the mantle and they allow to the reconstruction of the local mantle geotherm (Pearson et al., 2003).

In the Mercaderes zone, mantle and lower crustal xenoliths are mainly exposed in the Granatifera Tuff, situated in NVZ. As reported in Figure 1.20, most common mantle xenoliths are represented by garnet-free websterite and spinel-bearing peridotite, while crustal xenoliths are represented by hornblendite, pyroxenites, granulite and gneisses into the amphibolite to granulite facies (Rodriguez-Vargas et al., 2005). Both crustal and mantle xenoliths provide a complete sampling from the mantle wedge to the continental lithosphere.

Xenoliths in the Mercaderes area have different types of host rocks, such as tuffaceous matrix, lamprophyre or andesite fragments, all inside the Granatifera Tuff, and present different size, where mantle xenoliths are up to 12 cm while crustal xenoliths are about 20 cm. The specific characteristics of each types of xenoliths will be explain in detail below.

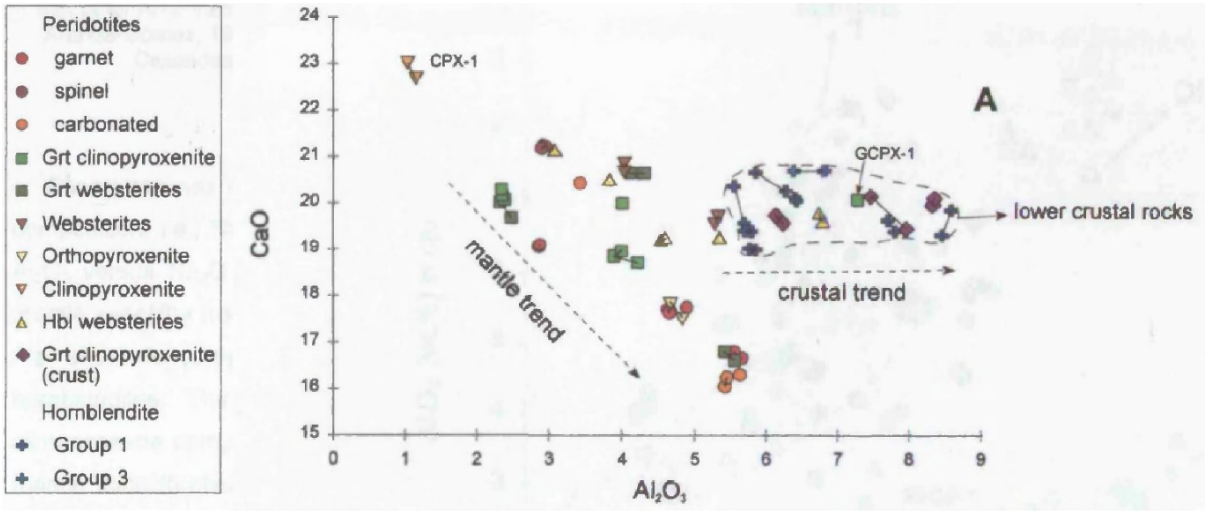

Figure 1.20 *Different compositional trend for peridotites which came from mantle and lower crust of Mercaderes zone* (Weber, 1998).

1.5.1 Mantle xenoliths

In a subduction context, mantle xenoliths could represent part of the metasomatized mantle wedge above the subduction zone or, simply, the mantle lithosphere not closely related to the subduction process (Pearson et al., 2003).

Garnet-bearing rocks ranging from peridotite to websterite are the most abundant mantle xenoliths and, in minor amount, it is possible to find also garnet-free spinel–bearing peridotites

and websterites. Through some studies based on these xenoliths, it was possible to constrain their formation conditions, in terms of temperature and pressure.

The very different compositions of these xenoliths underline how they derive from three different sources. In particular, garnet-free websteriste xenoliths exhibit a MORB isotopic signature, with pressure (P) of 1,6 GPa and temperature (T) about 1065° C. These data have been obtained through $^{87}Sr/^{86}Sr$ and $^{143}Nd/^{144}Nd$ methods. Instead, garnet-bearing peridotite and websterite xenoliths exhibit two different sources of provenance: the first one with intermediate conditions between 29 to 3,5 GPa in P and T about 1250-1295 ° C, which values are closest to sub-oceanic geotherm in OIB context. The second one shows conditions of a sub-continental geothermal with P > 3,8 GPa and T about 1140-1175° C.

Garnet-bearing peridotite xenoliths which show an OIB signature are in agreement with the tectonic setting of the region, where subduction of the Nazca Plate under the South America Plate is currently going forward (Rodriguez-Vargas et al., 2005).

The huge difference in terms of signature between these two types of mantle xenoliths underline the presence of a differentiated mantle. In the Mercaderes zone, the mantle has experienced a long and complex history of evolution processes. An interpretation key for the complex composition of this mantle could be linked to an event that occurred 1.0 Gyr ago, which provoked an intense recycling of continental crust during the Greenvillian Orogneny (Rodriguez-Vargas et al., 2005).

1.5.2 Lower crustal xenoliths

Crustal xenoliths permit to have a complete sampling on the continental crust over the subduction zone. These xenoliths present a wide range of composition, including amphibolites, pyroxenites, granulites and orthogneisses (Weber, 1998).

In the Mercaderes area, crustal xenoliths could be classified briefly as hornblendite and pyroxenite, which are the most abundant xenoliths in the Granatifera Tuff, and it was possible to define them in this way (Fig. 1.21):

Hornblendite: it is an ultramafic igneous rock where hornblende is the main phase.
Pyroxenite: it is an ultrabasic igneous rock, where pyroxene is the main phase and feldspar is absent.

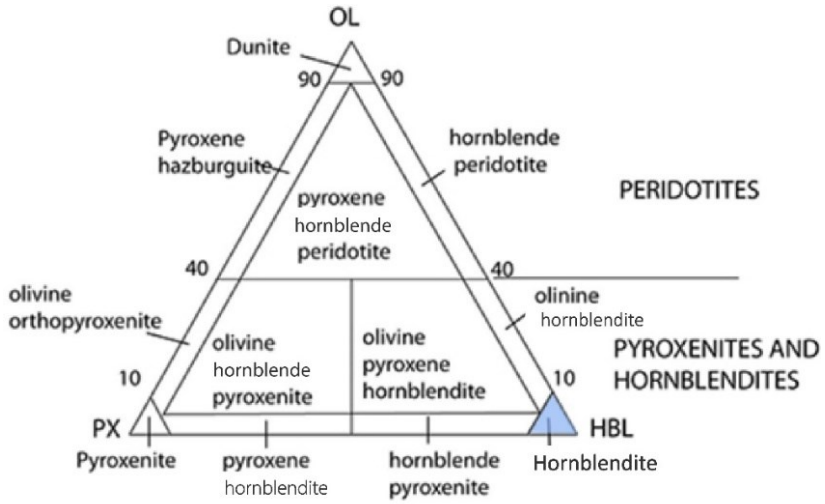

Fig 1.21 *Olivine(Ol) – pyroxene (Px) – hornblende (Hbl) diagram for ultramafic rocks.*

These two types of rocks have been further divided into several subgroups:

- **Garnet pyroxene hornblendites**: the principal phases are represented by Grt + Cpx + Hbl (mineral abbreviations after Whitney and Evans 2010) which is also the predominant phase, and accessory phases represented by Ap – Ttn – Rt.
  The presence of amphibole in these xenoliths underlines an highly hydrous lower crust in the northern Andes (Weber, 1998).
  This group has been further divided in other three groups, on the base of mineral texture and optical properties (Weber, 1998):
  1. Group 1 hornblendites: composed by coarse amphibole, clinopyroxene and xenomorphic garnet;
  2. Group 2 hornblendites: garnets are both xenomorphic and idiomorphic with different size. Many inclusions are present inside the garnet, such as rutile, apatite and occasionally some quartz;
  3. Group 3 hornblendites: they represent the only one crustal xenoliths type which contain orthopyroxene.

- **Garnet pyroxenite**: they essentially consist of bi-mineralic assemblage, with Grt – Cpx. (Weber, 1998).

Moreover, xenoliths could be classified also in:

- **Garnet pyribolite**: these include all the samples that contain any amount of felsic phase. Depending on the type of the felsic mineral, it is possible to recognize Group 1 pyribolites, where feldspar is the main felsic phase, or Group 2 pyribolites where scapolite is the principal felsic phase (Weber, 1998).
- **Granulite:** these rocks contain Grt – Cpx – Pl – Qz and Scp as main phases, whereas accessory phases are Ap – Rt -Ttn (Weber, 1998).
- **Gneiss:** it is composed by Grt – Pl – Bt – Amp - Cpx and it is also possible to find in low quantity Bt – Ep – Pl (Weber, 1998).

- **Pyriclasite and pyrigarnites:** these two types of xenoliths are similar in terms of mineral assemblage and the high content of apatite. Pyrigarnites presents Pl such as feldspar main phase, Grt and Cpx, in which it is possible to find small inclusion of Bt. Scp is also present, but in low quantity respect to Pl. In pyriclasites, the main felsic phase is represented by Scp, which is present in a small quantity and there is also Pl, which is lesser than Scp. There are also Grt and Cpx and Rt and Ap like accessory.

Garnet is an important phase, and it appears in every xenolith category. Its composition is not constant for each group, as reported in Fig. 1.22.

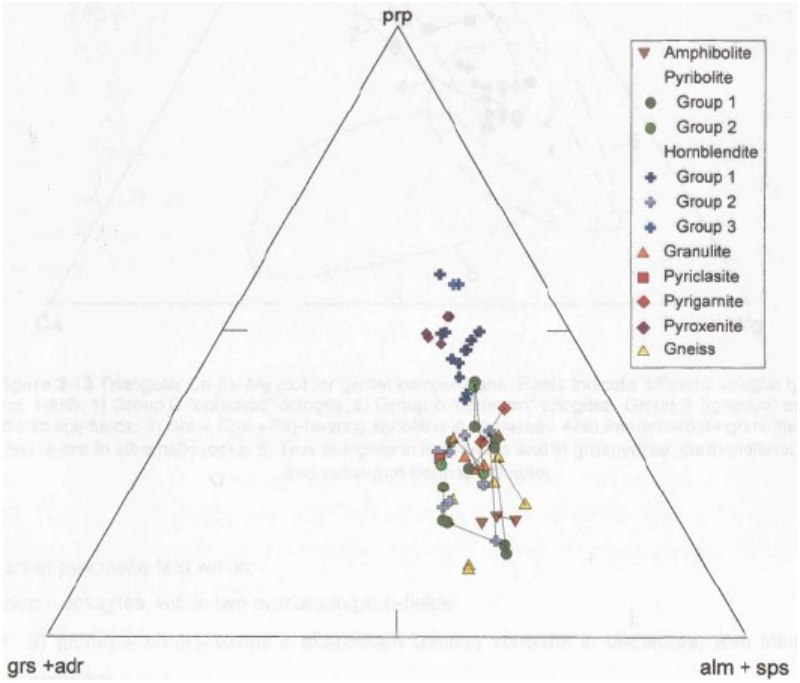

Figure 1.22 *Garnet composition for the Mercaderes - Rio Mayo lower crustal xenoliths* (Weber, 1998).

Through different analysis performed on garnets it was possible to calculate an evaluation of temperature and pressure.

Temperature of lower crustal xenoliths

The temperature of xenoliths has been estimated using garnet core and rim analyses, through three different geothermometers: the first by Krogh (1988) and the second by Ellis and Green (1979) are based on Fe^{2+} and Mg^{2+} exchange between garnet and pyroxene, while the third one by Graham and Powell (1984) is still based on Fe^{2+} and Mg^{2+} exchange, but between garnet and hornblende. To obtain a valid result using a geothermometer, it is important that minerals in xenoliths should be at equilibrium conditions. Indeed, if minerals are not at equilibrium, the temperature calculated does not represent the formation conditions, but only a general temperature or pressure which minerals have reached at a certain time. A good geothermometer presents a standard deviation of $\pm$ 50° C.

Some garnet samples, which belong to the previous xenoliths groups, were analyzed and the different results obtained are reported in Table 1.1.

		Krogh				E&G				G&P			
rock	sample	core	σ-1	rim	σ-1	core	σ-1	rim	σ-1	core	σ-1	rim	σ-1
pyribolites													
Group 1	**920-1**	683*		725*		721*		757*		735		779	
	PB-A-2	733*		750	5	776*		792	4	718		740	13
	PB-A-3	580	17	735	31	623	16	776	28	585	0	755	11
	PB-A-4	617*		783*		657*		808*		660*		820*	
	PB-A-6	782*		817*		808*		837*		721*		708*	
	PB-A-7	760	13	799	39	789	11	821	35	778	4	803	24
Group 2	**PB-B-1**	871		925		883		929		853		872	
	PB-B-2	708*	10	845	37	744	9	868	32	695*		798	13
hornblendites													
Group 1	**HBL-A-1**	999	30	1102	27	986	25	1096	23				
	HBL-A-2	831	39	818	77	891	34	878	69	928	15	963	9
	HBL-A-3	859	33	837	34	890	29	875	28	867	3	872	12
	HBL-A-4	828	23	835	26	861	19	868	22	881	6	877	5
	HBL-A-5	759	2	809	4	814	6	877	15	846	37	858	24
	HBL-A-6	798	3	807	5	855	26	867	9	778	11	771	10
	HBL-A-7	904	21	898	52	927	18	922	43	1011	2	1013	8
Group 2	**HBL-B-1**	807*		840*		828*		859*		844*		841*	
	HBL-B-2	607*		739* 710*		647*		790* 761*		569*		679* 687*	
	HBL-B-3	721*	37	851 970	36 13	754*	34	868 971	34 10	772*	13	861 876	18 12
	HBL-B-4	870	38	886	32	882	33	896	27	857	14	850	12
Group 3	**HBL-C-1**	910	6	944	0	902	9	937	8	861	3	866	10
granulite													
	GRL-1	978	11	960	36	998	8	981	31				
	GRL-2	858	9	1043 999	23 28	875	5	1030 998	19 23				
	GRL-3	920	54	974	24	927	45	976	52				
pyriclasite													
	PCL-1	979	47	958*		995	30	965*					
pyrigarnite													
	PGR-1	1010	33	1001	27	1038*		1025*					
pyroxenites													
	PX-2	957	22	984	22								
	PX-3	1007	61	1007	51								

Table 1.1 *Temperature calculations for Mercaderes lower crustal xenoliths obtained with Krogh = Grt-Cpx geothermometer (Krogh, 1988); E&G = Grt-Cpx geothermometer (Ellis and Green, 1979); G&P = Grt-Hbl geothermometer (Graham and Powell, 1984) (from Weber, 1998).*

In their history, lower crustal xenoliths have undergone an increase in temperature and also in metamorphic grade. They have reached the amphibolite – granulite transition through the amphibole and biotite dehydration reaction, but due to the high temperature any evidence of this process has been removed. In some rocks the temperature was maintained high enough to permit the complete chemical homogenization of minerals in the assemblage (Weber, 1998).

Pressure of lower crustal xenoliths

Pressure conditions for lower crustal xenoliths has been quite difficult to determine because in many samples an appropriate mineral assemblage is not preserved. Few results have been obtained with a comparison between the observed mineral assemblages and known phase stability field, only when the whole rock composition is in agreement.

Using pyribolite mineral assemblage (Grt – Pl – Cpx - Qz), pressure has been calculated with the Kohn and Spear (1990) barometer suggesting that a partial equilibrium has been obtained between 0,9 and 1,4 GPa. Although these values were approximate, it is clear how these rocks have undergone high pressure metamorphism typical of granulite facies but not in the eclogite

facies. The presence of clinopyroxene rather than orthopyroxene associated with garnet confirmed these pressure conditions, indeed a hypothetical presence of orthopyroxene would have indicated a low-pressure assemblage (Weber, 1998).

For the pyribolite group, the best P (0,9 – 1,4 GPa) and T (580-660°C) estimation values have been obtained respect to other rocks groups (Weber, 1998).

As reported in Bloch et al. (2017), in terms of depth most of Mercaderes crustal xenoliths have been equilibrated between 60 – 80 km along a continental geothermal gradient, more or less between 7 – 27 km under the seismically determined Moho (about 53 $\pm$ 3.5 Km). This gradient is typical of adiabatically upwelling mantle material at greater depths. Moreover, the lack of retrograde zonation in primary phases and major elements inside the xenoliths highlights how these rocks did not stay for a long time in shallow portions and consequently this means that the rise up has been fast and shortly before the eruption.

Chapter 2 - PETROGRAPHY

2.1 Introduction

My thesis work did not include field activity, indeed all samples were supplied by Dr. Fabio Ferri who collected them during his research activity in Colombia in the frame of the MAKEARTH Cariparo project. In total there are 20 thin sections of crustal xenoliths from Mercaderes - Rio Mayo, and each of them has been carefully observed under optical microscope. After an initial study, six samples have been selected to conduct the more detailed analysis described below.

These samples are:

- 18XC1
- 18XC5
- 18XC6
- 18XC10
- 18XC15
- 18XC20

The petrographic analysis of these samples has been made using an optical microscope, where both thin (30 μm) and thick (200 μm) sections were observed with reflected and transmitted light.

In order to examine in more detail all sections and the MI which are contained inside of them, I used the Scanning Electron Microscope (SEM) at the Department of Geosciences, Padua University. This SEM is a CamScan MX 3000 equipped with micro-chemical analyzer (EDAX). All observations were performed with a 20kV emission from filament in lanthanum hexaboride (LaB_6).

I also performed SEM analyses with the ESEM – FEI Quanta 200 of CEASC (Centro di Analisi e Servizi per la Certificazione), Padua University.

Below, I report the petrographic description of the studied samples.

Even if only three of them (18XC1, 18XC10, 18XC20) contain melt inclusions, all the six samples were completely analyzed with SEM and electron microprobe analyzer (EMPA) in order to obtain more complete chemical and petrographic information.

2.2 Sample 18XC1

The mineral assemblage of this sample is Grt – Pl - Amp – Cpx - Scap as main phases and Ap as accessory (Fig. 2.1a). Here and throughout the text, minerals in assemblages are listed in order of decreasing abundance, visually estimated.

The textural and microstructural description of 18XC1 and all other samples is quite complex. Xenoliths have an intricate genesis, therefore it is not very easy to distinguish a metamorphic texture from a magmatic one, moreover in many cases they tend to display a hybrid texture.

In order to describe in an accurate way the general structure of this section, it is useful to divide 18XC1 in two different parts.

In the first part the structure could be defined as inequigranular interlobate with garnet porphyroblast. The contact among phases are quite corroded, especially where different phases are in contact with garnets (Fig 2.1a).

In the other part, the texture could be defined as seriate interlobate, still with garnet porphyroblast. This side is much more fractured and with more corroded textures than the previous one, indeed garnet is intensely fractured and filled with small and thin crystals of secondary origin.

The intense resorption of crystals in this section could be probably caused by interaction with the host lava. This is supported by the previously mentioned filled fractures which crosscut garnets and other phases.

Sample 18XC1 does not display layering and from a textural point of view, it could be defined isotropic.

Garnet

Garnet is the main phase of this sample, and it shows an anhedral shape with variable size; some crystals are 2 -7 mm in size, while in other cases a few relict fragments are much smaller (200-500 µm). Most garnets are strongly fractured.

Locally, some fractures are filled by aggregates of small crystals, possibly representing the crystallization products of melt which infiltrated from the host lava (Fig. 2.1b).

The contact boundaries with other phases are in place linear, but sometimes they appear resorbed. Especially inside larger garnets many mineral inclusions, such as Cpx – Pl – and Amp are present.

Many garnets in sample 18XC1, especially the two which are located in the middle of the section (Fig. 2.1b), contain melt inclusions, which will be treated separately in the next section.

Plagioclase

Plagioclase is the second abundant phase after garnet. Plagioclase is distributed in homogeneous way throughout the section, with variable size ranging from 100 µm to 1,7 mm. It often presents lobate boundaries with other phases (Fig. 2.1c), even if in some cases boundaries tend to be corroded. In terms of shape, Pl could be defined as xenomorphic.

Many crystals display polysynthetic twinning.

Amphibole

Amphibole occurs in the entire section in heterogeneous way, indeed it is possible to identify some zones where it is most abundant.

Amphibole has a variable size ranging from 300 µm to 1,8 mm and has xenomorphic shape. The contact boundaries with other phases are lobate and well defined, only exceptionally non-linear (Fig. 2.1d).

Some crystals display the typical cleavage at 60°/120° (Fig. 1d).

Under plane polarized light (PPL) amphibole shows a nutsy brown pleochroic color, while under crossed polarizers (XPL) it appears dark green, with second order interference colors.

Clinopyroxene

It is present in homogeneous way inside the entire section with different size ranging from 400 µm to 700 µm and with anhedral shape. The larger crystals are present mainly near the garnets, while smaller ones are randomly distributed through the section. Moreover, Cpx tends to be very altered and fractured, with lobate boundaries in contact with other phases.

Under PPL Cpx is light-green, while under XPL it appears blue - orange – yellow, with third order interference maximum colors.

Scapolite

It is rare in this rock, and occurs as scattered crystals of variable size (Fig. 2.1e).

Apatite

It is present mostly as inclusion in the main rock phases, with rounded shape and high relief.

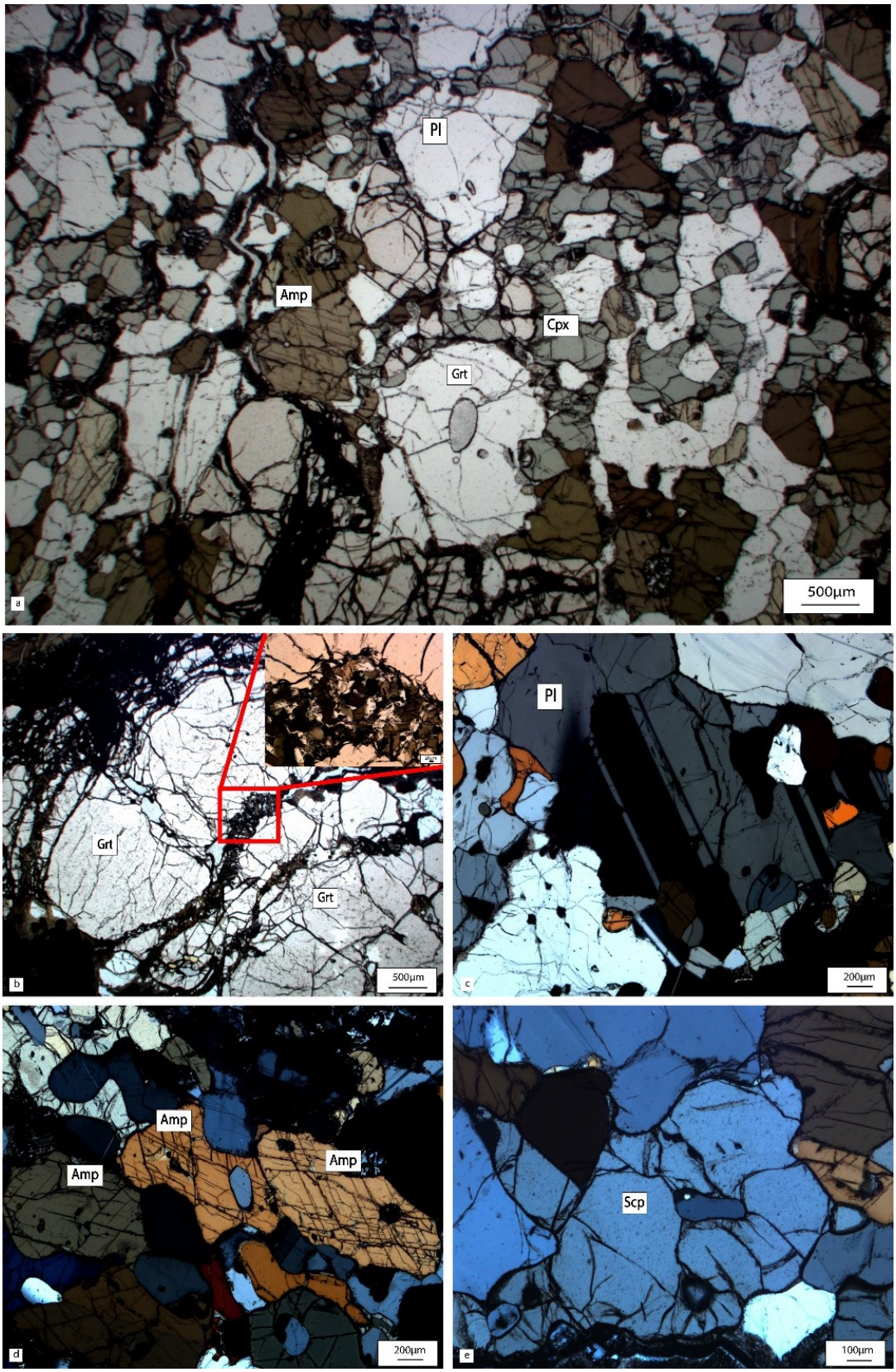

***Figure 2.1**: **(a)** General petrographic aspect of thin section 18XC1 under plane polarized light (PPL); **(b)** Fractured Grt with zoom on the fracture filled of minerals; **(c)** Plagioclase with polysynthetic twinning under crossed-polarizers (XPL); **(d)** Amphibole at crossed polarizers with its characteristic cleavage; **(e)** Scapolite under XPL.*

2.3 Sample 18XC5

The mineral assemblage of 18XC5 is Grt - Cpx - Amp – Pl - Scp as main phases and Rt – Ap as accessory (Fig. 2.2a). The general structure of this section could be considered granoblastic interlobate, without layering and with isotropic texture.

Garnet

It represents the main phase in 18XC5, and presents anhedral shape. Garnet is variable in size from 1mm to 3,5mm. Garnet is often surrounded by Cpx, and presents lobate boundaries toward other phases (Fig. 2.2b).

Inside the Grt some inclusions are often present, such as Ap, Pl or Cpx. Inclusions have a rounded shape.

Inside the Grt, it is also possible to find some MI both isolated and along trails.

In this section Grt appears very fractured.

Clinopyroxene

Clinopyroxene represents the second most abundant phase inside the thin section after Grt.

Clinopyroxene shows an anhedral shape, it is smaller than Grt and surrounds the latter. It shows size ranging from 300 µm to 4mm.

The boundaries with the other minerals are regular, but in some cases corroded (Fig. 2.2c) and filled with former melt.

Many crystals are fractured and only in a few cases Cpx contains Ap or Pl.

Under PPL clinopyroxene shows a light green color, while under XPL it appears fuchsia, yellow and light blue, with third order maximum interference color.

Amphibole

Amphibole is not abundantly present in 18XC5 thin section. It exhibits an anhedral shape and its size is between 400 µm and 2,5mm. It often displays a typical cleavage with angles of 60/120 degrees (Fig. 2.2d).

Under PPL amphibole shows a light brown pleochroic color, while under XPL it appears dark green, with second order maximum interference color.

Plagioclase

Plagioclase has an anhedral shape, with variable size in the range 800 µm - 1 mm. The boundaries with other phases are linear but often altered.

Scapolite

Scapolite is rare in 18XC5. The few crystals in the section are about 1,2 mm in size with lobate boundaries and occur as interstitial grains (Fig. 2.2e). Scapolite is often in contact with garnet. Some MI, which are organized in clusters, have been found inside scapolite, too.

Rutile

Rutile is present as an accessory phase, and shows acicular or rounded shapes. Rutile is present mostly included in the main phases, like Grt where it displays its characteristic orange -brown color and high relief.

Apatite

Apatite is present as an accessory phase inside the main minerals like Grt or Cpx. It is colorless, with a very high relief, and displays a light gray interference color.

Figure* 2.2: *(a) *General petrographic aspect of section 18XC5 under PPL;* ***(b)*** *Fractured garnet with lobate boundaries under XPL;* ***(c)*** *Clinopyroxene under XPL with corroded margins;* ***(d)*** *Amphibole under XPL with typical cleavage at 60/120°;* ***(e)*** *Scapolite rich in MI under XPL.*

2.4 Sample 18XC6

The mineral assemblage of this section is Grt - Pl - Cpx - Amp as main phases and Rt as accessory phase (Fig. 2.3a).

To describe the general structure of 18XC6 in an accurate way, it is useful to divide the section in two different sides. One side exhibits a seriate interlobate structure with garnet porphyroblasts, which are surrounded by Pl and Cpx. In the other side, the structure could be defined as inequigranular interlobate always with garnets porphyroblast but in this case they are surrounded almost exclusively by Pl.

From a textural point of view, 18XC6 could be defined isotropic and does not present any layering.

Garnet

Garnet is the main phase of this section and it is present with subhedral shape. The size of Grt is variable from 200 µm to 3 mm, but the pervasive network of fractures which pass through the mineral makes the measurement of the size quite difficult.

Garnet is extremely rich in inclusions of other minerals, especially Pl and Rt.

The boundaries with the other phases are strongly irregular but clear and devoid of films of former glass (Fig. 2.3b).

Plagioclase

Plagioclase represents the second phase after garnet in order of abundance, and its size varies from 800 µm to 2 mm.

Plagioclase is rich in mineral inclusions mostly composed by Rt, Ap, Qz (Fig. 2.3d) or other small and rounded Pl with different orientation.

The Pl-Pl boundaries tend to be linear, whereas when Pl is in contact with other phases, boundaries are extremely lobate. Only locally, plagioclase displays triple junction with 120 degrees, between them or with other phases (Fig. 2.3c).

Plagioclase shows typical polysynthetic twinning (Fig. 2.3c).

Clinopyroxene

Clinopyroxene is present in low amounts and in heterogenous way, and it is principally located at the center or at margins of the section. Clinopyroxene presents an anhedral shape, and it is often in contact with Pl and Grt.

Clinopyroxene appears as relicts of earlier coarser crystals, and for this reason its size presents a variable range between 200 µm to 1,4 mm and its margins are extremely lobate (Fig. 2.3e).

Under PPL clinopyroxene shows a light green color, while under XPL it appears purple – blue, with third order maximum interference color.

Amphibole

Only a few crystals of Amp are present in this section.

Amphibole exhibits an anhedral shape and it is commonly in contact with Cpx or Pl. Its size varies between 200 µm and 800 µm.

Under PPL amphibole shows green color, while under XPL it appears dark green, with second order maximum interference color.

Rutile

This mineral is present in large amount throughout the section, in homogeneous way. Rutile is present as inclusions or isolated crystals with variable size in the range between 100 and 300 µm (Fig. 2.3f).

Quartz

This mineral is presents in very low quantity often inside of plagioclase as an inclusion (Fig. 2.3g).

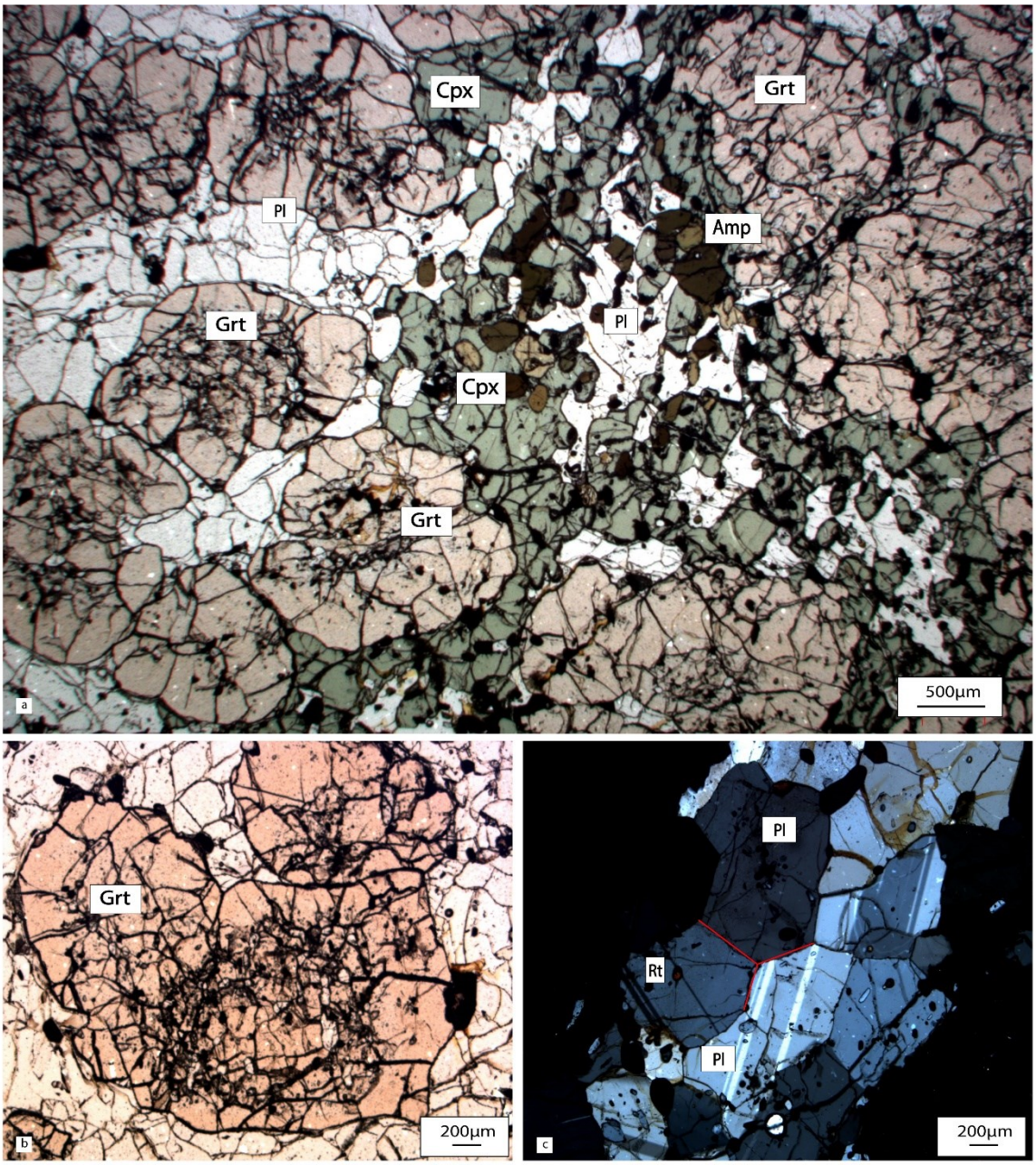

Figure 2.3 (a) *General petrographic aspect of thin section 18XC6 under PPL;* ***(b)*** *Garnet rich in inclusions under PPL;* ***(c)*** *Plagioclase with well-equilibrated triple junctions under XPL;*

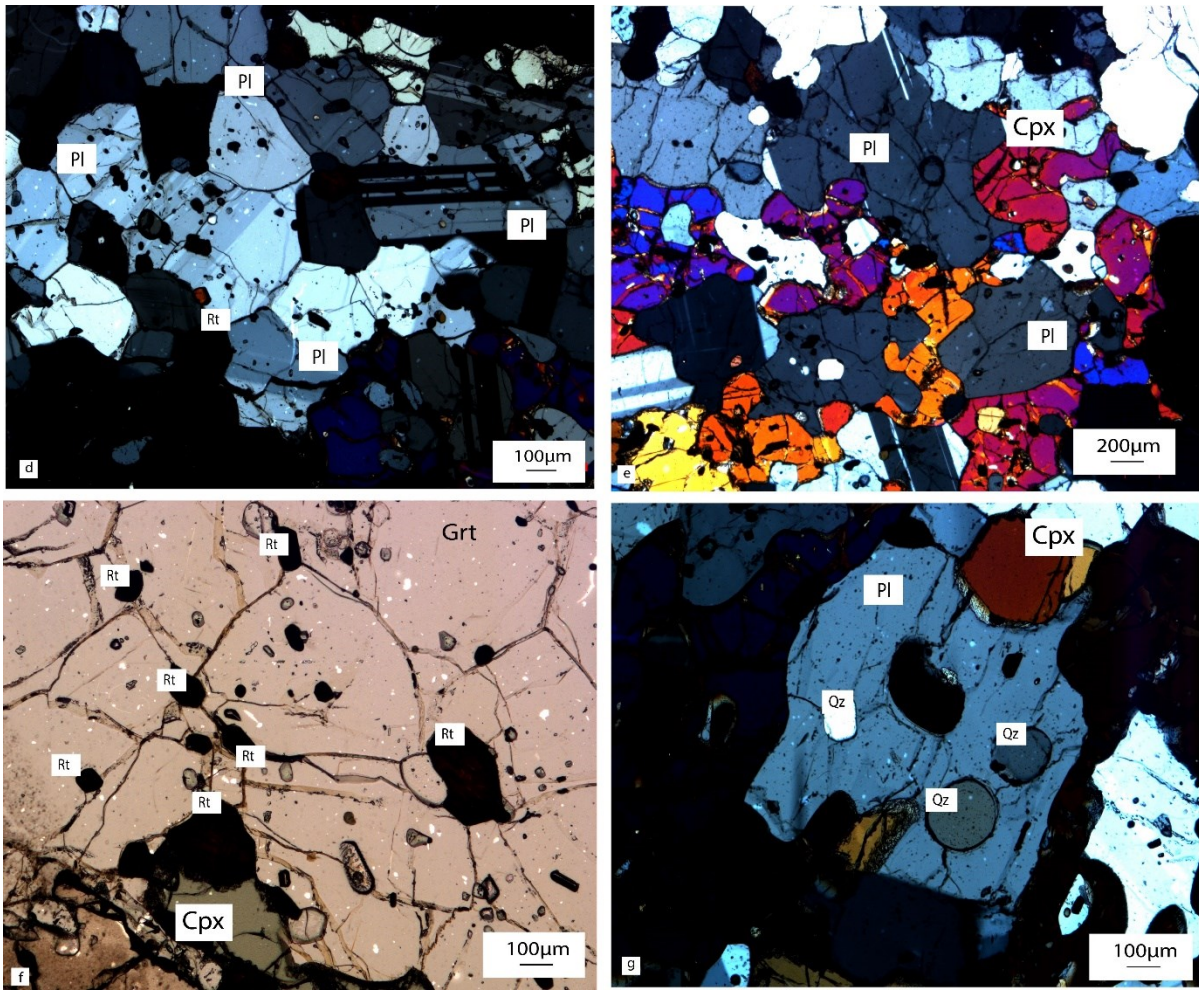

Figure 2.3 (d) *Plagioclase under XPL with polysynthetic twinning and Rt inclusion;* ***(e)*** *Lobate margins between Plagioclase and Clinopyroxene under XPL;* ***(f)*** *Rutile inside Grt under PPL;* ***(g)*** *Plagioclase under XPL with Qz inclusions.*

2.5 Sample 18XC10

The mineral assemblage of this section is Grt – Cpx – Pl – Amp as main phases and Qz, Rt and Ap as accessory phases (Fig 2.4a).

The general structure of 18XC10 could be defined as granoblastic. In the middle of the section there is a band of garnet (hereafter called "vein") which crosses the whole section dividing it into two parts with different features (Fig. 2.4b). The inner structure of garnets inside the vein can be defined as polygonal.

On one side of the vein Ap is present as accessory mineral, and some Grt contains small inclusions of Qz. On the other side of the vein there are neither Ap nor Qz (Fig. 2.4c).

The texture of section is slightly anisotropic due to the weak layering imparted by the garnet-rich band (Fig. 2.4d).

This section is unique compared to the others mentioned above, not only for the abundance of Grt but also because it contains a small remnant of lava from the Granatifera Tuff (Fig. 2.4e).

Garnet

It represents the main phase, and it is present in homogeneous way in the whole section.

Garnet has roughly constant size, and exhibits a subhedral shape. Under plane polarized light it is possible to see widespread triple junctions between different garnet crystals (Fig. 2.4d).

Inside the vein, garnet has a more variable size, with range between 100 µm to 700 µm. In the vein, the garnet dimensions tend to increase in one direction as indicate the red arrow in Figure 2.4b.

Outside the vein, the range size of Grt is more or less similar than the previous one, but it is possible to find also some larger crystals with 1-1,6 mm in size.

Garnet outside of the vein is often fractured and, in the core, it may contain many mineral inclusions of Cpx, Rt, Pl or Qz (Fig. 2.4f), as well as beautiful glass inclusions.

Clinopyroxene

Clinopyroxene distribution on the section is not homogeneous, indeed it tends to be organized in little cluster surrounding garnets.

It presents variable size around the section, ranging from 100 µm to 1,8 mm. The larger crystals are intensely fractured and contain many mineral inclusions as Amp and Pl.

Grain boundaries with the other phases tends to be linear or slightly lobate.

Under PPL clinopyroxene shows a light green color, while under XPL it appears purple – blue, with third order maximum interference color.

Plagioclase

Plagioclase distribution is heterogeneous in term of size, indeed it is mainly located on one side of the vein especially for the largest crystals (1-1,5 mm), while the small ones (100-400 µm) are randomly distributed in the section, with a greater abundance on the other side. Plagioclase is often fractured.

The contact margins with the other phases are linear only in some cases lobate.

In most crystals it is possible to find the classical polysynthetic twinning.

Amphibole

Amphibole is quite rare inside the section and it is present only in one side of the vein. The few crystals present are small in size (400-800 µm) with linear margins.

In some crystals it is possible to see typical cleavage at 60/120 degrees.

Under PPL amphibole shows a light brown color, while under XPL it appears yellow-orange, with second order maximum interference color.

Quartz

Quartz is present only on one side of the vein, in low quantity, and only as inclusions in Grt. The inclusions are small in size (50-150 µm) and sometimes exhibit an elongate shape. They often form clusters of many inclusions in the Grt cores, sometimes associated with MI (Fig. 2.4f). It is worth to highlight the total lack of quartz in the rock matrix outside garnet.

Rutile

Rutile is fairly abundant inside the section, with different shape and variable size in the range 100-200 μm. In many cases, rutile is not present as inclusions in other phases, but as single crystal in the matrix (Fig. 2.4g).

Under plane-polarized light rutile display orange – brown color and high relief; under crossed polarizers it is orange. Its shape is variable, from rounded to needle-like.

Apatite

It is often present as single mineral inside the vein or like an inclusion inside garnets, but only on the side of the vein where also quartz occurs (see Fig. 2.4c).

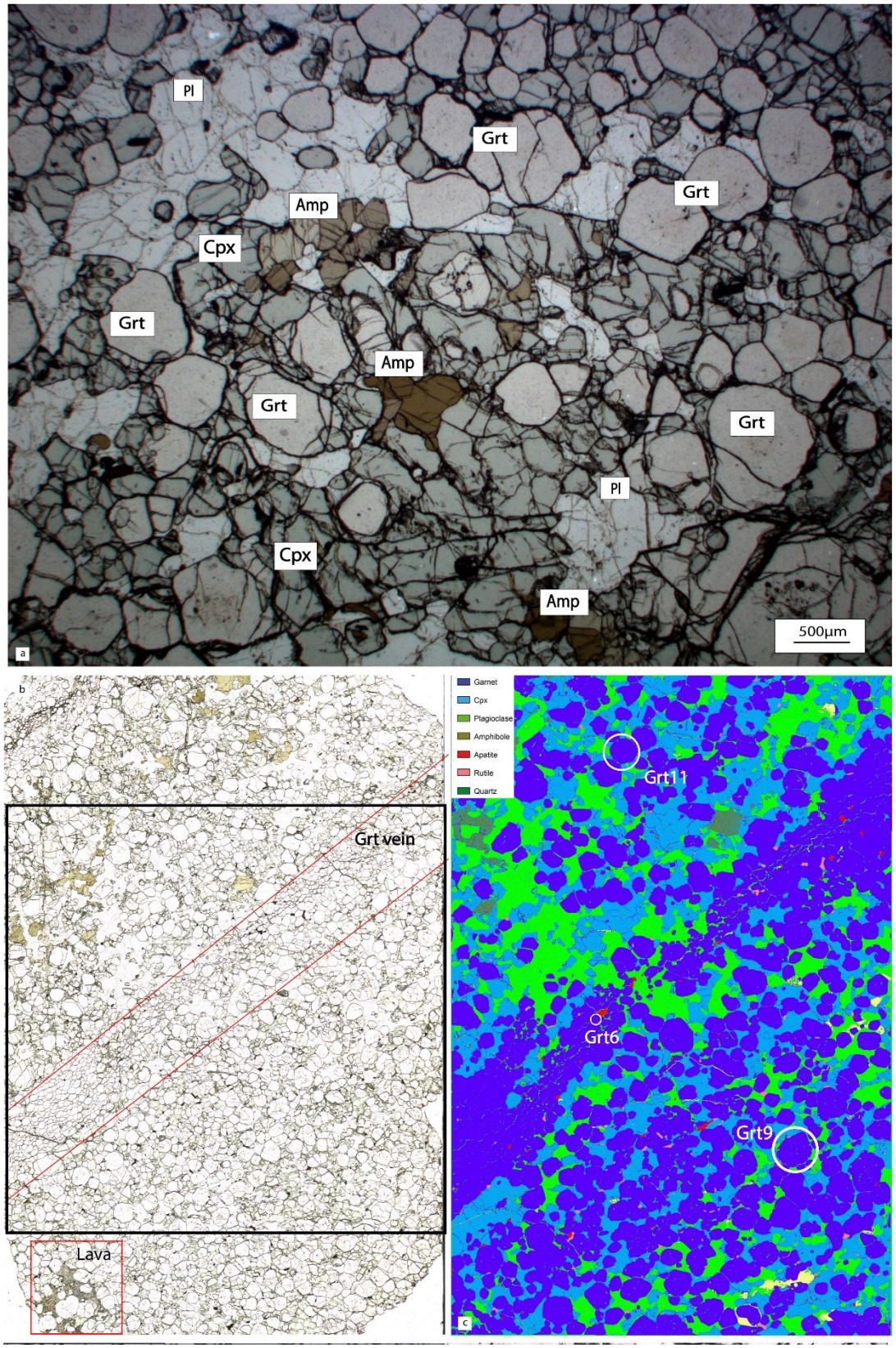

Figure 2.4: ***(a)*** *General petrographic aspect of 18XC10 under PPL;* ***(b)*** *Scan of thin section 18XC10 which underlines the principal features of this sample. The compositional SEM map was made into the black rectangle area. The red arrow indicates the increasing in size of garnets on the vein;* ***(c)*** *Compositional SEM map of 18XC10 which underlie the presence of Qz and Ap below the vein. The with circles indicate some of analyzed garnets.*

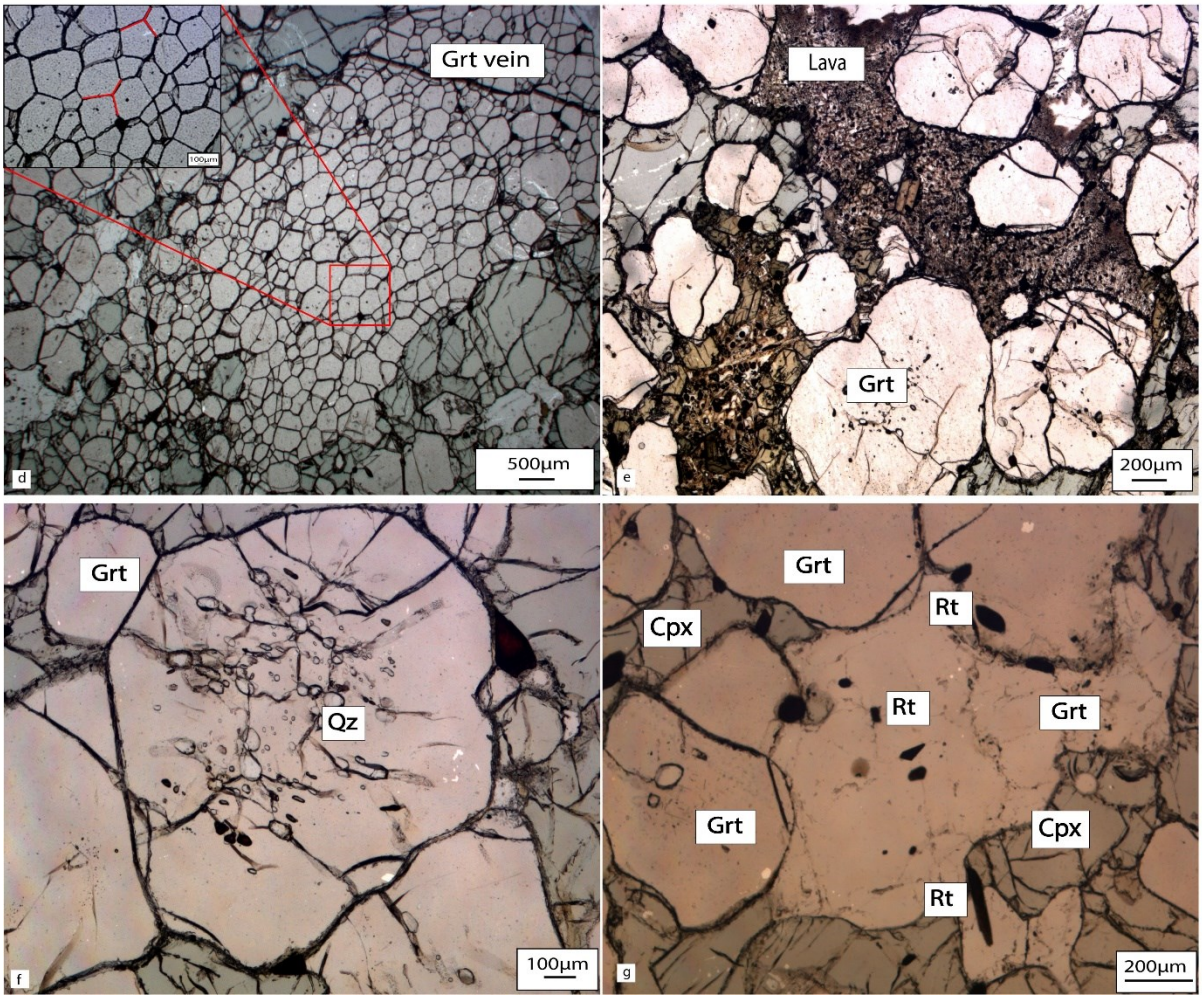

Figure 2.4: ***(d)*** *Garnet vein with the presence of triple junctions in garnets under PPL;* ***(e)*** *Lava inside the section under PPL;* ***(f)*** *Garnet with inclusions of Qz located below the vein under PPL;* ***(g)*** *Rutile under PPL.*

2.6 Sample 18XC15

The mineral assemblage of this section is Grt – Pl – Cpx as main phases and Rt - Scp and opaque represent the accessory phases (Fig. 2.5a).

The general structure of this section could be defined granofelsic interlobate with porphyroblastic garnet.

The texture of the section is isotropic and does not present any layering.

Garnet

Garnet represents the main phase in this section and crystals present a variable shape from subhedral to anhedral with extremely different size.

In terms of size garnet is present with a bimodal distribution:

1- Single and larger crystals (2,4-4,4 mm) located preferentially in the middle of the section (Fig. 2.5b).
2- Clusters located at the margin of the sample where minerals present roughly the same dimensions and smaller size respect previous one (from 100 µm to 1,2 mm) (Fig. 2.6c).

In both cases, garnet is strongly fractured.

Especially when the garnet is present as porphyroblasts, inside them it is possible to see many inclusions of Rt and Pl (Fig. 2.5b).

The boundaries with other minerals tend to be well defined.

Plagioclase

Plagioclase represents the second most abundant phase in this section, it shows anhedral shape with variable size, from 100 µm to 1,6 mm. Plagioclase surrounds garnets in homogeneous way.

Under crossed polarizers, in some plagioclase crystals polysynthetic twinning is clearly visible.

Boundaries with other phases tend to be linear or slightly lobate (Fig. 2.5d).

Clinopyroxene

Clinopyroxene is abundant in this section, and shows an anhedral shape. In terms of size, its range is variable from 100 µm to 2 mm.

Clinopyroxene has a heterogeneous distribution as it is mainly located at the edge of the section instead in the central part it is rare, small and always in contact with Grt.

Clinopyroxene is intensely fractured.

Under PPL clinopyroxene shows a light green color, while XPL it appears fuchsia – blue and orange with third order interference color.

Scapolite

Scapolite is present in this section in small quantity. It is often in contact with garnets and plagioclase, which it is easy to distinguish from Scp because it shows polysynthetic twinning.

Rutile

Rutile is present with variable size from 100 µm to 400 µm, as inclusion in main phases.

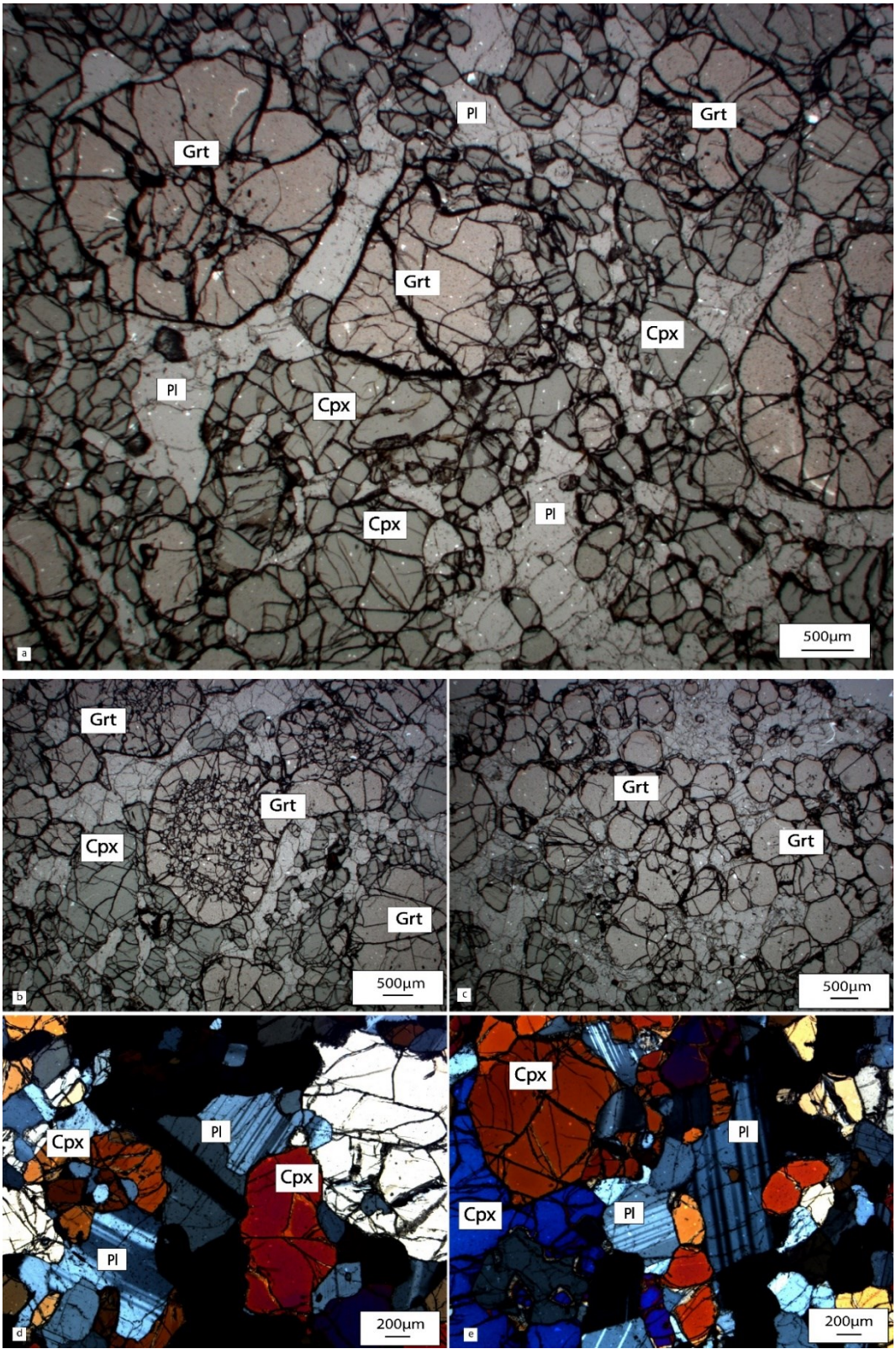

Figure 2.5: ***(a)*** *General petrographic aspect of thin section 18XC15 under PPL;* ***(b)*** *Garnet organized as a single crystal and rich in inclusions under PPL;* ***(c)*** *Garnet organized in cluster with roughly the same size under PPL;* ***(d)*** *Plagioclase with polysynthetic twinning under XPL;* ***(e)*** *Plagioclase and clinopyroxene under XPL.*

2.7 Sample 18XC20

The mineral assemblage of this section is Amp – Grt - Cpx - Pl as main phases, and Apt and Rt as accessory phases (Fig. 2.6b).

The general structure of 18XC20 could be defined as inequigranular interlobate and displays a grain-size layering. From a textural point of view, the section is anisotropic.

The distribution of the different phases is quite complex, indeed in term of quantity each phase is equally distributed in all section, but in terms of size many minerals present a bimodal distribution.

Amphibole

Amphibole is present in homogeneous way in the entire section, but in the uppermost part of 18XC20, as depicted in Fig. 2.6a, grain size varies from 1,2 mm to 4 mm, whereas in the lowermost part it is present with small crystals with size from 200 µm to 1 mm (Fig. 2.6a).

In several crystals it is possible to see the typical cleavage of 60/120 degrees (Fig. 2.6c).

Amphibole boundaries are often linear with respect to all phases present in this section (Fig. 2.6d).

Amphibole, especially when located in the uppermost part of the section, is intensely fractured and rich in small mineral inclusions, especially of Pl.

Under PPL amphibole shows a green-brown pleochroic color, while under XPL appears light pink or orange with second order maximum interference colors.

Garnet

In terms of size garnet is distributed in heterogeneous way, indeed in the uppermost part garnet is larger than the lowermost part. The medium size in the upper part is between 1,2 mm to 2 mm, whereas in the lower part it is between 1 mm to 1,6 mm.

Garnet in this section presents an euhedral shape, it is intensely fractured and rich in small mineral inclusions of Rt and Pl.

The boundaries with other phases are well defined.

Clinopyroxene

Clinopyroxene is present in the entire section with an anhedral shape, often in contact with Grt and Pl.

Clinopyroxene is present in well-developed crystal, ranging from 1,2 mm to 2 mm in size, or in little crystals (size range: 200 - 600 µm).

The boundaries with other phases are variable: some crystals display linear contacts whereas other present resorbed boundaries (Fig. 2.6e).

Under PPL clinopyroxene shows a light green color, while under XPL it appears fuchsia or light blue with third order maximum interference colors.

Plagioclase

Plagioclase occurs in a heterogeneous way in the section, and in the uppermost part of the section it is rare and form small crystals or inclusion in other phases. In terms of dimensions, plagioclase occurs as crystals from 200 µm to 1,8 mm in size. Plagioclase presents an euhedral shape, typical of a mineral that crystallizes from a melt (Fig. 2.6f).

Plagioclase always display its classical polysynthetic twinning.

The boundaries with other phases are well defined, and in some cases they could appear slightly lobate (Fig. 2.6f).

Rutile

It is present as small crystals included in the main phases, mostly inside garnet.

Apatite

It is present as rounded inclusions in the main phases.

Under PPL it is colorless with very high relief, while under XPL it is light gray.

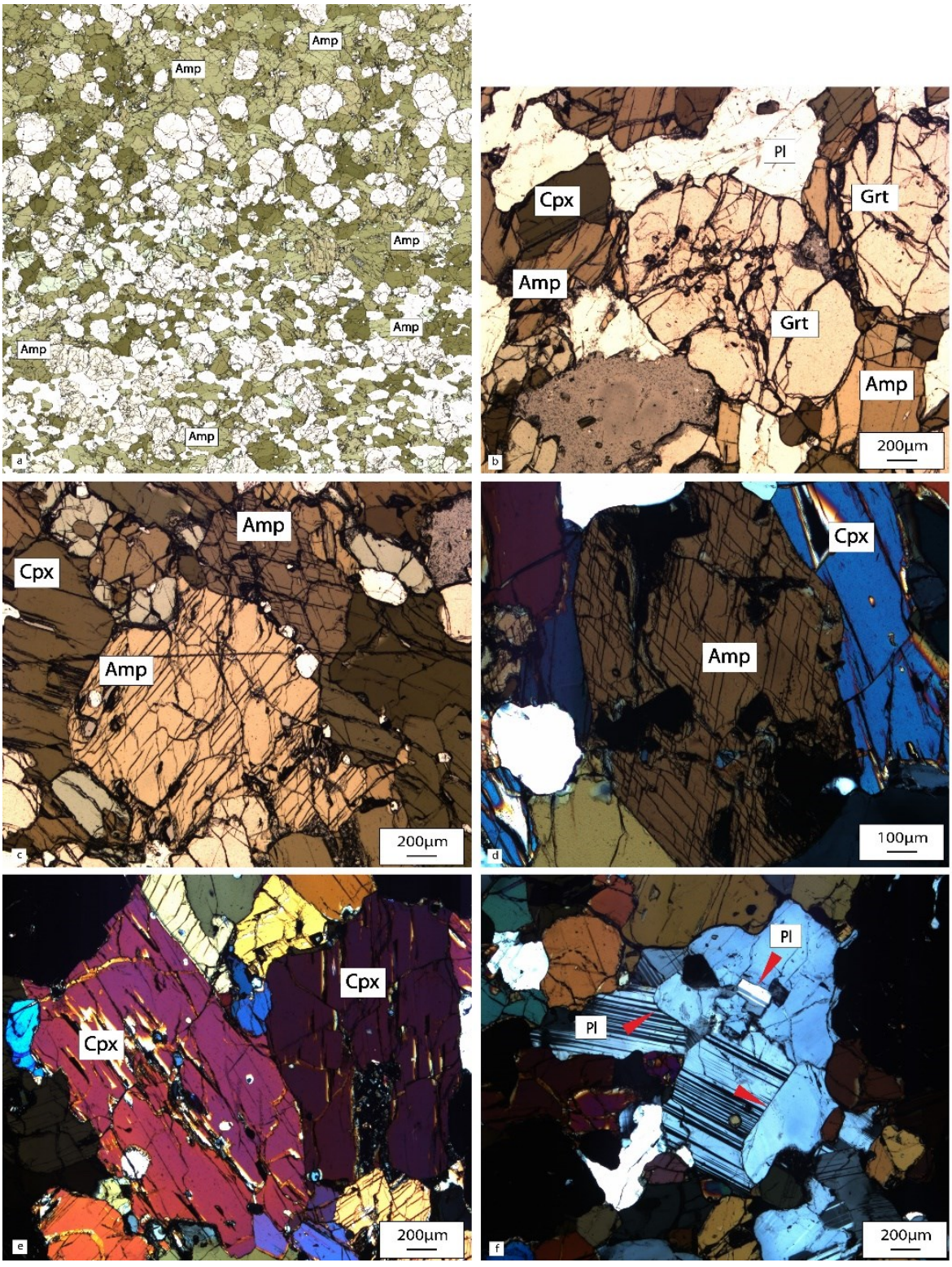

Figure 2.6: (a) Scan of thin section 18XC20 with underlines the different distributions of Amp; (b) General petrographic aspect of thin section 18XC20 under PPL; (c) Amphibole displays its classical cleavage at 60/120° under XPL; (d) Basal section of Amp under PPL; (e) Clinopyroxene under PPL; (f) Plagioclase displays straight euhedral faces in some crystals (arrows) under XPL.

In order to recap the mineral assemblage of each analyzed sample, below is reported a summary table which lists the different phases (Tab. 2.1):

Sample	*18XC1*	*18XC5*	*18XC6*	*18XC10*	*18XC15*	*18XC20*
Garnet	●	●	●	●	●	●
Clinopyroxene	●	●	■	●	●	●
Amphibole	■	■	■	▼		●
Plagioclase	●	■	●	■	●	■
Scapolite	▼	▼			▼	
Rutile		▼	■	■	▼	▼
Apatite	▼	▼		▼		▼
Quartz			▼	▼		

Table 2.1: *Summary table of mineral assemblages presents in each analyzed sample, where the different symbols indicate: ● = very abundant, ■ = present, ▼ =scarce.*

Chapter 3 – MINERAL AND BULK ROCK CHEMISTRY

3.1 Introduction

The chemical analysis of minerals in the samples mentioned before (Chapter 2), and also of the MI, was performed using an electron microprobe analyzer (EMPA) at the Department of Earth Sciences – University of Milan.

The analysis was made using the microprobe JEOL JXA-8200 WD/ED, and the different phases were analyzed through measuring complete mineral profiles or with single spots at core/or rim of crystals.

All analyses were performed with a 15 kV emission from the W filament and a 5 nA beam current. The utilized beam has a diameter of 1 μm when it is focused, and of 3-6 μm in the defocused case. The defocused beam was utilized only for the chemical analysis of MI. The acquisition time at the peak was of 10 seconds, while at the background 5 seconds.

Both thin (30 μm) and thick sections (200 μm) were analyzed.

The elements analyzed for the main mineralogical phases and MI are: Si, Ti, Al, Fe^{2+}, Mg, Ca, Na, K, P, Cr, S and Cl.

A total of about 1200 data points were acquired, and all analyses are reported in Appendix. After the acquisition, mineral data were normalized through a spreadsheet available from Microprobe Laboratory of Geosciences Department – Padua University.

Below, the number of oxygens used for the normalizations of different phases is reported (Tab 3.1).

Garnet	12 Oxygens
Clinopyroxene	6 Oxygens
Amphibole	23 Oxygens
Plagioclase	8 Oxygens

Table 3.1 *Normalizations criteria adopted for the main phases.*

The results obtained for single minerals, are treated in details for each sample.

3.2 Garnet

Garnet is the main phase in all samples. All studied and analyzed MI have been found inside Grt, that consequently represents the most important phase for this research.

Several garnet crystals have been analyzed in each sample, through rim to rim chemical profiles or as single rim – core points. Representative garnet analyses from all studied samples are reported in Table 3.2.

In terms of composition, garnet is a quaternary solution of almandine (Alm), pyrope (Pyr), grossular (Grs) and spessartine (Sps), where the concentrations of each end-members are calculated as: X_{Alm} [Fe/(Fe+Mg+Ca+Mn)], X_{Pyr} [Mg/(Fe+Mg+Ca+Mn)], X_{Gros} [Ca/(Fe+Mg+Ca+Mn)] and X_{Sps} [Mn/(Fe+Mg+Ca+Mn)].

	18XC1						18XC5						
	GR4	**GR4**	**GR7**	**GR7**	**GR1**	**GR1**	**GR2**	**GR2**	**GR3**	**GR3**	**GR5**	**GR5**	**GR6**
	Core	**Rim**	**Core**	**Rim**	**Core**	**Rim**	**Core**	**Rim**	**Core**	**Rim**	**Core**	**Rim**	**Core**
SiO_2	41,75	40,64	40,79	40,11	39,00	39,95	40,78	40,89	40,46	40,82	39,65	39,52	39,19
TiO_2	0,15	0,13	0,14	0,14	0,10	0,12	0,10	0,14	0,07	0,06	0,14	0,11	0,12
Al_2O_3	22,21	22,99	22,37	22,81	22,23	22,42	23,03	23,51	23,13	23,12	22,03	22,38	22,08
FeO	20,58	17,62	18,19	18,00	25,65	19,59	16,34	16,64	17,15	16,82	26,04	25,83	25,20
MnO	0,09	0,14	0,18	0,15	0,58	0,23	0,24	0,25	0,21	0,32	0,61	0,45	0,44
MgO	7,37	8,05	9,14	8,44	6,17	7,81	12,13	12,38	12,09	12,16	6,05	6,61	4,70
CaO	11,40	12,62	11,59	12,23	8,26	11,55	8,53	7,73	8,00	8,02	8,53	7,68	9,87
Total	**103,65**	**102,27**	**102,55**	**102,04**	**102,13**	**101,83**	**101,32**	**101,80**	**101,25**	**101,41**	**103,27**	**102,70**	**101,79**
Si	3,06	3,00	3,01	2,98	2,97	2,99	2,99	2,98	2,98	2,99	2,99	2,99	3,00
Ti	0,01	0,01	0,01	0,01	0,01	0,01	0,01	0,01	0,00	0,00	0,01	0,01	0,01
Al	1,92	2,00	1,94	2,00	2,00	1,98	1,99	2,02	2,01	2,00	1,96	1,99	1,99
Fe^{2+}	1,26	1,09	1,12	1,12	1,63	1,23	1,00	1,01	1,06	1,03	1,64	1,63	1,61
Mn	0,01	0,01	0,01	0,01	0,04	0,01	0,02	0,02	0,01	0,02	0,04	0,03	0,03
Mg	0,81	0,89	1,00	0,93	0,70	0,87	1,33	1,35	1,33	1,33	0,68	0,74	0,54
Ca	0,90	1,00	0,92	0,97	0,67	0,93	0,67	0,60	0,63	0,63	0,69	0,62	0,81
Total	**7,97**	**7,99**	**8,02**	**8,02**	**8,02**	**8,02**	**8,01**	**8,00**	**8,01**	**8,01**	**8,03**	**8,01**	**8,00**
Grs	30	33	30	32	22	30	22	20	21	21	23	21	27
Alm	43	36	37	37	54	40	33	34	35	34	54	54	54
Pyr	27	30	33	31	23	29	44	45	44	44	22	25	18
Sps	0,00	0,00	0	0	1	0	0	0	0	1	1	1	1
X_{Mg}	0,39	0,45	0,47	0,46	0,30	0,42	0,57	0,57	0,56	0,56	0,29	0,31	0,25

	18XC10					18XC15				18XC20			
	GR3	**GR3**	**GR11**	**GR11**	**GR11**	**GR2**	**GR2**	**GR6**	**GR6**	**GR6**	**GR6**	**GR9**	**GR9**
	Core	**Rim**	**Rim-L**	**Core**	**Rim-R**	**Core**	**Rim**	**Core**	**Rim**	**Core**	**Rim**	**Core**	**Rim**
SiO_2	40,04	40,61	38,85	39,11	39,16	39,40	39,20	39,75	40,73	39,52	39,90	39,68	40,12
TiO_2	0,10	0,13	0,15	0,15	0,10	0,13	0,10	0,13	0,11	0,10	0,16	0,11	0,10
Al_2O_3	22,76	22,80	22,76	22,26	22,73	21,72	23,01	22,90	23,09	22,43	22,53	22,59	22,50
FeO	20,52	20,68	20,50	20,03	19,97	22,94	20,13	19,32	18,69	23,37	21,70	22,04	21,03
MnO	0,31	0,34	0,34	0,27	0,31	1,01	0,50	0,20	0,14	1,25	0,79	0,92	0,62
MgO	10,63	10,79	11,09	10,29	10,44	7,36	8,51	8,36	10,58	7,43	8,26	7,28	8,46
CaO	6,89	6,29	6,05	7,39	6,91	8,36	9,46	10,48	8,95	7,94	9,54	9,73	9,17
Total	**101,32**	**101,68**	**99,77**	**99,63**	**99,66**	**100,99**	**100,94**	**101,38**	**102,50**	**102,15**	**103,08**	**102,42**	**102,06**
Si	2,98	3,01	2,94	2,97	2,96	3,00	2,95	2,98	2,99	2,98	2,97	2,97	2,99
Ti	0,01	0,01	0,01	0,01	0,01	0,01	0,01	0,01	0,01	0,01	0,01	0,01	0,01
Al	2,00	1,99	2,03	1,99	2,03	1,95	2,04	2,02	2,00	1,99	1,98	1,99	1,98
Fe^{2+}	1,28	1,28	1,30	1,27	1,26	1,46	1,27	1,21	1,15	1,47	1,35	1,32	1,28
Mn	0,02	0,02	0,02	0,02	0,02	0,07	0,03	0,01	0,01	0,08	0,05	0,06	0,04
Mg	1,18	1,19	1,25	1,16	1,18	0,84	0,96	0,93	1,16	0,84	0,92	0,81	0,94
Ca	0,55	0,50	0,49	0,60	0,56	0,68	0,76	0,84	0,70	0,64	0,76	0,78	0,73
Total	**8,02**	**7,99**	**8,04**	**8,03**	**8,02**	**8,02**	**8,02**	**8,01**	**8,01**	**8,01**	**8,04**	**8,00**	**8,00**
Grs	18	17	16	20	19	22	25	28	23	21	25	26	24
Alm	42	43	42	42	42	48	42	40	38	49	44	46	43
Pyr	39	40	41	38	39	27	32	31	38	28	30	27	31
Sps	1	1	1	1	1	2	1	0	0	3	2	2	1
X_{Mg}	0,48	0,48	0,49	0,48	0,48	0,36	0,43	0,44	0,50	0,36	0,40	0,38	0,42

Table 3.2 *Representative analyses of garnets from the studied samples*

Fig. 3.1 reports a ternary plot of all analyzed garnets that will be discussed in more detail below. In the ternary plot the garnet composition is expressed only through three components, Alm – Pyr – Grs, because the concentration of Sps is quite low (max. 2%) in all samples. It is possible to see how analyses from each sample form well-defined clusters, with a partial overlap in compositions only for samples 18XC15, 18XC20 and 18XC1.

The composition of all samples is located in the middle of the plot with a concentration of Alm between 35% and 55%.

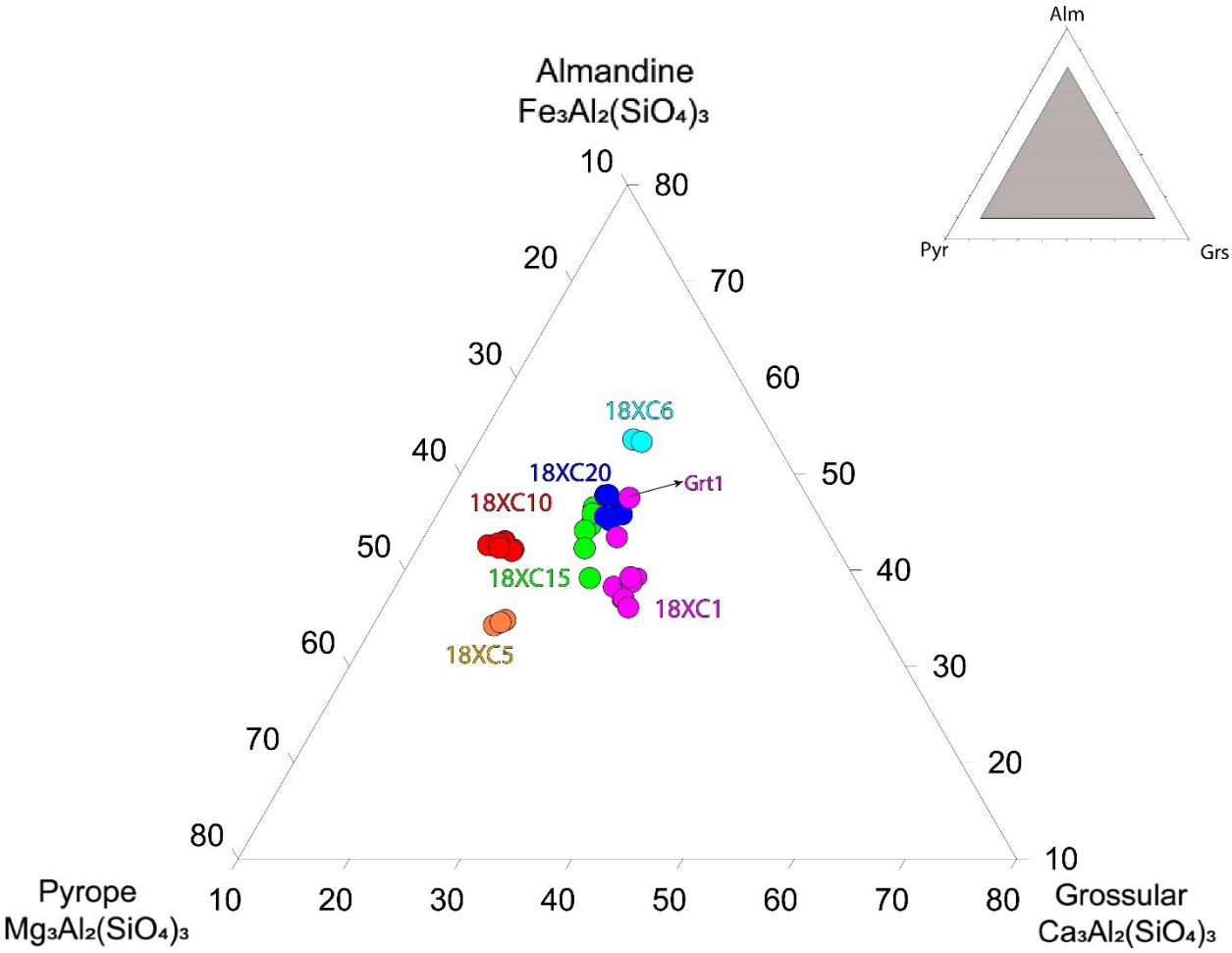

***Figure 3.1** Ternary plot of all analyzed garnets for the different samples.*

3.2.1 Sample 18XC1

A chemical composition profile has been analyzed for two garnets, GRT4 (Fig. 3.2a) and GRT7. Moreover, a third crystal (GRT8) has been analyzed with single points at the rim and at the core (Fig.3.2b).

Using the chemical compositions of the analyzed profile and its length, the following graphs were obtained in terms of X_{Alm} – X_{Pyr} – X_{Sps} – $X_{Grs,}$ which show the garnet composition and the possible zoning, if present.

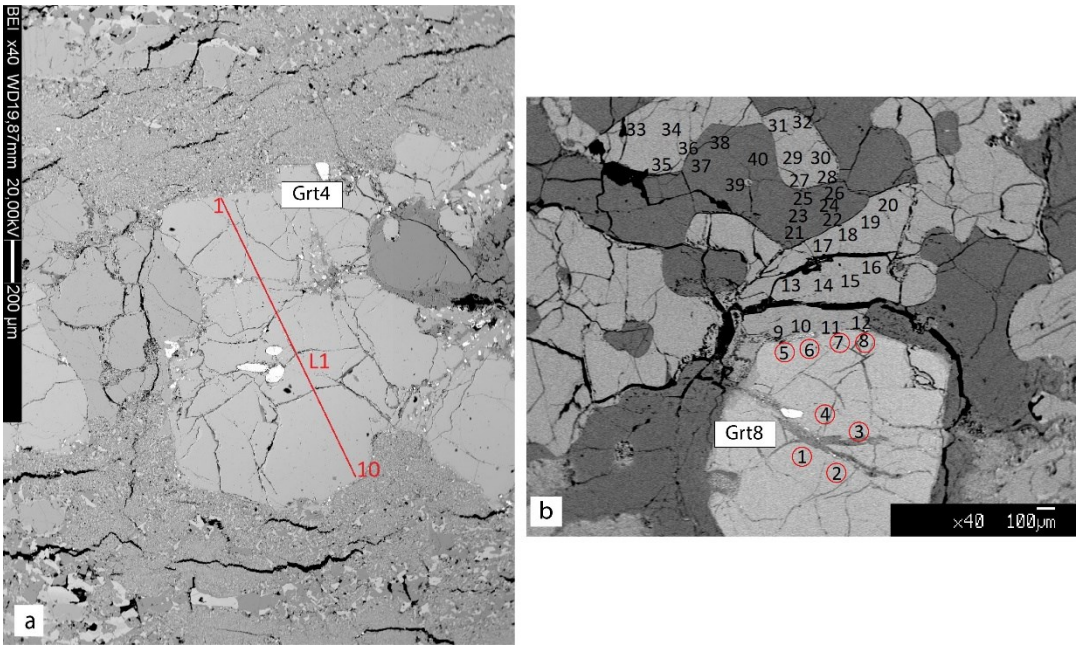

Figure. 3.2 *BSE images of sample 18XC1;*
(a) *Chemical profile analysis of Grt 4;* ***(b)*** *Core (1-4) and rim (5-8) analyses of Grt 8.*

Main components are represented by Alm – Pyr and Grs, whereas the quantity of Sps is very low.

Observing the data of GRT4, the curvature of Alm and Pyr profiles, underlines the presence of a slight zoning (Fig. 3.3a). In the zoned portion, the X_{Alm} concentration increases from about 0,36 in the rim to 0,43 in the core while the concentration of X_{Pyr} decreases from 0,30 to 0,27. Also X_{Grs} decreases from 0,33 at the rim to 0,30 at the core.

The profile of GRT7 is flat and indicates a constant composition of the crystal (Fig. 3.3b). Also, in this case the main components are represented by Alm – Pyr – Grs.

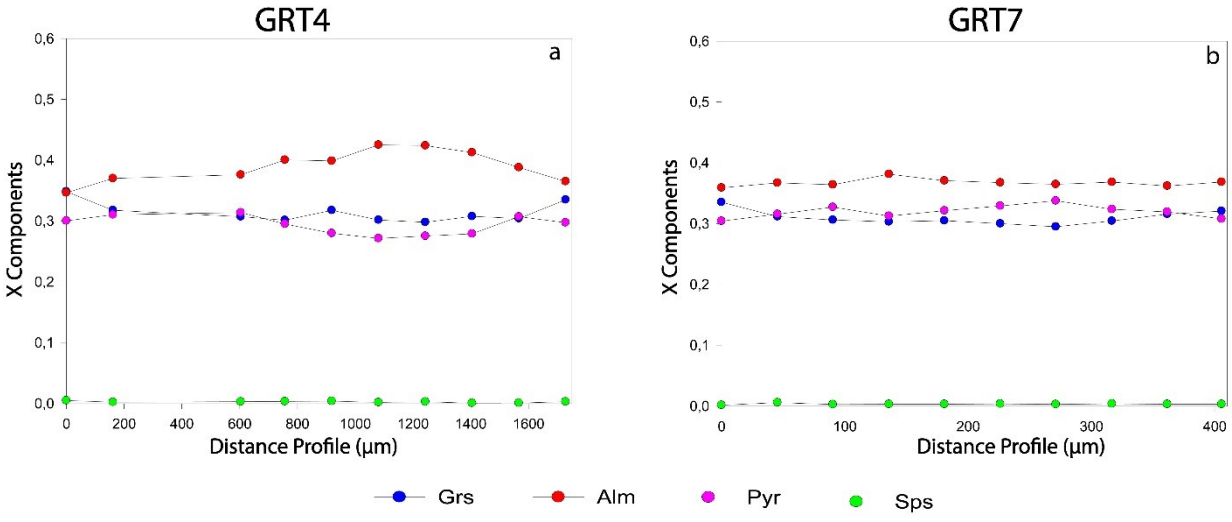

Figure 3.3 (a) *Compositional profile of Grt 4-18XC1* ***(b)*** *Compositional profile of Grt 7-18XC1*

Observing the summary table reported above (Tab. 3.2), it is possible to see how GRT4 and GRT7 present a comparable composition, whereas one crystal (GRT1) tends to deviate considerably from the others.
In GRT1 the X_{Alm} is present with a higher concentration which tends to vary significantly from the core with 0,54 to the rim with 0,40.
Also X_{Pyr} and X_{Grs} concentrations change from the core to rim, but in opposite way respect to Alm. Indeed, in these cases the higher values of both X_{Pyr} (0,29) and X_{Grs} (0,30) are at the rim, and the lower ones are at the core with X_{Pyr} 0,23 and X_{Grs} 0,22.

The X_{Mg} value for all reported garnets in Tab 3.2 varies from 0,30 to 0,47. This range also includes the values of GR1, whose core has the lower X_{Mg} content (0,30).

After these considerations, is possible to conclude that garnets in 18XC1 tend to be chemically rather homogeneous with a weak zoning within this compositional range $\boldsymbol{Alm_{36-43}\ Pyr_{27-33}\ Grs_{30-32}\ Sps_{0-1}}$. These values, do not consider results for GRT1, which tend to deviate from the average behavior. In Fig. 3.1, it is possible to see how the point which representing GRT1 is located outside the cluster characteristic for the total average composition of Grt in 18XC1. The composition of GRT1 is much more similar to the Grt in the sample 18XC20.

3.2.2 Sample 18XC5

In the sample 18XC5 three chemical profiles were analyzed: GRT1, GRT2 and GRT3, but in this case, randomly distributed core and rim analyses have not been collected.

In Fig. 3.4 it is possible to see how for each profile Pyr is the most abundant component (>43%) and Sps tends to zero. From a chemical point of view, profiles are comparable among them, and observing the general trend of all garnets they do not present any zoning.

Considering Table 3.2 reported above, is possible to conclude that the garnets in sample 18XC5 have a quite homogeneous composition with an elevated quantity of Pyr which reached the highest value on the rim of GRT2, with a concentration of X_{Pyr} 0,45. The average composition of garnet in this sample can be expressed through this range: $\boldsymbol{Alm_{33-35}Pyr_{44-45}Grs_{20-22}Sps_{0-1}}$. For what concerns the X_{Mg} value, considering all garnets, its variation is negligible, varying from 0,56 to 0,57.

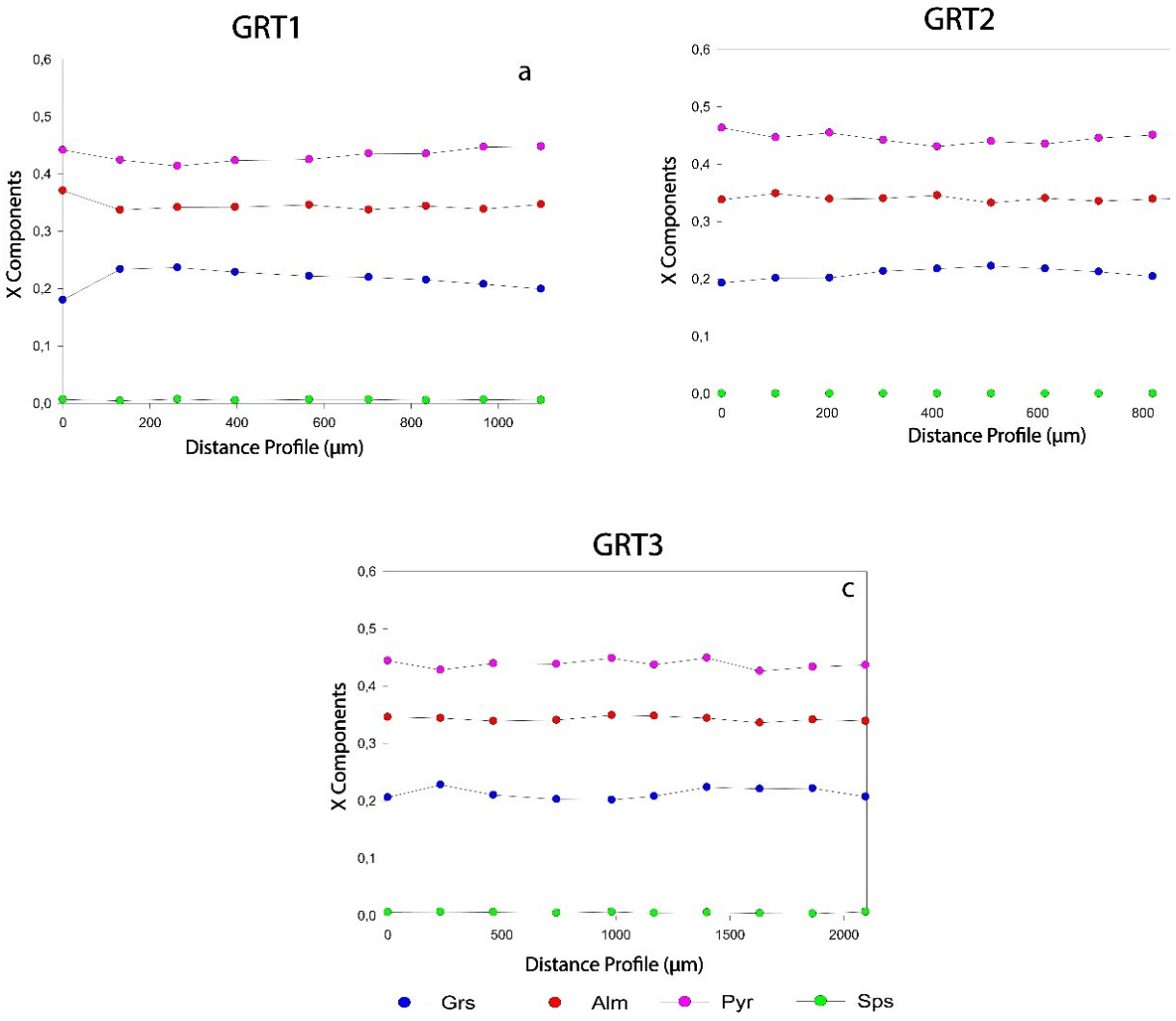

Figure 3.4 (a) *Chemical profile of GRT1 – 18XC5;* ***(b)*** *Chemical profile of GRT2 – 18XC5;* ***(c)*** *Chemical profile of GRT3-18XC5*

3.2.3. Sample 18XC6

In this sample two chemical profiles were, GRT5 and GRT6, and also some points at the rim of the latter one.

In figure 3.5 are reported both profiles, which show how GRT5 lacks any zoning, whereas for GRT6 a slight zoning for X_{Pyr} and X_{Grs} can be observed.

The X_{Grs} displays a concave profile where its concentration reaches the maximum with 0,27 at the core and decreases to 0,20 at the rim. On the contrary, the concentration of X_{Pyr} tends to decrease at the core, where the lower value (0,18) is shown, and increases to 0,25 at the rim. The zoning of GRT6 is also visible for the X_{Mg}, with 0,25 at the core and 0,32 at the rims.

Concerning the Alm component, for both analyzed garnets it is over 50%.

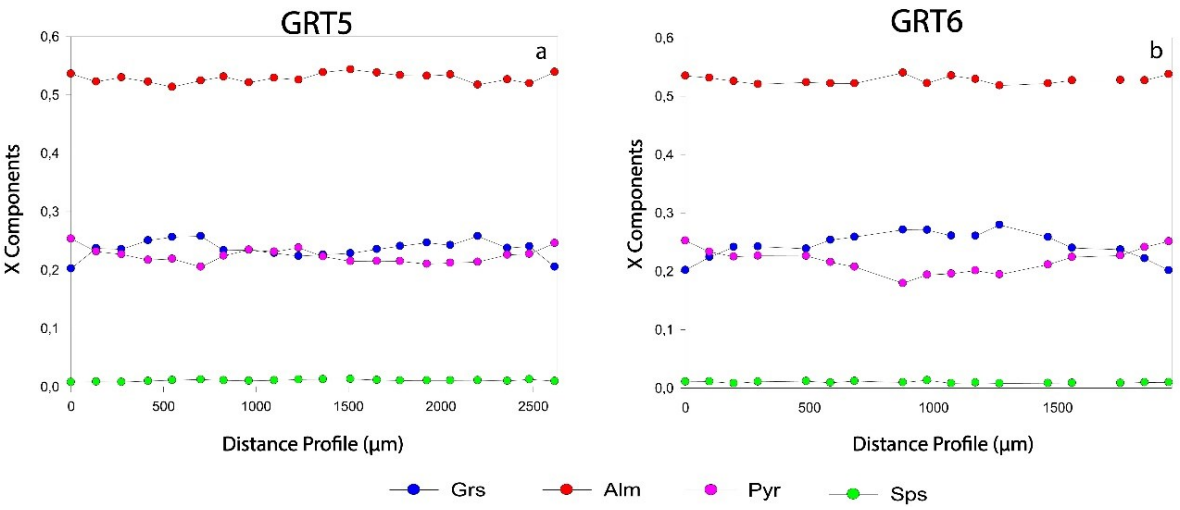

Figure 3.5 (a) *Chemical profile of GRT5-18XC6;* ***(b)*** *Chemical profile of GRT6-18XC6*

To sum up, observing the data in Table 3.2, the composition of garnets in this sample can be described through this range: $Alm_{54}\ Pyr_{18\text{-}25}\ Grs_{20\text{-}27}\ Sps_{1.}$ On the other hand, X_{Mg} varies from 0,25 to 0,32.

3.2.4 Sample 18XC10

Due to the characteristic features of this sample previously mentioned (Chapter 2), the analyzed garnets have been chosen in different positions (Fig. 2.4 – garnets in the white circles - chapter2) relative to the cross-cutting vein, in order to assess any chemical variation related to their spatial distribution. Two chemical profiles were taken in opposite parts of the vein (GRT3 – GRT11) and another one on the vein (GRT6). Moreover, few single points at cores and rims were collected.

Observing the different graphs reported in figure 3.6, garnets do not present any zoning. A slightly curvature can be identified only for X_{Grs} in the GRT11 profile.

In terms of compositions, all garnets display high Alm contents (X_{Alm} >0,40), while X_{Grs} is slightly higher in GRT11 (0,16-0,20) compared to the others (0,16-0,18).

Therefore, considering the values in the Table 3.2 it is possible to define the following chemical compositional range for garnets in this sample: $Alm_{42\text{-}43}\ Pyr_{38\text{-}41}Grs_{16\text{-}20}Sps_{1}$.

X_{Mg} values remain constant in all garnets at about 0,48-0,49.

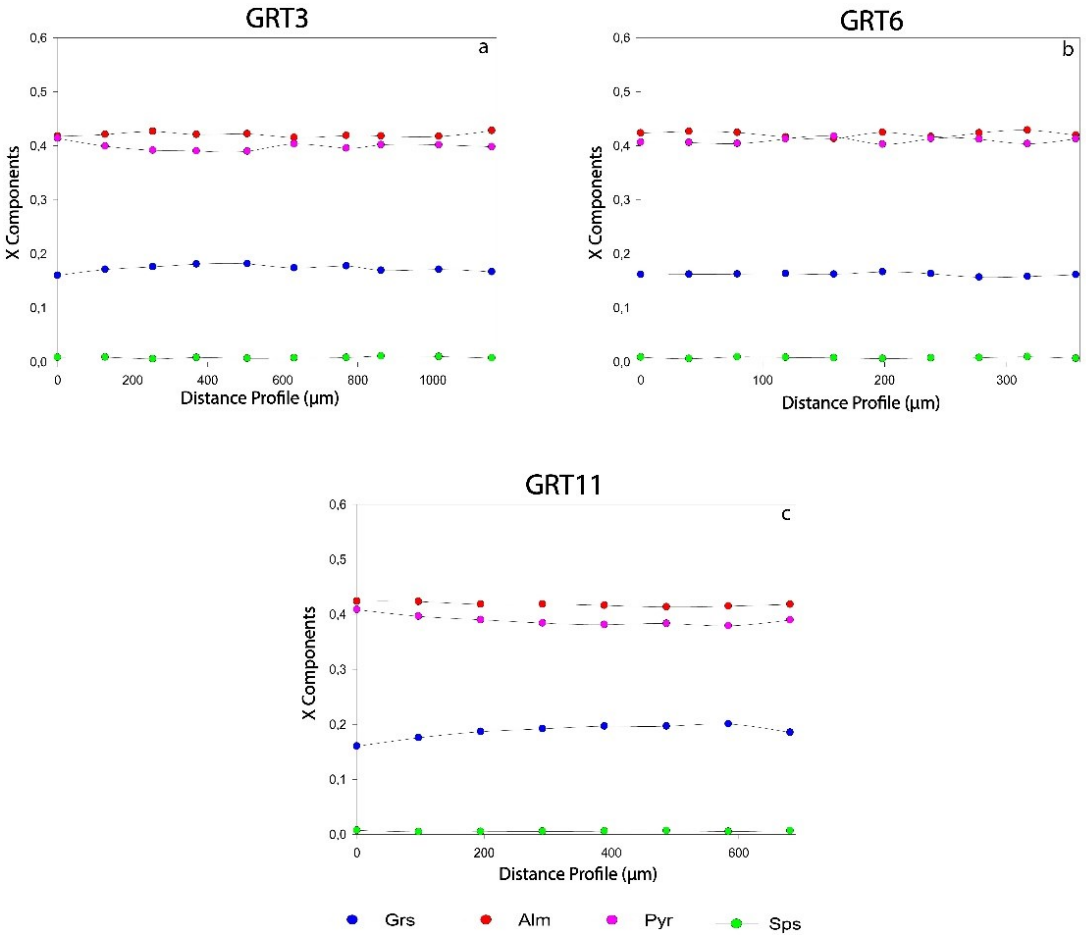

Figure 3.6 (a) *Chemical profile of GRT3-18XC10 in one side of the vein;* ***(b)*** *Chemical profile of GRT6-18XC10 on the vein,* **(c)** *Chemical profile of GRT11-18XC10 in the other side of the vein.*

3.2.5 Sample 18XC15

In this sample many chemical profiles were analyzed, but GRT1, GRT2 and GRT6 are the most representative ones. Moreover, some single points at cores and rims were collected.

Observing the three chemical profiles (Fig. 3.7), it is possible to see how GRT1 exhibits nearly a linear trend for each component, whereas GRT2 and GRT6 display a clear-zoning for Pyr and Grs, and only for GRT2, also for Alm.

In GRT2 (Fig. 3.7b), zoning tends to be accentuated especially for X_{Alm} component which reaches the maximum value 0,48 at the core and then decreases to 0,42 at the rim. Conversely, for X_{Grs} and X_{Pyr} the highest values are at the rim and the lower ones at the core. For X_{Grs} the zoning ranges from 0,22 to 0,25, while for X_{Pyr} from 0,27 to 0,32. In GRT2 also X_{Sps} does not present a constant concentration, but varies form core (0,01) to rim (0,02).

In GRT6 (Fig. 3.7c), X_{Grs} has the most pronounced zoning where the concentration tends to decreases from 0,28 at the core and to 0,23 at the rim. Instead the concentration of X_{Pyr} increases from 0,31 at the core to 0,38 at the rim.

Additionally, the X_{Mg} value follows the zoning trend varying significantly from core to rim for GRT2 and GRT6, where for the first one it ranges from 0,36 to 0,43, and for the second it varies from 0,44 to 0,50.

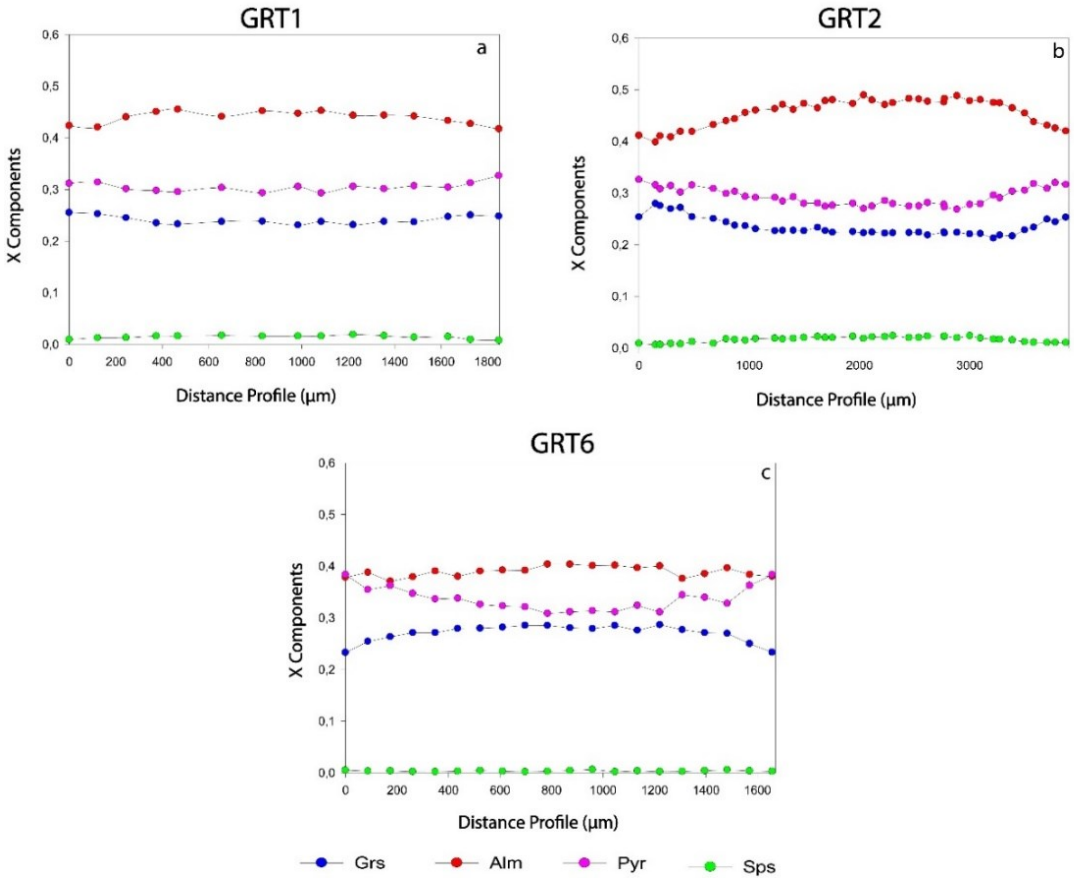

Figure 3.7 *(**a**) Chemical profile of Grt1 -18XC15; (**b**) Chemical profile of Grt2 -18XC15; (**c**) Chemical profile of GRT6 - 18XC15.*

In this sample the presence of zoning affects the general composition of garnets, which in this way appear rather heterogeneous. So, their composition is quite wide, but can be resumed through this range: $Alm_{38\text{-}48}\, Pyr_{27\text{-}38}\, Grs_{22\text{-}28}\, Sps_{0\text{-}2}$.

3.2.6 Sample 18XC20

In sample 18XC20 different chemical profiles for garnets were analyzed, and many of them exhibit about the same trend reported in Figure 3.8b, except for GRT6 which presents zoning for X_{Alm} and X_{Grs} (Fig. 3.8a).

The GRT9 exhibits a higher concentration of X_{Alm} (0,43-0,46), and approximately the same amount of X_{Grs} (0,24-0,26) and X_{Pyr} (0,27-0,31).

In GRT6 X_{Alm} tends higher (0,49) at the core and lower (0,44) at the rim, while X_{Grs} tends to increase from 0,21 at the core and to 0,25 at the rim. In this garnet, also X_{Sps} seems to form a very slight zoning, and its concentration varies from 0,03 at the core to 0,02 at the rim.

Observing the data on Table 3.2, is possible to see how X_{Mg} range from 0,36 to 0,42.

Always through the Table 3.2, from a chemical point of view garnets are comparable and with rather homogeneous composition even if GRT6 presents some zoning.

The compositional range is: $Alm_{43-49}\,Pyr_{27-31}\,Grs_{21-26}\,Sps_{1-3}$.

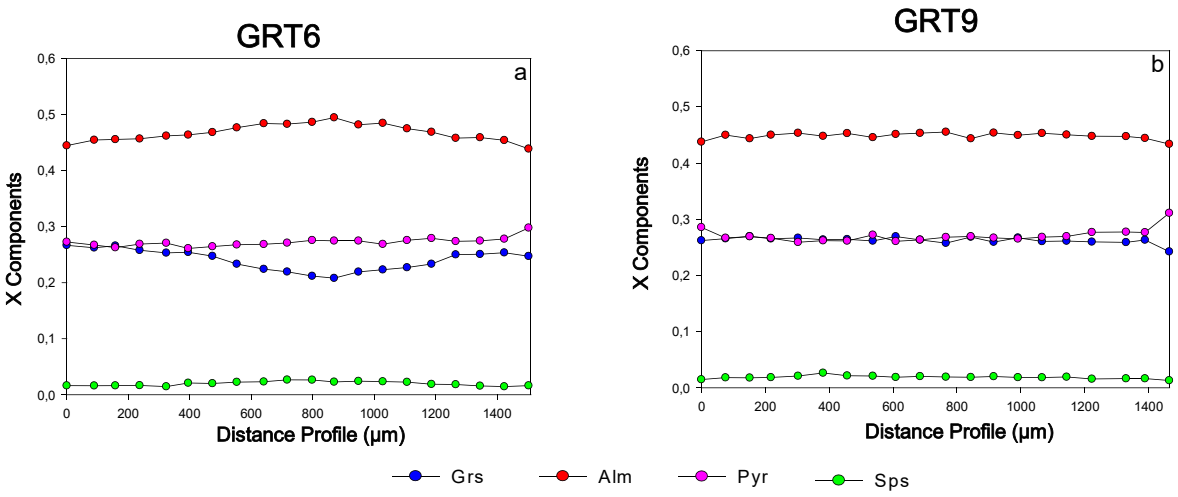

Figure 3.8 (a) *Chemical profile of GRT6 – 18XC20* ***(b)*** *Chemical profile of GRT9 – 18XC20*

3.3 Clinopyroxene

After Grt, clinopyroxene is another important phase which is presents in every samples.

It was not possible to classify and name these clinopyroxenes, because they deviate from the ideal parameters of the classical WEF (Wollastonite – Enstatite – Ferrosilite) nomenclature. This because they present an important concentration of Jadeite (Jd) and an excess of Al distributed between the tetrahedral and octahedral site, linked to a calcium Tschermak replacement.

For clinopyroxenes, chemical profiles have been obtained reporting four analyzed parameters (Ca – Al – Na - X_{Mg}) and the length of profile itself, with X_{Mg} = (Mg /(Mg+Fe^{2+}), considering all iron as Fe^{2+}.

Representative clinopyroxene analyses from all studied samples are reported below in Table 3.3.

	18XC1				18XC5						18XC6				
	CPX3	CPX3	CPX5	CPX5	CPX1	CPX1	CPX2	CPX2	CPX3	CPX3	CPX4	CPX4	CPX4	CPX5	CPX5
	Core	Rim	Core	Rim	Core	Rim	Core	Rim	Core	Rim	Core	33,00	Rim	Core	Rim
SiO_2	46,08	45,77	46,10	46,26	50,83	50,73	51,43	50,82	50,94	50,87	51,39	53,04	50,93	51,47	51,86
TiO_2	1,40	1,61	1,20	1,35	0,74	0,76	0,59	0,73	0,75	0,70	0,57	0,60	0,53	0,54	0,53
Al_2O_3	12,51	13,70	12,43	13,38	8,35	8,66	7,78	8,35	8,13	8,44	6,19	9,04	5,96	6,10	5,95
FeO	8,35	7,90	7,73	7,95	5,75	5,96	5,58	5,96	5,67	5,89	10,99	8,43	11,09	11,61	11,21
MnO	0,05	0,07	0,03	0,04	0,01	0,09	0,01	0,07	0,02	0,05	0,06	0,00	0,06	0,10	0,04
MgO	9,18	8,52	9,28	8,89	12,17	12,06	12,30	11,78	12,12	12,10	10,20	8,51	10,36	10,47	10,25
CaO	20,53	20,52	20,18	20,28	19,84	19,63	19,92	19,73	20,07	19,93	17,96	17,59	18,20	18,14	18,08
Na_2O	1,56	1,65	1,72	1,67	1,87	1,90	1,97	1,82	1,97	1,88	2,38	3,46	2,45	2,37	2,77
Total	**99,81**	**99,88**	**98,78**	**99,96**	**99,71**	**100,02**	**99,79**	**99,50**	**99,84**	**100,07**	**99,91**	**100,77**	**99,78**	**100,99**	**100,88**
Si	1,72	1,70	1,73	1,72	1,86	1,86	1,88	1,87	1,87	1,86	1,92	1,93	1,91	1,91	1,92
Ti	0,04	0,05	0,03	0,04	0,02	0,02	0,02	0,02	0,02	0,02	0,02	0,02	0,02	0,02	0,01
Al	0,55	0,60	0,55	0,59	0,36	0,37	0,34	0,36	0,35	0,36	0,27	**0,39**	0,26	0,27	0,26
Fe^{2+}	0,26	0,25	0,24	0,25	0,18	0,18	0,17	0,18	0,17	0,18	0,34	0,26	0,35	0,36	0,35
Mn	0,00	0,00	0,00	0,00	0,00	0,00	0,00	0,00	0,00	0,00	0,00	0,00	0,00	0,00	0,00
Mg	0,51	0,47	0,52	0,49	0,67	0,66	0,67	0,65	0,66	0,66	0,57	0,46	0,58	0,58	0,57
Ca	0,82	0,82	0,81	0,81	0,78	0,77	0,78	0,78	0,79	0,78	0,72	0,69	0,73	0,72	0,72
Na	0,11	0,12	0,13	0,12	0,13	0,13	0,14	0,13	0,14	0,13	0,17	0,24	0,18	0,17	0,20
Total	**4,02**	**4,01**	**4,02**	**4,01**	**4,00**	**4,00**	**4,00**	**3,99**	**4,01**	**4,00**	**4,01**	**3,98**	**4,03**	**4,03**	**4,03**
X_{Mg}	0,66	0,66	0,68	0,67	0,79	0,78	0,80	0,78	0,79	0,79	0,62	0,64	0,62	0,62	0,62
Jd	11	12	13	12	13	13	14	13	14	13	17	**24**	18	17	20

	18XC10				18XC15				18XC20			
	CPX1 Core	CPX1 Rim	CPX2 Core	CPX2 Rim	CPX5 Core	CPX5 Rim	CPX9 Core	CPX9 Rim	CPX1 Core	CPX1 Rim	CPX2 Core	CPX2 Rim
SiO_2	50,60	50,93	50,63	50,42	50,40	49,84	49,96	50,26	50,47	50,38	50,89	50,25
TiO_2	0,59	0,54	0,60	0,72	0,77	0,75	0,77	0,83	0,47	0,61	0,57	0,60
Al_2O_3	6,43	6,31	6,39	6,58	7,83	7,70	7,88	8,05	7,98	8,48	8,46	8,73
FeO	8,16	8,43	8,33	8,87	7,82	7,82	6,81	6,87	9,45	9,69	9,57	9,81
MnO	0,08	0,11	0,08	0,06	0,10	0,13	0,03	0,06	0,11	0,09	0,08	0,12
MgO	12,10	12,18	11,90	11,84	11,20	11,17	11,94	11,80	9,99	9,96	9,63	9,54
CaO	18,78	18,72	18,71	18,47	19,85	19,78	19,96	19,91	18,45	18,24	18,64	18,32
Na_2O	2,23	2,08	2,13	2,06	1,52	1,62	1,55	1,59	2,60	2,51	2,33	2,66
Total	**99,19**	**99,53**	**99,00**	**99,17**	**99,61**	**98,98**	**99,08**	**99,57**	**99,60**	**100,03**	**100,33**	100,06
Si	1,89	1,89	1,89	1,89	1,87	1,86	1,86	1,86	1,88	1,87	1,88	1,87
Ti	0,02	0,02	0,02	0,02	0,02	0,02	0,02	0,02	0,01	0,02	0,02	0,02
Al	0,28	0,28	0,28	0,28	0,34	0,34	0,35	0,35	0,35	0,37	0,37	0,38
Fe^{2+}	0,25	0,25	0,26	0,26	0,24	0,24	0,21	0,21	0,29	0,30	0,30	0,30
Mn	0,00	0,00	0,00	0,00	0,00	0,00	0,00	0,00	0,00	0,00	0,00	0,00
Mg	0,67	0,67	0,66	0,66	0,62	0,62	0,66	0,65	0,56	0,55	0,53	0,53
Ca	0,75	0,75	0,75	0,75	0,79	0,79	0,79	0,79	0,74	0,72	0,74	0,73
Na	0,16	0,16	0,15	0,15	0,11	0,12	0,11	0,11	0,19	0,18	0,17	0,19
Total	**4,03**	**4,03**	**4,02**	**4,02**	**3,99**	**4,00**	**4,01**	**4,00**	**4,02**	**4,02**	**4,00**	**4,02**
X_{Mg}	0,73	0,73	0,72	0,72	0,72	0,72	0,76	0,75	0,65	0,65	0,64	0,63
Jd	16	16	15	15	11	12	11	11	19	18	17	19

Table 3.3 *Representative analyses of clinopyroxene from the studied samples.*

3.3.1 Sample 18XC1

Chemical profiles have been analyzed for two clinopyroxenes, CPX1 and CPX3 (Fig. 3.9). Moreover, some additional single core and rim spot analyses were obtained from crystals CPX4 and CPX5. Although the profile of CPX1 (Fig. 3.9a) was obtained from a low number of analyses, it is possible to see how the trends in Fig. 3.9 are similar, showing the same tendency for each cation. Ca is >0,8 atom per formula unit (apfu), Al_{tot} about 0,55 apfu, and the Jadeite (Jd) content 12%. X_{Mg} ranges from 0,66 to 0,68. With the exception of one outermost rim of crystal CPX3, clinopyroxene does not exhibit appreciable zoning.

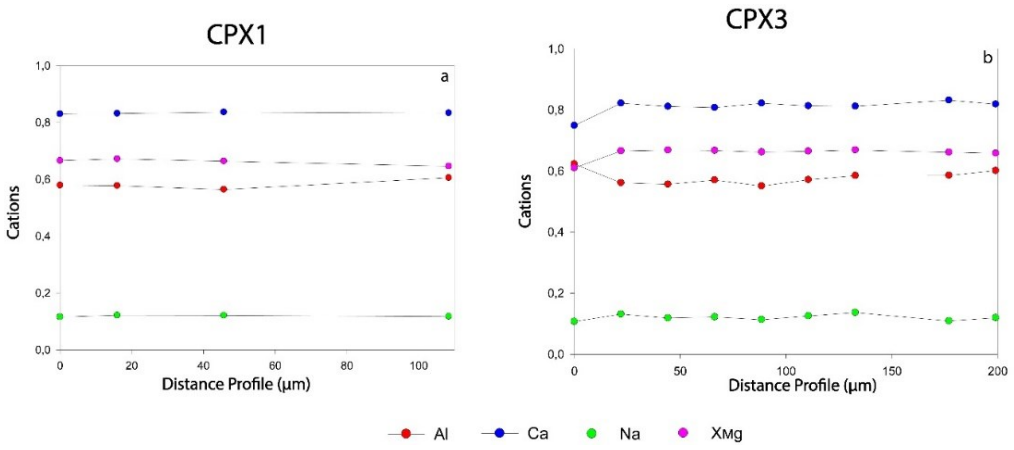

Figure 3.9 (a) *Chemical profile of CPX1 – 18XC1;* ***(b)*** *Chemical profile of CPX3 – 18XC1.*

Considering also the single data points from crystals CPX4 and CPX5, some of which are reported in Table 3.3 the compositional range of clinopyroxene in this sample is: $Na_{0,11\text{-}0,13}Ca_{0,81\text{-}0,82}Al_{0,55\text{-}0,60}Fe_{0,24\text{-}0,26}Mg_{0,47\text{-}0,52}Si_{1,72\text{-}1,73}O_6$

3.3.2 Sample 18XC5

In this sample Cpx has not been investigated with chemical profiles, but only a few core and rim spot analyses were taken for different clinopyroxenes, such as CPX1, CPX2 and CPX3.

Observing the summary Table 3.3, is possible to see how all analyzed clinopyroxenes present a comparable and rather homogeneous composition. The amount of Jd tends to be similar for both clinopyroxenes, and varies in a narrow range (13-14%). Also the X_{Mg} tends to remain quite constant ranging from 0,78 to 0,80.

Thus, the compositional range of clinopyroxenes in sample 18XC5 is: $Na_{0,13\text{-}0,14}Ca_{0,77\text{-}0,78}Al_{0,34\text{-}0,37}Fe_{0,17\text{-}0,18}Mg_{0,65\text{-}0,67}Si_{1,86\text{-}1,88}O_6$

3.3.3 Sample 18XC6

Chemical profiles have been made for two crystals, CPX4 and CPX5 (Fig.3.10), and also some rim-core points were taken for CPX2 and CPX3.

In both graph the general trend appears quite linear without zoning. A stranger tendency, can be observed for two singles points of Na and Al_{tot} in CPX4, which describe a sort of peak shifted towards higher values. In these points Al_{tot} 0,39 (apfu) and Na 0,24 (apfu), both strongly deviating from the general trend in which Al_{tot} is 0,26-0,27 (apfu) and Nais 0,17-0,18 (apfu).

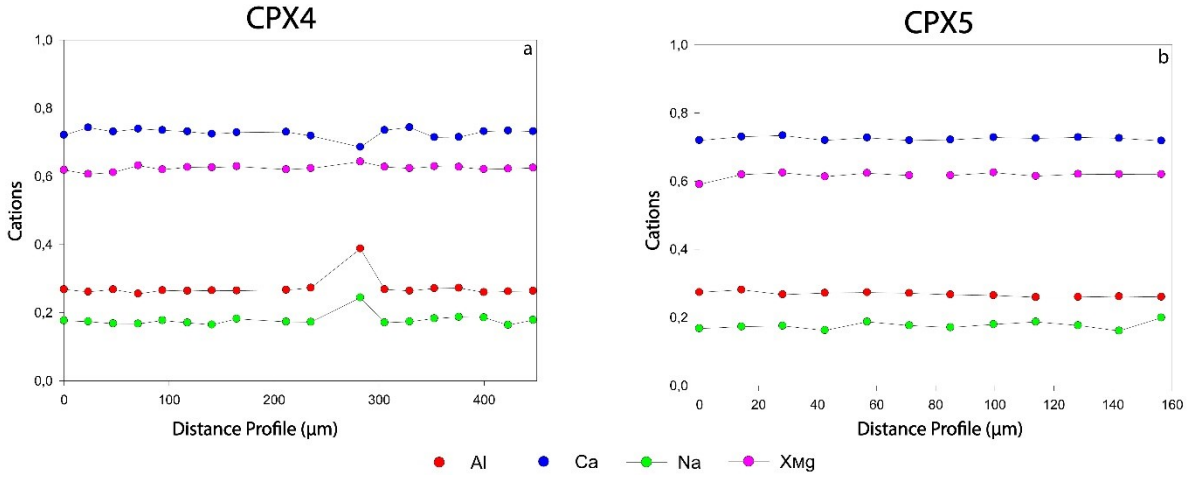

Figure 3.10 (a) *Chemical profile of CPX4 – 18XC6;* ***(b)*** *Chemical profile of CPX5 – 18XC6*

In Table 3.3 are reported the analyses for these two profiles, and it is possible to notice that they are chemically quite homogeneous. The composition of clinopyroxenes in sample 18XC6 fall within this range: $Na_{0,17\text{-}0,20}Ca_{0,72\text{-}0,73}Al_{0,26\text{-}0,27}Fe_{0,34\text{-}0,36}Mg_{0,57\text{-}0,58}Si_{1,91\text{-}1,93}O_6$.

The Jd content varies from 17 to 20% while X_{Mg} remains constant for all analyzed points with a value 0,62.

All these ranges do not consider the values for point 33 (Table 3.3), which strongly deviate from the average composition.

3.3.4 Sample 18XC10

In this sample no chemical profiles were done for Cpx, but only a few rim-core points were analyzed.

Table 3.3 clearly shows that the composition of CPX1 and CPX2 tends to remain quite constant without significant variations. The Jd content is about 15-16% and the XMg value ranges from 0,72 to 0,73.

So, the compositional range of clinopyroxenes in this sample, can be reassume by this formula: $Na_{0,15\text{-}0,16}Ca_{0,75}Al_{0,28}Fe_{0,25\text{-}0,26}Mg_{0,66\text{-}0,67}Si_{1,89}O_6$.

3.3.5 Sample 18XC15

In this sample only rim-core points for seven different clinopyroxenes have been analyzed, without chemical profiles.

In Table 3.3 are reported two of seven of analyzed clinopyroxenes, and it is possible to see how they appear chemically homogeneous and well-comparable.

The Jd content is constant with about 11-12%, while the X_{Mg} value tends to vary slightly more ranging from 0,72 to 0,76.

The composition of clinopyroxenes in sample 18XC15 is: $Na_{0,11\text{-}0,12}Ca_{0,79}Al_{0,34\text{-}0,35}Fe_{0,21\text{-}0,24}Mg_{0,72\text{-}0,76}Si_{1,86\text{-}1,87}O_6$.

3.3.6 Sample 18XC20

Chemical profiles have been analyzed for two clinopyroxenes, CPX1 and CPX2 (Fig. 3.11) No single rim-core points were collected.

In Figure 3.11 are reported both profiles, which exhibit a well-defined linear trend, without any zoning. Also from a chemical points of view they are quite similar, indeed all cations seem to have about the same tendency (see also Table 3.3).

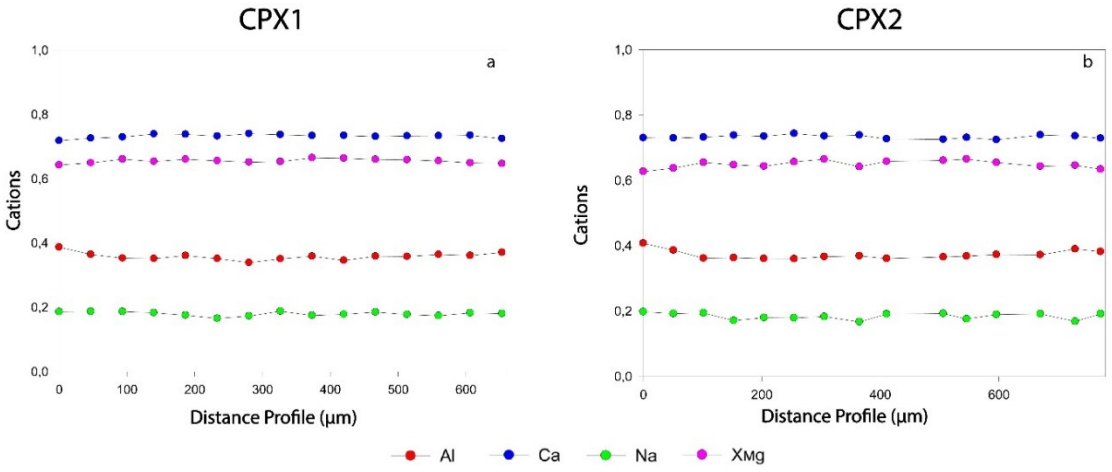

Figure 3.11 (a) *Chemical profile of CPX1 – 18XC20;* ***(b)*** *Chemical profile of CPX2 – 18XC20.*

Jd content and X_{Mg} vary in a narrow range, respectively 17-19% for Jd and 0,63-0,65 for $X_{Mg.}$

The compositional range for clinopyroxenes in sample 18XC20 can be resumed through this formula: $Na_{0,17\text{-}0,19}Ca_{0,72\text{-}0,74}Al_{0,35\text{-}0,38}Fe_{0,29\text{-}0,30}Mg_{0,53\text{-}0,56}Si_{1,87\text{-}1,88}O_6$.

3.4 Amphibole

Amphibole is the unique mineralogical main phase which is not present in all analyzed samples. In fact, Amp does not appear in sample 18XC5.

For the samples where Amp is present, the analysis method is the same as for the previous minerals, through complete chemical profiles or single points at rims or cores. The reference parameters utilized for the representation of each profile are: ^{IV}Al- ^{VI}Al - Na – Ca and X_{Mg}. The latter has been calculated considering all iron as Fe^{2+}.

The normalization file used for the recalculation of cations after the acquisition of data with microprobe also provided the mineralogical classification of each analyzed points.

Representative amphibole analyses from all studied samples are reported in Table 3.4.

	18XC1				18XC5		18XC6			
	AMP1	AMP1	AMP1a	AMP1a	AMP1	AMP1	AMP1	AMP1	AMP2	AMP2
	Core	Rim	Core	Rim	Core	Rim	Core	Rim	Core	Rim
SiO_2	40,29	39,55	38,79	39,12	42,90	43,00	42,47	41,83	42,56	41,90
TiO_2	2,32	2,23	2,05	2,17	1,91	2,05	2,71	2,73	2,60	2,73
Al_2O_3	17,01	16,67	18,05	18,34	15,00	15,13	12,58	12,67	13,20	13,09
FeO	11,61	11,72	11,23	11,35	8,46	8,48	16,05	16,19	15,70	16,08
MnO	0,01	0,03	0,05	0,00	0,06	0,07	0,06	0,02	0,00	0,01
MgO	10,54	10,80	11,14	11,09	14,72	14,38	10,33	9,90	9,87	10,11
CaO	11,10	11,15	11,08	10,92	10,60	10,61	9,60	9,90	9,69	9,54
Na_2O	2,18	2,29	2,47	2,55	2,86	2,89	2,83	2,69	2,66	2,72
K_2O	1,76	1,73	1,69	1,71	1,03	0,97	1,17	1,24	1,22	1,21
Total	**96,92**	**96,24**	**96,62**	**97,39**	**97,71**	**97,78**	**97,89**	**97,37**	**97,69**	**97,69**
Si	6,08	6,01	5,75	5,75	6,12	6,14	6,26	6,24	6,29	6,20
Ti	0,26	0,25	0,23	0,24	0,20	0,22	0,30	0,31	0,29	0,30
Al	3,03	2,98	3,16	3,18	2,52	2,55	2,19	2,23	2,30	2,28
Fe^{2+}	1,46	1,49	1,06	1,05	0,41	0,51	1,34	1,52	1,47	1,30
Mn	0,00	0,00	0,01	0,00	0,01	0,01	0,01	0,00	0,00	0,00
Mg	2,37	2,45	2,46	2,43	3,13	3,06	2,27	2,20	2,17	2,23
Ca	1,79	1,81	1,76	1,72	1,62	1,62	1,52	1,58	1,53	1,51
Na	0,64	0,67	0,71	0,73	0,79	0,80	0,81	0,78	0,76	0,78
K	0,34	0,34	0,32	0,32	0,19	0,18	0,22	0,24	0,23	0,23
Total	**15,98**	**16,01**	**15,79**	**15,60**	**15,60**	**15,60**	**15,54**	**15,60**	**15,53**	**15,52**
^{IV}Al	1,92	1,99	2,25	2,25	1,88	1,86	1,74	1,76	1,71	1,80
^{VI}Al	1,11	0,99	0,91	0,93	0,64	0,69	0,44	0,46	0,59	0,48
X_{Mg}	0,62	0,62	0,70	0,70	0,89	0,86	0,63	0,59	0,60	0,63

	18XC10				18XC20			
	AMP1	AMP1	AMP3	AMP3	AMP9	AMP9	AMP11	AMP11
	Core	Rim	Core	Rim	Core	Rim	Core	Rim
SiO_2	42,63	42,49	41,94	41,77	40,82	40,75	40,82	41,11
TiO_2	2,29	2,67	2,49	2,62	2,08	2,07	2,08	2,09
Al_2O_3	13,46	13,51	13,48	13,41	15,11	14,78	15,11	15,64
FeO	10,51	10,69	11,22	11,28	14,09	14,26	14,09	14,27
MnO	0,09	0,08	0,03	0,04	0,05	0,04	0,05	0,11
MgO	14,03	13,61	13,55	13,29	10,58	10,68	10,58	10,75
CaO	9,84	9,72	9,74	9,80	9,86	9,85	9,86	10,04
Na_2O	3,04	3,10	3,14	3,11	3,22	2,75	3,22	3,21
K_2O	0,83	0,80	0,83	0,79	1,17	1,27	1,17	1,24
Total	**96,91**	**96,69**	**96,58**	**96,31**	**97,51**	**96,65**	**97,35**	**98,55**
Si	6,16	6,16	6,10	6,10	6,00	6,05	6,04	5,99
Ti	0,25	0,29	0,27	0,27	0,24	0,23	0,23	0,23
Al	2,29	2,31	2,31	2,31	2,58	2,59	2,64	2,69
Fe^{2+}	0,42	0,54	0,51	0,51	1,02	1,07	1,21	1,15
Mn	0,01	0,01	0,01	0,00	0,01	0,01	0,01	0,01
Mg	3,02	2,94	2,94	2,94	2,41	2,36	2,34	2,34
Ca	1,52	1,51	1,52	1,52	1,55	1,57	1,56	1,57
Na	0,85	0,87	0,87	0,89	0,87	0,79	0,92	0,91
K	0,15	0,15	0,15	0,15	0,23	0,24	0,22	0,23
Total	**15,53**	**15,53**	**15,56**	**15,57**	**15,64**	**15,60**	**15,71**	**15,71**
^{IV}Al	1,84	1,84	1,84	1,90	2,00	1,95	1,96	2,01
^{VI}Al	0,45	0,46	0,42	0,42	0,59	0,63	0,68	0,68
X_{Mg}	0,88	0,85	0,85	0,85	0,70	0,69	0,66	0,67

Table 3.4 *Representative analyses of amphibole from the studied samples*

3.4.1 Sample 18XC1

In this sample I analyzed one chemical profile (AMP1) and also some scattered points at rim and core.

The profile of AMP1 (Fig. 3.12) describes a homogeneous mineral, without any zoning. The average X_{Mg} value from AMP1 is about 0,62, while looking at Table 3.4, it is possible to see how the rest of analyzed Amphiboles tend to be quite richer in Mg with a X_{Mg} value of 0,70. Amp also contains significant quantities of Na (0,64-0,73 apfu) and Ti (0,23-0,26 apfu).

From a chemical point of view all these amphiboles are classified as ferroan pargasite.

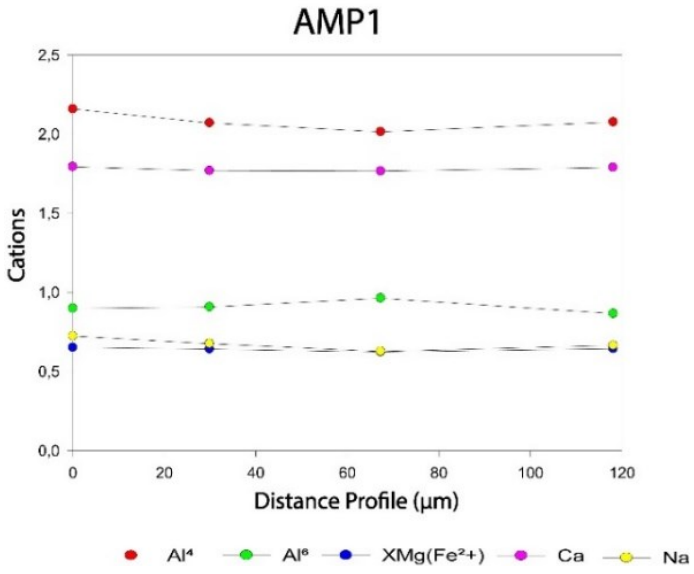

Figure 3.12 *Chemical profile of AMP1 -18XC1.*

3.4.2 Sample 18XC5

For this sample only one pair of core-rim points was analyzed.

Considering the Table 3.4 in which are reported all values for both core and rim of AMP1, the X_{Mg} value tends to vary from 0,89 at the core to 0,86 at the rim. The AMP1 has an elevated quantity of Mg (3,06-3,13 apfu) respect to the low quantity of Fe (0,41-0,51 apfu), but also the content of Ti (0,20-0,22 apfu) and Na (0,79-0,80 apfu) is considerable.

From a chemical point of view, the core of AMP1 can be classified as a ferroan pargasite, while its rim has a more pargasitic composition. The different composition from core to rim underlines the presence of a slight zoning in AMP1.

3.4.3 Sample 18XC6

In this sample two chemical profiles were analyzed, for AMP1 and for AMP2, and no additional rim-core points were collected.

In Fig. 3.13 both profiles for analyzed Amp are represented. Their general trend is quite similar, except for ^{VI}Al of AMP2 which tends to overlap the X_{Mg} values, describing a very slight zoning. The concentration of ^{VI}Al (0,44 - 0,59 apfu) tends to increase towards the core and then deceases at the rim.

But in general, neither AMP1 nor AMP2 exhibit a significant zoning.

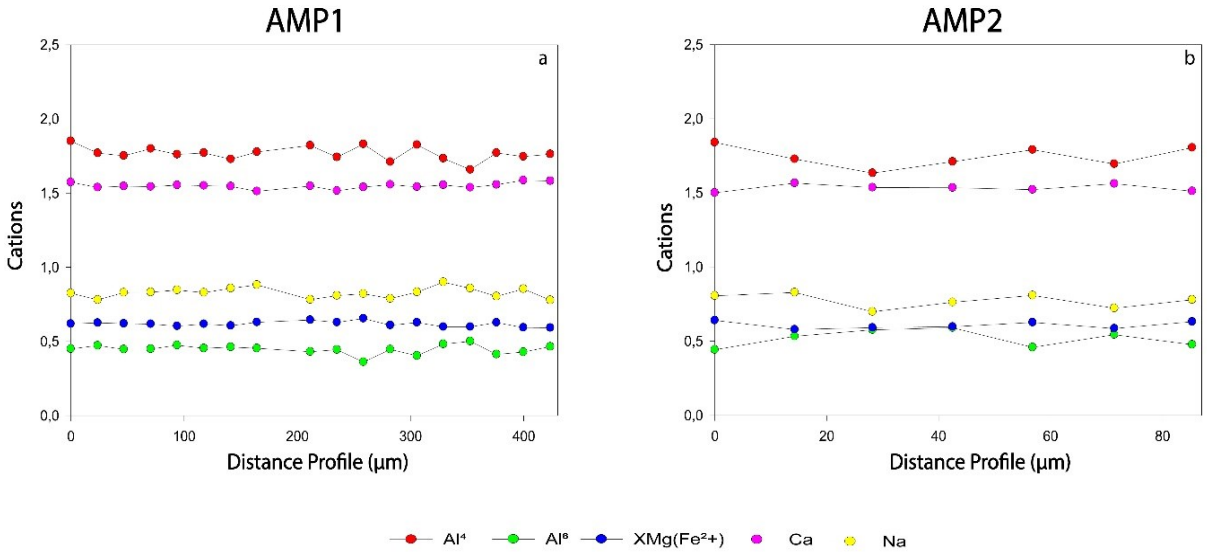

Figure 3.13 *(a) Profile of AMP1 – 18XC6;* ***(b)*** *Profile of AMP2 – 18XC6.*

In the Table 3.4 are reported the X_{Mg} values for both analyzed profiles, and it tends to remain about constant ranging from 0,59 to 0,63. Moreover, the amount of Na (0,76-0,81 apfu) and Ti (0,29-0,31 apfu) for AMP1 and AMP2 inside them are quite relevant.

From a chemical point of view, these two profiles are slightly different, as AMP1 can be classified as ferroan pargasite, while AMP2 has an intermediate composition between ferroan pargasite and ferroan pargasite hornblende.

3.4.4 Sample 18XC10

No chemical profile was taken in this sample, but only rim-core points were measured.

Table 3.4 reports the data for the analyzed amphiboles AMP1 and AMP3, and it is possible so see how the X_{Mg} values tend to vary in a narrow range from 0,85 to 0,88. Instead both amphiboles contain a notable quantity of Na (0,85-0,89 apfu) and Ti (0,25-0,29 apfu).

From a chemical point of view, both amphiboles are classified as pargasite.

3.4.5 Sample 18XC20

Sample 18XC20 has been analyzed for chemical profiles on two crystals, AMP9 and AMP11 and also a pair of rim-core points for AMP10 were analyzed.

Profiles reported in Fig. 3.14, exhibit a similar trend. The global trend is not well-linear, but there is no evidence of a clear zoning.

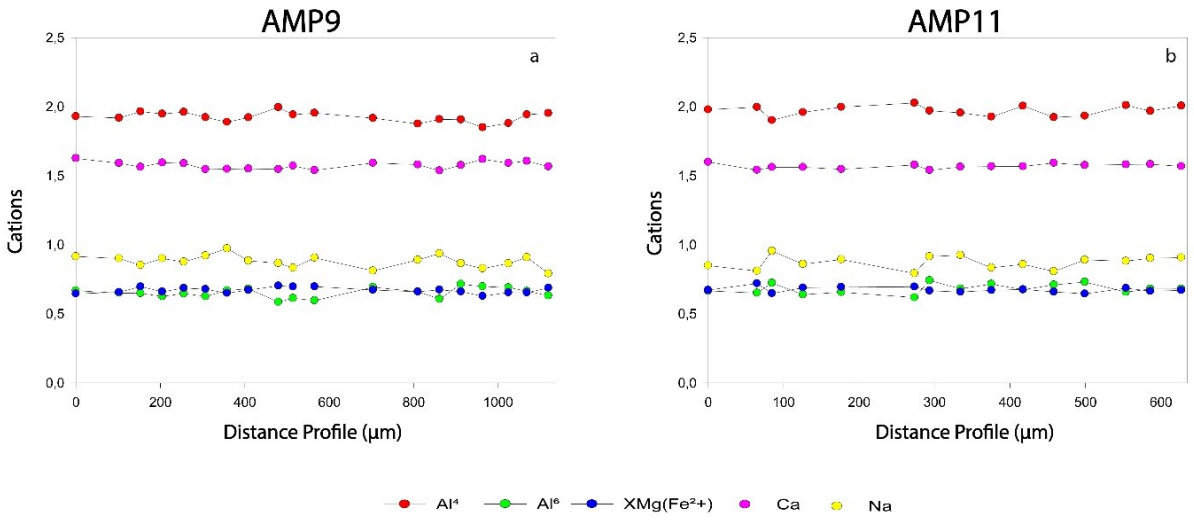

Figure 3.14 (a) *Chemical profile of AMP9 -18XC20;* ***(b)*** *Chemical profile of AMP11 – 18XC20.*

Observing the data reported in Table 3.4, it is possible to compare AMP1 and AMP2 from several points of view. The first one regards the X_{Mg} value, which range from 0,66 to 0,70 and the second one regards the considerable amount of Na (0,79-0,92 apfu) and Ti (0,23-0,24 apfu) inside of these amphiboles.

These two Amp present a homogeneous composition and can be classified as ferroan pargasite.

3.5 Plagioclase

Plagioclase represents the fourth and the last main phase present in all samples.

The method used to analyze the chemical composition of Pl is, as before, through measure of complete profiles or by acquisition of single core and rim points.

The parameters which were considered to describe the composition of Pl are the respective concentration of the albite (Ab) – anorthite (An) and orthoclase (Or) end-members. The concentration of each component has been calculated in this way: X_{An} = [Ca/(Ca+Na+K)], X_{Ab} [Na/(Ca+Na+K)], X_{Or} = [K/(Ca+Na+K)]. These concentrations, with the length of corresponding analyzed profile, were plotted in order to obtain the chemical profile of every analyzed Pl.

Representative plagioclase analyses from all studied samples are reported in Table 3.5.

	18XC1						18XC6				18XC10			
	PL1	**PL1**	**PL2a**	**PL2a**	**PL3**	**PL3**	**PL2**	**PL2**	**PL3**	**PL3**	**PL5**	**PL5**	**PL8**	**PL8**
	Core	**Rim**	**Core**	**Rim**	**Core**	**Rim**	**Core**	**Rim**	**Core**	**Rim**	**Core**	**Rim**	**Core**	**Rim**
SiO_2	54,33	55,98	43,00	43,35	55,41	54,99	63,13	62,48	62,91	63,10	61,50	61,87	61,30	60,89
Al_2O_3	26,57	24,49	33,27	32,81	27,15	27,09	22,68	22,92	22,66	22,43	24,17	24,40	24,18	24,14
CaO	11,28	10,03	19,73	19,46	10,22	10,56	4,33	4,32	4,23	4,21	5,40	5,39	5,25	5,44
Na_2O	4,80	5,38	0,13	0,15	5,27	5,16	8,31	8,50	8,33	**8,13**	8,21	8,32	8,08	8,07
K_2O	0,36	0,39	0,01	0,00	0,40	0,36	0,64	0,65	0,64	0,62	0,44	0,46	0,45	0,44
Total	**97,53**	**96,62**	**97,11**	**96,74**	**98,86**	**98,56**	**99,53**	**99,34**	**99,01**	**98,96**	**100,03**	**100,73**	**99,59**	**99,50**
Si	2,52	2,61	2,06	2,08	2,53	2,52	2,81	2,79	2,81	2,82	2,73	2,73	2,73	2,72
Al	1,45	1,34	1,88	1,86	1,46	1,46	1,19	1,21	1,19	1,18	1,27	1,27	1,27	1,27
Ca	0,56	0,50	1,01	1,00	0,50	0,52	0,21	0,21	0,20	0,20	0,26	0,25	0,25	0,26
Na	0,43	0,49	0,01	0,01	0,47	0,46	0,72	0,74	0,72	0,70	0,71	0,71	0,70	0,70
K	0,02	0,02	0,00	0,00	0,02	0,02	0,04	0,04	0,04	0,04	0,02	0,03	0,03	0,03
Total	**4,98**	**4,97**	**4,99**	**4,98**	**4,98**	**4,99**	**4,97**	**4,99**	**4,97**	**4,95**	**5,00**	**5,00**	**4,99**	**5,00**
Ab	43	48	1	1	47	46	75	75	75	75	72	72	72	71
An	55	50	99	99	51	52	22	21	21	21	26	26	26	26
Or	2	2	0	0	2	2	4	4	4	4	3	3	3	3

	18XC15				18XC20			
	PL1	**PL1**	**PL3**	**PL3**	**PL1**	**PL1**	**PL2**	**PL2**
	Core	**Rim**	**Core**	**Rim**	**Core**	**Rim**	**Rim**	**Core**
SiO_2	58,63	59,13	58,91	58,49	61,41	60,83	61,21	61,22
Al_2O_3	24,51	24,63	24,95	24,65	22,82	22,84	24,03	22,81
CaO	7,77	7,65	7,60	7,64	5,63	6,09	6,08	5,57
Na_2O	6,87	6,65	6,59	6,35	7,93	7,54	7,75	7,75
K_2O	0,23	0,31	0,27	0,27	0,57	0,51	0,50	0,59
Total	**98,28**	**98,69**	**98,59**	**97,80**	**98,65**	**98,20**	**99,94**	**98,25**
Si	2,67	2,67	2,66	2,67	2,77	2,76	2,72	2,77
Al	1,31	1,31	1,33	1,32	1,21	1,22	1,26	1,22
Ca	0,38	0,37	0,37	0,37	0,27	0,30	0,29	0,27
Na	0,61	0,58	0,58	0,56	0,69	0,66	0,67	0,68
K	0,01	0,02	0,02	0,02	0,03	0,03	0,03	0,03
Total	**4,98**	**4,97**	**4,96**	**4,95**	**4,98**	**4,98**	**4,99**	**4,98**
Ab	61	60	60	59	69	67	68	69
An	38	38	38	39	27	30	29	27
Or	1	2	2	2	3	3	3	3

Table 3.5 *Representative analyses of plagioclases from the studied samples.*

3.5.1 Sample 18XC1

Both profiles and rim core points were analyzed in this sample, in order to obtain the chemical composition of Pl in detail.

Fig. 3.15 reports the rim-core chemical profile of PL1, displaying a clear zoning, where the rim (which is in contact with scapolite) has the highest values for Ca (X_{An} 0,55), while towards the core X_{An} drops to 0,50.

The Or content is very low with only 2%.

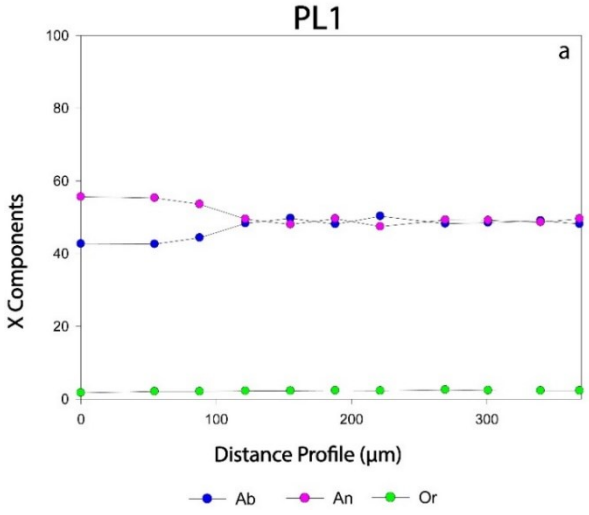

Figure 3.15 *Chemical profile of PL1 – 18XC1.*

The average composition of plagioclase in sample 18XC1 is well represented by the composition of PL1 and PL3 with an anorthite content between 50-55% and albite ranging from 46% to 48% (see appendix). Nevertheless, the Table 3.5 shows that the rock contains also crystals (PL2a) that can be classified as pure anorthite (99%). Among all analyzed plagioclases in this section, PL2a is the only one which has this composition.

3.5.2 Sample 18XC6

In this sample two chemical profiles have been analyzed, without rim-core analyses.

Fig. 3.16 exhibits the compositional trend for the analyzed minerals, PL2 and PL3, which tend to be very similar and contain a high concentration of Ab (75%), and also non-negligible concentrations of Or (4%).

The linear trend for each component underlines the absence of zoning.

Observing the results on Table 3.5, the composition of both analyzed plagioclases appears to be homogeneous, with about the same values for Ab (~75%) and An (21%).

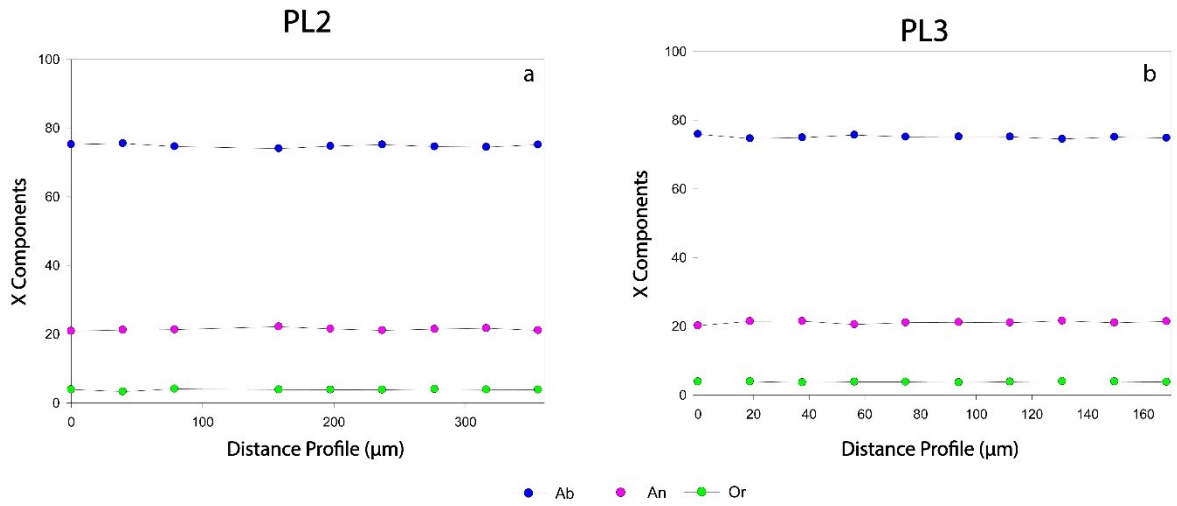

Figure 3.16 (a) *Chemical profile of PL2 – 18XC6;* ***(b)*** *Chemical profile of PL3 -18XC6.*

3.5.3 Sample 18XC10

In sample 18XC10 only rim-core points have been analyzed for 8 different Pl, located in different parts respect to the vein position.

In Table 3.5 are reported the data for some of analyzed crystals, PL5 and PL8, which present a rather homogeneous composition of Ab (71-72%), An (26%) and Or (3%).

3.5.4 Sample 18XC15

In sample 18XC15 both chemical profiles and rim-core points were analyzed.

In Fig. 3.17 the compositional profiles of PL1 and PL3 are reported, which exhibit a linear global trend without the presence of any zoning.

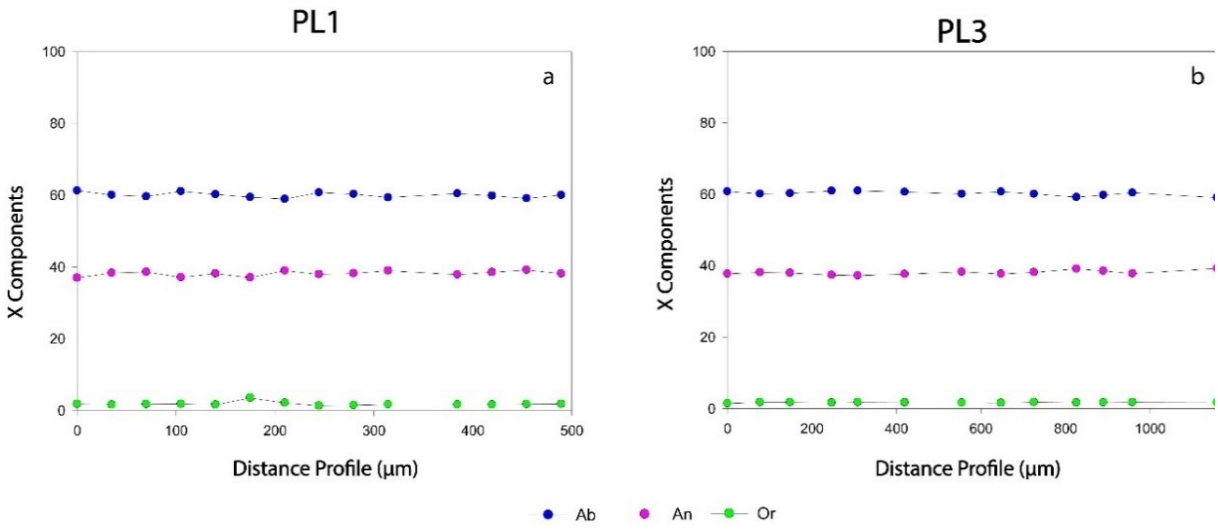

Figure 3.17 (a) *Chemical profile of PL1 – 18XC15;* ***(b)*** *Chemical profile of PL3 – 18XC15.*

Observing the Table 3.5 in which are reported all analyses for both profiles, is possible to see how from a chemical point of view they appear extremely homogeneous in terms of Ab (59-61%) and An (38-39%).

3.5.5 Sample 18XC20

In this sample only two profiles have been analyzed, for PL1 and PL2, without rim-core analyses.

In Figure 3.18 are reported both profiles, which exhibit the same linear trend without evident zoning. In the Table 3.5 are reported the data for these analyzed plagioclases, which are chemically homogeneous and similar in terms of Ab (67-69%), An (27-30%) and Or (3%).

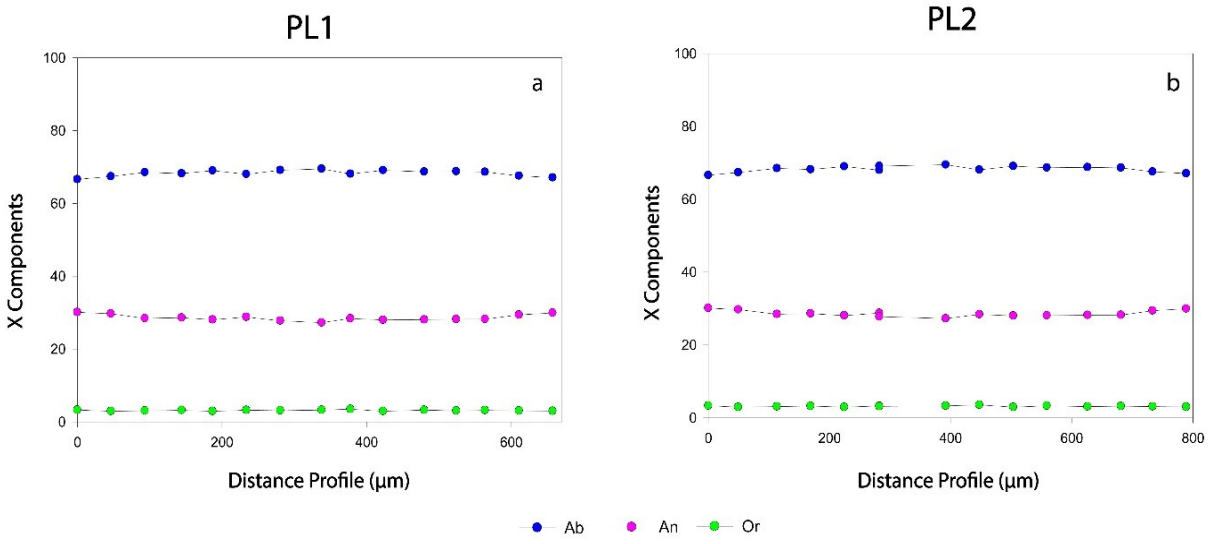

Figure 3.18 (a) *Chemical profile of PL1 – 18XC20;* ***(b)*** *Chemical profile of PL2 -18XC20.*

3.6 BULK ROCK COMPOSITION

The chemical bulk rock composition has been calculated for two samples, 18XC1 and 18XC20 (Fig. 3.19).

In order to determine the bulk composition, SEM maps have been firstly acquired and subsequently they have been processed with Multispec and ImageJ – two imaging software applications, which have permitted to quantify the modal amount of the different mineralogical phases.

Afterwards, the bulk composition was obtained using the mode calculated through the SEM maps for the different minerals combined with the average chemical composition (obtained by microprobe) of each mineral phase.

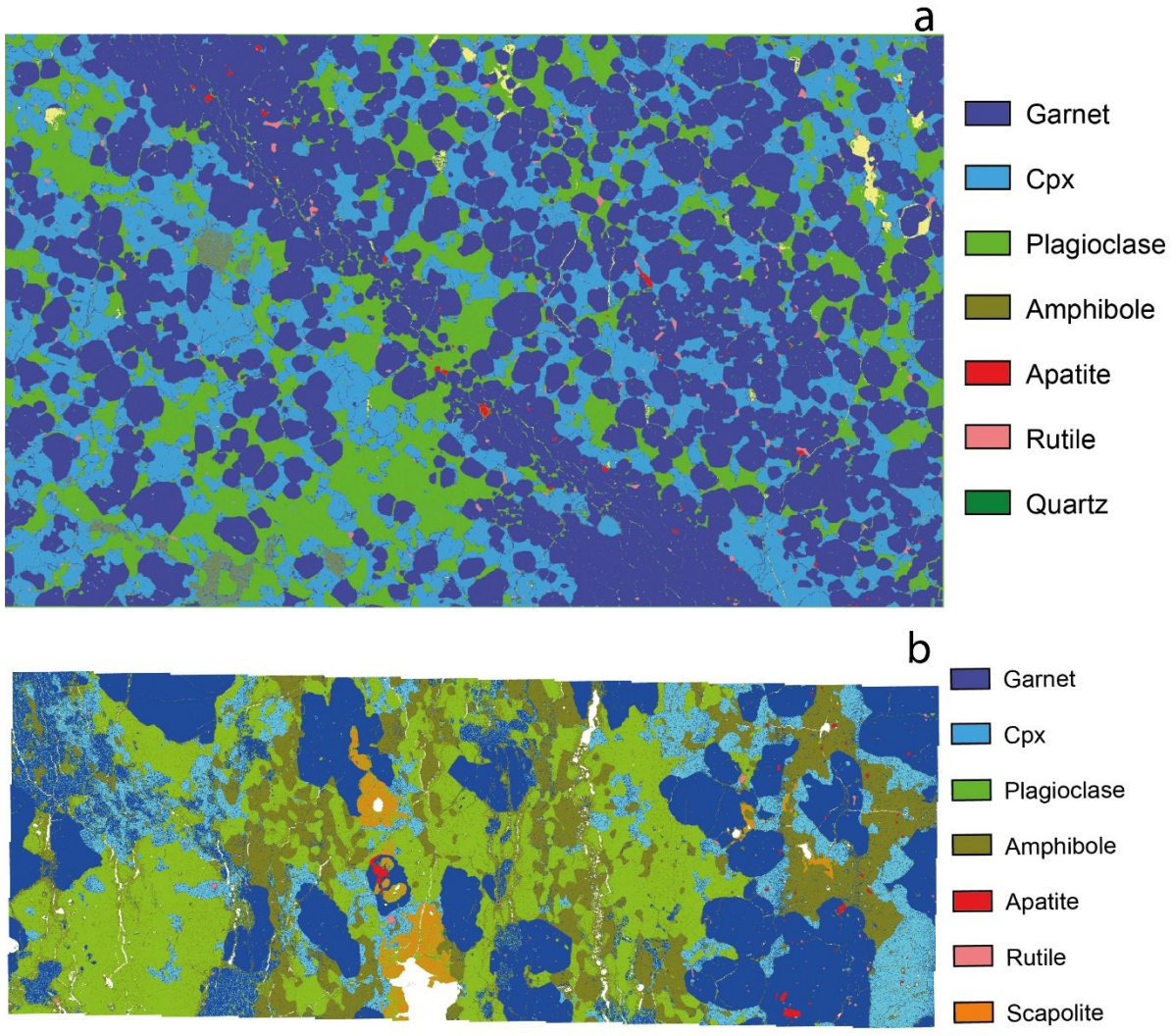

Figure 3.19 (a) *SEM compositional map of sample 18XC10;* ***(b)*** *SEM compositional map of sample 18XC1.*

From a mineralogical point of view, the two samples exhibit about the same mineral assemblage, except for scapolite and quartz, where the first one is presents only in sample 18XC1, whereas the Qz is observed exclusively in sample 18XC10.

Table 3.6 reports the calculated bulk composition for both samples, 18XC1 and 18XC10, expressed in oxides (wt.%).

	18XC1	*18XC10*
SiO_2	45,26	46,61
TiO_2	0,17	0,53
Al_2O_3	21,23	17,61
FeO	8,54	13,11
MnO	0,00	0,27
MgO	8,94	10,19
CaO	13,07	9,79
Na_2O	2,27	1,79
K_2O	0,08	0,07
H_2O	0,45	0,04
Total	100,00	100,00

Table 3.6 *Bulk composition expressed in oxides (wt.-%) for samples 18XC1 and 18XC10*

Table 3.6 shows that the two samples do not have a similar chemical composition.

Sample 18XC10 has an elevated concentration in FeO (13,11%) and MgO (10,19%), and fair amounts of CaO (9,79%) and Na_2O (1,79%) with a very low content in K_2O.

By contrast the sample 18XC1, has relatively low amounts of FeO (8,54%) and MgO (8,94%) compared to the previous sample 18XC10, but higher Al_2O_3 (21,23%) CaO (13,07%) and Na_2O (2,27%) concentrations.

Another important difference between the two samples regards the H_2O content, which is then times greater in 18XC1 (0,45%) compared to 18XC10 (0,04%). This discrepancy is mainly related to the fact that the sample 18XC1 has a higher modal proportion of amphibole (23%) than 18XC10 (2%).

4.1.1 Introduction

Among the analyzed samples three of them contain melt inclusions (MI), which were studied in detail by the same analytical methods mentioned in the previous chapters.

The studied inclusions are glassy and optically isotropic and therefore re-homogenization by heating stage or piston cylinder was not performed.

Most of the investigated MI were observed in garnet, but in some samples they have been noticed also in scapolite or oxides. For the purpose of this thesis only MI in garnet are discussed.

Besides MI, it was also possible to analyze by microprobe the chemical composition of few points of intergranular melt, which occurs at grain boundaries, and the lava of the Granatifera Tuff.

After the acquisition of the data, all melt analyses were corrected for alkali loss using different anhydrous and hydrous glass standards of known composition (see appendix for more details about the alkali correction method).

The samples which will be discussed in more detail below are:

- 18XC1
- 18XC10
- 18XC20

4.1 Microstructures of MI in sample 18XC1

Several MI were individuated in this sample.

Observing MI through the optical microscope under PPL, they appear brownish or colorless with variable shapes ranging from irregular to negative crystal shape. Their size varies from 5 to 50 μm.

Not all inclusions can be classified as primary, as some of them seem to lie along trails, a typical feature of secondary inclusions (Fig. 4.1a). The primary ones instead do not present a zonal arrangement but they are isolated or organized in small clusters randomly distributed inside the host (Fig. 4.1b-c). However, even after a careful observation, it was not possible to undoubtedly determine the origin of all MI.

Many glassy inclusions present one or more shrinkage bubbles which may results from of the higher thermal contraction of the inclusion compared to the surrounding host crystal. The generated empty space inside the MI is then occupied by the bubble. Another reason linked to the formation of the bubble relies on the composition of the melt itself. If the melt is rich in volatile phases, the latter could be exsolved during the cooling and decompression within the inclusions, and form the bubble.

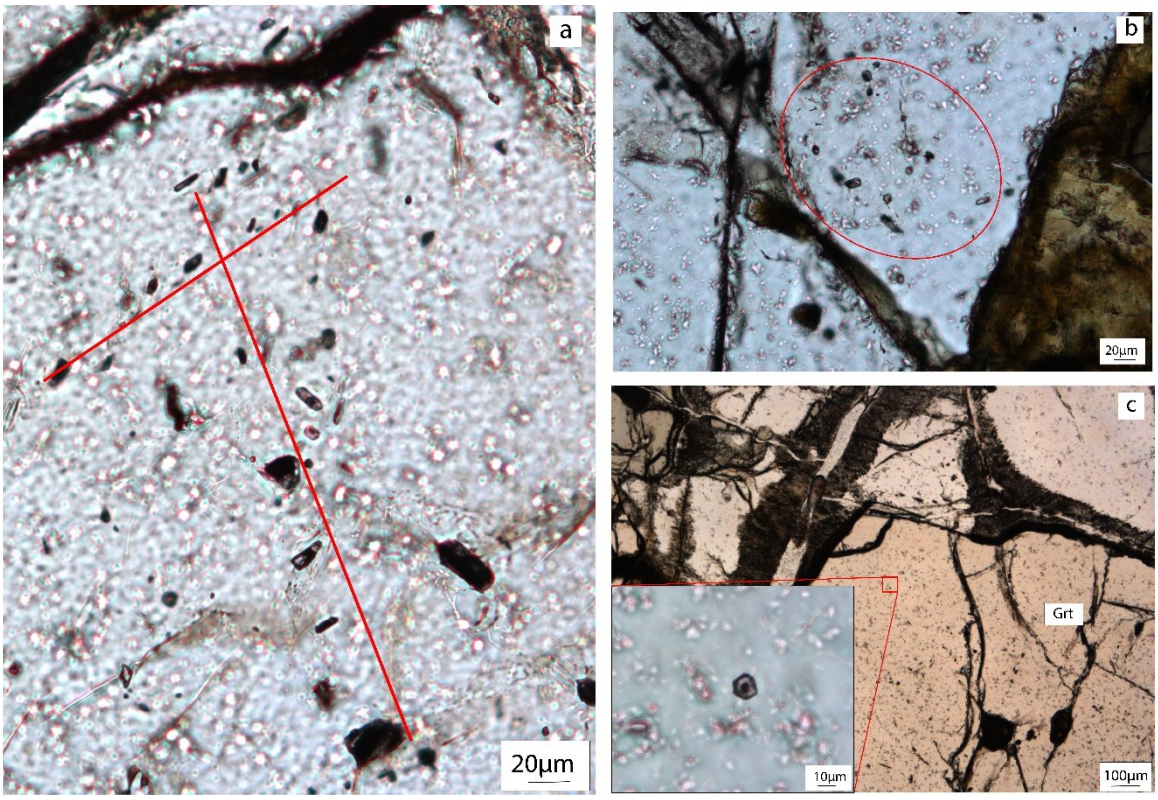

Figure 4.1 (a) *Secondary MI along trails under PPL;* ***(b) C****luster of MI located at the rim of Grt under PPL;* ***(c)*** *Primary MI located near the rim of Grt under PPL.*

Investigation of MI by SEM imaging allowed to observe with more detail their internal structure, and allowed to choose the most suitable MI for subsequent microprobe analyses.

In particular, it was possible to observe that MI in sample 18XC1 are not homogeneous but present small white dots, which could be identified as an early stage of crystallization of a new phase, probably ilmenite or magnetite (Fig. 4.2a and 4.2b).

The nanocrystals have a sub - micrometric size and are too small for a chemical analysis by SEM-EDAX or microprobe and therefore precise chemical composition of these phases is still unknown.

By SEM imaging it was also possible to find some inclusions within different hosts, especially oxides (Fig. 4.2c-d). A MI with a negative crystal shape and a shrinkage bubble has been found in rutile which also displays some trace of exsolutions, represented by the white domains which cross the mineral (Fig. 4.2c-inset 4.2d).

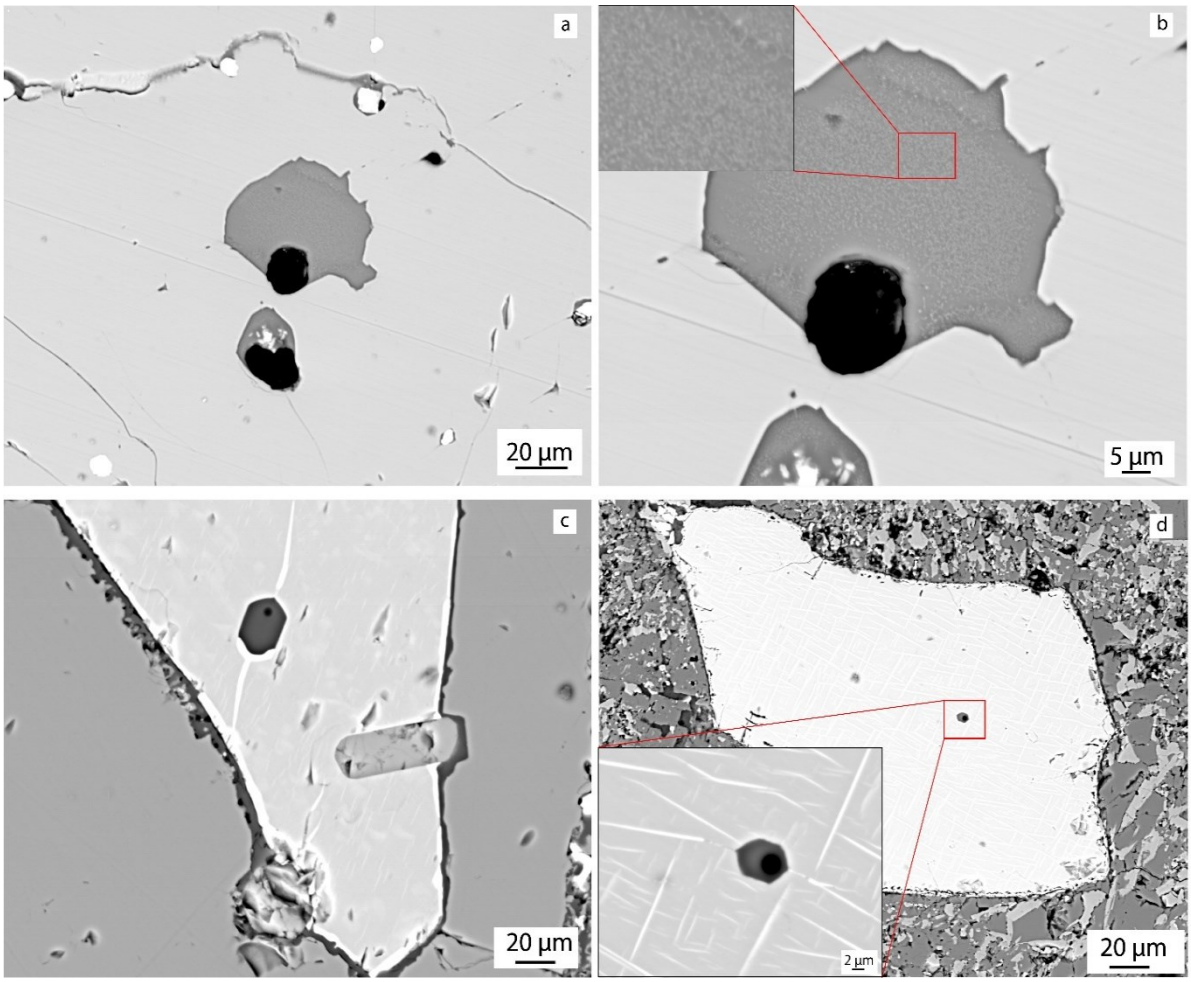

Figure 4.2 (a) *BSE image of an irregular-shaped MI in Grt host, showing a shrinkage bubble;* ***(b)****BSE image of the same MI as (a) which exhibits an early stage of crystallization and rich in nanocrystals (see inset);* ***(c)****BSE image of MI with negative crystal shape in Rt.;* ***(d)*** *BSE image of MI in Rt, the latter showing exsolutions.*

4.1.2 Microstructures of MI in sample 18XC10

Under PPL, MI appear brownish with multiple shapes, from irregular, to rectangular-square or negative crystal shape (Fig. 4.3a-c-d) with variable sizes ranging from 10 to 50 µm.

In this sample both primary and secondary inclusions have been found, where in the most cases the primary ones are isolated and located near to the core of the host (Fig. 4.3a). MI frequently present multiple bubbles and sometime inside the latter it is possible to see a small crystal (Fig. 4.3a).

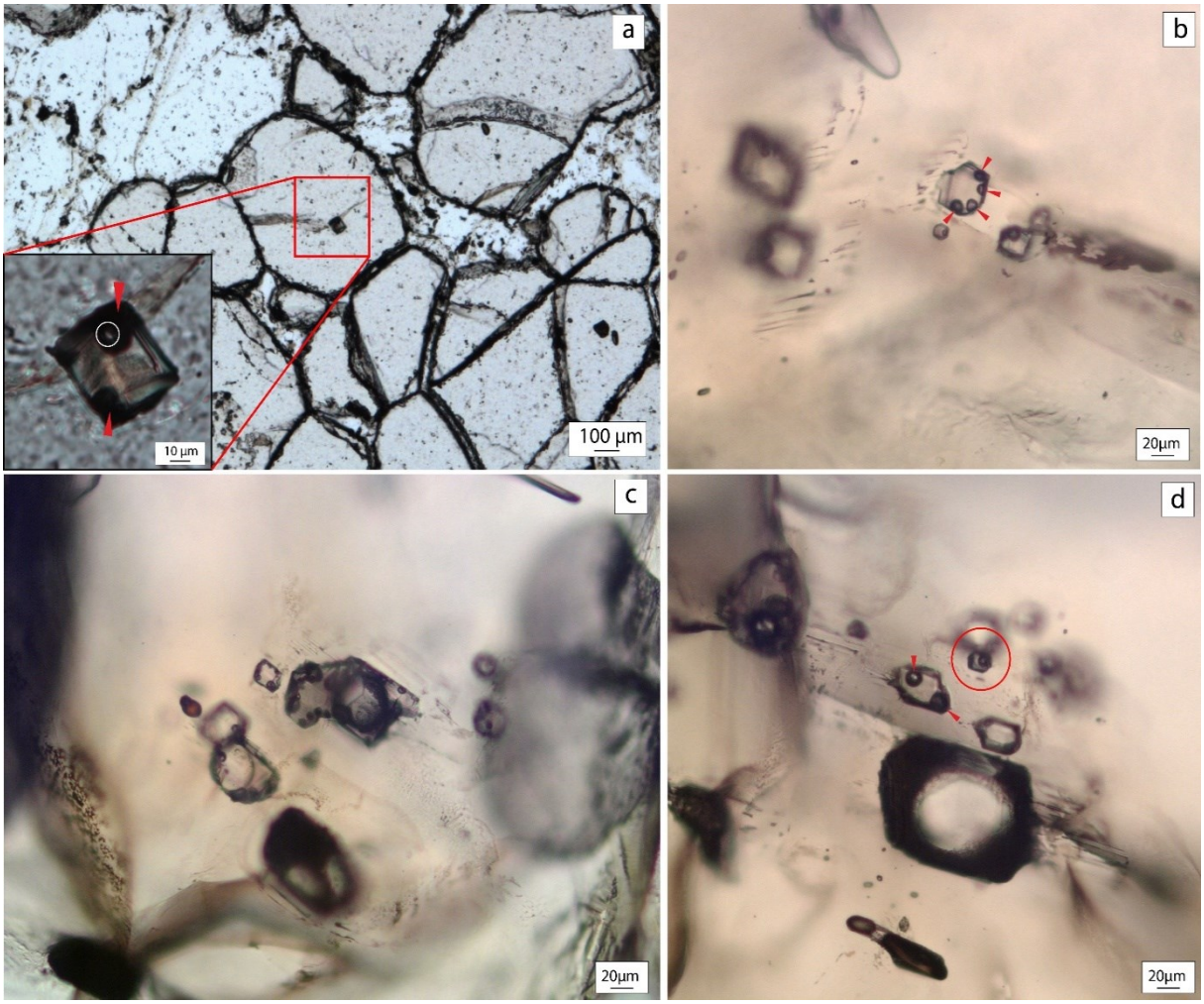

Figure 4.3 *Melt inclusions in garnet.* ***(a)*** *Image under PPL of a primary MI located near the core of the host (Grt) with double bubble and a small crystal inside (white circle);* ***(b)*** *Image under PPL of a primary MI with multiple shrinkage bubbles as indicated by the red arrow;* ***(c)*** *Image under PPL of several MI with different shapes;* ***(d)*** *Image under PPL of MI with double shrinkage bubbles and the red circle highlights the presence of a MI with negative crystal shape.*

Studying MI by SEM, it was possible to understand more details about their microstructures. As in sample 18XC1, also some melt inclusions in sample 18XC10 present the nanocrystals, even though other are perfectly homogeneous (Fig. 4.4a). The nanocrystals distribution is not always homogeneous within the MI, in some cases they tend to stay preferentially near the bubble and in the middle of the inclusion, leaving the edges free (Fig. 4.4b and Fig. 4.4c). In others cases, instead, they are evenly distributed on the entire volume of the MI (Fig. 4.5f).

Furthermore, the size of the nanocrystals is not constant, but changes among the different MI (see Fig. 4.4b-c).

As mentioned before, the MI have variable shapes and in figure 4.5a it is possible to observe two inclusions with perfect negative crystal shape which refer to the dodecahedral symmetry of their host, but probably they can not be considered as primary because they are on a fracture.

Also the MI in Figure 4.5b exhibits a crystal negative shape, but in this case the MI is linked to a larger one through a melt-filled crack.

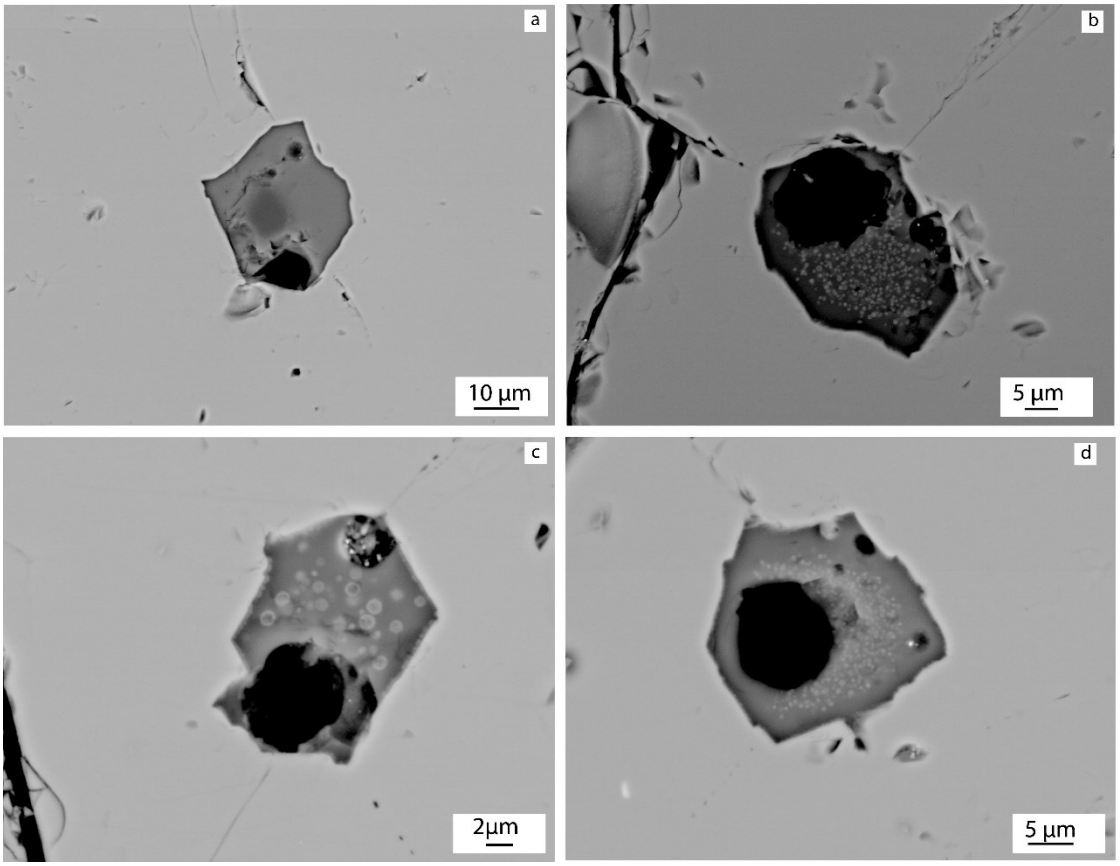

Figure 4.4(a) *BSE image of homogeneous MI located near to the core of Grt;* ***(b)*** *BSE image of MI which presents small white nanocrystals;* ***(c)*** *BSE image of MI where nanocrystals are located preferentially near to the bubble, while edges are free;* ***(d)*** *SEM-BSE image of MI with perfect negative crystal shape.*

The inclusions exhibit several open shrinkage bubbles (Fig.4.5), which have been opened as a consequence of the sample preparation processes, as indicated by the red arrows in several images (Fig. 4.5d-e). The MI in this sample contain different solid phases, predominantly trapped Rt (Fig. 4.5b-c) but also Qz has been observed (Fig. 4.5b).

Figure 4.5d-e-f show the presence of decrepitation tails, which occur in natural glassy inclusions when they undergo relevant isothermal decompression after the entrapment.

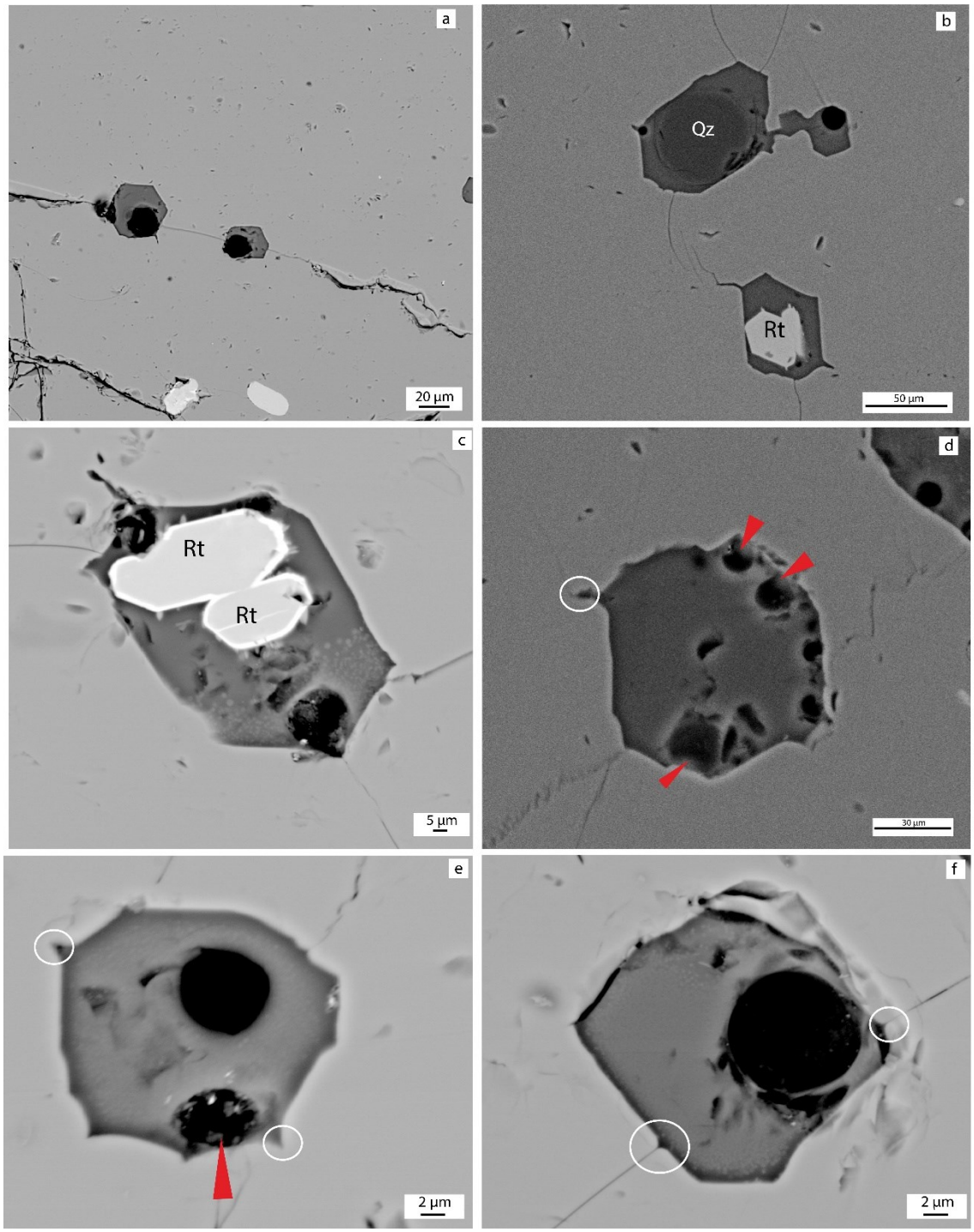

Figure 4.5 (a) *BSE image of MI with negative crystal shape;* ***(b)*** *BSE image of two different inclusions where the first exhibits a negative crystal shape and it is linked to another one through a melt-filled crack. The second one contains an oxide inclusions and has two decrepitation tails;* ***(c)*** *BSE image of MI which has two oxide inclusions;* ***(d)*** *BSE image of MI with presents decrepitation tails (with ellipse) and several shrinkage bubbles;* ***(e)*** *BSE image of MI with open bubbles and decrepitation tails;* ***(f)*** *BSE image of MI which presents two decrepitation tails, and nanocrystals homogeneously distributed.*

By SEM analysis it was possible to clearly observe the remnants of the lava from the Granatifera Tuff (Fig. 4.6 a-b), which have been analyzed by microprobe.

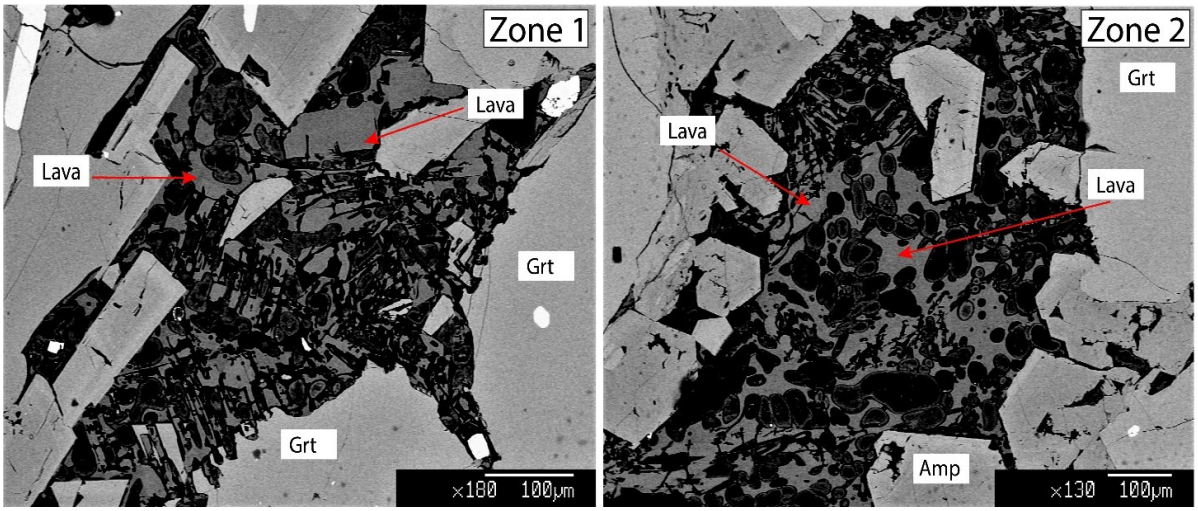

Figure 4.6a-b *BSE Images showing the remnants trace of lava from the Granatifera Tuff.*

4.1.3 Microstructures of MI in sample 18XC20

Under PPL, MI appear brownish or colorless, with different shapes, from irregular to negative crystal shape (Fig. 4.7c). The MI have a variable size ranging from 20 to 70 µm.

Both primary and secondary inclusions were found, where the primary ones are isolated and located near to the core of the host, while secondary MI seem to be organized along trails (Fig. 4.7a) or lie on fractures. Often MI exhibit multiple shrinkage bubbles (Fig. 4.7b).

For what concerns the nanocrystals they are also present in this sample, with a more irregular distribution, depending on the investigated MI. Figure 4.8b show the nanocrystals, located only in the inner part of the MI and not on inclusion walls, whereas in figure 4.8d they are situated only near to the walls. A more uncommon distributions is shown in figure 4.8c, where the nanocrystals are placed only on one side of the MI, and they are absent at the contact with Bt, forming a crystal free-band. Moreover, their size tends to increase from the bottom to the top (Fig. 4.8c yellow arrow).

The MI exhibits some solid phases, which are represented by oxides (Fig. 4.8a-b) and Bt (Fig. 4.8c). Also in this sample, several open shrinkage bubbles are present.

Decrepitation tails have been noticed only in few MI (Fig. 4.8a-b).

Thanks to the elevated resolution of the SEM, it was also possible to find some portions of intergranular melt (Fig. 4.9b-c) and devitrified glass (Fig. 4.9a).

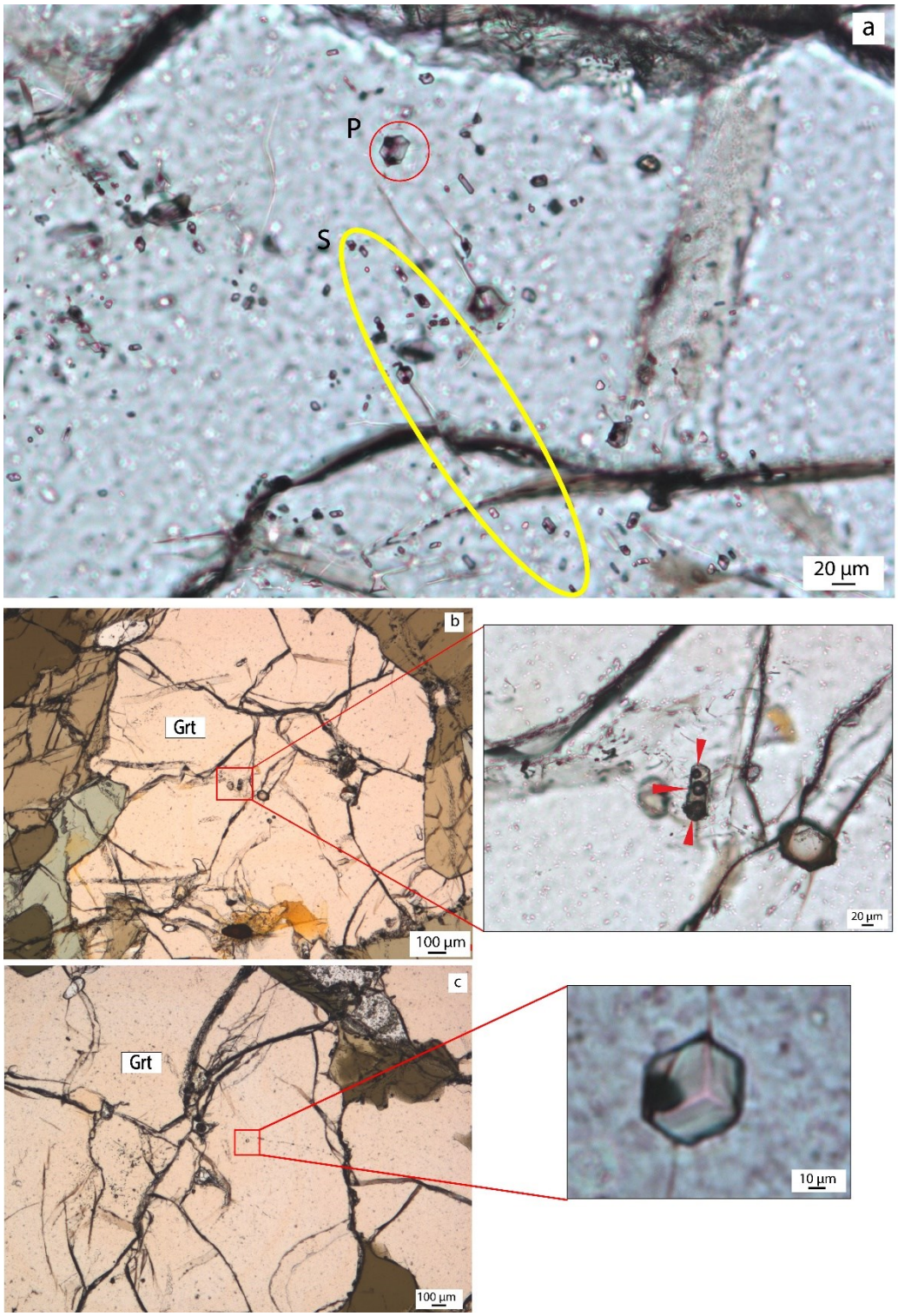

Figure 4.7 (a) *Image under PPL of primary (P) and secondary (S) MI;* ***(b)*** *Image under PPL of MI with multiple shrinkage bubbles;* ***(c)*** *Image under PPL of MI with negative crystal shape.*

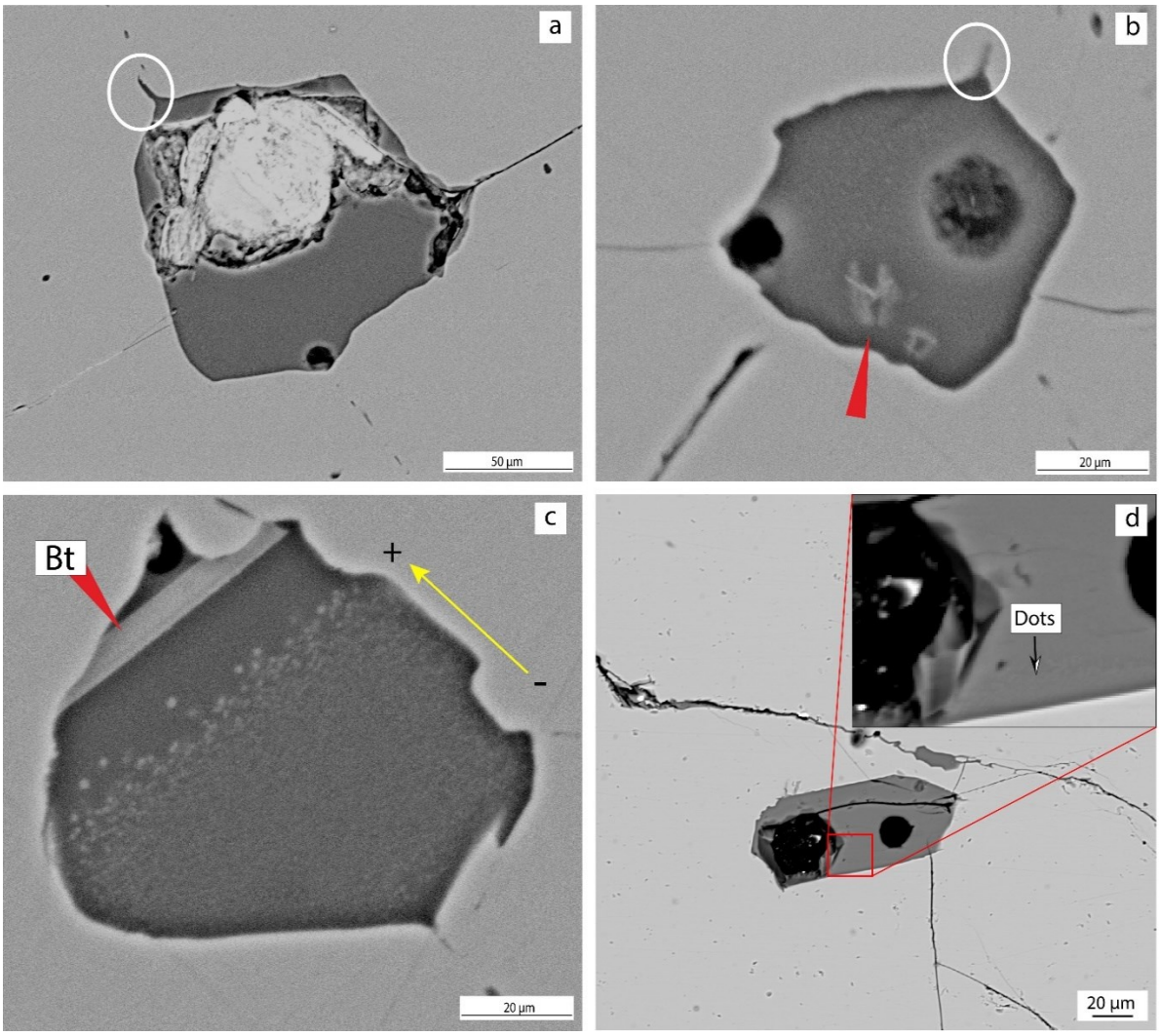

Figure 4.8 (a) *BSE image of MI with decrepitation tails;* ***(b)*** *BSE image of MI with some solid phases inside, white nanocrystals and decrepitation tails;* ***(c)*** *BSE image of MI which presents a particular arrangement of the nanocrystals and with a Bt inclusion. The yellow arrow indicates the increases in size of nanocrystals from the bottom to the top;* ***(d)*** *BSE image of MI with different location of withe nanocrystals and double shrinkage bubbles.*

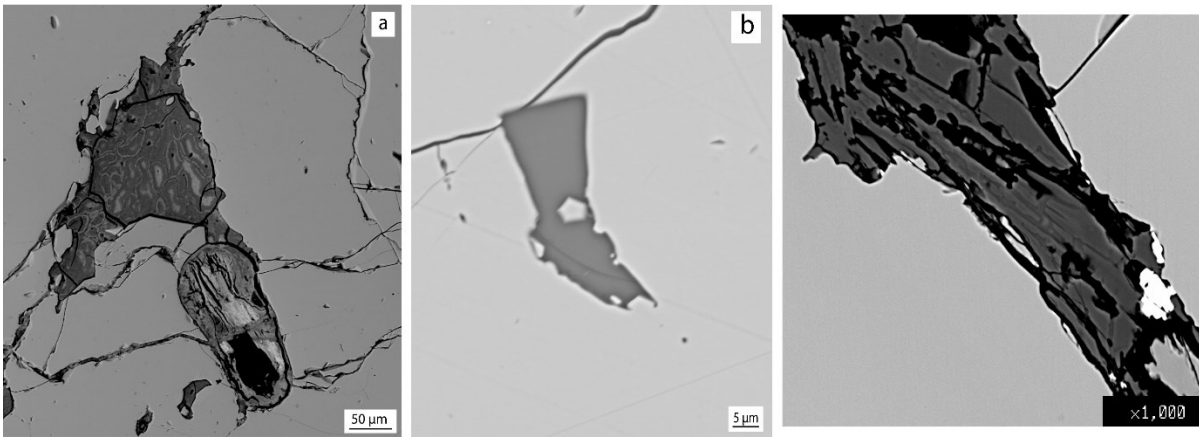

Figure 4.9 (a) *BSE image of devitrified glass;* ***(b)****BSE image of intergranular melt (MeltGRT4); (c) BSE image of intergranular melt (MELT2).*

4.2 Chemical analysis of MI

After an accurate observation by SEM, the most suitable melt inclusions were selected for the analysis of their chemical composition by microprobe.

The intergranular melt was analyzed for two samples, i.e. 18XC10 and 18XC20, whereas the MI were analyzed for all the samples mentioned above.

In figure 4.10 it is reported a TAS diagram (Total Alkali vs. Silica), which shows the chemical composition of the analyzed MI and the intergranular melt.

Regarding the melt inclusions, they were plotted in the TAS diagram in two distinct ways, because during the analysis of single MI several points were taken, both in portions with and without the white nanocrystals. Therefore, for some MI, the presence of the nanocrystals may have affected the reproducibility of the analysis. Consequently, when the results of the same MI deviate strongly from each other, they were plotted singularly, while average values were reported in the case of negligible chemical differences.

In the TAS, it is possible to observe how all MI for each sample describe an approximately well-defined cluster.

The MI in sample 18XC1 presents an intermediate silica-content (57-63 wt.%) and only two points lie near the transition toward acidic melts. Instead, the alkali content ranges from 6 to 8 wt.%. Most MI from this sample have a trachyandesite-andesite composition, and only two points fall in the trachydacite-dacite field.

Melt inclusions from sample 18XC10, describe the best-defined cluster, as is also observed from the analyses of the intergranular melt. From a compositional point of view, the inclusions mostly have a rhyolitic composition, and only few points lie on the border with the dacite field. Their silica content is strongly acidic, indeed these MI presents the higher concentration in silica (up to 75 wt.%) than the others samples. In sample 18XC10 the alkali content tends to vary from 4 to 7 wt.%.

The inclusions from sample 18XC20 describe a well-defined cluster, except for one point which falls in the trachyandesite field, whereas the intergranular melt has a more scattered distribution with a dacitic-rhyolitic composition. The melt inclusions instead have predominantly an intermediate trachydacite-dacite composition, where several points are located exactly on the border between these two fields. Only a few points have a rhyolitic composition. Their silica content is acidic, ranging from 63 to 71 wt.% but less than the MI in sample 18XC10, while two points of the intergranular melt have silica content comparable to the MI in sample 18XC10. In this sample, the alkali content is quite variable from 5 to 9 wt.%.

In sample 18XC20 the composition of the intergranular melt is extremely variable and does not reflect the chemistry of the MI.

Also in the sample 18XC10 the compositions of MI and the intergranular melt are not comparable, but in this case the compositions of the latter seem to be less variable.

In order to well-define the chemical composition of the studied MI and intergranular melt, chemical analyses were plotted in the diagram of Chappell and White (1974), who proposed the first modern geochemical scheme for the classification of granitic (s.l.) rock. They have

proposed two distinct granitoid types: The S-type (sedimentary type) derived from metasedimentary rocks and the I-type (igneous type) inferred to have formed from metaigneous sources. The graph expresses the ratio between aluminum saturation index (ASI), where ASI is defined as: [ASI = mol. Al_2O_3/(CaO+Na_2O+K_2O)] and the alkalinity index (AI) is defined as: [AI = mol. Al_2O_3 – (Na_2O+K_2O)].

Observing the global trend of the plot (Fig. 4.11), it is possible to say that most of the analyzed melt inclusions are mainly located in the peraluminous zone or are slightly metaluminous, i.e. ASI = 1,0-1,1.

This means that the most analyzed MI and intergranular melt correspond to I-type granitoids and only few inclusions and intergranular melt are classified as S-type granitoids.

In particular, for the sample 18XC1 half of the points fall in peraluminous zone, and the only three points are located closely to the metaluminous field, i.e. ASI 0,8-1,1 and the AI=0,10-0,12. All inclusions of 18XC1 correspond to I-type granitoids.

Sample 18XC10, is the only one in which melt inclusions tend to define a denser cluster. The distribution of the largest part of the analyses falls into the 1,0-1,1 ASI interval (i.e. peraluminous melts). The entire dataset for sample 18XC10 has ASI= 0,9-1,2 and AI= 0,02-0,08. The interstitial melt follows the trend of the MI previously described. The inclusions and the melt in this sample belong to both granitoid type groups, even if the larger part is represented by I-type.

The MI in the sample 18XC20, do not present a uniform distribution, indeed they fall both in metaluminous (ASI = 0,8-1,0) and strongly peraluminous (ASI = 1,1-1,4) zones. Their AI value vary from 0,6 to 0,10. For what concerns the intergranular melts they reflect the same general trend as the MI.

Most analyzed inclusions in this sample belong to the I-type granitoids, and only a small number to S-type granitoids.

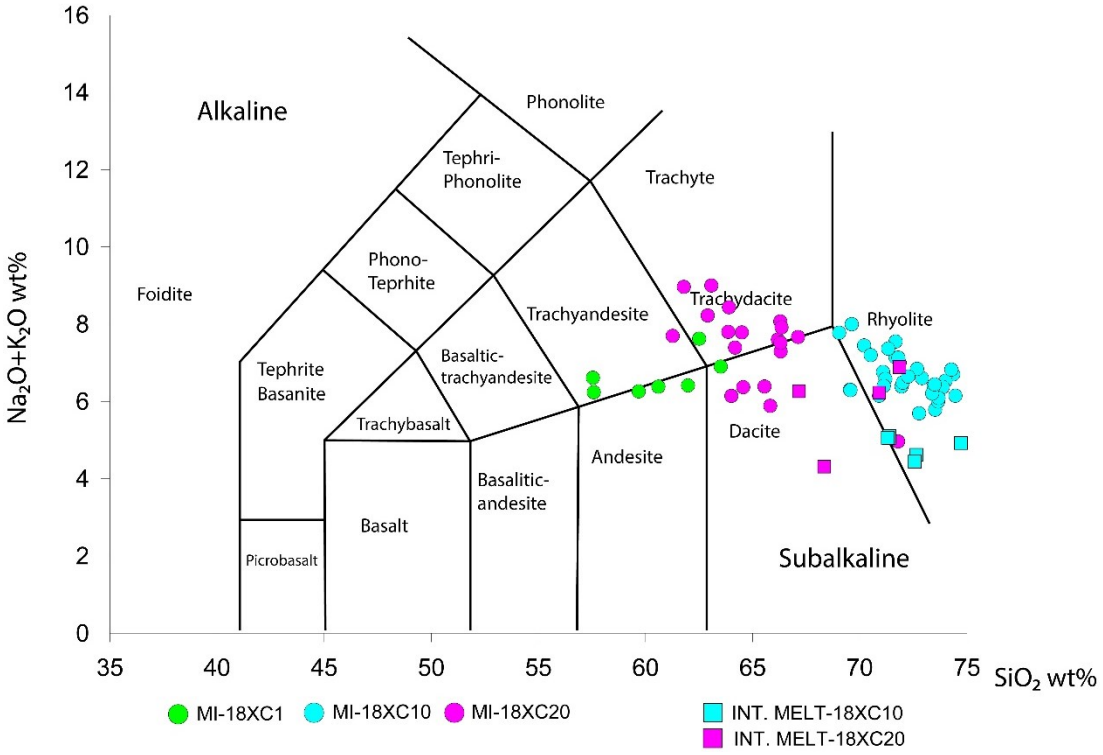

Figure 4.10 *TAS diagram of all analyzed MI and intergranular melts (labelled ad INT. MELT).*

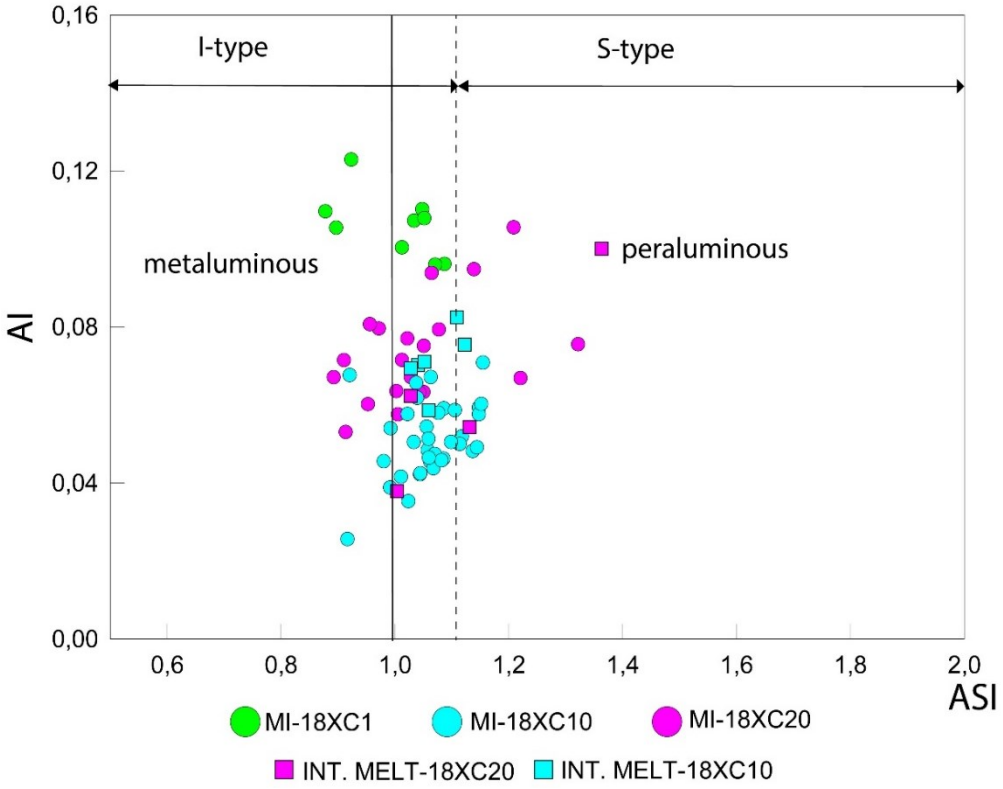

Figure 4.11 *Plot of aluminum saturation index [ASI = molar Al_2O_3/(CaO+Na_2O+K_2O)] vs alkalinity index [AI = molar Al_2O_3-(Na_2O+K_2O)].*

After this general introduction on the chemical compositions of the analyzed melts, a more detailed description for each sample will be given below.

4.2.1 Composition of MI in sample 18XC1

For sample 18XC1 three melt inclusions have been analyzed, where two of them are situated in the same host.

For MI1-GRT1, which displays the white nanocrystals (Fig. 4.12a) it was possible to take several analyses at different positions. A couple of points were taken near the edges where white nanocrystals are absent or present with low concentration, and another one was taken in the middle of the MI where the concentration of the dots is high (Fig. 4.12a).

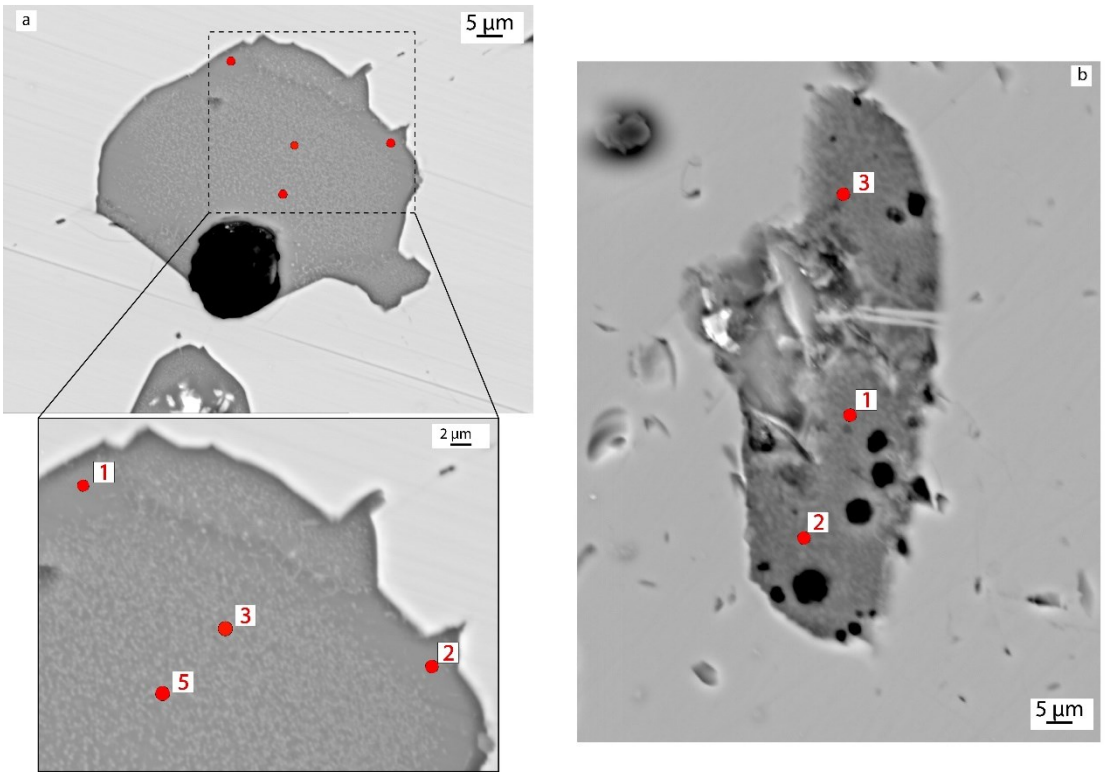

Figure 4.12 (a) *BSE image of analyzed points in MI1-GRT1 sample 18XC1;* ***(b)*** *BSE image of analyzed points in MI1-GRT6 sample 18XC1*

Below is reported a summary table (Tab. 4.1) which shows the results for these points. In all tables will be reported the data for the oxides corrected for alkali and normalized at 100, whereas the total is the pure value from the microprobe analyses without any correction or normalization.

GRT1	SiO_2	TiO_2	Al_2O_3	FeO	MnO	MgO	CaO	Na_2O	K_2O	Total
MI1-1	59,7	0,5	20,0	5,9	0,2	1,5	5,7	3,7	2,6	95,8
MI1-2	60,6	0,5	19,9	5,2	0,2	1,4	5,6	3,8	2,6	95,4
MI1-3	57,6	0,6	19,7	7,7	0,3	2,2	5,5	3,6	2,6	96,0
MI1-5	57,6	0,6	19,5	7,7	0,2	2,2	5,5	3,9	2,7	96,1

Table 4.1 *Obtained results for MI1-GRT1 for the three analyzed points. Totals are form the raw EMPA analyses.*

Also for MI1-GRT6 (Fig. 4.12b) several points were analyzed at different locations, but in this case the obtained results are very similar to each other (Tab 4.2), even if this MI shows the nanocrystals.

GRT6	SiO_2	TiO_2	Al_2O_3	FeO	MnO	MgO	CaO	Na_2O	K_2O	Total
MI1-1	61,8	0,1	20,9	2,6	0,0	0,5	7,8	3,3	2,7	95,6
MI1-2	62,5	0,2	19,8	2,8	0,1	0,8	7,1	3,4	3,2	95,3
MI1-3	61,8	0,1	20,4	2,6	0,0	0,6	7,7	3,8	2,8	97,7

Table 4.2 *Results for MI1-GRT6 for the three analyzed points. Totals are from the EMPA analyses.*

For the melt inclusions in sample 18XC1, Harker diagrams for the major elements (Al_2O_3-CaO-FeO-MgO-Na_2O-K_2O) have been made. These diagrams indicate how the elements vary in respect to their SiO_2 content (Fig. 4.13). For Harker diagrams, each point was individually plotted for MI and no average values were used.

The trends for FeO and MgO describe a negative correlation with SiO_2 until 61%, whereas above this value the correlation changes and becomes positive. For Al_2O_3 and K_2O, the correlation seems to remain constant with increasing values of silica. For what concerns CaO and Na_2O they do not show any correlation with silica.

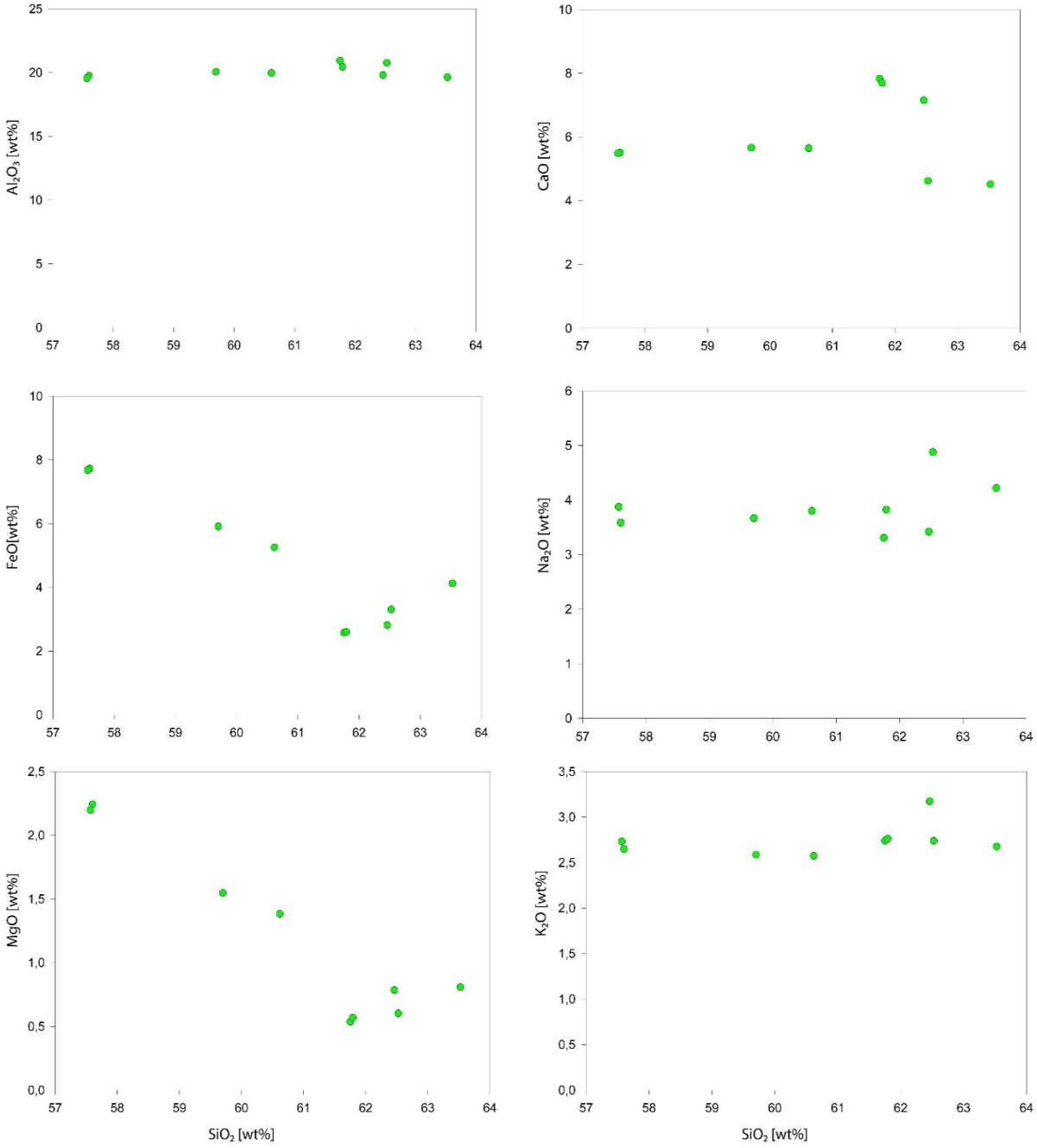

Figure 4.13 *Harker diagrams for major elements of MI sample 18XC1.*

4.2.2 Composition of MI in sample 18XC10

In this sample both MI and intergranular melts have been analyzed.

More than 25 MI were analyzed, with half of them containing the bright nanocrystals. Their compositional range is reported in table (Tab. 4.3), except for four MI which displays a low concentration in FeO, MgO and K_2O, even if the other parameters are comparable (Table 4.4).

	SiO_2	TiO_2	Al_2O_3	FeO	MnO	MgO	CaO	Na_2O	K_2O	Total
Max	74,5	0,5	16,5	3,4	0,1	1,2	4,6	5,6	3,0	99,3
Average	*72,2*	*0,4*	*14,8*	*2,6*	*0,0*	*0,8*	*2,3*	*4,4*	*2,3*	*97,9*
Min	69,1	0,2	13,4	1,1	0,0	0,1	1,7	3,7	0,9	94,0

Table 4.3 *Compositional range of analyzed MI with higher FeO concentrations. Totals are from the row EMPA analyses.*

	SiO_2	TiO_2	Al_2O_3	FeO	MnO	MgO	CaO	Na_2O	K_2O	Total
Max	75,2	0,6	16,3	1,0	0,1	0,3	3,1	5,7	1,8	98,6
Average	*73,0*	*0,4*	*15,6*	*0,8*	*0,1*	*0,1*	*3,0*	*5,1*	*1,5*	*98,3*
Min	71,7	0,3	14,3	0,7	0,0	0,0	2,7	4,3	1,3	97,9

Table 4.4 *Compositional range of 4 MI that deviate from the others reported in Table 4.3. Totals are from the row EMPA analyses.*

In this sample, the intergranular melt is represented by the remnants of the Granatifera Tuff lava. For the latter one, two neighboring zones were analyzed (Fig. 4.6), from which several points were measured, and their average composition is reported below (Tab. 4.5). Table 4.5 shows that values for the different zones are well comparable.

	SiO_2	TiO_2	Al_2O_3	FeO	MnO	MgO	CaO	Na_2O	K_2O	Total
ZONE1	73,3	0,2	14,5	2,8	0,1	0,6	3,3	3,7	1,0	94,8
ZONE2	71,4	0,4	14,9	3,1	0,1	0,7	3,6	4,1	1,0	96,1

Table 4.5 *Average composition of intergranular melts from Zone1 and Zon2 in sample-18XC10. Totals are from the row EMPA analyses.*

In the Harker diagrams, the Al_2O_3 trend describes a well-defined negative correlation with SiO_2, as also FeO, MgO and Na_2O but for these two latter elements the correlation is less defined and quite approximate. On the other hand, K_2O and CaO are highly scattered and no correlation with silica can be observed (Fig.4.14).

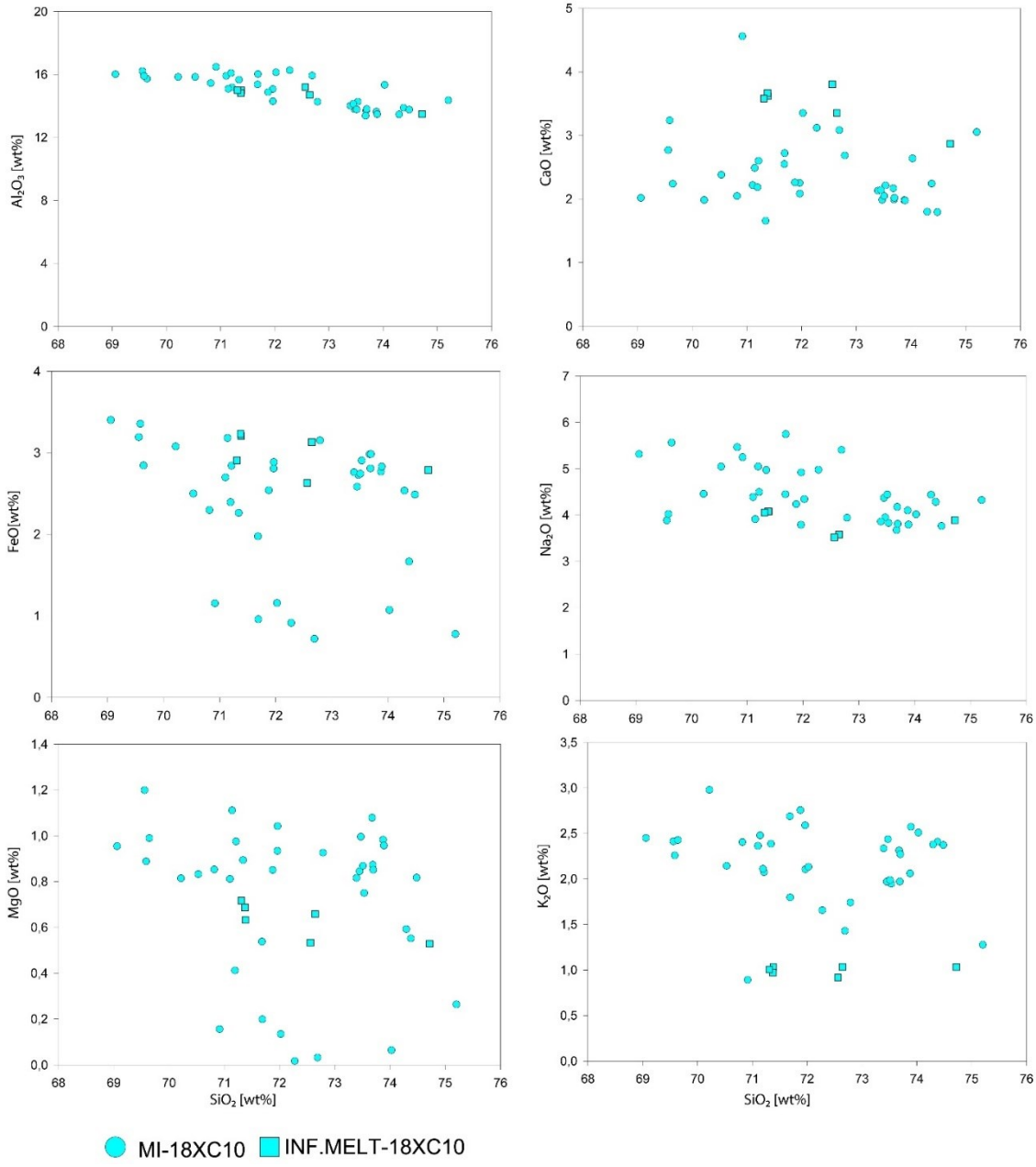

Figure 4.14 *Harker diagrams for major elements of MI and intergranular melt in sample 18XC10*

4.2.3 Composition of MI in sample 18XC20

Both MI and intergranular melts have been analyzed in this sample.

More than 20 MI were analyzed, and several of them have nanocrystals. In many cases their presence was not a problem during the analysis because the compositions do not change too much, but in other cases some differences have been noticed (ex. MI2-GRT6t) (Fig. 4.15).

For MI2-GRT6t the portion with nanocrystals, one-point analysis (yellow square point 6-Fig. 4.15) was acquired using a beam of 6 µm in size, with the aim to obtain a more homogeneous analyses, while the rest of the points and the crystal-free portion (red points Fig. 4.15) were analyzed using the classical dimension of the beam, i.e. about 1 µm.

The chemical composition of solid phase (Bt) was determined by a qualitative EDS analysis.

Table (Tab. 4.6) reports the results obtained for the analyses in the different portions of the MI.

It is possible to see that the concentration of some elements tends to vary as a function of the spot analysis. In the crystal-rich part, there is a higher concentration in MgO, K_2O and FeO which tends to be three times respect to the crystal-free part, while CaO, and SiO_2 are higher in the crystal-free domain.

In this case, it is clear how the presence of the nanocrystals, heavily affects the analyses.

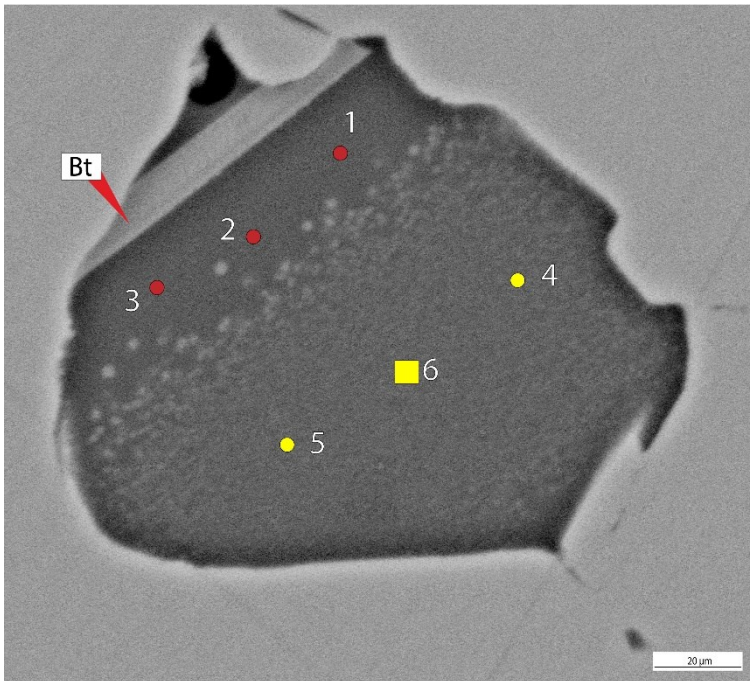

Figure 4.15 *BSE image of the analyzed points in MI2-GRT6t. The yellow square in point 6 indicates the analysis with 6 µm beam.*

	SiO_2	TiO_2	Al_2O_3	FeO	MnO	MgO	CaO	Na_2O	K_2O	Total
MI1-1	66,3	0,1	19,2	1,2	0,1	0,0	5,0	6,4	1,6	95,6
MI1-2	66,3	0,1	19,7	1,1	0,0	0,0	5,0	5,9	1,6	95,3
MI1-3	66,4	0,1	19,3	1,1	0,0	0,1	5,0	6,2	1,7	95,2
MI1-4	63,9	0,1	19,4	3,6	0,2	0,9	4,1	5,5	2,3	96,1
MI1-5	62,9	0,1	19,4	4,4	0,2	0,8	3,9	5,8	2,4	95,9
MI1-6	63,1	0,1	18,9	3,8	0,1	0,8	3,9	6,7	2,3	95,9

Table 4.6 *Obtained values from the analysis of MI2-GRT6. Totals are from the raw EMPA analyses.*

All analyzed melt inclusions, from a chemical point of view, exhibit about the same compositional range as reported in Table 4.7.

Concerning Na_2O there are two MI (MI1-GRT7 and MI2-GRT4t) which are particularly rich in sodium with a concentration over 6 wt.%.

About the silica content, there is one MI (MI1-GRT6 – Fig. 4.8d) which has a higher concentration in SiO_2, almost 72 wt.%. This MI was analyzed in three different spots.

	SiO_2	TiO_2	Al_2O_3	FeO	MnO	MgO	CaO	Na_2O	K_2O	Total
Max	71,9	0,8	21,0	5,6	0,3	1,7	5,0	6,8	3,0	98,3
Average	*65,3*	*0,2*	*18,3*	*4,0*	*0,2*	*1,1*	*3,7*	*4,9*	*2,1*	*95,9*
Min	61,3	0,1	13,7	1,1	0,0	0,0	1,7	3,2	1,6	93,1

Table 4.7 *Compositional range of all analyzed MI in sample 18XC20. Totals are from the raw EMPA analyses*

About the intergranular melt (Fig. 4.9b-c) its composition is reported in the table below (Tab. 4.8). Observing the data, the composition of the intergranular melt seems to be more or less constant, even if some values tend to deviate slightly.

	SiO_2	TiO_2	Al_2O_3	FeO	MnO	MgO	CaO	Na_2O	K_2O	Total
MELT1	71,8	0,2	14,1	3,7	0,1	0,9	2,1	5,0	1,9	97,8
MELT2	70,9	0,1	14,1	4,7	0,3	1,1	2,1	3,3	2,9	97,9
MGR4-1	67,2	0,2	15,7	5,7	0,1	1,4	3,3	4,5	1,7	97,5
MGR4-2	68,3	0,2	16,2	6,2	0,0	1,3	3,2	2,4	1,9	97,9

Table 4.8 *Chemical composition of intergranular analyzed melts in sample 18XC20. Totals are from the raw EMPA analyses*

Al_2O_3, CaO and Na_2O have a negative correlation with silica, which is particularly pronounced for Al_2O_3. On the other hand, FeO exhibits a weak positive correlation with silica. MgO and K_2O do not present any type of correlation with silica, being highly scattered. Similarly, the trends observed for the intergranular melt follow those described for the MI (Fig. 4.16).

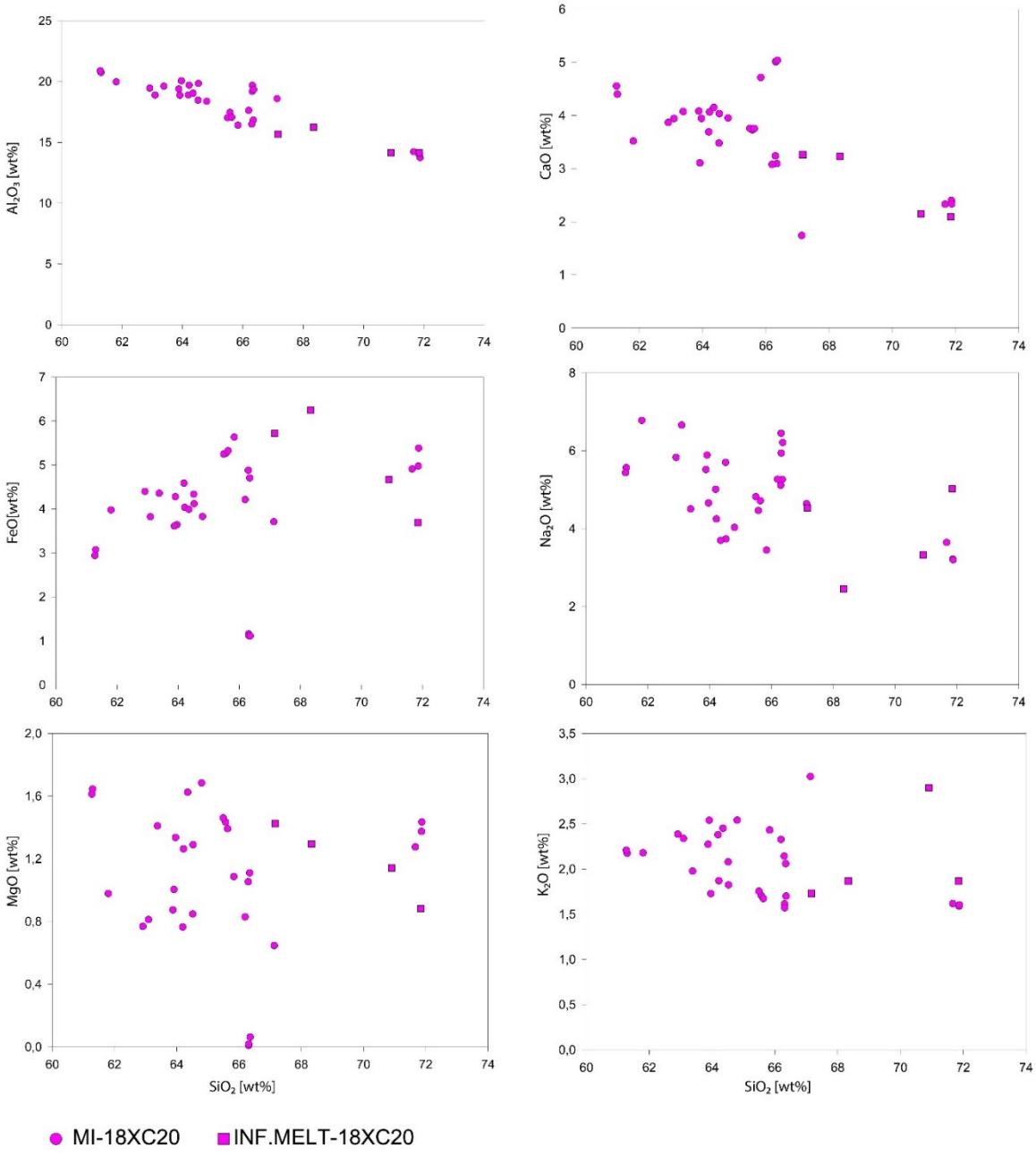

Figure 4.16 *Harker diagrams for major elements of MI and intergranular melt in sample 18XC20*

Chapter 5 – GEOTHERMOBAROMERTY

5.1 Introduction

Samples containing MI, i.e. 18XC1, 18XC10 and 18XC20, were investigated through geothermometry, in order to determine the temperature conditions experienced by these xenoliths.

The chosen geothermometer, proposed by Nakamura (2009), is calibrated on the garnet-clinopyroxene pairs, two phases particularly abundant in these samples.

The thermometer of Nakamura (2009) considers as Fe_{tot} only as Fe^{2+}, without Fe^{3+}. This because the estimation of Fe^{3+} from stoichiometry is highly dependent on accuracy of the analyzed chemical composition, which can lead to overestimated or underestimated K_D (Fe^{2+}/Mg) values both for garnet and clinopyroxene (Nakamura, 2009).

Compared to other garnet-clinopyroxene thermometers, the thermometer of Nakamura (2009) does not overestimate temperatures for Ca-rich garnets and therefore it is well indicated for the xenoliths investigated in this thesis, where X_{Grs} in garnet ranges from 0,16 to 0,36.

By contrast, one drawback related to this thermometer is the pressure dependence, which was not possible to be constrained for this thesis. Indeed, calculations were done assuming a pressure range from 0,5 to 3 GPa. This means that a more accurate temperature interval can be obtained only after the determination of pressure.

The standard deviation (S.D) estimated for this thermometer is 74°C (Nakamura, 2009).

All temperature values were calculated with the formula reported in Figure 5.1:

$$T(^\circ\mathrm{C}) = \{2784 + 14.52\ P + (2601 + 1.44\ P)(2X_{grs}X_{prp} - A) + (1183 + 6.98\ P)(X_{grs}^2 - A) - 105(2X_{grs}X_{alm} + B) + (814.6 + 3.61P)(X_{grs}^2 + B) - (254.6 + 8.42\ P)(2X_{prp}X_{alm} - X_{alm}^2 + C) - 83.6(X_{prp}^2 - 2X_{prp}X_{alm} + C) + 1388\,X_{sps} - 462(X_{Mg}^{Cpx} - X_{Fe}^{Cpx})\}/\{\ln K_D + 1.431 + 0.695(2X_{grs}X_{prp} + X_{grs}^2 - 2A) + 0.203(X_{grs}^2 - 2X_{grs}X_{alm}) + 0.922X_{sps}\} - 273,$$

where T = temperature, P = pressure (kbar), $A = 0.5\ X_{grs}\ (X_{prp} - X_{alm} - X_{sps})$, $B = 0.5\ X_{grs}\ (X_{prp} - X_{alm} + X_{sps})$, $C = 0.5\ (X_{grs} + X_{sps})\ (X_{prp} - X_{alm})$, $X_{prp} = Mg/(Fe^{2+} + Mn + Mg + Ca)^{Grt}$, $X_{alm} = Fe/(Fe^{2+} + Mn + Mg + Ca)^{Grt}$, $X_{sps} = Mn/(Fe^{2+} + Mn + Mg + Ca)^{Grt}$, $X_{grs} = Ca/(Fe^{2+} + Mn + Mg + Ca)^{Grt}$, $X_{Mg}^{Cpx} = Mg/(Al + Fe^{total} + Mg)^{Cpx}$, $X_{Fe}^{Cpx} = Fe^{2+}/(Al + Fe^{total} + Mg)^{Cpx}$, $K_D = (Fe^{2|+}/Mg)^{Grt}/(Fe^{2+}/Mg)^{Cpx}$, Grt = garnet, Cpx = clinopyroxe

Figure 5.1 *Thermometer formula calculation from Nakamura (2009).*

When possible, temperatures were calculated using core and rim analyses of garnets and clinopyroxenes lying in contact with each other. For sample 18XC20 only the rim points for both minerals were chosen.
When more than one point of rim or core were present, the average value was considered.
The final temperature is the result of the average temperature between the values obtained for pairs core-rim, or in case of sample 18XC20 only for the rim.

5.2 Results

Below is reported a summary table for each sample, which shows the different temperatures in the pressure range from 0,5 to 3 GPa.

18XC1	**GRT7CPX3**			
	Core	***Rim***		
Kd	*2,20*	*2,04*		
(GPa)	T (°C)	T (°C)	T Avg.	S.D
0,5	1167	1226	1196	30
1	1198	1258	1228	30
1,5	1229	1291	1260	31
2	1260	1323	1292	31
2,5	1291	1355	1323	32
3	1322	1388	1355	33

18XC10	**GRT14CPX1-2**				**GRT8CPX8**			
	Core	***Rim***			***Core***	***Rim***		
Kd	2,63	*2,53*			*2,88*	*2,52*		
(GPa)	T(°C)	T(°C)	T Avg.	S. D.	T(°C)	T (°C)	T Avg.	S. D
0,5	964	977	971	6	921	980	950	30
1	991	1004	998	7	947	1008	978	30
1,5	1019	1032	1025	7	974	1035	1005	31
2	1046	1060	1053	7	1001	1063	1032	31
2,5	1073	1087	1080	7	1027	1091	1059	32
3	1101	1115	1108	7	1054	1119	1086	32

18XC20	**GRT10 CPX3 (r 1- 4)**	**GRT11CPX3 (r 4-6)**	**GRT12CPX4**	**GRT8 CPX**	
Kd	*2,62*	*2,62*	*2,65*	*2,63*	
(GPa)	Temp (°C)	Temp (°C)	Temp (°C)	Temp (°C)	T Avg.
0,5	1039	1040	1032	1030	1035
1	1069	1069	1062	1059	1065
1,5	1099	1099	1091	1088	1094
2	1128	1128	1121	1118	1124
2,5	1158	1158	1150	1147	1153
3	1188	1188	1179	1177	1183

Table 5.1 *Temperature (T) values obtained for each sample. Pressure (P) ranging from 0,5 to 3 GPa.*

Table 5.1 and Figure 5.2 report all temperature values determined for the three samples.

Each sample defines a fairly narrow temperature range of equilibration, that increases in order 18XC10, 18XC20, 18XC1 (Fig. 5.3). Assuming a reference pressure of 1,5 GPa, which represents the reference value of pressure in the lower crust zone, the xenolith 18XC1 has experienced a temperature between 1229 and 1291°C. The xenolith 18XC10 records temperatures in the range 974 to 1035 °C and the xenolith 18XC20 records temperature in the range 1089 to 1099°C.

These temperatures are compatible with the thermal conditions that can be attained in the deep roots of continental arcs (Kelemen et al., 2004).

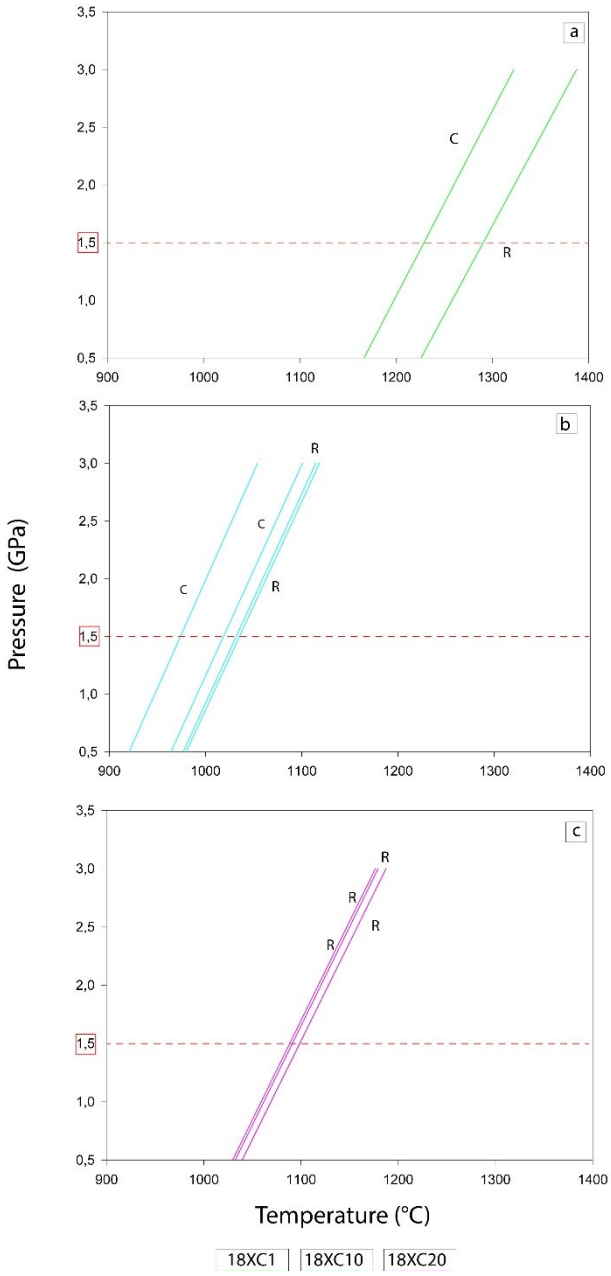

Figure 5.2 *Plots for each sample in terms of pressure and temperature.* ***(a)*** *Sample 18XC1;* ***(b)*** *Sample 18XC10;* ***(c)*** *Sample 18XC20. In diagrams a-b are plotted the average temperature between core and rim, while in the diagram (c) the temperature regards only rim points. The red lines indicate the value of reference pressure. Thermometer of Nakamura (2009).*

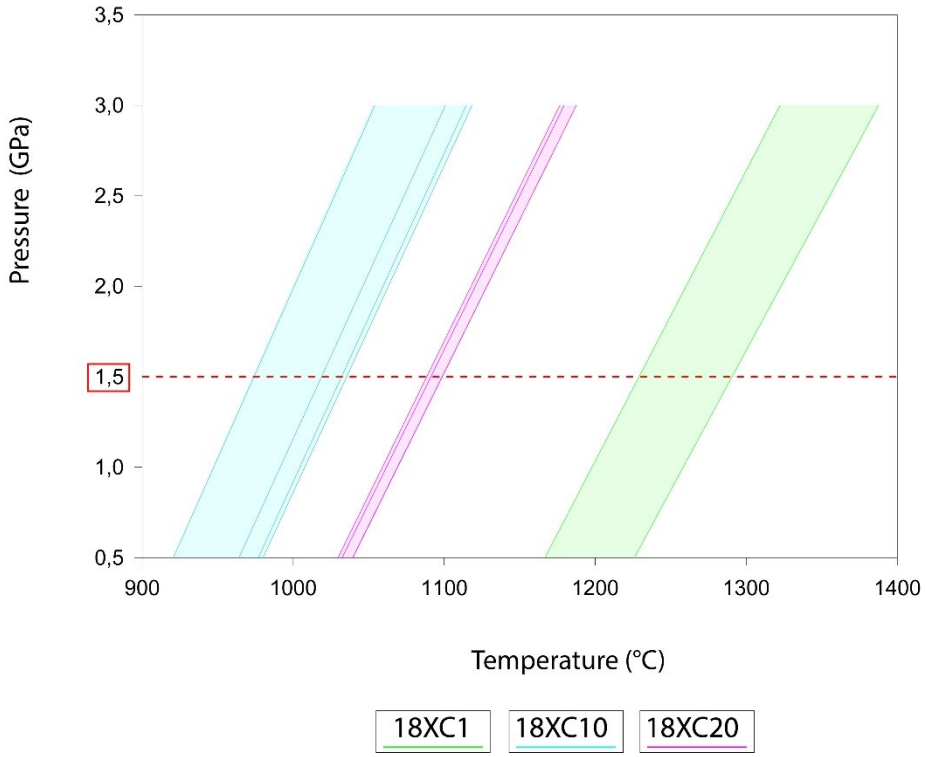

Figure 5.3 *Location of different samples in function of the temperature conditions. The red lines indicate the reference pressure value. Thermometer of Nakamura (2009).*

Chapter 6 – DISCUSSION

6.1 Comparison between the studied MI

After the presentation of all data about MI and their composition, it is important to understand if the analyzed MI can be compared among them. Among all the studied inclusions, some are primary in origin and this is very important because these of MI allow to obtain some information about the composition of the melt which has been contemporarily formed during the growth of their host. In this context, it is also important to know if MI were trapped during an incongruent melting process (anatexis context) – melt producing process - or during an igneous crystallization – melt-consuming process. This aspect will be treated in more detail further below.

As reported in the TAS diagram (Figure 4.10) MI have a different composition, with an increasing silica-content passing from 18XC1 (57-64 wt.%) to 18XC10 with 69-75 wt.%, while the sample 18XC20 presents an intermediate concentration ranging from 61 to 72 wt.%. The MI in 18XC1 can be classified as trachyandesite-andesite, those in 18XC10 as rhyolite and in 18XC20 as trachydacitic-dacitic to rhyolitic.

Below are reported some summary Harker diagrams (Fig. 6.1) for the major elements (Al_2O_3-CaO-FeO-MgO-Na_2O-K_2O) which indicate how the latter vary depending on the SiO_2 content for all the analyzed inclusions.

Observing the general trend of the Harker diagrams, it is possible to notice how all three samples exhibit a negative correlation in terms of Al_2O_3, CaO and FeO, while for MgO, Na_2O and K_2O they appear quite scattered without a clear correlation trend. Moreover, the diagrams show the MI of sample 18XC1 have a close affinity with those of sample 18XC20, whereas those of 18XC10 tend to define an isolated cluster.

Concerning CaO, the highest concentrations is observed for MI in sample 18XC1, then smoothly decreasing from sample 18XC20 to sample 18XC10. A similar behavior is also reflected in the composition of the garnet hosts, where the Grs component in garnet on 18XC1 is about 30-36%, whereas in 18XC10 is between 16-20%, and in 18XC20 about 20-29%. This suggests that the chemical composition of the trapped melt in the three xenoliths is closely related (and probably also spatially-dependent) to the specific bulk chemical system in which each xenolith has been formed.

The Harker diagrams also show that some melt analyses belonging to 18XC1 (notably those with Si_2O < 60 wt.%) tend to deviate from the general trend in terms of Al_2O_3, CaO, FeO and MgO. All these analyses were collected in the nanocrystal-rich portion of the same inclusion (MI1-GRT1; see Fig. 4.12). This indicates that the presence of the nanocrystals may influence the results of all analyzed melt. Micro-scale heterogeneities in a single inclusion have been also observed in sample 18XC20 (MI2-GRT6t; see Figure 4.15), where the melt analyzed near to a daughter Bt crystal is notably FeO, MgO (both with lowest points in Fig. 6.1) and K_2O-poorer compared to the portion of the inclusion having nanocrystals.

Another relevant observation arising from my results is that the silica content of the MI in the three xenolith is inversely correlated with temperature obtained applying the Grt-Cpx geothermometer of Nakamura (2009). In order of increasing silica content, the samples and their estimated temperatures are as follows: 18XC1 (1229-1291 °C), 18XC20 (1089-1099°C) and 18XC10 (974-1035°C).

To conclude, it is possible to affirm that samples 18XC1 and 18XC20 are more similar to each other than 18XC10, both in terms of mineral assemblage and composition of MI.

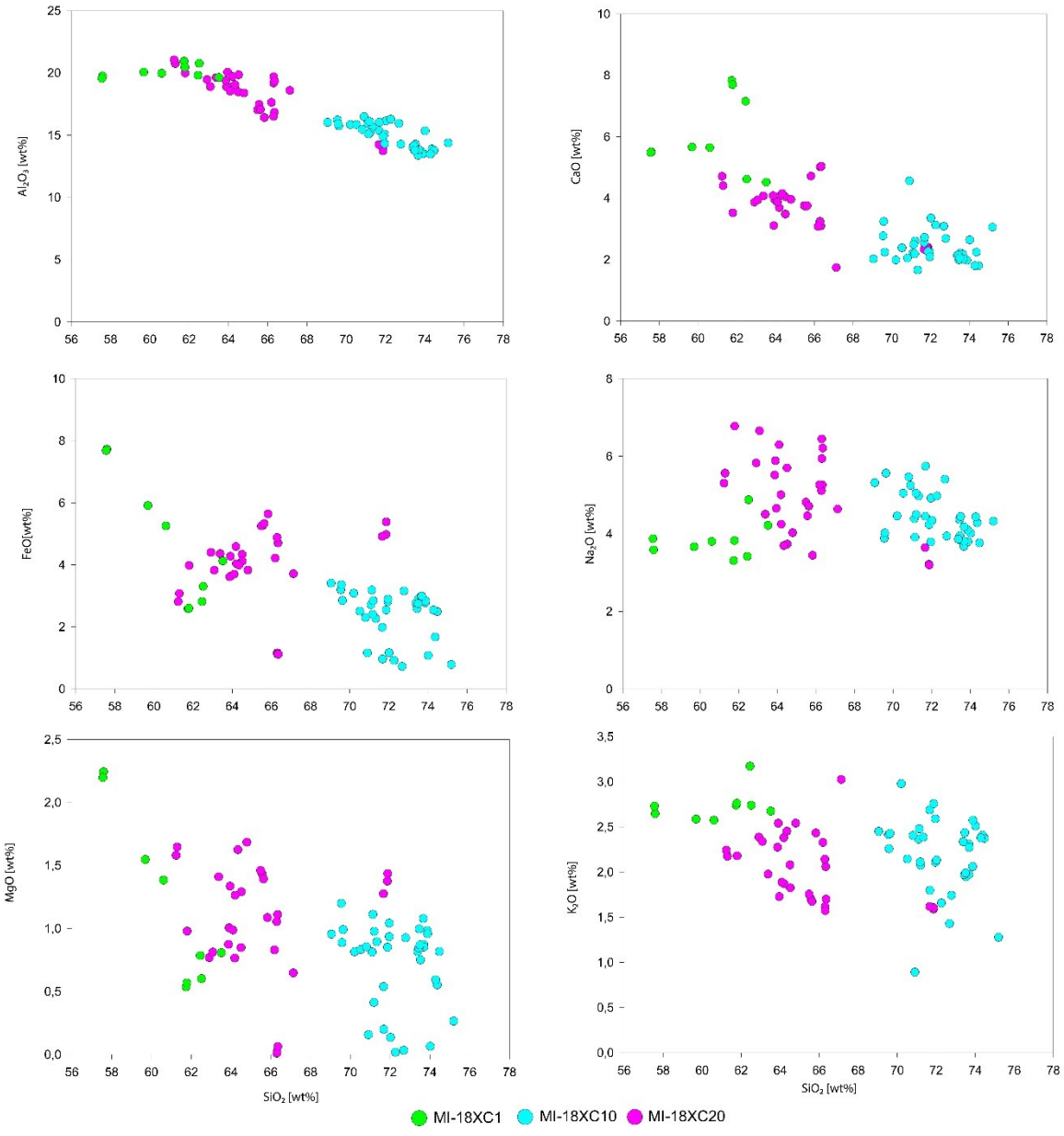

Figure 6.1 *Harker diagrams for the major elements of MI in the three studied samples.*

6.2 Comparison between garnets in the studied xenoliths and in other works

6.2.1 Studied garnets vs. results obtained by Weber (1998)

The garnets composition of xenoliths 18XC1, 18XC10 and 18XC20, can be compared with the results obtained by Weber in her PhD project (1998).

In Figure 6.2 it is reported a ternary diagram in terms of Alm + Sps – Pyr – Grs + Adr which allows to compare the garnets composition of the studied xenoliths, and the results obtained by Weber (1998).

For garnets of the studied samples, which do not present important zoning, the average compositions are reported, while composition measured by Weber (1998) are given as single rim-core points.

The garnets of sample 18XC10 present a higher concentration in Pyr with respect to 18XC1 and 18XC20, and are located near the hornblendite and pyribolite groups defined by Weber (1998). By contrast, xenoliths 18XC1 and 18XC20, are located in the lower part of the diagram, close to the pyriclasites and granulites.

Especially for sample 18XC20, the garnets can be described using the compositional range proposed by Weber for these rocks: Pyr_{30} – Alm_{45} – Grs_{25}.

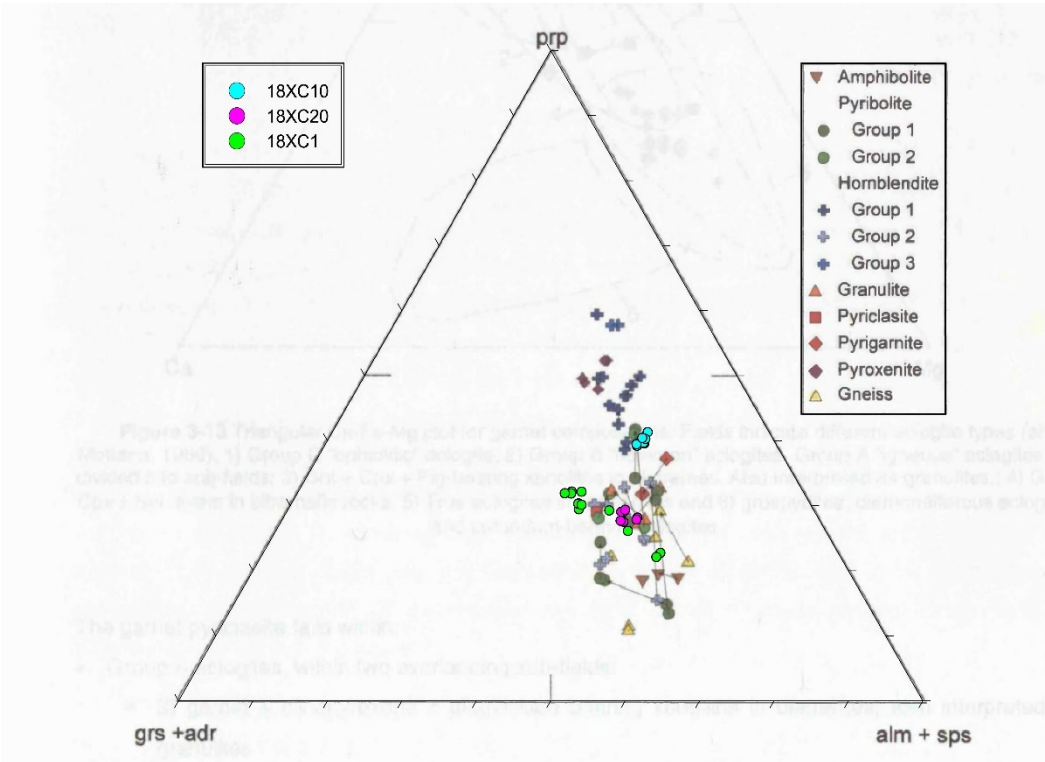

Figure 6.2 *Comparison between garnets compositions from this thesis and the results obtained by Weber (1998). Modified from Weber (1998).*

After these considerations, it is possible to conclude that the analyzed garnets tend to deviate from the results obtained by Weber (1998). Indeed, sample 18XC10 is located near to the garnets of the amphibolite field, even if in this thesis it has been classified as a granulite. On the other hand, garnets in 18XC1 and in 18XC20 appear similar to garnets of the granulite and pyribolite fields, even if especially 18XC20 has been classified as garnet-pyroxene hornblendite. Following the nomenclature proposed by Weber (1998), garnets of sample 18XC20 should be more akin to garnets of the hornblendite Group 1.

6.2.2 Bulk composition of sample 18XC10 vs. results obtained by Bloch et al. (2017)

The bulk composition of the sample 18XC10, here classified as granulite, can be compared with the bulk composition obtained by Bloch et al. (2017) for garnet-clinopyroxenites (Table 6.1).

Observing the proportions between garnet (40-60%) and clinopyroxene (50-60%) reported by Bloch et al. (2017), they are higher with respect to 18XC10 in which Grt is about 54% and Cpx 25% (Table 6.1).

For what concerns SiO_2, there is not a big difference between 18XC10 (~47 wt.%) and the values reported by Bloch et al. (2017), which range from 43 to 49 wt.%.

The results obtained by Bloch et al. (2017) tend to strongly deviate from sample 18XC10 especially for TiO_2 (0,8 -1,5%), MgO (10-18,9%) and CaO (13-15,5%), which are higher than values obtained for sample 18XC10 (Table 6.1). For what concerns the other oxides, Al_2O_3 (11,3-18,5%), FeO (5-13,6%) and MnO (0,1-0,4%) in garnet-clinopyroxenites they tend to be similar to sample 18XC10, with only Na_2O (1,79%) being higher in 18XC10 compared to the samples of Bloch et al. (2017).

The differences in composition are compatible with the presence and abundance of plagioclase in sample 18XC10. Conversely, this phase is absent in the clinopyroxenites studied by Bloch (2017).

a

	18XC10
% Grt	54
% Cpx	25
SiO_2	46,61
TiO_2	0,53
Al_2O_3	17,61
FeO	13,11
MnO	0,27
MgO	10,19
CaO	9,79
Na_2O	1,79
K_2O	0,07
H_2O	0,04
Total	100,00

b

Sample	MEMX6	MMXP08	MEMX2	MEMX5	MEMX7
% grt	40 (10)	45 (10)	60 (5)	45 (15)	50 (10)
% cpx	60 (10)	55 (10)	40 (5)	55 (15)	50 (10)
SiO_2	49.0 (1.2)	43.3 (0.8)	40.7 (0.2)	46.2 (0.1)	42.3 (0.6)
TiO_2	0.8 (0)	1.5 (0.1)	1.5 (0.1)	0.9 (0)	1.3 (0.1)
Al_2O_3	11.3 (2)	15.6 (1.2)	18.5 (0.4)	13.3 (1.8)	16.4 (1.2)
Cr_2O_3	0.8 (0.1)	0.1 (0)	0.0 (0)	0.1 (0)	0.0 (0)
FeO	5.0 (0.4)	13.1 (0.9)	15.1 (0.5)	9.3 (0.6)	13.6 (0.9)
MnO	0.1 (0)	0.3 (0)	0.2 (0)	0.2 (0)	0.4 (0.1)
MgO	18.9 (0.4)	10.3 (0.1)	8.3 (0)	16.2 (0.1)	10.0 (0)
CaO	13.0 (1.4)	14.4 (1)	15.5 (0.5)	13.2 (1.3)	15.4 (1.1)
Na_2O	1.0 (0.2)	1.2 (0.2)	0.5 (0.1)	0.5 (0.1)	0.6 (0.1)
Mg#	87.2 (0.7)	58.4 (1.5)	49.4 (0.9)	75.7 (1.1)	56.8 (1.8)
Density contrast (%)	2.7 (1)	7.2 (1.4)	9.6 (0.7)	4.9 (1.2)	7.8 (1.4)

Values wihich strongly deviate between Bloch (2017) and sample 18XC10
Values wihich slightly deviate between Bloch (2017) and sample 18XC10
Highest values are reported in sample 18XC10 than Bloch (2017)

Table 6.1 *(a) Bulk composition of sample 18XC10; (b) Bulk composition of garnet-clinopyroxenites from Bloch (2017).*

A more detailed discussion will be focused only on sample 18XC10 and 18XC20, without considering 18XC1. This because the former two present textures and characteristics which permitted to make some hypotheses on their genesis.

Mafic Grt-Cpx-bearing xenoliths containing melt inclusions in the garnet can develop in the lower crust either by (fractional) crystallization of basaltic-andesitic melts (igneous-cumulate origin) (Fig. 6.3 point a) at high pressure conditions (Alonso-Perez et al., 2009; Bloch et al., 2017), or by partial melting of mafic rocks (anatectic origin) (Fig. 6.3 point b), leaving a garnet-bearing granulitic residuum at the base of the arc (Atherton & Petford, 1993) (Fig. 6.3). Observing the studied xenoliths, it is not possible to establish a single context of formation. Indeed, sample 18XC10 shows some typical features related to anatexis, whereas in sample 18XC20 some characteristics of a magmatic origin are present.

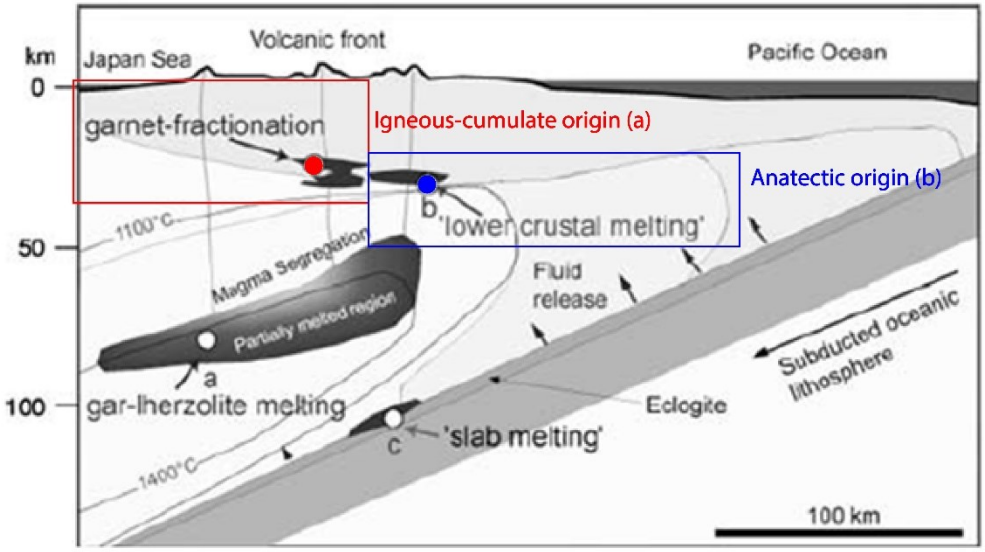

Figure 6.3 *Potential localities/ process where garnet could be involved in the genesis of andesitic magma at convergent-plate margins. Modified from Alonso-Perez (2009).*

6.2 Origin of sample 18XC10

Sample 18XC10 presents this mineral assemblage: Grt – Cpx – Pl and few Amp and Qz. Garnets from this sample contain primary MI with rhyolitic composition, and inside garnet is possible to find some inclusions of Qz (Fig. 6.4), a mineral which is not observed in the rock matrix. All evidences mentioned before, suggest an anatectic genesis for sample 18XC10.

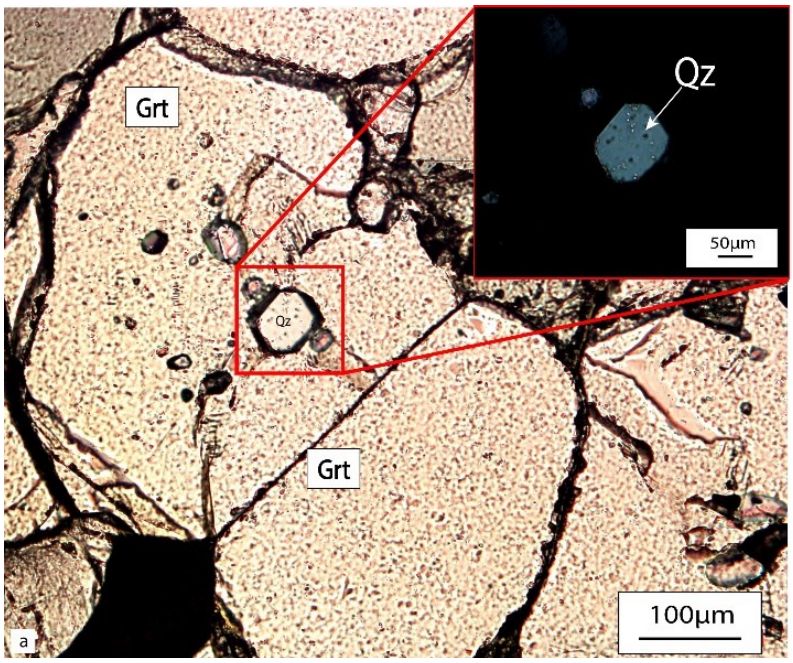

Figure 6.4 *Garnet from sample 18XC10 with inclusions of Qz under PPL and XPL.*

Due to the abundance of garnets and clinopyroxenes in this xenolith, sample 18XC10 can be defined as a mafic granulite (e.g. Griffin et al. 1990).

In fact, the mineral assemblage of granulite is generally represented by clinopyroxene + orthopyroxene + garnet + feldspar + quartz ± hornblende (Wolf & Wyllie, 1993) with a low content of hydrous minerals.

The sample 18XC10 could be the product of the partial melting of an amphibolitic precursor (plagioclase + hornblende + quartz), favored by the dehydration of Amp, which after the segregation of melt permitted the formation of a mafic granulite restite (Wolf & Wyllie, 1993). Palin et al. (2016) have shown that only for low degrees of partial melting, the silica trend in the melt produced from the anatexis of an amphibolite is strongly acidic. This might possibly explain the rhyolitic composition in the MI entrapped in the garnets of 18XC10, as well as the occurrence of Qz only as inclusions in Grt: the Qz present in the protolith completely reacted out during melting, and was preserved only as inclusion in the garnet core that formed in the early melting stages as attested by the presence of primary MI.

The presence of hydrous phases in the lower continental crust is fundamental to permitted partial melting. Indeed, anatexis in the lower crust occurs mainly by dehydration-melting, during which H_2O from dissociating hydrous minerals dissolves directly into a H_2O-undersatured silicate liquid (Wolf & Wyllie, 1994).

The presence of amphibolite in the lower crust is linked to the metamorphism of mafic rocks with basaltic-andesitic composition, directly produced in arc itself. Indeed, if these mafic rocks, due to the development and the growth of the arc, reach higher temperatures and pressures, they could be metamorphosed to amphibolites. When the partial melting of these amphibolites occurs, new peritectic phases can appear. For example, garnet tends to be stable at pressures > 0,95 GPa, and the appearance of garnet coincides with the loss of orthopyroxene. If pressure continues to increase the final mineral assemblage will be orthopyroxene-free (Fig.

6.5) (Palin et al., 2016). Garnet tends to remain stable in a wide range of temperature excess of 750°C (at 1,2 GPa).

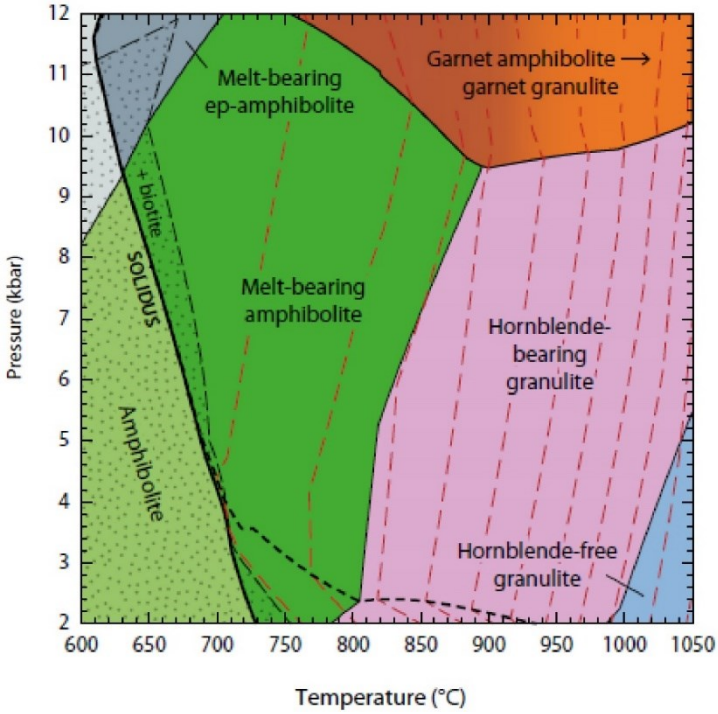

Figure 6.5 *Calculated P-T pseudosection for the MORB bulk composition showing equilibrium phases assemblage for modal proportion of melt. From Palin et. al (2016).*

The final and complete mineral assemblage of sample 18XC10, can be explained quantitatively through Fig. 6.6, which represents how the composition of an amphibolite with tholeiitic composition changes during a partial melting process increasing the temperature at a fixed pressure value of 1,2 GPa. With increasing temperature and melting degree, the partial melt generally becomes richer in Al_2O_3, CaO, MgO and FeO, and poorer in SiO_2, K_2O and Na_2O (Palin et al., 2016). These means that for producing melt with high silica content, as in sample 18XC10, low to medium degrees of melting are required, in this case is about 20-40 mol% melt for T > 900°C (Palin et al., 2016). The final composition of the residue is strongly dependent on the H_2O content of the precursor rock and, for amphibolite at 1,2 GPa, Palin et al. (2016) have estimated that ~7 mol% of H_2O is needed to saturate solidus. Although the H_2O content in the studied MI has not been quantified, the EMPA totals indicate that a significant amount of H_2O is dissolved in the melt and that this amount may possibly range between ~1 and 3 wt.% (see appendix). This may therefore corroborate the hypothesis that sample 18XC10 originated from fluid-absent melting of a hydrous mafic precursor (amphibolite).

Considering temperatures between 920 and 1000°C (Fig. 6.6), which are quite similar to the temperatures obtained by the geothermometry for this sample, it is possible to see that together with the liquid also Grt + Pl + Cpx + Amp + Rt + Qz (only al lower temperature) are present.

At T=1000°C, the residue is represented by a garnet granulite (Palin et al., 2016), which is consistent with the mineral assemblage observed for 18XC10. The only difference with the

assemblage described by Palin et al. (2016) with respect to the sample 18XC10, concerns the amount of Amp, which is quite larger (~8%) in respect to the 2% contained in 18XC10, but in both cases it is thought to represent the residumm of the amphibolitic precursor.

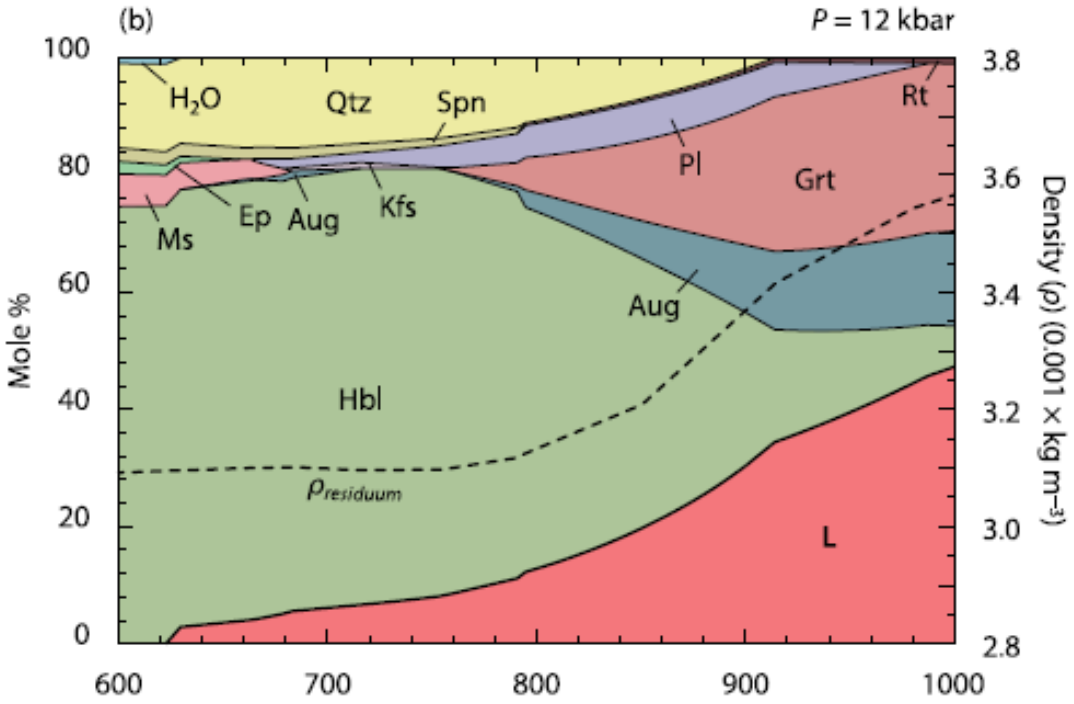

Figure 6.6 *Calculated phase assemblage for the tholeiite bulk composition metamorphosed at 1,2 GPa. From Palin et al. (2016).*

Furthermore, in terms of P-T conditions, the values obtained for the xenolith 18XC10 at a pressure of about 1,5 GPa, range from 974 –1035 °C. These temperatures are in agreement with the values reported by Weber et al. (2002) for the granulite-facies rocks located in the lower crust of Mercaderes, which are 950-1050°C at 1,3 – 1,5 GPa.

6.3 Origin of sample 18XC20

Sample 18XC20 presents MI with an intermediate composition, mostly between dacite and trachyandesite, with some minor rhyolites. In this case, Qz is not present in the mineral assemblage. Some crystals, such as plagioclase, exhibit euhedral faces (Fig. 6.7) and Cpx in this section has lobated/resorbed shapes, suggesting that they may have crystallized from a melt. All these evidences can be defined as characteristic features of a cumulate texture.

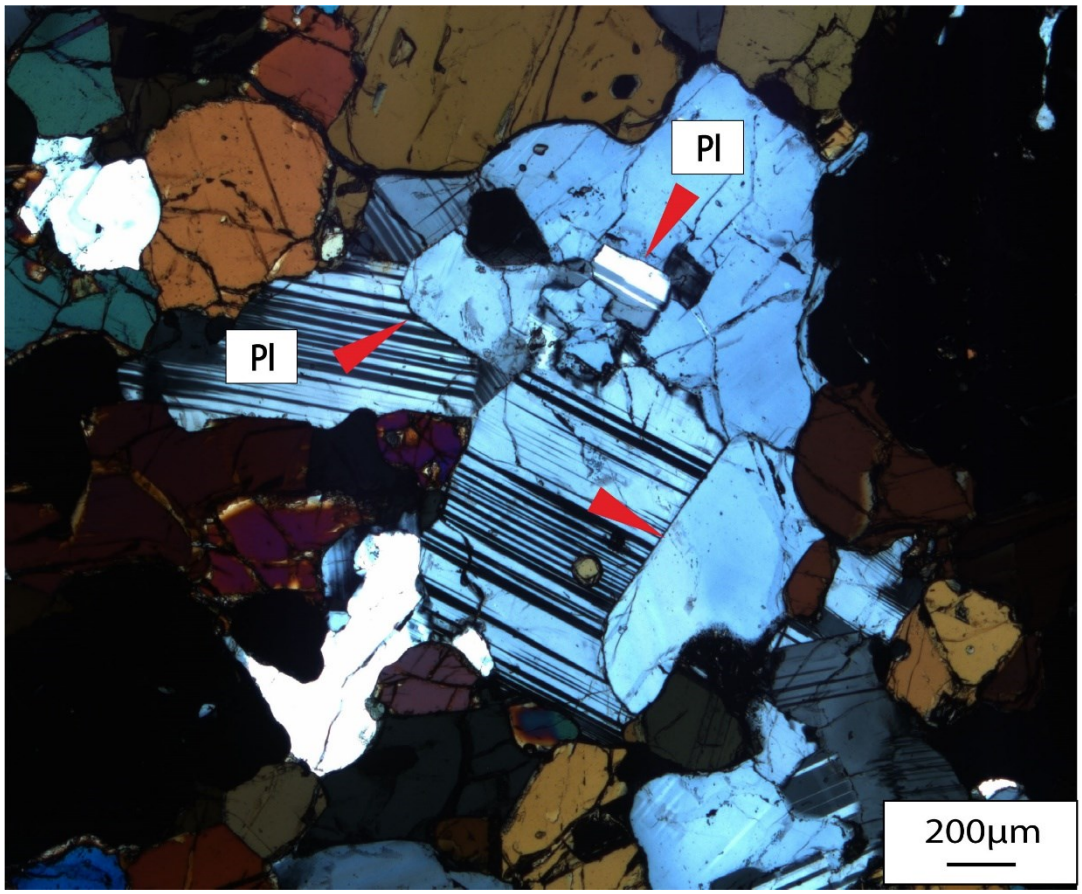

Figure 6.7 *Plagioclase under XPL where the red arrows display the euhedral faces in some crystals from sample 18XC20.*

Sample 18XC20 has this mineral assemblage: Amp (very abundant) + Grt + Cpx ± Pl, resembling the rocks defined by Weber et al. (2002) as garnet-pyroxene hornblendites. A striking difference is represented by the fact that the sample 18XC20 exhibits an evident cumulate texture, while Weber et al. (2002) do not report such texture in their xenoliths.

As mentioned above, the Amp represents the main phase in sample 18XC20, but it does not display a homogeneous chemical composition.

As reported in the Harker diagrams (Fig. 6.8) the Amp inclusions inside garnet tends to deviate in terms of major elements as Al_2O_3-CaO-FeO-MgO-Na_2O-K_2O-Ti_2O and X_{Mg} from the other ones present inside the matrix or in clinopyroxenes.

Indeed, Amp in the matrix and in clinopyroxenes describe a well-defined cluster, and for each element they tend to show the same chemical composition.

A possible hypothesis which can explain this discrepancy between the Amp inside the Grt and those in the matrix and clinopyroxenes, could be probably linked by the different origin. For example, the inclusions inside the garnet could represent relicts of early fractionated amphiboles, whereas the Amp in the matrix and Cpx could be formed later in the fractionation sequence.

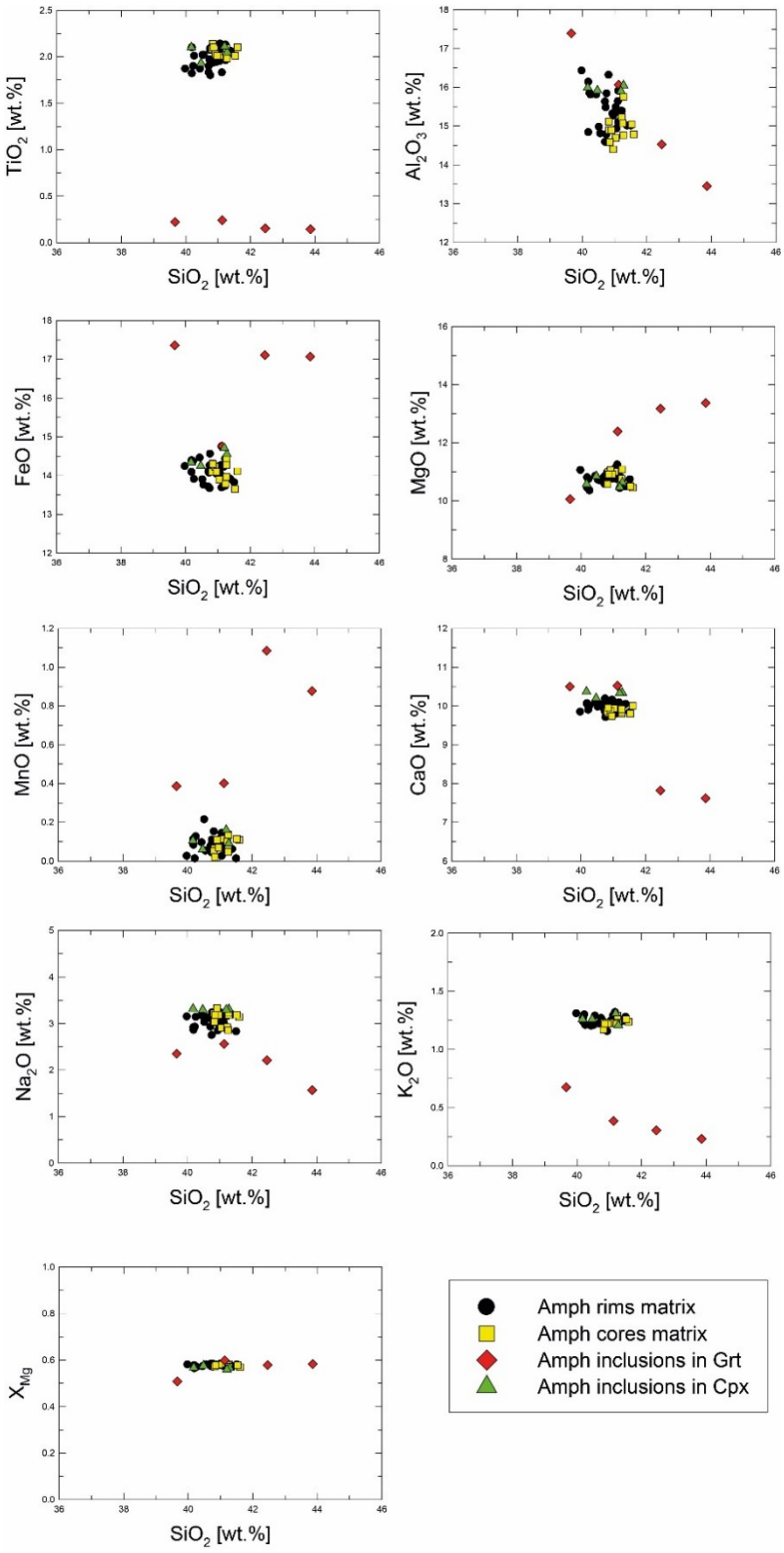

Figure 6.8 *Harker diagram of different Amp in the sample 18XC20.*

The mineral assemblage of sample 18XC20 may be related to the H_2O content of the liquid during the igneous crystallization of the magmatic arc. Indeed, increasing the H_2O concentration in the liquid, the crystallization sequence can change, leading to the crystallization of amphibole and garnet, and delaying the crystallization of plagioclase (Müntener et al., 2001).

Magmatic garnet was found in andesitic to dacitic calc-alkaline volcanics, and its fractionation and crystallization at high-pressure at a depth of 25-45 km can influence in several ways the production of these kinds of lavas.

Considering pressure of about 1,2 GPa, garnet represents the most stable phase together with clinopyroxene under low H_2O contents in the liquid, whereas for considerable H_2O content (8 wt.%) the amount of amphibole becomes larger than that of garnet, which is progressively reduced (Fig. 6.9) and the liquidus temperature decreases significantly. This situation can be mirrored by the larger amount of Amp than Grt observed in 18XC20 (Alonso-Perez et. al 2009).

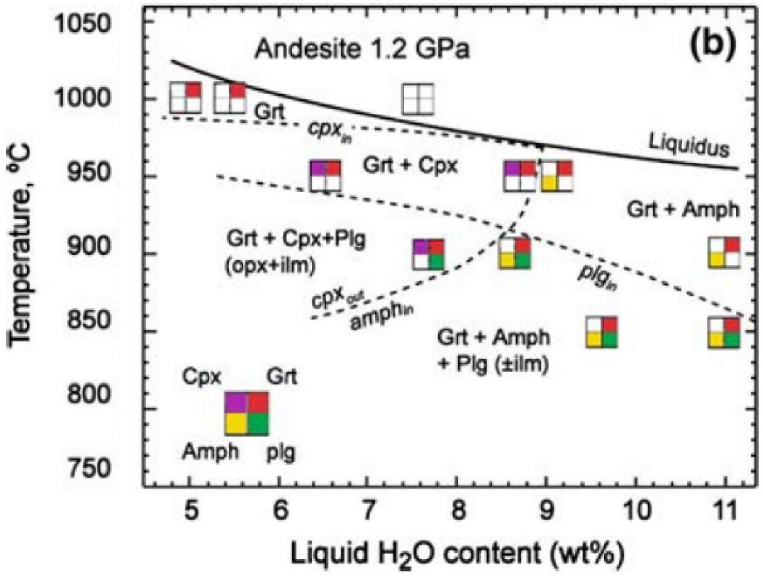

Figure 6.9 *Isobaric T-X (H_2O) phase diagram for andesitic liquids at 1,2 GPa from Alonso et al. (2009).*

This means that if we consider a volcanic arc or the lower crust setting and the melts which are produced in this context, which range from basaltic to andesitic, their composition in terms of major and minor elements, could be modified due to the fraction of the igneous garnet and amphibole (Alonso-Perez et al., 2009). Consequently, the sample 18XC20 could represent a high-pressure cumulate which ponded at the base of the arc and that has been derived from Grt/Hbl fractionation of a hydrous basalt or basaltic andesite (Fig. 6.10) (Lee et. al 2006). The cumulate hypothesis could therefore explain the magmatic texture found in the xenolith.

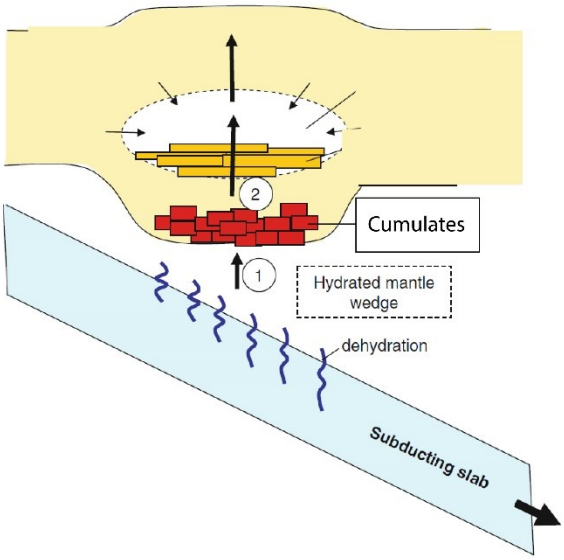

Figure 6.10 *Schematic diagram which shows the cumulate formations (2) starting from the rise up of hydrous basalt or basaltic andesites generated by the wet mantle wedge (1). Modified from Lee (2006).*

It has to be stressed that the pressure considered by Alonso-Perez et al. (2009) is about 1,2 GPa, which does not reflect entirely the pressure (1,5 GPa) considered in this thesis work for geothermometry. Nevertheless, in all literature experiments, 1,2 GPa is considered as the reference value to describe the pressure conditions of the lower crust in a volcanic arc. Despite this difference, a cumulate origin can explain the genesis and the mineral assemblage of the xenolith 18XC20 in a reasonable way.

6.4 Final considerations about the studied xenoliths

In the lower crust of a continental arc, melts with different compositions can be present. These different compositions affect in several ways the evolution and the maturation of the arc itself. The studied melts, contain a significant content of H_2O, which is a key parameter to understand the rock-forming processes occurring above a subducting slab.

Considering the MI of sample 18XC10 and 18XC20, they have a different composition, respectively rhyolitic and trachydacitic-dacitic. This can be explained through to the different processes which have permitted the genesis of both xenoliths. Indeed, the entrapped melt of 18XC20 could derived from a magmatic evolution process, whereas the melt of sample 18XC10 is linked to an anatectic context.

In the lower crust of a continental arc, the Grt-rich cumulates such as those studied in this thesis can have higher density (> 3.5 g/cm^3) than the mantle or the subcontinental lithosphere (3.3 g/cm^3). In this way these negatively buoyant crustal cumulates tend to sink (crustal-delamination process). Conditions for cumulates formation appear to be common in the lower crust and the delamination process could take place at the base of volcanic arcs as in the Mercaderes context (Bloch et al., 2017). The delamination process is very important, because it can affect the composition of the lower arc crust itself but also represents an important mechanism to introduce water in the mantle (Wolf & Wyllie, 1993).

The density reversal is not related only to magmatic xenoliths, but also the anatectic ones, and also in the metasedimentary deep crust. An example of the latter one is represented by the Ulten Zone (UZ) where the HP anatexis of metapelites formed Grt-Ky-rich residual rocks with a density of about 3.7 g/cm^3. This high density may have caused the delamination process in which continental material was involved the Variscan Orogen (Braga et al., 2007).

After these considerations, and resuming the genesis of the studied samples, we can conclude that they can represent portions of these garnet-clinopyroxene-bearing granulites which derived from magmas ponding in the lower crustal zone, or from their subsequent reworking and anatexis. These witnesses of the lower crust were brought up to the surface through the volcanic activity, before they may sink in the mantle by delamination. This hypothesis in agreement with the interpretations of Bloch et al. (2017), who suggested that the Mercaderes xenoliths represent the youngest lower-crustal record of the lithospheric foundering from a thick continental arc.

Chapter 7 - CONCLUSION AND OUTLOOK

7.1 Conclusion

This work has permitted for the first time to study the MI contained in the lower crustal xenoliths from the Mercaderes – Rio Mayo Zone.

These MI are mainly located inside garnets, and were trapped both during melt-consuming (igneous regime) and melt-producing melting (anatexis regime) processes.

This study on MI from Mercaderes aimed to understand and determine the petrographic features, and the chemical composition of these xenoliths and of the MI inside them.

A detailed study with SEM on MI was done, which has permitted to investigate also the intergranular melts and some remains of lava from the Granatifera Tuff, as well as the nanocrystals inside the MI. The composition of nano-crystals is still unknown, due to their small dimensions that prevented their analysis at the microprobe, but they are most likely magnetite or ilmenite. An interesting point is represented by the fact that in some cases these nanocrystals affect the analyses of MI, altering significantly the concentration of some elements (i.e. FeO – MgO - Na_2O - CaO) in the residual glass.

The composition of MI varies among samples, and the silica content increases considerably from sample 18XC1 (57-64 wt.%) to 18XC10 (69-75 wt.%), while intermediate values (61-72 wt.%) are observed in 18XC20.

Classifying these xenoliths has been quite difficult and still uncertain, because their origin (cumulate vs. residue) is texturally complex to interpret, and because their mineralogical composition deviates from the classical parameters which would have permitted to classify them as garnet-clinopyroxenite or clinopyroxene-bearing garnetite. For these reasons only two sample (18XC10 – 18XC20) were classified and named. 18XC10 is interpreted as a granulite, whereas 18XC20 is a garnet-pyroxene hornblendite.

The temperature of equilibration of the three samples has been determined by applying the Grt-Cpx exchange thermometer of Nakamura (2009).

At the reference pressure of 1,5 GPa, value which represents the pressure conditions of the lower crust, at the base of the Andes, the temperature tends to decrease from sample 18XC1 (1229-1291°C), through 18XC20 (1089-1099 °C), to 18XC10 (974-1035 °C).

The dependence of this thermometer with the pressure is elevated, and for this reason a more accurate temperature interval will be obtained only after the determination of a well-constrained pressure.

7.2 Outlook

This thesis leaves several interesting questions open for future research. Some of them are of relevance for a better understanding of general petrological processes. Some others for refining our knowledge of the geological and geodynamic evolution of the Mercaderes area. Here are some possible follow-ups.

- As reported in Chapter 6, the genesis of sample 18XC10 is linked to an anatectic context. To obtain more detailed information about its formation conditions, it is important to constrain the pressure of equilibration of this xenolith. In this respect it could be very useful to apply Raman-based elastic geobarometry on the Qz inclusions in Grt. In this way, it would be possible to determine how the pressure evolve during metamorphic growth in garnet crystals. The quartz inclusions in garnet preserve a record of the pressure of the host growth, allowing detailed reconstruction of the metamorphic condition of the rock itself (Ashley et al., 2014).

- In order to clarify the mantle vs. crustal origin of some xenoliths, and therefore their provenance within the geological column above a subduction zone, the bulk rock and the single minerals of the xenoliths could be investigated by an isotopic survey of their Sr – Nd – Pb contents. This geochemical approach makes possible to understand if they present also a mantle signature.

- The peculiarity of the studied rocks resides mainly in their abundant and well-preserved MI in several host minerals. The major element contents of these MI have been investigated here. The analyses of the trace elements in the same MI would provide further information and constrain about their origin and melting processes. For the cumulate xenoliths it could allow estimates of the composition and nature of the slab components, and constrain the thermal condition of the mantle-wedge (Portnyagin et al., 2007). For the residual anatectic xenoliths it could constrain the nature of the reactant phases now unknown, and provide data for a better understanding of the intermediate to acidic volcanism observed in the Mercaderes region. Also the direct measurement of the volatile contents (H_2O and CO_2) in the MI would provide valuable information for both attempting to constrain a volatile budget in the lower crust and evaluating the potential explosivity of the magmas in case of eruption.

Acknowledgments

Vorrei ringraziare davvero di cuore il Professore Bernardo Cesare e il Dottor Omar Gianola per la disponibilità nei mei confronti durante tutto questo percorso, per l'enorme pazienza che hanno sempre avuto nel revisionare la tesi, e per tutti i preziosi consigli che mi hanno dato durante questo percorso. Da voi ho davvero imparato molto, grazie.

Ringrazio inoltre: il Dottor Fabio Ferri che mi ha fornito i campioni per questo lavoro di tesi; il Dipartimento di Geoscienze - Università degli Studi di Padova - per l'utilizzo dei laboratori di microscopia e l'utilizzo del SEM; Andrea Risplendente - Dipartimento di Scienze della Terra Università degli Studi di Milano Statale - per l'aiuto e il supporto durante le molteplici sessioni di microsonda; il CESAC – Università degli Studi di Padova per la disponibilità e l'utilizzo del SEM.

References

Alonso-Perez, R., Müntener, O., & Ulmer, P. (2009). Igneous garnet and amphibole fractionation in the roots of island arcs: Experimental constraints on andesitic liquids. *Contributions to Mineralogy and Petrology*, *157*(4), 541–558. https://doi.org/10.1007/s00410-008-0351-8

Ashley, K. T., Caddick, M. J., Steele-Macinnis, M. J., Bodnar, R. J., & Dragovic, B. (2014). Geothermobarometric history of subduction recorded by quartz inclusions in garnet. *Geochemistry, Geophysics, Geosystems*, *15*(2), 350–360. https://doi.org/10.1002/2013GC005106

Atherton, M. P., & Petford, N. (1993). Generation of sodium-rich magmas from newly underplated basaltic crust. *Nature*. https://doi.org/10.1038/362144a0

Bartoli, O., Acosta-Vigil, A., Ferrero, S., & Cesare, B. (2016). Granitoid magmas preserved as melt inclusions in high-grade metamorphic rocks. *American Mineralogist*, *101*(7), 1543–1559. https://doi.org/10.2138/am-2016-5541CCBYNCND

Bloch, E., Ibañez-Mejia, M., Murray, K., Vervoort, J., & Müntener, O. (2017). Recent crustal foundering in the Northern Volcanic Zone of the Andean arc: Petrological insights from the roots of a modern subduction zone. *Earth and Planetary Science Letters*, *476*, 47–58. https://doi.org/10.1016/j.epsl.2017.07.041

Braga, R., Massonne, H.-J., & Morten, A. L. (2007). An early metamorphic stage for the Variscan Ulten Zone gneiss (NE Italy): evidence from mineral inclusions in kyanite. *Mineralogical Magazine*, *71*(06), 593–610. https://doi.org/10.1180/minmag.2007.071.6.593

Cembrano, J., Lavenu, A., Reynolds, P., Arancibia, G., López, G., & Sanhueza, A. (2002). Late Cenozoic transpressional ductile deformation north of the Nazca-South America-Antarctica triple junction. *Tectonophysics*, *354*(3–4), 289–314. https://doi.org/10.1016/S0040-1951(02)00388-8

Cesare, Acosta-Vigil, A., Ferrero, S., & Bartoli, O. (2011). Melt inclusions in migmatites and granulites. *Journal of the Virtual Explorer*, *38*. https://doi.org/10.3809/jvirtex.2011.00268

Cesare, B., Acosta-Vigil, A., Bartoli, O., & Ferrero, S. (2015). What can we learn from melt inclusions in migmatites and granulites? *Lithos*, *239*, 186–216. https://doi.org/10.1016/j.lithos.2015.09.028

Cesare, Bernardo, Ferrero, S., Salvioli-Mariani, E., Pedron, D., & Cavallo, A. (2009). "Nanogranite" and glassy inclusions: The anatectic melt in migmatites and granulites. *Geology*, *37*(7), 627–630. https://doi.org/10.1130/G25759A.1

Daly, C. (1989). Correlations between Nazca/Farallon plate kinematics and forearc basin evolution in ecuador. *Tectonics*, 8(4), 769–790.

Frezzotti, M. L. (2001). Silicate-melt inclusions in magmatic rocks: Applications to petrology. *Lithos*, *55*(1–4), 273–299. https://doi.org/10.1016/S0024-4937(00)00048-7

Goldstein, R. H. (2003). Petrographic analysis of fluid inclusions. *Fluid Inclusions-Analysis and Interpretation*, *32*(April), 9–54.

Jaillard, E., Hérail, G., Monfret, T., Diaz-Martinez, E., Baby, P., Lavenu, A., & Dumont, J. F. (2000). Tectonic evolution of the Andes of Ecuador, Peru, Bolivia and Northernmost Chile. In Tectonic evolution of South America (Cordani, U.; Milani, E.; Thomaz Filho, A.; Campos; D.; editors). *International Geological Congress : . Río de Janeiro.*, *31*(January), 481–559.

Kelemen, P. B., Rilling, J. L., Parmentier, E. M., Mehl, L., & Hacker, B. R. (2004). Thermal structure due to solid-state flow in the mantle wedge beneath arcs. *Geophysical Monograph Series*, *138*, 293–311. https://doi.org/10.1029/138GM13

Lee, C. T. A., Cheng, X., & Horodyskyj, U. (2006). The development and refinement of continental arcs by primary basaltic magmatism, garnet pyroxenite accumulation, basaltic recharge and delamination: Insights from the Sierra Nevada, California. *Contributions to Mineralogy and Petrology*, *151*(2), 222–242. https://doi.org/10.1007/s00410-005-0056-1

Manley, C. R. (1996). Morphology and maturation of melt inclusions in quartz phenocrysts from the Badlands rhyolite lava flow, southwestern Idaho. *American Mineralogist*. https://doi.org/10.2138/am-1996-1-220

Marín-Cerón, M. I., Leal-Mejía, H., Bernet, M., & Mesa-García, J. (2019). Late Cenozoic to modern-day volcanism in the Northern Andes: A geochronological, petrographical, and geochemical review. In *Frontiers in Earth Sciences*. https://doi.org/10.1007/978-3-319-76132-9_8

Marriner, G. F., & Millward, D. (1984). The petrology and geochemistry of Cretaceous to Recent volcanism in Colombia: the magmatic history of an accretionary plate margin. *Journal of the Geological Society*. https://doi.org/10.1144/gsjgs.141.3.0473

Maya, M., & González, H. (1995). Unidades litodemicas en la Cordillera Central de Colombia. *Boletín Geológico*.

McCourt, W. J., Aspden, J. A., & Brook, M. (1984). New geological and geochronological data from the Colombian Andes: continental growth by multiple accretion. *Journal of the Geological Society*. https://doi.org/10.1144/gsjgs.141.5.0831

Meschede, M., & Barckhausen, U. (2000). *7 . P LATE T ECTONIC E VOLUTION OF THE C OCOS -N AZCA S PREADING C ENTER 1*. *170*(August).

Müntener, O., Kelemen, P. B., & Grove, T. L. (2001). The role of H2O during crystallization of primitive arc magmas under uppermost mantle conditions and genesis of igneous pyroxenites: An experimental study. *Contributions to Mineralogy and Petrology*, *141*(6), 643–658. https://doi.org/10.1007/s004100100266

Nakamura, D. (2009). A new formulation of garnet-clinopyroxene geothermometer based on accumulation and statistical analysis of a large experimental data set. *Journal of Metamorphic Geology*, *27*(7), 495–508. https://doi.org/10.1111/j.1525-1314.2009.00828.x

Palin, R. M., White, R. W., Green, E. C. R., Diener, J. F. A., Powell, R., & Holland, T. J. B. (2016). High-grade metamorphism and partial melting of basic and intermediate rocks. *Journal of Metamorphic Geology*, *34*(9), 871–892. https://doi.org/10.1111/jmg.12212

Palin, Richard M., White, R. W., & Green, E. C. R. (2016). Partial melting of metabasic rocks and the generation of tonalitic–trondhjemitic–granodioritic (TTG) crust in the Archaean: Constraints from phase equilibrium modelling. *Precambrian Research*, *287*, 73–90. https://doi.org/10.1016/j.precamres.2016.11.001

Pearson, D. G., Canil, D., & Shirey, S. B. (2003). Mantle Samples Included in Volcanic Rocks: Xenoliths and Diamonds. In *Treatise on Geochemistry*. https://doi.org/10.1016/B0-08-043751-6/02005-3

Portnyagin, M., Hoernle, K., Plechov, P., Mironov, N., & Khubunaya, S. (2007). Constraints on mantle melting and composition and nature of slab components in volcanic arcs from volatiles (H2O, S, Cl, F) and trace elements in melt inclusions from the Kamchatka Arc. *Earth and Planetary Science Letters*, *255*(1–2), 53–69.

https://doi.org/10.1016/j.epsl.2006.12.005

Poveda, E., Julià, J., Schimmel, M., & Perez-Garcia, N. (2018). Upper and Middle Crustal Velocity Structure of the Colombian Andes From Ambient Noise Tomography: Investigating Subduction-Related Magmatism in the Overriding Plate. *Journal of Geophysical Research: Solid Earth*, *123*(2), 1459–1485. https://doi.org/10.1002/2017JB014688

Rodriguez-Vargas, A., Koester, E., Mallmann, G., Conceição, R. V., Kawashita, K., & Weber, M. B. I. (2005). Mantle diversity beneath the Colombian Andes, Northern Volcanic Zone: Constraints from Sr and Nd isotopes. *Lithos*, *82*(3-4 SPEC. ISS.), 471–484. https://doi.org/10.1016/j.lithos.2004.09.027

Roedder, E. (1984). Introduction to fluid inclusions. *Reviews in Mineralogy, Volume 12: Fluid Inclusions, (Mineralogical Society of America)*.

Rudnick, R. L., & Taylor, S. R. (1987). The composition and petrogenesis of the lower crust: A xenolith study. *Journal of Geophysical Research: Solid Earth*, *92*(B13), 13981–14005. https://doi.org/10.1029/jb092ib13p13981

Rudnick, Roberta L. (1992). Xenoliths — samples of the lower continental crust. *Continental Lower Crust*, *January*, 269–316.

Stern, C. R. (2008). Holocene tephrochronology record of large explosive eruptions in the southernmost Patagonian Andes. *Bulletin of Volcanology*. https://doi.org/10.1007/s00445-007-0148-z

Sun, M. (2001). Geochemical variation among small eruptive centers in the central SVZ of the Andes: An evaluation of subduction, mantle, and crustal influences. *Doctoral Dissertation, Florida International University.*, *2001*, 316.

Van Den Kerkhof, A. M., & Hein, U. F. (2001). Fluid inclusion petrography. *Lithos*, *55*(1–4), 27–47. https://doi.org/10.1016/S0024-4937(00)00037-2

Viti, C., & Frezzotti, M. L. (2001). Transmission electron microscopy applied to fluid inclusion investigations. *Lithos*. https://doi.org/10.1016/S0024-4937(00)00042-6

Weber, M. B. I. (1998). *The Mercaderes-Rio Mayo xenoliths, Colombia: their bearing on mantle and crustal processes in the Northern Andes*. *PhD Thesis*(July).

Weber, M. B. I., Tarney, J., Kempton, P. D., & Kent, R. W. (2002). Crustal make-up of the Northern Andes: Evidence based on deep crustal xenolith suites, Mercaderes, SW Colombia. *Tectonophysics*, *345*(1–4), 49–82. https://doi.org/10.1016/S0040-1951(01)00206-2

Whitney, D. L., & Evans, B. W. (2010). Abbreviations for names of rock-forming minerals. *American Mineralogist*, *95*(1), 185–187. https://doi.org/10.2138/am.2010.3371

Winter, J. D. (2014). Classification and nomenclature of igneous rocks. In *Principles of Igneous and Metamorphic Petrology*.

Wolf, M. B., & Wyllie, P. J. (1993). Garnet growth during amphibolite anatexis: implications of a garnetiferous restite. *Journal of Geology*, *101*(3), 357–373. https://doi.org/10.1086/648229

Wolf, Michael B., & Wyllie, P. J. (1994). Dehydration-melting of amphibolite at 10 kbar: the effects of temperature and time. *Contributions to Mineralogy and Petrology*, *115*(4), 369–383. https://doi.org/10.1007/BF00320972

Appendix

In the following tables, EMP analyses of all mineral phases and for MI are reported.

For both MI and intergranular melt, after the acquisition of the data, analyses were corrected for alkali loss using different spreadsheets, anhydrous or hydrous, depending on the total closure values of each single EMPA analyses.

The analyses which present a closure value ranging from 98 to 92 were corrected using the hydrous spreadsheet using as a reference value a glass standard with known composition of 5,52 wt.% H_2O. When the closure value was less than 92, alkalis were corrected considering a standard with 10,11 wt.% of H_2O. If the closure value was > 98, the analyzed points were considered anhydrous and corrected using an anhydrous glass standard. Below is reported a summary table (Table A) which reports the correction factors for Na_2O and K_2O for the different spreadsheets.

Most of the analyzed points fall in the hydrous field with the closure value ranging from 98 to 92, and only one point exceeds 98. Correction factors for Na2O and K2O were determined analyzing the three different standards, at the same conditions as the unknown glasses, during each analytical session.

In all tables below are reported the raw data from EMPA analyses for both melt inclusions and intergranular melt.

Correction factors	Na_2O	K_2O
Hydrous (10,11 wt.% H_2O)	1,87	1,19
Hydrous (5,52 wt.% (H_2O)	1,44	1,09
Anhydrous	1,31	1,04

Table A: Correction factors for Na_2O and K_2O

MI Sample 18XC1

	MI1-Gr1	MI1-2Gr1	MI1-3Gr1	MI2-Gr1	MI3-Gr1	MI1-5Gr1	MI1-Gr6	MI1-2Gr6	MI1-3Gr6
SiO_2	57,95	58,60	56,05	62,95	62,25	56,11	59,75	60,32	61,25
TiO_2	0,53	0,48	0,60	0,32	0,41	0,56	0,14	0,18	0,13
Al_2O_3	19,45	19,28	19,20	19,43	20,65	19,04	20,23	19,10	20,25
FeO	5,73	5,07	7,51	4,08	3,28	7,48	2,49	2,71	2,57
MnO	0,23	0,17	0,28	0,11	0,09	0,18	0,03	0,05	0,00
MgO	1,50	1,34	2,18	0,80	0,60	2,14	0,52	0,76	0,56
CaO	5,49	5,45	5,35	4,47	4,59	5,34	7,57	6,90	7,62
Na_2O	2,47	2,55	2,42	2,90	3,37	2,62	2,22	2,29	2,63
K_2O	2,31	2,29	2,37	2,44	2,51	2,45	2,44	2,82	2,52
Total	95,78	95,35	96,04	97,60	97,86	96,10	95,57	95,32	97,75

MI Sample 18XC10

	MI1-Gr1t	MI3-Gr3t	MI2-Gr2t	MI1-Gr3t	MI1-Gr4t	MI1-Gr6t	MI1_2-Gr6t	MI2-Gr6t	MI1-Gr7t	MI1-Gr8t	MI2-Gr9t	MI1-Gr10t	MI1-Gr11t	MI1-Gr12t
SiO_2	71,26	71,36	73,80	71,39	73,06	73,21	71,64	73,04	71,54	72,48	68,28	72,21	71,97	70,69
TiO_2	0,41	0,44	0,34	0,44	0,21	0,40	0,48	0,54	0,51	0,38	0,44	0,34	0,35	0,27
Al_2O_3	15,26	14,93	13,76	14,76	15,12	13,50	14,22	13,57	15,98	15,87	15,82	14,00	16,70	15,80
FeO	1,96	2,78	1,65	2,52	1,05	2,74	2,87	2,78	0,95	0,71	3,36	2,85	0,71	2,68
MnO	0,06	0,00	0,00	0,04	0,02	0,00	0,00	0,06	0,04	0,14	0,04	0,04	0,01	0,00
MgO	0,53	0,92	0,55	0,84	0,06	0,97	1,04	0,86	0,20	0,03	0,94	0,74	0,00	0,81
CaO	2,53	2,23	2,22	2,24	2,60	1,96	2,07	1,97	2,71	3,07	1,99	2,17	2,27	2,20
Na_2O	3,07	2,85	2,95	2,92	2,75	2,82	3,40	3,14	3,98	4,09	3,65	2,61	6,00	3,31
K_2O	2,46	2,47	2,20	2,52	2,28	1,88	1,93	1,88	1,65	1,37	2,23	1,76	0,96	2,26
Total	97,85	98,16	97,73	97,82	97,29	97,69	97,88	98,05	97,90	98,36	97,07	96,90	99,29	98,28

	MI1-GR13t	MI1-Gr14t	MI1-Gr2	MI2-Gr2	MI1-Gr3	MI2-Gr4	MI1-Gr5	MI1-Gr6	MI2-Gr6	MI3-Gr6	MI1-Gr7	MI2-Gr8	MI3-Gr8	MI1-Gr9
SiO_2	68,21	69,89	73,45	68,93	74,07	73,20	70,49	73,04	70,72	73,19	70,07	74,75	70,07	71,66
TiO_2	0,43	0,36	0,36	0,42	0,37	0,44	0,30	0,38	0,36	0,33	0,32	0,55	0,32	0,35
Al_2O_3	14,96	15,75	13,38	16,05	13,67	13,27	15,01	13,70	14,98	13,70	15,72	14,26	16,27	16,04
FeO	2,16	3,06	2,81	3,16	2,47	2,96	2,81	2,71	3,16	2,96	2,48	0,77	1,14	1,15
MnO	0,03	0,00	0,03	0,00	0,00	0,04	0,07	0,03	0,00	0,02	0,05	0,04	0,00	0,04
MgO	0,85	0,81	0,95	1,19	0,81	1,07	0,96	0,99	1,10	0,84	0,83	0,26	0,15	0,13
CaO	1,58	1,97	1,96	2,74	1,78	2,15	2,57	1,97	2,47	2,00	2,36	3,03	4,50	3,33
Na_2O	3,30	3,08	2,86	2,92	2,84	2,77	3,09	2,98	2,95	2,87	3,48	3,26	3,60	3,28
K_2O	2,10	2,73	2,46	2,30	2,27	2,21	1,89	2,33	2,37	2,17	1,96	1,22	0,81	2,04
Total	93,98	97,94	98,40	98,08	98,45	98,39	97,46	98,37	98,38	98,31	97,65	98,31	97,15	98,37

	MI1-Gr10	MI1-Gr11	MI2-Gr12	MI1-Gr13	MI1-Gr14B	MI2-Gr14B	MI3-Gr14B	MI1-Gr15	MI1-Gr16	MI1-Gr19
SiO_2	72,16	68,88	73,18	73,32	72,89	71,17	70,38	69,53	73,04	72,68
TiO_2	0,33	0,39	0,38	0,37	0,29	0,31	0,28	0,39	0,34	0,28
Al_2O_3	16,23	15,54	13,96	13,27	14,01	16,07	15,34	15,87	14,30	13,61
FeO	0,91	2,81	2,75	2,50	2,56	2,39	2,28	3,35	3,16	2,71
MnO	0,11	0,07	0,05	0,00	0,04	0,03	0,08	0,00	0,00	0,01
MgO	0,02	0,98	0,81	0,58	0,84	0,41	0,85	0,89	0,93	0,86
CaO	3,11	2,21	2,12	1,77	2,12	2,18	2,03	3,23	2,69	2,02
Na_2O	3,77	3,82	2,92	3,04	3,29	3,83	3,77	3,05	3,00	3,05
K_2O	1,59	2,21	2,24	2,16	1,88	2,03	2,20	2,17	1,68	1,81
Total	98,58	97,03	98,69	97,16	98,12	98,67	97,53	98,86	99,33	97,37

MI Sample 18XC20

	MI1-Gr3	MI1-Gr4	MI1-2Gr4	MI1-3Gr4	MI1-Gr5	MI2-Gr5	MI2-2Gr5	MI1-Gr6	MI1-2Gr6	MI1-3Gr6	MI3-Gr7	MI1-Gr7	MI1-Gr8	MI1-2Gr8
SiO_2	65,28	63,93	64,46	64,80	64,08	60,96	60,54	69,29	69,67	70,31	66,54	62,02	65,98	65,98
TiO_2	0,15	0,18	0,15	0,16	0,27	0,71	0,77	0,26	0,19	0,17	0,30	0,42	0,28	0,33
Al_2O_3	16,25	17,00	16,73	16,82	18,32	20,60	20,78	13,45	13,30	13,94	18,41	17,91	16,72	16,40
FeO	5,58	5,13	5,16	5,25	4,30	3,05	2,77	4,79	5,21	4,81	3,67	3,57	4,67	4,85
MnO	0,07	0,08	0,22	0,16	0,16	0,18	0,12	0,26	0,19	0,05	0,04	0,04	0,19	0,20
MgO	1,08	1,40	1,44	1,37	0,84	1,63	1,56	1,32	1,39	1,25	0,64	0,95	1,10	1,05
CaO	4,67	3,63	3,69	3,70	3,45	4,37	4,65	2,31	2,26	2,28	1,72	3,74	3,07	3,22
Na_2O	2,59	3,02	3,29	3,23	3,93	3,84	3,64	2,15	2,15	2,48	3,19	4,23	3,97	3,86
K_2O	2,32	1,53	1,59	1,52	1,90	1,99	2,04	1,41	1,43	1,46	2,76	1,68	1,97	2,05
Total	98,24	96,03	96,83	97,17	97,43	97,58	97,06	95,34	95,85	96,88	97,47	94,74	98,11	98,21

	MI2-Gr8	MI1-Gr2t	MI1-2Gr2t	MI1-3Gr2t	MI1-4Gr2t	MI2-Gr2t	MI1-Gr3t	MI1-2Gr3t	MI2-Gr4	MI2-1Gr6t	MI2-2Gr6t	MI2-3Gr6t	MI2-4Gr6t	MI2-5Gr6t
SiO_2	65,94	61,50	60,61	61,56	61,21	60,96	61,22	60,72	59,78	64,74	64,67	64,49	62,55	61,58
TiO_2	0,19	0,22	0,22	0,24	0,25	0,20	0,25	0,27	0,33	0,09	0,07	0,10	0,07	0,08
Al_2O_3	17,54	18,89	18,74	19,28	18,76	17,92	17,34	17,95	19,30	18,71	19,18	18,77	18,96	19,02
FeO	4,19	3,92	4,16	3,50	3,84	4,35	3,61	3,76	3,84	1,13	1,09	1,08	3,53	4,30
MnO	0,10	0,27	0,19	0,31	0,24	0,18	0,21	0,17	0,27	0,09	0,00	0,00	0,17	0,19
MgO	0,82	1,23	1,35	1,28	1,20	0,72	1,59	1,53	0,95	0,01	0,02	0,06	0,85	0,75
CaO	3,06	3,84	3,89	3,79	3,87	3,50	3,73	3,91	3,40	4,89	4,88	4,89	3,99	3,78
Na_2O	3,98	2,47	2,99	3,11	2,81	3,30	2,64	2,42	4,55	4,37	4,02	4,19	3,75	3,96
K_2O	2,23	1,60	1,74	1,53	1,64	2,08	2,21	2,13	1,94	1,45	1,41	1,52	2,05	2,15
Total	98,26	94,08	94,15	94,74	93,93	93,33	93,12	93,10	94,55	95,58	95,62	95,20	96,09	95,95

Intergranular melt sample 18XC10

	ZONE1-1	ZONE1-2	ZONE1-3	ZONE1-2	ZONE2-2	ZONE2-3
SiO_2	69,14	68,70	73,20	69,27	69,07	70,10
TiO_2	0,22	0,25	0,17	0,38	0,48	0,44
Al_2O_3	14,00	14,39	13,22	14,54	14,35	14,75
FeO	2,98	2,49	2,73	3,11	3,13	2,86
MnO	0,10	0,04	0,19	0,08	0,14	0,13
MgO	0,63	0,51	0,52	0,61	0,67	0,70
CaO	3,19	3,60	2,81	3,51	3,55	3,52
Na_2O	2,37	2,32	2,65	2,75	2,74	2,77
K_2O	0,91	0,80	0,93	0,92	0,87	0,91
Total	94,06	93,59	96,72	95,75	95,50	97,01

Intergranular melt sample 18XC20

	MELT1	MELT2	MGR4-1	MGR4-2
SiO_2	71,44	70,31	66,51	67,53
TiO_2	0,22	0,08	0,22	0,24
Al_2O_3	14,06	14,03	15,53	16,05
FeO	3,67	4,63	5,66	6,17
MnO	0,06	0,26	0,13	0,03
MgO	0,88	1,13	1,41	1,28
CaO	2,08	2,13	3,23	3,19
Na_2O	3,47	2,29	3,12	1,68
K_2O	1,71	2,65	1,58	1,70
Total	97,76	97,92	97,52	97,94

GRT profiles sample 18XC1

GRT7	G7-1	G7-2	G7-3	G7-4	G7-5	G7-6	G7-7	G7-8	G7-9	G7-10
	Rim	Rim			Core	Core			Rim	Rim
SiO_2	39,99	40,22	40,27	40,53	40,54	40,79	39,72	40,73	40,39	40,11
TiO_2	0,13	0,13	0,11	0,15	0,15	0,14	0,14	0,13	0,13	0,14
Al_2O_3	21,50	21,82	21,93	22,51	21,95	22,37	22,26	22,17	22,47	22,81
FeO	17,52	18,27	17,69	18,62	17,86	18,19	18,12	17,94	17,54	18,00
MnO	0,07	0,28	0,14	0,15	0,15	0,18	0,14	0,18	0,15	0,15
MgO	8,33	8,81	8,92	8,56	8,69	9,14	9,41	8,84	8,68	8,44
CaO	12,77	12,10	11,61	11,55	11,47	11,59	11,44	11,57	11,94	12,23
Total	**100,44**	**101,77**	**100,85**	**102,18**	**101,04**	**102,55**	**101,49**	**101,73**	**101,36**	**102,04**
Si	3,02	3,00	3,02	3,00	3,03	3,01	2,97	3,02	3,01	2,98
Ti	0,01	0,01	0,01	0,01	0,01	0,01	0,01	0,01	0,01	0,01
Al	1,91	1,92	1,94	1,97	1,93	1,94	1,96	1,94	1,97	2,00
Fe^{2+}	1,11	1,14	1,11	1,15	1,12	1,12	1,13	1,11	1,09	1,12
Mn	0,00	0,02	0,01	0,01	0,01	0,01	0,01	0,01	0,01	0,01
Mg	0,94	0,98	1,00	0,95	0,97	1,00	1,05	0,98	0,96	0,93
Ca	1,03	0,97	0,93	0,92	0,92	0,92	0,92	0,92	0,95	0,97
Total	**8,02**	**8,03**	**8,01**	**8,01**	**8,00**	**8,02**	**8,05**	**8,00**	**8,00**	**8,02**
X_{Grs}	0,34	0,31	0,31	0,30	0,30	0,30	0,29	0,30	0,32	0,32
X_{Alm}	0,36	0,37	0,36	0,38	0,37	0,37	0,36	0,37	0,36	0,37
X_{Pyr}	0,30	0,32	0,33	0,31	0,32	0,33	0,34	0,32	0,32	0,31
X_{Sps}	0,00	0,01	0,00	0,00	0,00	0,00	0,00	0,00	0,00	0,00
X_{Mg}	0,46	0,46	0,47	0,45	0,46	0,47	0,48	0,47	0,47	0,46

GRT4	G4-1	G4-2	G4-3	G4-4	G4-5	G4-6	G4-7	G4-8	G4-9	G4-10
	Rim	Rim			Core	Core			Rim	Rim
SiO_2	39,77	40,18	39,92	40,07	41,48	41,75	40,09	40,41	40,37	40,64
TiO_2	0,12	0,14	0,16	0,11	0,12	0,15	0,15	0,13	0,10	0,13
Al_2O_3	23,03	22,88	22,68	22,68	23,25	22,21	23,22	22,96	23,24	22,99
FeO	16,96	18,20	18,28	19,60	19,35	20,58	20,57	19,90	18,99	17,62
MnO	0,23	0,10	0,14	0,16	0,18	0,09	0,14	0,03	0,04	0,14
MgO	8,25	8,56	8,68	8,10	7,62	7,37	7,49	7,55	8,43	8,05
CaO	13,32	12,19	11,65	11,51	12,03	11,40	11,28	11,58	11,61	12,62
Total	**101,92**	**102,49**	**101,70**	**102,36**	**104,29**	**103,65**	**103,08**	**102,74**	**103,00**	**102,27**
Si	2,95	2,97	2,98	2,98	3,02	3,06	2,97	2,99	2,97	3,00
Ti	0,01	0,01	0,01	0,01	0,01	0,01	0,01	0,01	0,01	0,01
Al	2,02	1,99	1,99	1,99	1,99	1,92	2,03	2,01	2,02	2,00
Fe^{2+}	1,05	1,13	1,14	1,22	1,18	1,26	1,27	1,23	1,17	1,09
Mn	0,01	0,01	0,01	0,01	0,01	0,01	0,01	0,00	0,00	0,01
Mg	0,91	0,94	0,95	0,90	0,83	0,81	0,83	0,83	0,93	0,89
Ca	1,06	0,97	0,93	0,92	0,94	0,90	0,89	0,92	0,92	1,00
Total	**8,03**	**8,02**	**8,02**	**8,02**	**7,98**	**7,97**	**8,01**	**8,00**	**8,01**	**7,99**
X_{Grs}	0,36	0,33	0,31	0,31	0,32	0,30	0,30	0,31	0,31	0,33
X_{Alm}	0,32	0,36	0,37	0,39	0,40	0,43	0,42	0,41	0,38	0,36
X_{Pyr}	0,31	0,32	0,32	0,30	0,28	0,27	0,28	0,28	0,31	0,30
X_{Sps}	0,00	0,00	0,00	0,00	0,00	0,00	0,00	0,00	0,00	0,00
X_{Mg}	0,46	0,46	0,45	0,42	0,41	0,39	0,39	0,40	0,44	0,45

GRT profiles sample 18XC5

GRT1	G1-1	G1-2	G1-3	G1-4	G1-5	G1-6	G1-7	G1-8	G1-9
	Rim				Core				Rim
SiO_2	40,22	41,12	40,70	40,67	41,01	41,26	40,60	40,81	40,86
TiO_2	0,11	0,10	0,09	0,14	0,10	0,11	0,10	0,13	0,13
Al_2O_3	19,94	23,29	23,21	23,17	23,07	23,23	22,97	23,10	23,31
FeO	**19,61**	**16,46**	**16,69**	**16,54**	**17,26**	**16,72**	**16,86**	**16,83**	**17,28**
MnO	0,35	0,21	0,35	0,24	0,33	0,33	0,26	0,32	0,28
MgO	13,09	11,62	11,33	11,48	11,90	12,11	11,96	12,46	12,52
CaO	7,44	8,91	9,02	8,64	8,64	8,50	8,23	8,06	7,76
Total	**101,01**	**101,84**	**101,63**	**101,18**	**102,45**	**102,49**	**101,13**	**101,85**	**102,33**
Si	3,01	3,00	2,99	3,00	2,99	3,00	2,99	2,98	2,97
Ti	0,01	0,01	0,01	0,01	0,01	0,01	0,01	0,01	0,01
Al	1,76	2,00	2,01	2,01	1,98	1,99	1,99	1,99	2,00
Fe^{2+}	1,23	1,00	1,02	1,02	1,05	1,02	1,04	1,03	1,05
Mn	0,02	0,01	0,02	0,02	0,02	0,02	0,02	0,02	0,02
Mg	1,46	1,26	1,24	1,26	1,29	1,31	1,31	1,36	1,36
Ca	0,60	0,70	0,71	0,68	0,67	0,66	0,65	0,63	0,60
Total	**8,10**	**8,00**	**8,00**	**7,99**	**8,02**	**8,00**	**8,01**	**8,02**	**8,02**
X_{Grs}	0,18	0,23	0,24	0,23	0,22	0,22	0,22	0,21	0,20
X_{Alm}	0,37	0,34	0,34	0,34	0,35	0,34	0,34	0,34	0,35
X_{Pyr}	0,44	0,42	0,41	0,42	0,43	0,44	0,44	0,45	0,45
X_{Sps}	0,01	0,00	0,01	0,01	0,01	0,01	0,01	0,01	0,01
X_{Mg}	0,54	0,56	0,55	0,55	0,55	0,56	0,56	0,57	0,56

GRT2	G2-1	G2-2	G2-3	G2-4	G2-5	G2-6	G2-7	G2-8	G2-9	G2-10
	Rim				Core	Core				Rim
SiO_2	40,96	43,88	41,16	41,11	40,50	40,78	40,93	40,85	40,54	40,89
TiO_2	0,10	0,03	0,03	0,12	0,13	0,10	0,09	0,10	0,06	0,14
Al_2O_3	23,24	22,40	23,04	23,13	23,53	23,03	23,28	23,41	23,29	23,51
FeO	16,39	16,55	17,04	16,86	16,73	16,34	16,94	16,51	16,59	16,64
MnO	0,27	0,13	0,21	0,19	0,28	0,24	0,30	0,30	0,26	0,25
MgO	12,60	11,87	12,81	12,28	11,69	12,13	12,14	12,30	12,37	12,38
CaO	7,30	7,46	7,91	8,25	8,22	8,53	8,45	8,16	7,80	7,73
Total	**100,99**	**102,34**	**102,26**	**102,06**	**101,25**	**101,32**	**102,19**	**101,78**	**101,00**	**101,80**
Si	3,00	3,15	2,99	2,99	2,98	2,99	2,98	2,98	2,98	2,98
Ti	0,01	0,00	0,00	0,01	0,01	0,01	0,00	0,01	0,00	0,01
Al	2,01	1,90	1,97	1,99	2,04	1,99	2,00	2,01	2,02	2,02
Fe^{2+}	1,00	0,99	1,04	1,03	1,03	1,00	1,03	1,01	1,02	1,01
Mn	0,02	0,01	0,01	0,01	0,02	0,02	0,02	0,02	0,02	0,02
Mg	1,38	1,27	1,39	1,33	1,28	1,33	1,32	1,34	1,36	1,35
Ca	0,57	0,57	0,62	0,64	0,65	0,67	0,66	0,64	0,61	0,60
Total	**7,99**	**7,90**	**8,02**	**8,01**	**8,00**	**8,01**	**8,02**	**8,01**	**8,01**	**8,00**
X_{Grs}	0,19	0,20	0,20	0,21	0,22	0,22	0,22	0,21	0,20	0,20
X_{Alm}	0,34	0,35	0,34	0,34	0,35	0,33	0,34	0,34	0,34	0,34
X_{Pyr}	0,46	0,45	0,45	0,44	0,43	0,44	0,44	0,45	0,45	0,45
X_{Sps}	0,00	0,00	0,00	0,00	0,00	0,00	0,00	0,00	0,00	0,00
X_{Mg}	0,58	0,56	0,57	0,56	0,55	0,57	0,56	0,57	0,57	0,57

GRT3	G3-1	G3-2	G3-3	G3-4	G3-5	G3-6	G3-7	G3-8	G3-9	G3-10
	Rim				Core	Core				Rim
SiO_2	41,08	40,63	40,92	41,16	40,70	40,46	40,40	41,19	40,57	40,82
TiO_2	0,10	0,15	0,08	0,16	0,13	0,07	0,14	0,11	0,14	0,06
Al_2O_3	22,99	23,05	23,31	23,38	23,60	23,13	23,06	23,31	23,01	23,12
FeO	17,01	16,68	16,62	17,08	17,40	17,15	16,60	16,57	16,69	16,82
MnO	0,28	0,31	0,28	0,23	0,31	0,21	0,25	0,18	0,16	0,32
MgO	12,25	11,64	12,09	12,33	12,54	12,09	12,16	11,79	11,88	12,16
CaO	7,90	8,63	8,04	7,93	7,84	8,00	8,43	8,50	8,46	8,02
Total	**101,78**	**101,20**	**101,45**	**102,44**	**102,62**	**101,25**	**101,23**	**101,81**	**101,01**	**101,41**
Si	3,00	2,99	2,99	2,99	2,95	2,98	2,97	3,00	2,99	2,99
Ti	0,01	0,01	0,00	0,01	0,01	0,00	0,01	0,01	0,01	0,00
Al	1,98	2,00	2,01	2,00	2,02	2,01	2,00	2,00	2,00	2,00
Fe^{2+}	1,04	1,03	1,02	1,04	1,06	1,06	1,02	1,01	1,03	1,03
Mn	0,02	0,02	0,02	0,01	0,02	0,01	0,02	0,01	0,01	0,02
Mg	1,33	1,28	1,32	1,33	1,36	1,33	1,33	1,28	1,30	1,33
Ca	0,62	0,68	0,63	0,62	0,61	0,63	0,66	0,66	0,67	0,63
Total	**8,03**	**7,99**	**8,01**	**8,02**	**8,02**	**8,01**	**8,00**	**8,00**	**8,00**	**8,01**
X_{Grs}	0,21	0,23	0,21	0,20	0,20	0,21	0,22	0,22	0,22	0,21
X_{Alm}	0,35	0,34	0,34	0,34	0,35	0,35	0,34	0,34	0,34	0,34
X_{Pyr}	0,44	0,43	0,44	0,44	0,45	0,44	0,45	0,43	0,43	0,44
X_{Sps}	0,01	0,01	0,01	0,00	0,01	0,00	0,01	0,00	0,00	0,01
X_{Mg}	0,56	0,55	0,56	0,56	0,56	0,56	0,57	0,56	0,56	0,56

GRT profiles sample 18XC6

GRT5	G5-1	G5-2	G5-3	G5-4	G5-5	G5-6	G5-7	G5-8	G5-9	G5-10
	Rim	Rim								Core
SiO_2	39,72	39,50	39,49	39,62	39,36	38,97	39,71	39,80	39,85	39,73
TiO_2	0,09	0,10	0,09	0,11	0,14	0,15	0,12	0,15	0,04	0,11
Al_2O_3	22,22	22,05	22,55	22,26	22,50	22,26	22,23	22,37	22,49	22,51
FeO	25,77	25,05	25,86	25,02	24,49	24,90	25,32	24,59	24,87	24,94
MnO	0,38	0,41	0,39	0,46	0,53	0,58	0,52	0,47	0,50	0,57
MgO	6,84	6,23	6,21	5,84	5,86	5,47	6,00	6,21	6,10	6,34
CaO	7,59	8,88	8,97	9,38	9,54	9,56	8,69	8,63	8,40	8,29
Total	**102,72**	**102,29**	**103,72**	**102,76**	**102,53**	**102,01**	**102,88**	**102,36**	**102,36**	**102,60**
Si	3,00	3,00	2,96	2,99	2,98	2,97	3,00	3,01	3,01	2,99
Ti	0,01	0,01	0,01	0,01	0,01	0,01	0,01	0,01	0,00	0,01
Al	1,97	1,97	2,00	1,98	2,01	2,00	1,98	1,99	2,00	2,00
Fe^{2+}	1,63	1,59	1,62	1,58	1,55	1,59	1,60	1,55	1,57	1,57
Mn	0,02	0,03	0,02	0,03	0,03	0,04	0,03	0,03	0,03	0,04
Mg	0,77	0,70	0,69	0,66	0,66	0,62	0,68	0,70	0,69	0,71
Ca	0,61	0,72	0,72	0,76	0,77	0,78	0,70	0,70	0,68	0,67
Total	**8,02**	**8,02**	**8,03**	**8,01**	**8,01**	**8,02**	**8,01**	**7,99**	**7,99**	**8,00**
X_{Grs}	0,20	0,24	0,24	0,25	0,26	0,26	0,23	0,23	0,23	0,22
X_{Alm}	0,54	0,52	0,53	0,52	0,51	0,52	0,53	0,52	0,53	0,53
X_{Pyr}	0,25	0,23	0,23	0,22	0,22	0,21	0,22	0,23	0,23	0,24
X_{Sps}	0,01	0,01	0,01	0,01	0,01	0,01	0,01	0,01	0,01	0,01
X_{Mg}	0,32	0,31	0,30	0,29	0,30	0,28	0,30	0,31	0,30	0,31
	G5-11	**G5-12**	**G5-13**	**G5-14**	**G5-15**	**G5-16**	**G5-17**	**G5-18**	**G5-19**	**G5-20**
	Core								Rim	Rim
SiO_2	39,65	39,81	39,69	39,45	39,48	39,01	39,77	39,82	39,75	39,52
TiO_2	0,14	0,21	0,05	0,11	0,18	0,24	0,14	0,32	0,11	0,11
Al_2O_3	22,03	21,94	22,35	21,88	22,09	22,08	21,74	22,50	22,40	22,38
FeO	26,04	25,76	25,62	25,49	25,83	25,35	24,67	25,14	24,62	25,83
MnO	0,61	0,61	0,53	0,50	0,51	0,50	0,53	0,47	0,59	0,45
MgO	6,05	5,72	5,75	5,76	5,72	5,64	5,72	6,05	6,04	6,61
CaO	8,53	8,46	8,75	8,98	9,34	8,97	9,60	8,86	8,89	7,68
Total	**103,27**	**102,67**	**102,94**	**102,26**	**103,32**	**102,00**	**102,27**	**103,34**	**102,55**	**102,70**
Si	2,99	3,02	3,00	3,00	2,98	2,98	3,02	2,99	3,00	2,99
Ti	0,01	0,01	0,00	0,01	0,01	0,01	0,01	0,02	0,01	0,01
Al	1,96	1,96	1,99	1,96	1,97	1,99	1,94	1,99	1,99	1,99
Fe^{2+}	1,64	1,63	1,62	1,62	1,63	1,62	1,57	1,58	1,55	1,63
Mn	0,04	0,04	0,03	0,03	0,03	0,03	0,03	0,03	0,04	0,03
Mg	0,68	0,65	0,65	0,65	0,64	0,64	0,65	0,68	0,68	0,74
Ca	0,69	0,69	0,71	0,73	0,76	0,73	0,78	0,71	0,72	0,62
Total	**8,03**	**7,99**	**8,01**	**8,02**	**8,02**	**8,01**	**8,00**	**8,00**	**8,00**	**8,01**
X_{Grs}	0,23	0,23	0,24	0,24	0,25	0,24	0,26	0,24	0,24	0,21
X_{Alm}	0,54	0,54	0,54	0,53	0,53	0,53	0,52	0,53	0,52	0,54
X_{Pyr}	0,22	0,22	0,22	0,21	0,21	0,21	0,21	0,23	0,23	0,25
X_{Sps}	0,01	0,01	0,01	0,01	0,01	0,01	0,01	0,01	0,01	0,01
X_{Mg}	0,29	0,28	0,29	0,29	0,28	0,28	0,29	0,30	0,30	0,31

GRT6	G6-1	G6-2	G6-3	G6-4	G6-6	G6-7	G6-8	G6-10	G6-12
	Rim	Rim						Core	Core
SiO_2	39,57	39,50	39,41	39,35	39,95	39,37	39,16	39,19	39,21
TiO_2	0,10	0,10	0,12	0,09	0,13	0,23	0,14	0,12	0,13
Al_2O_3	21,96	21,96	21,95	21,95	22,37	22,04	22,12	22,08	21,93
FeO	25,83	25,41	24,85	24,86	24,93	24,47	24,86	25,20	25,34
MnO	0,52	0,53	0,37	0,50	0,55	0,42	0,56	0,44	0,37
MgO	6,84	6,26	5,97	6,07	6,04	5,67	5,55	4,70	5,20
CaO	7,61	8,37	8,91	9,04	8,87	9,28	9,63	9,87	9,64
Total	**102,68**	**102,35**	**101,77**	**101,99**	**102,95**	**101,52**	**102,05**	**101,79**	**101,93**
Si	2,99	2,99	3,00	2,99	3,00	3,01	2,98	3,00	2,99
Ti	0,01	0,01	0,01	0,01	0,01	0,01	0,01	0,01	0,01
Al	1,95	1,96	1,97	1,97	1,98	1,98	1,98	1,99	1,97
Fe^{2+}	1,57	1,55	1,57	1,54	1,56	1,56	1,54	1,61	1,58
Mn	0,03	0,03	0,02	0,03	0,04	0,03	0,04	0,03	0,02
Mg	0,77	0,71	0,68	0,69	0,68	0,65	0,63	0,54	0,59
Ca	0,62	0,68	0,73	0,74	0,71	0,76	0,78	0,81	0,79
Total	**8,00**	**8,00**	**8,00**	**8,00**	**8,00**	**8,00**	**8,00**	**8,00**	**8,00**
X_{Grs}	0,20	0,22	0,24	0,24	0,24	0,25	0,26	0,27	0,26
X_{Alm}	0,53	0,53	0,53	0,52	0,52	0,52	0,52	0,54	0,54
X_{Pyr}	0,25	0,23	0,23	0,23	0,23	0,22	0,21	0,18	0,20
X_{Sps}	0,01	0,01	0,01	0,01	0,01	0,01	0,01	0,01	0,01
X_{Mg}	0,33	0,31	0,30	0,31	0,30	0,29	0,29	0,25	0,27

	G6-11	G6-13	G6-14	G6-16	G6-17	G6-18	G6-19	G6-20
	Core						Rim	Rim
SiO_2	38,46	38,80	39,42	39,50	39,57	39,43	39,21	39,84
TiO_2	0,14	0,15	0,07	0,09	0,10	0,36	0,16	0,11
Al_2O_3	21,84	22,51	22,00	22,53	22,41	22,50	22,33	22,23
FeO	24,75	25,69	24,13	24,71	25,16	25,07	25,21	25,93
MnO	0,62	0,44	0,36	0,39	0,41	0,40	0,45	0,46
MgO	5,16	5,48	5,08	5,62	6,01	6,05	6,48	6,80
CaO	10,02	9,87	10,15	9,56	8,95	8,80	8,29	7,59
Total	**101,27**	**103,02**	**101,45**	**102,46**	**102,73**	**102,70**	**102,33**	**103,12**
Si	2,95	2,93	3,02	2,99	2,99	2,98	2,96	2,99
Ti	0,01	0,01	0,00	0,01	0,01	0,02	0,01	0,01
Al	1,98	2,00	1,99	2,01	1,99	2,00	1,99	1,97
Fe^{2+}	1,47	1,48	1,55	1,55	1,56	1,58	1,52	1,59
Mn	0,04	0,03	0,03	0,03	0,03	0,03	0,04	0,03
Mg	0,59	0,62	0,58	0,63	0,68	0,68	0,73	0,76
Ca	0,82	0,80	0,83	0,77	0,72	0,71	0,67	0,61
Total	**8,00**	**8,01**	**8,02**	**8,01**	**8,00**	**8,00**	**8,00**	**8,01**
X_{Grs}	0,27	0,26	0,28	0,26	0,24	0,24	0,22	0,20
X_{Alm}	0,52	0,53	0,52	0,52	0,53	0,53	0,53	0,54
X_{Pyr}	0,19	0,20	0,19	0,21	0,22	0,23	0,24	0,25
X_{Sps}	0,01	0,01	0,01	0,01	0,01	0,01	0,01	0,01
X_{Mg}	0,29	0,29	0,27	0,29	0,30	0,30	0,33	0,32

GRT profiles sample 18XC10

GRT3	G3-1	G3-2	G3-3	G3-4	G3-5	G3-6	G3-7	G3-8	G3-9	G3-10
	Rim				Core	Core				Rim
SiO_2	40,05	39,85	39,23	39,98	40,04	40,11	39,48	39,95	40,33	40,61
TiO_2	0,14	0,18	0,12	0,16	0,10	0,15	0,10	0,10	0,13	0,13
Al_2O_3	23,06	23,25	22,27	22,95	22,76	22,61	22,90	23,38	23,06	22,80
FeO	20,26	20,43	20,39	20,58	20,52	20,15	19,86	20,22	20,02	20,68
MnO	0,40	0,42	0,27	0,39	0,31	0,34	0,38	0,51	0,47	0,34
MgO	11,26	10,87	10,50	10,71	10,63	10,98	10,52	10,90	10,81	10,79
CaO	6,06	6,48	6,57	6,91	6,89	6,59	6,57	6,40	6,41	6,29
Total	**101,33**	**101,80**	**99,62**	**101,78**	**101,32**	**101,14**	**100,01**	**101,65**	**101,34**	**101,68**
Si	2,97	2,96	2,98	2,97	2,98	2,99	2,97	2,96	2,99	3,01
Ti	0,01	0,01	0,01	0,01	0,01	0,01	0,01	0,01	0,01	0,01
Al	2,02	2,03	1,99	2,01	2,00	1,98	2,03	2,04	2,02	1,99
Fe^{2+}	1,26	1,27	1,29	1,28	1,28	1,26	1,25	1,25	1,24	1,28
Mn	0,03	0,03	0,02	0,02	0,02	0,02	0,02	0,03	0,03	0,02
Mg	1,25	1,20	1,19	1,18	1,18	1,22	1,18	1,20	1,20	1,19
Ca	0,48	0,52	0,53	0,55	0,55	0,53	0,53	0,51	0,51	0,50
Total	**8,01**	**8,02**	**8,02**	**8,02**	**8,02**	**8,01**	**8,01**	**8,01**	**7,99**	**7,99**
X_{Grs}	0,16	0,17	0,18	0,18	0,18	0,17	0,18	0,17	0,17	0,17
X_{Alm}	0,42	0,42	0,43	0,42	0,42	0,42	0,42	0,42	0,42	0,43
X_{Pyr}	0,41	0,40	0,39	0,39	0,39	0,40	0,40	0,40	0,40	0,40
X_{Sps}	0,01	0,01	0,01	0,01	0,01	0,01	0,01	0,01	0,01	0,01
X_{Mg}	0,50	0,49	0,48	0,48	0,48	0,49	0,49	0,49	0,49	0,48

GRT6	G6-1	G6-2	G6-3	G6-4	G6-5	G6-6	G6-7	G6-8	G6-9	G6-10
	Rim				Core	Core				Rim
SiO_2	39,20	40,02	39,95	40,07	39,69	40,11	39,62	40,22	40,12	39,67
TiO_2	0,08	0,08	0,05	0,13	0,15	0,10	0,11	0,12	0,08	0,13
Al_2O_3	22,72	22,54	23,17	22,59	23,19	22,93	23,21	23,27	23,04	22,85
FeO	20,54	20,32	20,54	20,40	20,20	20,25	20,03	20,78	20,89	20,20
MnO	0,41	0,28	0,44	0,40	0,36	0,28	0,34	0,37	0,46	0,31
MgO	11,06	10,85	10,97	11,35	11,44	10,77	11,14	11,34	11,03	11,15
CaO	6,12	6,03	6,14	6,25	6,19	6,20	6,12	6,00	6,01	6,06
Total	**100,16**	**100,22**	**101,37**	**101,23**	**101,38**	**100,67**	**100,67**	**102,35**	**101,75**	**100,59**
Si	2,95	3,00	2,97	2,98	2,95	2,99	2,96	2,96	2,97	2,97
Ti	0,00	0,00	0,00	0,01	0,01	0,01	0,01	0,01	0,00	0,01
Al	2,02	1,99	2,03	1,98	2,03	2,02	2,04	2,02	2,01	2,02
Fe^{2+}	1,29	1,28	1,28	1,27	1,25	1,26	1,25	1,28	1,29	1,26
Mn	0,03	0,02	0,03	0,02	0,02	0,02	0,02	0,02	0,03	0,02
Mg	1,24	1,21	1,22	1,26	1,27	1,20	1,24	1,24	1,22	1,24
Ca	0,49	0,48	0,49	0,50	0,49	0,50	0,49	0,47	0,48	0,49
Total	**8,03**	**8,00**	**8,01**	**8,02**	**8,03**	**7,99**	**8,01**	**8,02**	**8,02**	**8,02**
X_{Grs}	0,16	0,16	0,16	0,16	0,16	0,17	0,16	0,16	0,16	0,16
X_{Alm}	0,42	0,43	0,42	0,42	0,41	0,42	0,42	0,42	0,43	0,42
X_{Pyr}	0,41	0,41	0,40	0,41	0,42	0,40	0,41	0,41	0,40	0,41
X_{Sps}	0,01	0,01	0,01	0,01	0,01	0,01	0,01	0,01	0,01	0,01
X_{Mg}	0,49	0,49	0,49	0,50	0,50	0,49	0,50	0,49	0,48	0,50

GRT11	G11-1	G11-2	G11-3	G11-4	G11-5	G11-6	G11-7	G11-8
	Rim				Core	Core		
SiO_2	38,85	38,88	39,26	39,38	39,11	38,66	39,31	39,16
TiO_2	0,15	0,10	0,16	0,12	0,15	0,15	0,13	0,10
Al_2O_3	22,76	22,15	22,22	22,62	22,26	22,18	22,04	22,73
FeO	20,50	20,28	20,01	20,08	20,03	19,90	19,76	19,97
MnO	0,34	0,22	0,23	0,25	0,27	0,31	0,25	0,31
MgO	11,09	10,66	10,47	10,34	10,29	10,35	10,13	10,44
CaO	6,05	6,57	6,97	7,19	7,39	7,39	7,46	6,91
Total	**99,77**	**99,04**	**99,43**	**100,19**	**99,63**	**99,15**	**99,21**	**99,66**
Si	2,94	2,97	2,98	2,97	2,97	2,95	2,99	2,96
Ti	0,01	0,01	0,01	0,01	0,01	0,01	0,01	0,01
Al	2,03	1,99	1,99	2,01	1,99	2,00	1,98	2,03
Fe^{2+}	1,30	1,29	1,27	1,27	1,27	1,27	1,26	1,26
Mn	0,02	0,01	0,01	0,02	0,02	0,02	0,02	0,02
Mg	1,25	1,21	1,18	1,16	1,16	1,18	1,15	1,18
Ca	0,49	0,54	0,57	0,58	0,60	0,60	0,61	0,56
Total	**8,04**	**8,03**	**8,02**	**8,02**	**8,03**	**8,04**	**8,01**	**8,02**
X_{Grs}	0,16	0,18	0,19	0,19	0,20	0,20	0,20	0,19
X_{Alm}	0,42	0,42	0,42	0,42	0,42	0,41	0,41	0,42
X_{Pyr}	0,41	0,40	0,39	0,38	0,38	0,38	0,38	0,39
X_{Sps}	0,01	0,00	0,00	0,01	0,01	0,01	0,01	0,01
X_{Mg}	0,49	0,48	0,48	0,48	0,48	0,48	0,48	0,48

GRT14	G14-1	G14-2	G14-3	G14-4	G14-5	G14-6	G14-7	G14-8	G14-9	G14-10
	Rim	Rim						Core		
SiO_2	39,92	40,12	39,75	39,85	39,61	39,66	39,68	40,57	40,32	39,69
TiO_2	0,08	0,10	0,15	0,13	0,10	0,17	0,11	0,11	0,08	0,09
Al_2O_3	22,88	23,00	22,93	22,87	22,69	22,96	22,99	22,59	23,20	22,95
FeO	19,52	20,20	20,12	20,24	20,02	19,49	19,76	20,59	20,32	20,22
MnO	0,43	0,35	0,42	0,37	0,37	0,45	0,48	0,43	0,48	0,45
MgO	11,85	11,21	11,08	10,96	10,92	10,90	10,72	11,16	11,38	10,89
CaO	**5,98**	**6,22**	**6,29**	**6,42**	**6,64**	**6,55**	**6,58**	**6,65**	**6,47**	**6,55**
Total	**100,73**	**101,29**	**100,94**	**101,05**	**100,54**	**100,35**	**100,57**	**102,14**	**102,39**	**100,97**
Si	2,97	2,98	2,97	2,97	2,97	2,97	2,97	2,99	2,97	2,96
Ti	0,00	0,01	0,01	0,01	0,01	0,01	0,01	0,01	0,00	0,00
Al	2,01	2,01	2,02	2,01	2,01	2,03	2,03	1,96	2,01	2,02
Fe^{2+}	1,22	1,25	1,26	1,26	1,26	1,22	1,24	1,27	1,25	1,26
Mn	0,03	0,02	0,03	0,02	0,02	0,03	0,03	0,03	0,03	0,03
Mg	1,32	1,24	1,23	1,22	1,22	1,22	1,20	1,23	1,25	1,21
Ca	0,48	0,49	0,50	0,51	0,53	0,53	0,53	0,53	0,51	0,52
Total	**8,02**	**8,01**	**8,01**	**8,02**	**8,02**	**8,01**	**8,01**	**8,02**	**8,02**	**8,02**
X_{Grs}	0,16	0,16	0,17	0,17	0,18	0,18	0,18	0,17	0,17	0,17
X_{Alm}	0,40	0,42	0,42	0,42	0,41	0,41	0,41	0,42	0,41	0,42
X_{Pyr}	0,43	0,41	0,41	0,40	0,40	0,41	0,40	0,40	0,41	0,40
X_{Sps}	0,01	0,01	0,01	0,01	0,01	0,01	0,01	0,01	0,01	0,01
X_{Mg}	0,52	0,50	0,50	0,49	0,49	0,50	0,49	0,49	0,50	0,49

	G14-11	G14-12	G14-13	G14-14	G14-15
				Rim	Rim
SiO_2	39,86	40,00	40,48	40,61	39,97
TiO_2	0,11	0,07	0,10	0,15	0,09
Al_2O_3	23,26	23,47	22,84	22,73	22,78
FeO	20,48	19,80	19,84	19,69	19,85
MnO	0,45	0,39	0,38	0,47	0,36
MgO	11,15	11,03	11,42	11,35	11,03
CaO	**6,43**	**6,28**	**6,19**	**6,08**	**6,08**
Total	**101,90**	**101,13**	**101,36**	**101,20**	**100,37**
Si	2,95	2,97	3,00	3,01	2,99
Ti	0,01	0,00	0,01	0,01	0,01
Al	2,03	2,05	1,99	1,98	2,01
Fe^{2+}	1,27	1,23	1,23	1,22	1,24
Mn	0,03	0,02	0,02	0,03	0,02
Mg	1,23	1,22	1,26	1,25	1,23
Ca	0,51	0,50	0,49	0,48	0,49
Total	**8,03**	**8,00**	**8,01**	**7,99**	**8,00**
X_{Grs}	0,17	0,17	0,16	0,16	0,16
X_{Alm}	0,42	0,41	0,41	0,41	0,42
X_{Pyr}	0,41	0,41	0,42	0,42	0,41
X_{Sps}	0,01	0,01	0,01	0,01	0,01
X_{Mg}	0,49	0,50	0,51	0,51	0,50

GRT profiles sample 18XC15

GRT1	G1-1	G1-2	G1-3	G1-4	G1-5	G1-6	G1-7	G1-8	G1-9	G1-10	G1-11	G1-12	G1-13	G1-14	G1-15
	Rim	Rim						Core						Rim	Rim
SiO_2	39,78	39,88	39,09	39,86	40,04	39,48	39,93	39,80	40,19	40,13	39,47	39,55	39,52	40,11	39,63
TiO_2	0,11	0,16	0,17	0,09	0,08	0,13	0,08	0,18	0,16	0,11	0,11	0,09	0,09	0,09	0,19
Al_2O_3	21,76	22,14	21,77	21,88	22,02	22,11	21,46	21,61	21,66	22,01	21,64	21,92	22,08	21,50	21,57
FeO	20,35	20,51	21,06	21,60	21,47	21,02	21,56	22,02	21,75	21,51	21,16	21,22	20,97	20,72	20,05
MnO	0,44	0,61	0,63	0,78	0,76	0,82	0,76	0,79	0,78	0,92	0,79	0,66	0,72	0,45	0,37
MgO	8,40	8,59	8,08	8,01	7,82	8,11	7,85	8,44	7,90	8,32	8,06	8,27	8,26	8,50	8,81
CaO	9,57	9,62	9,15	8,80	8,58	8,84	8,87	8,88	8,92	8,77	8,86	8,89	9,34	9,47	9,31
Total	**100,62**	**101,68**	**100,16**	**101,04**	**101,07**	**100,67**	**100,64**	**101,84**	**101,52**	**101,88**	**100,22**	**100,83**	**101,20**	**100,99**	**99,99**
Si	3,01	2,99	2,99	3,02	3,03	3,00	3,04	3,00	3,03	3,01	3,01	3,00	2,99	3,03	3,01
Ti	0,01	0,01	0,01	0,01	0,00	0,01	0,00	0,01	0,01	0,01	0,01	0,01	0,00	0,00	0,01
Al	1,94	1,96	1,96	1,95	1,96	1,98	1,92	1,92	1,92	1,95	1,95	1,96	1,97	1,91	1,93
Fe^{2+}	1,29	1,29	1,35	1,37	1,36	1,33	1,37	1,39	1,37	1,35	1,35	1,35	1,33	1,31	1,27
Mn	0,03	0,04	0,04	0,05	0,05	0,05	0,05	0,05	0,05	0,06	0,04	0,04	0,03	0,03	0,03
Mg	0,95	0,96	0,92	0,90	0,88	0,92	0,89	0,95	0,89	0,93	0,92	0,93	0,93	0,96	1,00
Ca	0,78	0,77	0,75	0,71	0,69	0,72	0,72	0,72	0,72	0,71	0,72	0,72	0,76	0,77	0,76
Total	**8,02**	**8,02**	**8,02**	**8,00**	**7,99**	**8,01**	**8,00**	**8,04**	**8,00**	**8,01**	**8,01**	**8,02**	**8,03**	**8,01**	**8,01**
X_{Grs}	0,26	0,25	0,25	0,24	0,23	0,24	0,24	0,23	0,24	0,23	0,24	0,24	0,25	0,25	0,25
X_{Alm}	0,42	0,42	0,44	0,45	0,46	0,44	0,45	0,45	0,45	0,44	0,44	0,44	0,43	0,43	0,42
X_{Pyr}	0,31	0,31	0,30	0,30	0,30	0,30	0,29	0,31	0,29	0,31	0,30	0,31	0,30	0,31	0,33
X_{Sps}	0,01	0,01	0,01	0,02	0,02	0,02	0,02	0,02	0,02	0,02	0,02	0,01	0,02	0,01	0,01
X_{Mg}	0,42	0,43	0,41	0,40	0,39	0,41	0,39	0,41	0,39	0,41	0,40	0,41	0,41	0,42	0,44

GRT2	G2-1	G2-2	G2-3	G2-4	G2-5	G2-6	G2-8	G2-9	G2-10	G2-11	G2-12	G2-13	G2-14	G2-15	G2-16
	Rim	Rim													
SiO_2	39,81	40,10	40,46	39,57	39,69	40,17	39,84	39,84	40,12	39,89	39,35	39,37	39,48	39,33	39,64
TiO_2	0,09	0,16	0,11	0,16	0,11	0,15	0,10	0,13	0,15	0,17	0,18	0,16	0,20	0,14	0,12
Al_2O_3	22,49	22,51	22,05	23,15	22,46	22,39	22,58	22,06	22,04	22,41	22,08	22,30	22,22	22,30	22,48
FeO	19,66	18,94	19,78	19,91	20,21	19,89	20,96	21,18	21,51	21,54	22,04	22,24	22,60	22,22	22,61
MnO	0,43	0,29	0,30	0,40	0,37	0,57	0,43	0,83	0,78	0,69	0,84	0,90	0,81	0,87	0,95
MgO	8,74	8,41	8,32	8,59	8,16	8,40	8,39	8,08	8,24	7,78	7,83	7,85	7,64	7,90	7,50
CaO	9,46	10,36	10,36	10,25	10,23	9,41	9,48	9,17	8,98	8,73	8,62	8,50	8,51	8,55	8,46
Total	**100,76**	**101,09**	**101,61**	**102,26**	**101,36**	**101,22**	**101,94**	**101,43**	**101,90**	**101,27**	**101,22**	**101,43**	**101,71**	**101,46**	**101,88**
Si	3,00	3,01	3,03	2,95	2,98	3,01	2,98	3,00	3,01	3,01	2,98	2,98	2,98	2,98	2,99
Ti	0,00	0,01	0,01	0,01	0,01	0,01	0,01	0,01	0,01	0,01	0,01	0,01	0,01	0,01	0,01
Al	1,99	1,99	1,94	2,03	1,99	1,98	1,99	1,96	1,95	1,99	1,97	1,99	1,98	1,99	2,00
Fe^{2+}	1,24	1,19	1,24	1,24	1,27	1,25	1,31	1,34	1,35	1,36	1,40	1,41	1,43	1,41	1,42
Mn	0,03	0,02	0,02	0,03	0,02	0,04	0,03	0,05	0,05	0,04	0,05	0,06	0,05	0,06	0,06
Mg	0,98	0,94	0,93	0,95	0,91	0,94	0,94	0,91	0,92	0,87	0,89	0,89	0,86	0,89	0,84
Ca	0,76	0,83	0,83	0,82	0,82	0,76	0,76	0,74	0,72	0,70	0,70	0,69	0,69	0,69	0,68
Total	**8,00**	**7,99**	**8,00**	**8,03**	**8,02**	**7,99**	**8,02**	**8,01**	**8,01**	**7,99**	**8,02**	**8,02**	**8,02**	**8,02**	**8,01**
X_{Grs}	0,25	0,28	0,28	0,27	0,27	0,25	0,25	0,24	0,24	0,24	0,23	0,23	0,23	0,23	0,23
X_{Alm}	0,41	0,40	0,41	0,41	0,42	0,42	0,43	0,44	0,44	0,46	0,46	0,46	0,47	0,46	0,47
X_{Pyr}	0,33	0,32	0,31	0,31	0,30	0,32	0,31	0,30	0,30	0,29	0,29	0,29	0,28	0,29	0,28
X_{Sps}	0,01	0,01	0,01	0,01	0,01	0,01	0,01	0,02	0,02	0,01	0,02	0,02	0,02	0,02	0,02
X_{Mg}	0,44	0,44	0,43	0,43	0,42	0,43	0,42	0,40	0,41	0,39	0,39	0,39	0,38	0,39	0,37

	G2-17	G2-18	G2-19	G2-20	G2-21	G2-22	G2-23	G2-24	G2-25	G2-26	G2-27	G2-28	G2-29	G2-30	G2-31
					Core	Core									
SiO_2	39,60	39,40	39,17	39,86	39,47	39,40	40,09	39,66	39,27	39,51	39,40	39,85	39,05	39,56	39,65
TiO_2	0,12	0,13	0,17	0,11	0,13	0,13	0,16	0,08	0,16	0,21	0,12	0,16	0,12	0,16	0,16
Al_2O_3	22,22	22,14	21,99	22,00	22,02	21,72	21,75	22,55	22,60	21,94	21,81	22,35	22,15	22,17	22,47
FeO	22,06	22,95	23,21	22,56	23,36	22,94	22,53	22,36	22,90	23,04	23,53	22,69	23,15	23,13	22,72
MnO	1,03	0,96	0,96	1,05	0,86	1,01	1,02	1,10	0,93	0,95	1,11	1,03	1,07	0,93	1,11
MgO	7,47	7,38	7,48	7,49	7,22	7,36	7,65	7,38	7,30	7,37	7,78	7,43	7,33	7,13	7,40
CaO	8,65	8,50	8,44	8,38	8,29	8,36	8,29	8,19	8,26	8,36	8,41	8,34	8,32	8,27	8,18
Total	**101,28**	**101,51**	**101,66**	**101,60**	**101,50**	**100,99**	**101,60**	**101,44**	**101,61**	**101,73**	**102,31**	**102,02**	**101,30**	**101,39**	**101,93**
Si	3,00	2,99	2,98	3,01	3,00	3,00	3,03	3,00	2,97	3,00	2,98	3,00	2,97	3,00	2,99
Ti	0,01	0,01	0,01	0,01	0,01	0,01	0,01	0,00	0,01	0,01	0,01	0,01	0,01	0,01	0,01
Al	1,98	1,98	1,97	1,96	1,97	1,95	1,94	2,01	2,02	1,96	1,94	1,98	1,99	1,98	2,00
Fe^{2+}	1,40	1,46	1,48	1,43	1,48	1,46	1,42	1,41	1,45	1,46	1,49	1,43	1,47	1,47	1,43
Mn	0,07	0,06	0,06	0,07	0,06	0,07	0,07	0,07	0,06	0,06	0,07	0,07	0,07	0,06	0,07
Mg	0,84	0,83	0,85	0,84	0,82	0,84	0,86	0,83	0,82	0,83	0,88	0,83	0,83	0,81	0,83
Ca	0,70	0,69	0,69	0,68	0,67	0,68	0,67	0,66	0,67	0,68	0,68	0,67	0,68	0,67	0,66
Total	**8,00**	**8,02**	**8,03**	**8,00**	**8,02**	**8,02**	**8,00**	**7,99**	**8,01**	**8,02**	**8,04**	**8,00**	**8,02**	**8,00**	**8,01**
X_{Grs}	0,23	0,23	0,22	0,23	0,22	0,22	0,22	0,22	0,22	0,22	0,22	0,22	0,22	0,22	0,22
X_{Alm}	0,46	0,48	0,48	0,47	0,49	0,48	0,47	0,47	0,48	0,48	0,48	0,48	0,48	0,49	0,48
X_{Pyr}	0,28	0,27	0,28	0,28	0,27	0,27	0,29	0,28	0,27	0,27	0,28	0,28	0,27	0,27	0,28
X_{Sps}	0,02	0,02	0,02	0,02	0,02	0,02	0,02	0,02	0,02	0,02	0,02	0,02	0,02	0,02	0,02
X_{Mg}	0,38	0,36	0,36	0,37	0,36	0,36	0,38	0,37	0,36	0,36	0,37	0,37	0,36	0,35	0,37

	G2-32	G2-33	G2-34	G2-35	G2-36	G2-37	G2-38	G2-39	G2-40
								Rim	Rim
SiO_2	39,98	40,12	39,90	39,71	39,94	39,68	40,27	40,07	39,20
TiO_2	0,14	0,15	0,13	0,09	0,15	0,08	0,08	0,12	0,10
Al_2O_3	21,84	21,96	22,48	22,48	22,64	22,40	22,91	22,61	23,01
FeO	22,93	23,16	22,59	22,01	21,71	20,59	20,60	20,70	20,13
MnO	0,90	0,81	0,79	0,73	0,56	0,50	0,50	0,51	0,50
MgO	7,46	8,09	7,76	8,06	8,17	8,39	8,28	8,73	8,51
CaO	8,24	8,09	8,12	8,01	8,51	8,58	9,30	9,26	9,46
Total	**101,66**	**102,43**	**101,98**	**101,28**	**101,81**	**100,33**	**102,14**	**102,18**	**100,94**
Si	3,02	3,01	3,00	3,00	2,99	3,01	3,00	2,99	2,95
Ti	0,01	0,01	0,01	0,01	0,01	0,00	0,00	0,01	0,01
Al	1,95	1,94	1,99	2,00	2,00	2,00	2,01	1,99	2,04
Fe^{2+}	1,45	1,45	1,42	1,39	1,36	1,30	1,28	1,29	1,27
Mn	0,06	0,05	0,05	0,05	0,04	0,03	0,03	0,03	0,03
Mg	0,84	0,90	0,87	0,91	0,91	0,95	0,92	0,97	0,96
Ca	0,67	0,65	0,65	0,65	0,68	0,70	0,74	0,74	0,76
Total	**8,00**	**8,02**	**8,00**	**8,00**	**8,00**	**7,99**	**7,99**	**8,02**	**8,02**
X_{Grs}	0,22	0,21	0,22	0,22	0,23	0,23	0,25	0,24	0,25
X_{Alm}	0,48	0,47	0,47	0,46	0,45	0,44	0,43	0,43	0,42
X_{Pyr}	0,28	0,30	0,29	0,30	0,31	0,32	0,31	0,32	0,32
X_{Sps}	0,02	0,02	0,02	0,02	0,01	0,01	0,01	0,01	0,01
X_{Mg}	0,37	0,38	0,38	0,39	0,40	0,42	0,42	0,43	0,43

GRT3	G3-1	G3-2	G3-3	G3-4	G3-5	G3-6	G3-7	G3-8	G3-9	G3-10	G3-11	G3-12	G3-13	G3-14	G3-15
	Rim	Rim													Core
SiO_2	40,08	39,45	40,44	39,98	39,92	39,86	39,82	40,02	40,06	40,40	40,00	39,63	40,18	39,78	39,81
TiO_2	0,12	0,12	0,11	0,11	0,15	0,10	0,08	0,13	0,19	0,11	0,13	0,11	0,18	0,17	0,08
Al_2O_3	23,10	22,90	22,35	23,23	22,75	22,41	22,82	22,35	21,90	22,03	22,45	22,30	22,42	21,93	21,90
FeO	20,47	20,25	20,84	21,13	21,59	21,52	22,55	22,06	21,77	21,61	21,55	22,06	22,51	22,13	22,39
MnO	0,47	0,58	0,49	0,47	0,68	0,74	0,57	0,80	0,81	0,73	0,93	0,87	1,04	0,99	1,13
MgO	8,81	8,43	8,53	8,55	8,39	8,21	8,16	7,54	8,10	8,09	7,75	7,88	7,58	7,66	7,30
CaO	9,25	9,35	9,17	8,91	8,51	8,45	8,38	8,51	8,51	8,49	8,76	8,64	8,43	8,90	8,78
Total	**102,44**	**101,24**	**102,02**	**102,56**	**102,07**	**101,44**	**102,58**	**101,69**	**101,53**	**101,64**	**101,77**	**101,59**	**102,49**	**101,61**	**101,49**
Si	2,97	2,97	3,01	2,97	2,98	3,00	2,97	3,01	3,02	3,03	3,00	2,99	3,01	3,00	3,01
Ti	0,01	0,01	0,01	0,01	0,01	0,01	0,00	0,01	0,01	0,01	0,01	0,01	0,01	0,01	0,00
Al	2,02	2,03	1,96	2,03	2,00	1,99	2,01	1,98	1,94	1,95	1,99	1,98	1,98	1,95	1,95
Fe^{2+}	1,27	1,27	1,30	1,31	1,35	1,35	1,41	1,39	1,37	1,36	1,35	1,39	1,41	1,40	1,42
Mn	0,03	0,04	0,03	0,03	0,04	0,05	0,04	0,05	0,05	0,05	0,06	0,06	0,07	0,06	0,07
Mg	0,97	0,94	0,95	0,95	0,93	0,92	0,91	0,85	0,91	0,91	0,87	0,89	0,85	0,86	0,82
Ca	0,73	0,75	0,73	0,71	0,68	0,68	0,67	0,69	0,69	0,68	0,71	0,70	0,68	0,72	0,71
Total	**8,01**	**8,01**	**8,00**	**8,01**	**8,01**	**8,00**	**8,02**	**7,99**	**8,00**	**7,99**	**7,99**	**8,01**	**7,99**	**8,01**	**8,01**
X_{Grs}	0,24	0,25	0,24	0,24	0,23	0,23	0,22	0,23	0,23	0,23	0,24	0,23	0,23	0,24	0,24
X_{Alm}	0,42	0,42	0,43	0,44	0,45	0,45	0,47	0,47	0,45	0,45	0,45	0,46	0,47	0,46	0,47
X_{Pyr}	0,32	0,31	0,31	0,32	0,31	0,31	0,30	0,28	0,30	0,30	0,29	0,29	0,28	0,28	0,27
X_{Sps}	0,01	0,01	0,01	0,01	0,01	0,02	0,01	0,02	0,02	0,02	0,02	0,02	0,02	0,02	0,02
X_{Mg}	0,43	0,43	0,42	0,42	0,41	0,40	0,39	0,38	0,40	0,40	0,39	0,39	0,38	0,38	0,37

	G3-16	G3-17	G3-18	G3-19	G3-20	G3-21	G3-22	G3-23	G3-24	G3-25	G3-26	G3-27	G3-28	G3-29	G3-30
	Core													**Rim**	**Rim**
SiO_2	39,89	40,15	39,78	37,91	39,91	39,96	39,30	39,76	39,41	39,81	39,98	40,10	39,57	39,90	39,94
TiO_2	0,16	0,14	0,15	0,13	0,09	0,15	0,14	0,13	0,08	0,08	0,12	0,10	0,10	0,11	0,13
Al_2O_3	22,18	22,11	22,19	22,08	22,07	21,93	22,30	22,24	22,06	22,61	22,68	22,47	22,22	22,56	22,49
FeO	23,10	22,09	21,69	22,76	22,30	21,43	21,75	21,55	21,70	21,56	21,29	20,98	21,18	20,68	19,89
MnO	1,08	1,08	1,12	1,15	1,13	0,98	0,90	0,94	0,99	0,91	0,66	0,61	0,62	0,54	0,40
MgO	7,28	7,37	7,29	7,76	7,41	7,77	7,86	7,87	8,28	8,09	8,20	8,30	8,19	8,62	8,54
CaO	8,66	8,64	8,73	8,77	8,84	8,94	9,09	8,89	9,01	9,10	9,13	9,23	9,40	9,29	9,36
Total	**102,56**	**101,71**	**101,12**	**100,88**	**101,98**	**101,29**	**101,50**	**101,50**	**101,63**	**102,29**	**102,18**	**101,85**	**101,43**	**101,88**	100,87
Si	3,00	3,02	3,01	2,92	3,01	3,02	2,97	3,00	2,97	2,98	2,99	3,00	2,98	2,98	3,00
Ti	0,01	0,01	0,01	0,01	0,00	0,01	0,01	0,01	0,00	0,00	0,01	0,01	0,01	0,01	0,01
Al	1,96	1,96	1,98	2,00	1,96	1,95	1,99	1,98	1,96	1,99	2,00	1,98	1,97	1,99	1,99
Fe^{2+}	1,45	1,39	1,37	1,46	1,41	1,35	1,37	1,36	1,37	1,35	1,33	1,31	1,34	1,29	1,25
Mn	0,07	0,07	0,07	0,07	0,07	0,06	0,06	0,06	0,06	0,06	0,04	0,04	0,04	0,03	0,03
Mg	0,82	0,83	0,82	0,89	0,83	0,88	0,89	0,88	0,93	0,90	0,91	0,93	0,92	0,96	0,96
Ca	0,70	0,70	0,71	0,72	0,71	0,72	0,74	0,72	0,73	0,73	0,73	0,74	0,76	0,74	0,75
Total	**8,01**	**7,99**	**7,99**	**8,08**	**8,01**	**8,00**	**8,03**	**8,01**	**8,04**	**8,03**	**8,01**	**8,00**	**8,03**	**8,01**	**7,99**
X_{Grs}	0,23	0,23	0,24	0,23	0,24	0,24	0,24	0,24	0,24	0,24	0,24	0,25	0,25	0,25	0,25
X_{Alm}	0,48	0,47	0,46	0,46	0,46	0,45	0,45	0,45	0,44	0,44	0,44	0,44	0,44	0,43	0,42
X_{Pyr}	0,27	0,28	0,28	0,28	0,28	0,29	0,29	0,29	0,30	0,30	0,30	0,31	0,30	0,32	0,32
X_{Sps}	0,02	0,02	0,02	0,02	0,02	0,02	0,02	0,02	0,02	0,02	0,01	0,01	0,01	0,01	0,01
X_{Mg}	0,36	0,37	0,37	0,38	0,37	0,39	0,39	0,39	0,40	0,40	0,41	0,41	0,41	0,43	0,43

GRT4	G4-1	G4-2	G4-3	G4-4	G4-5	G4-6	G4-7	G4-8	G4-9	G4-10
	Rim	**Rim**								**Core**
SiO_2	39,61	40,20	40,08	40,22	40,00	39,76	39,93	39,83	40,07	39,65
TiO_2	0,11	0,10	0,11	0,13	0,13	0,17	0,15	0,12	0,21	0,14
Al_2O_3	23,28	22,86	22,61	22,94	22,87	22,91	23,09	23,10	22,95	22,91
FeO	20,18	21,01	20,83	21,09	20,89	21,38	21,29	21,47	21,70	20,83
MnO	0,49	0,47	0,62	0,62	0,61	0,79	0,56	0,63	0,66	0,67
MgO	8,75	8,34	8,69	8,95	8,60	8,43	8,32	8,36	8,55	8,50
CaO	9,25	9,07	9,01	8,95	8,60	8,81	8,72	8,87	8,84	8,79
Total	**101,79**	**102,29**	**102,07**	**103,03**	**101,84**	**102,51**	**102,12**	**102,54**	**103,02**	**101,61**
Si	2,96	2,99	2,99	2,97	2,99	2,96	2,98	2,97	2,97	2,97
Ti	0,01	0,01	0,01	0,01	0,01	0,01	0,01	0,01	0,01	0,01
Al	2,05	2,01	1,99	2,00	2,01	2,01	2,03	2,03	2,00	2,02
Fe^{2+}	1,26	1,31	1,30	1,30	1,30	1,33	1,33	1,34	1,34	1,31
Mn	0,03	0,03	0,04	0,04	0,04	0,05	0,04	0,04	0,04	0,04
Mg	0,97	0,93	0,97	0,99	0,96	0,94	0,92	0,93	0,94	0,95
Ca	0,74	0,72	0,72	0,71	0,69	0,70	0,70	0,71	0,70	0,71
Total	**8,01**	**8,00**	**8,01**	**8,02**	**8,00**	**8,03**	**8,00**	**8,01**	**8,02**	**8,01**
X_{Grs}	0,25	0,24	0,24	0,23	0,23	0,23	0,23	0,23	0,23	0,23
X_{Alm}	0,42	0,44	0,43	0,43	0,44	0,44	0,44	0,44	0,44	0,43
X_{Pyr}	0,32	0,31	0,32	0,32	0,32	0,31	0,31	0,31	0,31	0,32
X_{Sps}	0,01	0,01	0,01	0,01	0,01	0,02	0,01	0,01	0,01	0,01
X_{Mg}	0,44	0,41	0,43	0,43	0,42	0,41	0,41	0,41	0,41	0,42

	G4-11	G4-12	G4-13	G4-14	G4-15	G4-16	G4-17	G4-18	G4-19	G4-20
	Core								Rim	Rim
SiO_2	40,05	40,49	40,16	40,12	40,62	39,61	39,93	40,28	40,42	40,28
TiO_2	0,15	0,14	0,15	0,22	0,16	0,13	0,10	0,14	0,13	0,14
Al_2O_3	22,45	22,71	22,83	22,89	22,66	23,03	22,96	22,39	22,69	21,95
FeO	21,12	20,83	21,04	20,59	21,20	20,46	20,73	21,06	20,65	19,35
MnO	0,55	0,68	0,62	0,60	0,62	0,53	0,59	0,60	0,46	0,37
MgO	8,14	8,09	8,47	8,23	8,08	8,65	8,36	8,35	8,53	8,58
CaO	8,87	8,89	9,09	8,90	8,95	8,73	8,71	9,32	9,68	9,42
Total	**101,51**	**101,96**	**102,49**	**101,73**	**102,44**	**101,25**	**101,44**	**102,24**	**102,76**	**100,18**
Si	3,01	3,02	2,98	3,00	3,02	2,97	2,99	3,00	2,99	3,04
Ti	0,01	0,01	0,01	0,01	0,01	0,01	0,01	0,01	0,01	0,01
Al	1,99	2,00	2,00	2,02	1,98	2,04	2,03	1,97	1,98	1,95
Fe^{2+}	1,33	1,30	1,31	1,29	1,32	1,28	1,30	1,31	1,28	1,22
Mn	0,03	0,04	0,04	0,04	0,04	0,03	0,04	0,04	0,03	0,02
Mg	0,91	0,90	0,94	0,92	0,90	0,97	0,93	0,93	0,94	0,97
Ca	0,71	0,71	0,72	0,71	0,71	0,70	0,70	0,74	0,77	0,76
Total	**8,00**	**7,98**	**8,01**	**7,99**	**7,98**	**8,01**	**7,99**	**8,01**	**8,02**	**7,98**
X_{Grs}	0,24	0,24	0,24	0,24	0,24	0,23	0,24	0,25	0,25	0,26
X_{Alm}	0,44	0,44	0,43	0,44	0,44	0,43	0,44	0,43	0,42	0,41
X_{Pyr}	0,31	0,30	0,31	0,31	0,30	0,32	0,31	0,31	0,31	0,32
X_{Sps}	0,01	0,01	0,01	0,01	0,01	0,01	0,01	0,01	0,01	0,01
X_{Mg}	0,41	0,41	0,42	0,42	0,40	0,43	0,42	0,41	0,42	0,44

GRT6	G6-1	G6-2	G6-3	G6-4	G6-5	G6-6	G6-7	G6-8	G6-9	G6-10
	Rim	Rim								Core
SiO_2	40,53	39,61	39,81	40,65	40,48	40,42	40,15	39,82	40,49	40,34
TiO_2	0,14	0,08	0,15	0,10	0,09	0,12	0,20	0,18	0,27	0,14
Al_2O_3	23,13	22,01	23,56	22,76	22,78	22,74	22,20	22,32	22,80	22,54
FeO	18,64	18,37	18,48	18,56	19,29	18,48	18,86	19,05	19,05	19,47
MnO	0,24	0,15	0,18	0,11	0,09	0,14	0,20	0,14	0,09	0,13
MgO	10,60	9,42	10,13	9,53	9,32	9,21	8,83	8,80	8,76	8,34
CaO	8,95	9,40	10,24	10,36	10,46	10,59	10,55	10,68	10,83	10,73
Total	**102,30**	**99,16**	**102,66**	**102,26**	**102,62**	**102,04**	**101,23**	**101,17**	**102,51**	**101,83**
Si	2,98	3,01	2,93	3,00	2,99	2,99	3,00	2,99	2,99	3,01
Ti	0,01	0,00	0,01	0,01	0,00	0,01	0,01	0,01	0,01	0,01
Al	2,00	1,97	2,04	1,98	1,98	1,98	1,96	1,97	1,99	1,98
Fe^{2+}	1,15	1,17	1,14	1,14	1,19	1,14	1,18	1,19	1,18	1,21
Mn	0,02	0,01	0,01	0,01	0,01	0,01	0,01	0,01	0,01	0,01
Mg	1,16	1,07	1,11	1,05	1,02	1,02	0,99	0,98	0,96	0,93
Ca	0,70	0,77	0,81	0,82	0,83	0,84	0,85	0,86	0,86	0,86
Total	**8,01**	**8,00**	**8,04**	**8,01**	**8,02**	**8,01**	**8,01**	**8,02**	**8,01**	**8,00**
X_{Grs}	0,23	0,25	0,26	0,27	0,27	0,28	0,28	0,28	0,29	0,29
X_{Alm}	0,38	0,39	0,37	0,38	0,39	0,38	0,39	0,39	0,39	0,40
X_{Pyr}	0,38	0,35	0,36	0,35	0,34	0,34	0,33	0,32	0,32	0,31
X_{Sps}	0,01	0,00	0,00	0,00	0,00	0,00	0,00	0,00	0,00	0,00
X_{Mg}	0,50	0,48	0,49	0,48	0,46	0,47	0,45	0,45	0,45	0,43

	G6-11	G6-12	G6-13	G6-14	G6-15	G6-16	G6-17	G6-18	G6-19	G6-20
	Core								Rim	Rim
SiO_2	39,75	40,02	40,04	39,96	40,89	40,07	40,12	38,93	40,93	40,73
TiO_2	0,13	0,18	0,21	0,09	0,16	0,12	0,11	0,14	0,08	0,11
Al_2O_3	22,90	22,93	23,05	22,93	22,42	22,76	22,98	22,15	23,05	23,09
FeO	19,32	19,52	19,32	19,37	19,16	18,32	18,76	19,02	18,69	18,69
MnO	0,20	0,30	0,09	0,18	0,10	0,13	0,19	0,27	0,17	0,14
MgO	8,36	8,56	8,40	8,87	8,35	9,41	9,27	8,83	9,90	10,58
CaO	10,48	10,60	10,70	10,50	10,70	10,53	10,30	10,11	9,50	8,95
Total	**101,38**	**102,33**	**102,05**	**102,06**	**101,92**	**101,54**	**101,92**	**99,66**	**102,58**	**102,50**
Si	2,98	2,97	2,98	2,97	3,03	2,98	2,98	2,97	3,00	2,99
Ti	0,01	0,01	0,01	0,01	0,01	0,01	0,01	0,01	0,00	0,01
Al	2,02	2,01	2,02	2,01	1,96	1,99	2,01	1,99	1,99	2,00
Fe^{2+}	1,21	1,21	1,20	1,20	1,19	1,14	1,16	1,21	1,15	1,15
Mn	0,01	0,02	0,01	0,01	0,01	0,01	0,01	0,02	0,01	0,01
Mg	0,93	0,95	0,93	0,98	0,92	1,04	1,02	1,00	1,08	1,16
Ca	0,84	0,84	0,85	0,84	0,85	0,84	0,82	0,83	0,75	0,70
Total	**8,01**	**8,01**	**8,01**	**8,03**	**7,98**	**8,02**	**8,02**	**8,04**	**7,99**	**8,01**
X_{Grs}	0,28	0,28	0,29	0,28	0,29	0,28	0,27	0,27	0,25	0,23
X_{Alm}	0,40	0,40	0,40	0,40	0,40	0,38	0,39	0,40	0,38	0,38
X_{Pyr}	0,31	0,31	0,31	0,32	0,31	0,34	0,34	0,33	0,36	0,38
X_{Sps}	0,00	0,01	0,00	0,00	0,00	0,00	0,00	0,01	0,00	0,00
X_{Mg}	0,44	0,44	0,44	0,45	0,44	0,48	0,47	0,45	0,49	0,50

GRT profiles sample 18XC20

GRT4	G4-1	G4-2	G4-3	G4-4	G4-5	G4-6	G4-7	G4-8	G4-9	G4-10
	Rim	Rim								Core
SiO_2	40,10	40,32	39,80	39,70	39,98	39,86	39,92	39,78	39,81	39,78
TiO_2	0,09	0,09	0,12	0,14	0,12	0,17	0,15	0,12	0,10	0,15
Al_2O_3	22,51	22,42	22,64	22,63	22,67	22,51	22,76	22,16	22,73	22,49
FeO	20,93	22,04	21,65	22,44	21,82	22,69	22,16	23,36	23,14	23,48
MnO	0,63	0,79	0,83	0,80	0,83	0,89	0,93	1,11	0,99	1,03
MgO	8,31	7,54	7,13	7,30	7,01	7,14	7,20	7,63	7,38	7,12
CaO	9,54	9,76	9,63	9,43	9,37	9,26	8,78	7,98	7,96	8,06
Total	**102,27**	**103,14**	**101,93**	**102,57**	**101,88**	**102,64**	**101,97**	**102,33**	**102,26**	**102,32**
Si	2,99	3,00	2,99	2,98	3,00	2,99	3,00	2,99	2,99	2,99
Ti	0,01	0,00	0,01	0,01	0,01	0,01	0,01	0,01	0,01	0,01
Al	1,98	1,97	2,01	2,00	2,01	1,99	2,01	1,97	2,01	1,99
Fe^{2+}	1,31	1,37	1,36	1,41	1,37	1,42	1,39	1,47	1,45	1,48
Mn	0,04	0,05	0,05	0,05	0,05	0,06	0,06	0,07	0,06	0,07
Mg	0,92	0,84	0,80	0,82	0,79	0,80	0,81	0,86	0,83	0,80
Ca	0,76	0,78	0,78	0,76	0,75	0,74	0,71	0,64	0,64	0,65
Total	**8,02**	**8,02**	**8,00**	**8,02**	**7,99**	**8,01**	**7,99**	**8,03**	**8,00**	**8,01**
X_{Grs}	0,25	0,26	0,26	0,25	0,25	0,25	0,24	0,21	0,21	0,22
X_{Alm}	0,43	0,45	0,46	0,46	0,46	0,47	0,47	0,48	0,49	0,49
X_{Pyr}	0,30	0,28	0,27	0,27	0,26	0,26	0,27	0,28	0,28	0,27
X_{Sps}	0,01	0,02	0,02	0,02	0,02	0,02	0,02	0,02	0,02	0,02
X_{Mg}	0,41	0,38	0,37	0,37	0,36	0,36	0,37	0,37	0,36	0,35

	G4-11	G4-12	G4-13	G4-14	G4-15	G4-16	G4-17	G4-18	G4-19	G4-20
	Core								Rim	Rim
SiO_2	40,01	39,44	39,62	39,98	39,85	39,96	39,59	40,18	40,54	39,89
TiO_2	0,11	0,14	0,07	0,15	0,07	0,11	0,10	0,10	0,07	0,10
Al_2O_3	22,31	22,05	22,31	22,58	23,03	23,31	22,77	22,92	22,67	22,87
FeO	23,37	23,05	23,44	23,45	22,55	23,14	22,54	22,02	22,05	21,22
MnO	1,10	1,16	0,96	0,88	1,00	0,86	0,89	0,79	0,72	0,70
MgO	7,68	7,55	7,28	7,16	7,51	7,32	7,70	7,35	7,65	7,89
CaO	8,21	8,48	8,60	8,68	8,69	8,78	9,12	9,36	9,56	9,57
Total	**103,02**	**102,06**	**102,36**	**103,10**	**102,72**	**103,60**	**102,88**	**102,87**	**103,40**	**102,32**
Si	2,99	2,98	2,98	2,99	2,97	2,96	2,96	2,99	3,00	2,98
Ti	0,01	0,01	0,00	0,01	0,00	0,01	0,01	0,01	0,00	0,01
Al	1,97	1,96	1,98	1,99	2,03	2,04	2,01	2,01	1,98	2,01
Fe^{2+}	1,46	1,46	1,48	1,47	1,41	1,44	1,41	1,37	1,37	1,32
Mn	0,07	0,07	0,06	0,06	0,06	0,05	0,06	0,05	0,05	0,04
Mg	0,86	0,85	0,82	0,80	0,84	0,81	0,86	0,82	0,84	0,88
Ca	0,66	0,69	0,69	0,70	0,70	0,70	0,73	0,75	0,76	0,77
Total	**8,02**	**8,04**	**8,02**	**8,01**	**8,01**	**8,02**	**8,04**	**8,00**	**8,01**	**8,01**
X_{Grs}	0,22	0,22	0,23	0,23	0,23	0,23	0,24	0,25	0,25	0,25
X_{Alm}	0,48	0,47	0,48	0,49	0,47	0,48	0,46	0,46	0,45	0,44
X_{Pyr}	0,28	0,28	0,27	0,26	0,28	0,27	0,28	0,27	0,28	0,29
X_{Sps}	0,02	0,02	0,02	0,02	0,02	0,02	0,02	0,02	0,01	0,01
X_{Mg}	0,37	0,37	0,36	0,35	0,37	0,36	0,38	0,37	0,38	0,40

GRT6	G6-1	G6-2	G6-3	G6-4	G6-5	G6-6	G6-7	G6-8	G6-9	G6-10
	Rim	Rim								Core
SiO_2	40,15	40,24	39,91	39,96	39,89	39,69	39,75	40,05	39,82	39,61
TiO_2	0,13	0,15	0,13	0,08	0,09	0,07	0,09	0,06	0,15	0,13
Al_2O_3	22,88	22,23	22,18	22,06	22,46	22,72	22,13	22,39	22,58	22,11
FeO	21,43	22,29	21,96	22,23	22,17	22,11	22,51	23,04	23,07	22,51
MnO	0,77	0,77	0,77	0,79	0,68	0,99	0,95	1,07	1,09	1,22
MgO	7,37	7,35	7,10	7,34	7,29	6,98	7,13	7,26	7,18	7,08
CaO	10,03	10,04	10,00	9,79	9,48	9,46	9,28	8,80	8,34	7,98
Total	**102,89**	**103,26**	**102,20**	**102,33**	**102,17**	**102,15**	**101,98**	**102,73**	**102,42**	**100,80**
Si	2,99	3,00	3,00	3,00	3,00	2,98	3,00	3,00	2,99	3,02
Ti	0,01	0,01	0,01	0,00	0,01	0,00	0,00	0,00	0,01	0,01
Al	2,01	1,95	1,97	1,95	1,99	2,01	1,97	1,98	2,00	1,99
Fe^{2+}	1,33	1,39	1,38	1,40	1,39	1,39	1,42	1,44	1,45	1,43
Mn	0,05	0,05	0,05	0,05	0,04	0,06	0,06	0,07	0,07	0,08
Mg	0,82	0,82	0,80	0,82	0,82	0,78	0,80	0,81	0,80	0,80
Ca	0,80	0,80	0,81	0,79	0,76	0,76	0,75	0,71	0,67	0,65
Total	**8,00**	**8,02**	**8,01**	**8,02**	**8,01**	**8,01**	**8,01**	**8,01**	**8,00**	**7,98**
X_{Grs}	0,23	0,25	0,26	0,27	0,27	0,28	0,28	0,28	0,29	0,29
X_{Alm}	0,38	0,39	0,37	0,38	0,39	0,38	0,39	0,39	0,39	0,40
X_{Pyr}	0,38	0,35	0,36	0,35	0,34	0,34	0,33	0,32	0,32	0,31
X_{Sps}	0,01	0,00	0,00	0,00	0,00	0,00	0,00	0,00	0,00	0,00
X_{Mg}	0,38	0,37	0,37	0,37	0,37	0,36	0,36	0,36	0,36	0,36

	G6-11	G6-12	G6-13	G6-14	G6-15	G6-16	G6-17	G6-18	G6-19	G6-20
	Core								Rim	Rim
SiO_2	39,52	39,51	39,96	39,55	39,45	39,55	39,89	40,05	40,21	39,90
TiO_2	0,10	0,12	0,10	0,11	0,11	0,15	0,09	0,03	0,16	0,16
Al_2O_3	22,43	22,54	22,35	22,07	22,30	22,60	22,50	22,81	22,90	22,53
FeO	23,37	24,08	23,15	23,38	22,86	22,58	21,89	22,29	21,99	21,70
MnO	1,25	1,10	1,15	1,12	1,06	0,89	0,86	0,75	0,70	0,79
MgO	7,43	7,50	7,40	7,27	7,44	7,54	7,34	7,48	7,55	8,26
CaO	7,94	7,91	8,22	8,40	8,53	8,77	9,33	9,50	9,58	9,54
Total	**102,15**	**102,90**	**102,45**	**102,12**	**101,84**	**102,24**	**102,16**	**103,05**	**103,33**	**103,08**
Si	2,98	2,97	3,00	2,99	2,98	2,97	3,00	2,98	2,98	2,97
Ti	0,01	0,01	0,01	0,01	0,01	0,01	0,01	0,00	0,01	0,01
Al	1,99	2,00	1,98	1,97	1,99	2,00	1,99	2,00	2,00	1,98
Fe^{2+}	1,47	1,51	1,45	1,48	1,44	1,42	1,38	1,39	1,36	1,35
Mn	0,08	0,07	0,07	0,07	0,07	0,06	0,05	0,05	0,04	0,05
Mg	0,84	0,84	0,83	0,82	0,84	0,85	0,82	0,83	0,84	0,92
Ca	0,64	0,64	0,66	0,68	0,69	0,71	0,75	0,76	0,76	0,76
Total	**8,01**	**8,03**	**8,00**	**8,02**	**8,02**	**8,02**	**8,00**	**8,01**	**8,01**	**8,04**
X_{Grs}	0,21	0,21	0,22	0,22	0,23	0,23	0,25	0,25	0,25	0,25
X_{Alm}	0,49	0,49	0,48	0,48	0,47	0,47	0,46	0,46	0,45	0,44
X_{Pyr}	0,28	0,27	0,27	0,27	0,28	0,28	0,27	0,27	0,28	0,30
X_{Sps}	0,03	0,02	0,02	0,02	0,02	0,02	0,02	0,02	0,01	0,02
X_{Mg}	0,36	0,36	0,36	0,36	0,37	0,37	0,37	0,37	0,38	0,40

GRT8	G8-1	G8-2	G8-3	G8-4	G8-5	G8-6	G8-7	G8-8	G8-9	G8-10
	Rim	Rim								Core
SiO_2	39,81	39,21	39,95	39,61	39,82	39,40	39,77	39,96	39,72	39,82
TiO_2	0,11	0,09	0,13	0,12	0,14	0,08	0,09	0,12	0,15	0,16
Al_2O_3	22,92	22,88	22,61	22,90	22,87	22,54	22,16	21,98	21,76	21,95
FeO	21,31	21,59	21,85	21,69	22,40	21,56	21,68	22,04	21,92	22,26
MnO	0,70	0,69	0,75	0,84	0,83	0,94	0,82	0,85	0,89	1,03
MgO	7,94	7,56	7,19	7,36	7,26	7,53	7,23	7,16	7,48	7,25
CaO	9,80	9,70	9,81	9,95	9,62	9,80	9,74	9,81	9,73	9,66
Total	**102,93**	**101,80**	**102,47**	**102,58**	**103,12**	**101,99**	**101,63**	**102,02**	**101,76**	**102,28**
Si	2,96	2,95	2,99	2,96	2,97	2,97	3,00	3,01	3,00	3,00
Ti	0,01	0,00	0,01	0,01	0,01	0,00	0,00	0,01	0,01	0,01
Al	2,01	2,03	2,00	2,02	2,01	2,00	1,97	1,95	1,94	1,95
Fe^{2+}	1,33	1,36	1,37	1,36	1,40	1,36	1,37	1,39	1,38	1,40
Mn	0,04	0,04	0,05	0,05	0,05	0,06	0,05	0,05	0,06	0,07
Mg	0,88	0,85	0,80	0,82	0,81	0,85	0,81	0,80	0,84	0,81
Ca	0,78	0,78	0,79	0,80	0,77	0,79	0,79	0,79	0,79	0,78
Total	**8,03**	**8,03**	**8,00**	**8,02**	**8,02**	**8,03**	**8,01**	**8,01**	**8,03**	**8,02**
X_{Grs}	0,26	0,26	0,26	0,26	0,25	0,26	0,26	0,26	0,26	0,25
X_{Alm}	0,44	0,45	0,46	0,45	0,46	0,44	0,45	0,46	0,45	0,46
X_{Pyr}	0,29	0,28	0,27	0,27	0,27	0,28	0,27	0,26	0,27	0,27
X_{Sps}	0,01	0,01	0,02	0,02	0,02	0,02	0,02	0,02	0,02	0,02
X_{Mg}	0,40	0,38	0,37	0,38	0,37	0,38	0,37	0,37	0,38	0,37

	G8-11	G8-12	G8-13	G8-14	G8-15	G8-16	G8-17	G8-18	G8-19	G8-20
	Core								Rim	Rim
SiO_2	40,06	39,42	39,58	39,94	39,99	39,85	39,93	39,68	39,87	39,85
TiO_2	0,15	0,11	0,08	0,11	0,13	0,12	0,12	0,14	0,09	0,14
Al_2O_3	21,84	22,29	21,39	21,55	21,89	21,93	21,68	21,86	21,47	21,78
FeO	22,38	22,20	22,57	21,82	22,16	21,84	21,90	22,10	21,77	21,68
MnO	1,17	1,21	0,97	1,04	1,02	0,83	0,90	0,88	0,87	0,78
MgO	7,26	7,24	7,33	7,00	7,30	7,34	7,19	7,22	7,36	7,28
CaO	9,59	9,55	9,82	9,94	9,72	9,76	9,85	9,94	10,06	10,26
Total	**102,52**	**102,17**	**101,78**	**101,63**	**102,29**	**101,91**	**101,64**	**101,96**	**101,57**	**101,87**
Si	3,01	2,97	3,00	3,03	3,01	3,01	3,02	3,00	3,02	3,01
Ti	0,01	0,01	0,00	0,01	0,01	0,01	0,01	0,01	0,01	0,01
Al	1,93	1,98	1,91	1,92	1,94	1,95	1,93	1,94	1,91	1,94
Fe^{2+}	1,41	1,40	1,43	1,38	1,39	1,38	1,38	1,40	1,38	1,37
Mn	0,07	0,08	0,06	0,07	0,07	0,05	0,06	0,06	0,06	0,05
Mg	0,81	0,81	0,83	0,79	0,82	0,83	0,81	0,81	0,83	0,82
Ca	0,77	0,77	0,80	0,81	0,78	0,79	0,80	0,80	0,82	0,83
Total	**8,02**	**8,04**	**8,04**	**8,01**	**8,02**	**8,01**	**8,01**	**8,03**	**8,02**	**8,02**
X_{Grs}	0,25	0,25	0,26	0,26	0,26	0,26	0,26	0,26	0,26	0,27
X_{Alm}	0,46	0,46	0,46	0,45	0,46	0,45	0,45	0,45	0,45	0,45
X_{Pyr}	0,27	0,27	0,27	0,26	0,27	0,27	0,27	0,26	0,27	0,27
X_{Sps}	0,02	0,03	0,02	0,02	0,02	0,02	0,02	0,02	0,02	0,02
X_{Mg}	0,37	0,37	0,37	0,36	0,37	0,37	0,37	0,37	0,38	0,37

GRT9	G9-1	G9-2	G9-3	G9-4	G9-5	G9-6	G9-7	G9-8	G9-9	G9-10
	Rim	Rim								Core
SiO_2	40,41	40,07	40,06	40,15	40,26	39,96	39,92	40,07	39,73	39,92
TiO_2	0,07	0,14	0,15	0,15	0,15	0,18	0,12	0,10	0,11	0,14
Al_2O_3	22,07	22,37	22,14	22,22	22,66	22,29	22,75	22,54	22,36	22,73
FeO	20,76	21,60	21,51	22,17	22,06	21,62	21,86	21,73	21,85	21,77
MnO	0,69	0,86	0,85	0,89	1,01	1,25	1,02	1,01	0,89	0,96
MgO	7,60	7,18	7,32	7,36	7,07	7,09	7,08	7,44	7,08	7,09
CaO	9,70	9,95	10,20	10,20	10,13	9,93	9,96	9,95	10,17	9,87
Total	**101,85**	**102,45**	**102,39**	**103,27**	**103,62**	**102,52**	**102,85**	**102,98**	**102,27**	**102,50**
Si	3,04	3,00	3,00	2,98	2,99	2,99	2,98	2,98	2,98	2,98
Ti	0,00	0,01	0,01	0,01	0,01	0,01	0,01	0,01	0,01	0,01
Al	1,96	1,97	1,95	1,95	1,98	1,97	2,00	1,98	1,98	2,00
Fe^{2+}	1,31	1,34	1,30	1,30	1,34	1,32	1,33	1,31	1,32	1,35
Mn	0,04	0,05	0,05	0,06	0,06	0,08	0,06	0,06	0,06	0,06
Mg	0,85	0,80	0,82	0,82	0,78	0,79	0,79	0,83	0,79	0,79
Ca	0,78	0,80	0,82	0,81	0,81	0,80	0,80	0,79	0,82	0,79
Total	**8,00**	**8,00**	**8,00**	**8,00**	**8,00**	**8,00**	**8,00**	**8,00**	**8,00**	**8,00**
X_{Grs}	0,26	0,27	0,27	0,27	0,27	0,26	0,26	0,26	0,27	0,26
X_{Alm}	0,44	0,45	0,44	0,45	0,45	0,45	0,45	0,45	0,45	0,45
X_{Pyr}	0,29	0,27	0,27	0,27	0,26	0,26	0,26	0,27	0,26	0,26
X_{Sps}	0,01	0,02	0,02	0,02	0,02	0,03	0,02	0,02	0,02	0,02
X_{Mg}	0,39	0,37	0,39	0,38	0,37	0,37	0,37	0,39	0,37	0,37

	G9-11	G9-12	G9-13	G9-14	G9-15	G9-16	G9-17	G9-18	G9-19	G9-20
	Core								Rim	Rim
SiO_2	39,68	39,96	39,67	40,17	40,45	40,25	40,84	40,40	40,12	40,12
TiO_2	0,11	0,14	0,11	0,07	0,12	0,14	0,11	0,11	0,12	0,10
Al_2O_3	22,59	22,44	21,79	21,81	22,31	21,77	22,25	22,06	22,04	22,50
FeO	22,04	21,40	22,04	21,40	22,05	21,87	21,45	21,75	21,31	21,03
MnO	0,92	0,89	0,96	0,86	0,88	0,92	0,74	0,78	0,77	0,62
MgO	7,28	7,29	7,27	7,08	7,32	7,34	7,44	7,56	7,44	8,46
CaO	9,73	10,10	9,83	9,92	9,90	9,90	9,71	9,82	9,85	9,17
Total	**102,42**	**102,28**	**101,75**	**101,37**	**103,19**	**102,28**	**102,76**	**102,54**	**101,85**	**102,06**
Si	2,97	2,99	2,99	3,04	3,00	3,02	3,04	3,02	3,01	2,99
Ti	0,01	0,01	0,01	0,00	0,01	0,01	0,01	0,01	0,01	0,01
Al	1,99	1,98	1,94	1,94	1,95	1,92	1,95	1,94	1,95	1,98
Fe^{2+}	1,32	1,31	1,31	1,35	1,33	1,35	1,34	1,34	1,32	1,28
Mn	0,06	0,06	0,06	0,06	0,06	0,06	0,05	0,05	0,05	0,04
Mg	0,81	0,81	0,82	0,80	0,81	0,82	0,83	0,84	0,83	0,94
Ca	0,78	0,81	0,79	0,80	0,79	0,80	0,77	0,79	0,79	0,73
Total	**8,00**	**8,00**	**8,00**	**8,00**	**8,00**	**8,00**	**8,00**	**8,00**	**8,00**	**8,00**
X_{Grs}	0,26	0,27	0,26	0,27	0,26	0,26	0,26	0,26	0,26	0,24
X_{Alm}	0,46	0,44	0,45	0,45	0,45	0,45	0,45	0,45	0,44	0,43
X_{Pyr}	0,27	0,27	0,27	0,27	0,27	0,27	0,28	0,28	0,28	0,31
X_{Sps}	0,02	0,02	0,02	0,02	0,02	0,02	0,02	0,02	0,02	0,01
X_{Mg}	0,38	0,38	0,38	0,37	0,38	0,38	0,38	0,39	0,39	0,42

GRT cores-rims sample 18XC1

	GR8	GR8	GR1	GR1	GR2	GR2	GR3	GR3	GR4	GR4	GR5	GR5	GR6	GR6	GR7	GR7
	Core	Rim	Core	Rim	Core	Rim	Core	Rim	Core	Rim	Core	Rim	Core	Rim	Core	Rim
SiO_2	40,66	40,35	39,00	39,95	39,82	39,93	39,35	40,02	40,04	39,74	40,25	40,09	40,00	40,36	40,25	39,35
TiO_2	0,15	0,16	0,10	0,12	0,16	0,18	0,12	0,11	0,13	0,11	0,06	0,13	0,14	0,13	0,10	0,13
Al_2O_3	22,99	22,99	22,23	22,42	22,31	22,26	22,63	22,44	22,54	22,33	22,68	22,49	22,25	22,35	22,84	22,40
FeO	17,63	17,37	25,65	19,59	19,20	17,46	23,22	18,05	19,30	18,04	19,22	18,02	19,39	18,32	17,99	17,52
MnO	0,12	0,13	0,58	0,23	0,03	0,13	0,75	0,17	0,12	0,12	0,13	0,23	0,08	0,12	0,11	0,15
MgO	8,94	8,38	6,17	7,81	9,09	8,21	7,42	8,19	8,05	8,31	8,25	8,07	8,01	8,22	9,10	8,08
CaO	11,77	12,58	8,26	11,55	9,90	12,42	8,32	12,14	11,43	11,94	11,41	11,98	11,27	11,83	10,88	12,58
Total	**102,46**	**102,06**	**102,13**	**101,83**	**100,62**	**100,77**	**102,03**	**101,33**	**101,80**	**100,78**	**102,16**	**101,22**	**101,25**	**101,50**	**101,53**	**100,34**
Si	2,99	2,98	2,97	2,99	2,99	3,00	2,97	2,99	2,99	2,99	2,99	3,00	3,00	3,01	2,99	2,97
Ti	0,01	0,01	0,01	0,01	0,01	0,01	0,01	0,01	0,01	0,01	0,00	0,01	0,01	0,01	0,01	0,01
Al	1,99	2,00	2,00	1,98	1,98	1,97	2,01	1,98	1,98	1,98	1,99	1,98	1,97	1,97	2,00	1,99
Fe^{2+}	1,08	1,07	1,63	1,23	1,21	1,10	1,47	1,13	1,21	1,13	1,19	1,13	1,22	1,14	1,12	1,11
Mn	0,01	0,01	0,04	0,01	0,00	0,01	0,05	0,01	0,01	0,01	0,01	0,01	0,00	0,01	0,01	0,01
Mg	0,98	0,92	0,70	0,87	1,02	0,92	0,83	0,91	0,90	0,93	0,91	0,90	0,90	0,91	1,01	0,91
Ca	0,93	1,00	0,67	0,93	0,80	1,00	0,67	0,97	0,91	0,96	0,91	0,96	0,91	0,95	0,87	1,02
Total	**8,00**	**8,01**	**8,02**	**8,02**	**8,01**	**8,01**	**8,02**	**8,01**	**8,01**	**8,01**	**8,01**	**8,00**	**8,01**	**8,00**	**8,00**	**8,02**
X_{Grs}	0,31	0,33	0,22	0,30	0,26	0,33	0,22	0,32	0,30	0,32	0,30	0,32	0,30	0,31	0,29	0,33
X_{Alm}	0,36	0,36	0,54	0,40	0,40	0,36	0,49	0,37	0,40	0,37	0,39	0,38	0,40	0,38	0,37	0,36
X_{Pyr}	0,33	0,31	0,23	0,29	0,34	0,30	0,28	0,30	0,30	0,31	0,30	0,30	0,30	0,30	0,34	0,30
X_{Sps}	0,00	0,00	0,01	0,00	0,00	0,00	0,02	0,00	0,00	0,00	0,00	0,00	0,00	0,00	0,00	0,00
X_{Mg}	0,47	0,46	0,30	0,42	0,46	0,46	0,36	0,45	0,43	0,45	0,43	0,44	0,42	0,44	0,47	0,45

GRT cores-rims sample 18XC6

	GR5	GR5	GR6
	Rim	Core	Rim
SiO_2	39,78	39,56	39,48
TiO_2	0,11	0,13	0,12
Al_2O_3	22,20	22,42	22,03
FeO	25,77	25,62	25,50
MnO	0,51	0,40	0,46
MgO	6,45	6,77	6,81
CaO	7,57	7,55	7,65
Total	**102,50**	**102,62**	**102,19**
Si	3,01	3,00	2,99
Ti	0,01	0,01	0,01
Al	1,98	1,98	1,97
Fe^{2+}	1,63	1,63	1,62
Mn	0,03	0,03	0,03
Mg	0,73	0,73	0,77
Ca	0,61	0,62	0,62
Total	**8,00**	**8,00**	**8,02**
X_{Grs}	0,20	0,20	0,20
X_{Alm}	0,54	0,54	0,53
X_{Pyr}	0,24	0,24	0,25
X_{Sps}	0,01	0,01	0,01
X_{Mg}	0,31	0,31	0,32

GRT cores-rims sample 18XC10

	GR2	GR2	GR4	GR4	GR5	GR5	GR7	GR7	GR8	GR8	GR9	GR9	GR10	GR10
	Core	Rim	Core	Rim	Core	Rim	Core	Rim	Core	Rim	Core	Rim	Core	Rim
SiO_2	39,91	40,06	40,00	40,16	39,99	39,26	38,89	38,61	39,28	38,90	38,74	39,17	39,26	38,79
TiO_2	0,10	0,13	0,11	0,10	0,20	0,14	0,20	0,05	0,10	0,10	0,14	0,12	0,15	0,08
Al_2O_3	22,97	22,90	22,76	23,28	22,48	22,93	21,97	23,14	22,47	22,73	22,25	22,95	22,41	22,65
FeO	20,06	20,43	20,28	20,63	20,78	20,19	20,76	20,53	20,41	20,22	20,11	20,56	20,52	20,10
MnO	0,38	0,36	0,41	0,39	0,39	0,32	0,37	0,38	0,40	0,40	0,30	0,26	0,28	0,31
MgO	10,45	10,89	10,55	11,18	10,46	11,43	10,43	11,02	10,39	11,07	10,16	11,28	10,59	11,18
CaO	7,25	6,25	6,76	6,33	7,09	6,07	7,09	6,21	6,56	6,16	7,84	6,34	7,04	6,09
Total	**101,24**	**101,14**	**100,97**	**102,17**	**101,52**	**100,38**	**99,81**	**100,06**	**99,82**	**99,84**	**99,67**	**100,84**	**100,36**	**99,43**
Si	2,97	2,98	2,99	2,96	2,98	2,94	2,96	2,92	2,97	2,94	2,95	2,93	2,96	2,94
Ti	0,01	0,01	0,01	0,01	0,01	0,01	0,01	0,00	0,01	0,01	0,01	0,01	0,01	0,00
Al	2,02	2,01	2,00	2,02	1,98	2,03	1,97	2,06	2,01	2,03	2,00	2,03	1,99	2,03
Fe^{2+}	1,25	1,27	1,27	1,27	1,30	1,27	1,32	1,30	1,29	1,28	1,28	1,29	1,29	1,28
Mn	0,02	0,02	0,03	0,02	0,02	0,02	0,02	0,02	0,03	0,03	0,02	0,02	0,02	0,02
Mg	1,16	1,21	1,17	1,23	1,16	1,28	1,18	1,24	1,17	1,25	1,15	1,26	1,19	1,26
Ca	0,58	0,50	0,54	0,50	0,57	0,49	0,58	0,50	0,53	0,50	0,64	0,51	0,57	0,50
Total	**8,01**	**8,01**	**8,01**	**8,02**	**8,02**	**8,04**	**8,05**	**8,05**	**8,01**	**8,04**	**8,05**	**8,05**	**8,04**	**8,04**
X_{Grs}	0,19	0,17	0,18	0,17	0,19	0,16	0,19	0,16	0,18	0,16	0,21	0,17	0,19	0,16
X_{Alm}	0,41	0,42	0,42	0,42	0,42	0,41	0,43	0,42	0,43	0,42	0,41	0,42	0,42	0,42
X_{Pyr}	0,39	0,40	0,39	0,41	0,38	0,42	0,38	0,40	0,39	0,41	0,37	0,41	0,39	0,41
X_{Sps}	0,01	0,01	0,01	0,01	0,01	0,01	0,01	0,01	0,01	0,01	0,01	0,01	0,01	0,01
X_{Mg}	0,48	0,49	0,48	0,49	0,47	0,50	0,47	0,49	0,48	0,49	0,47	0,49	0,48	0,50

GRT cores-rims sample 18XC15

	GR1	GR2	GR3	GR4	GR5	GR5	GR5	GR6	GR6
	Rim	Rim	Rim	Rim	Core	Rim	Rim	Rim	Rim
SiO_2	39,80	40,43	40,06	40,05	39,88	39,80	39,95	40,39	40,63
TiO_2	0,15	0,14	0,13	0,12	0,11	0,13	0,14	0,16	0,12
Al_2O_3	21,85	22,01	22,70	22,72	22,75	23,06	22,88	23,54	23,02
FeO	20,42	19,95	19,70	20,11	20,78	19,93	19,61	18,36	18,36
MnO	0,40	0,38	0,46	0,45	0,66	0,41	0,35	0,18	0,21
MgO	8,51	8,63	8,98	8,52	8,36	8,87	8,99	10,86	10,51
CaO	9,37	9,60	9,32	9,48	8,94	9,43	9,69	8,75	8,84
Total	**100,71**	**101,33**	**101,50**	**101,59**	**101,59**	**101,80**	**101,77**	**102,41**	**101,85**
Si	3,01	3,01	2,99	2,99	2,99	2,97	2,98	2,93	2,99
Ti	0,01	0,01	0,01	0,01	0,01	0,01	0,01	0,01	0,01
Al	1,95	1,95	2,00	2,00	2,01	2,03	2,01	2,01	2,00
Fe^{2+}	1,29	1,26	1,23	1,26	1,30	1,24	1,22	1,11	1,13
Mn	0,03	0,02	0,03	0,03	0,04	0,03	0,02	0,14	0,01
Mg	0,96	0,97	1,00	0,95	0,93	0,99	1,00	1,17	1,15
Ca	0,76	0,77	0,75	0,76	0,72	0,75	0,77	0,68	0,70
Total	**8,01**	**8,00**	**8,00**	**8,00**	**8,00**	**8,02**	**8,01**	**8,06**	**8,00**
X_{Grs}	0,25	0,26	0,25	0,25	0,24	0,25	0,26	0,22	0,23
X_{Alm}	0,43	0,42	0,41	0,42	0,43	0,41	0,41	0,36	0,38
X_{Pyr}	0,32	0,32	0,33	0,32	0,31	0,33	0,33	0,38	0,39
X_{Sps}	0,01	0,01	0,01	0,01	0,01	0,01	0,01	0,05	0,00
X_{Mg}	0,43	0,44	0,45	0,43	0,42	0,44	0,45	0,51	0,51

GRT cores-rims sample 18XC20

	GR4	GR6	GR6	GR8	GR9	GR10	GR10	GR11	GR11	GR12	GR12
	Rim	Rim	Rim	Rim	Rim	Core	Rim	Core	Rim	Core	Rim
SiO_2	40,10	40,30	40,24	40,05	40,16	40,01	40,07	40,00	40,67	40,11	40,41
TiO_2	0,07	0,15	0,09	0,14	0,12	0,12	0,11	0,14	0,15	0,11	0,10
Al_2O_3	22,83	22,57	22,68	21,89	22,46	22,62	22,37	22,54	22,75	22,77	22,80
FeO	21,38	21,48	21,28	21,57	21,31	22,15	21,35	21,77	21,30	22,20	21,06
MnO	0,61	0,73	0,64	0,65	0,65	0,74	0,64	0,70	0,68	0,78	0,64
MgO	7,72	7,66	8,18	8,35	7,90	7,46	8,08	7,42	8,12	7,51	8,11
CaO	9,53	9,84	9,33	9,30	9,88	9,69	9,53	9,71	9,67	9,45	9,34
Total	**102,43**	**102,84**	**102,59**	**102,04**	**102,69**	**102,96**	**102,28**	**102,43**	**103,41**	**103,08**	**102,59**
Si	2,99	3,00	2,99	3,00	2,99	2,98	2,99	2,99	3,00	2,98	3,00
Ti	0,00	0,01	0,01	0,01	0,01	0,01	0,01	0,01	0,01	0,01	0,01
Al	2,01	1,98	1,99	1,93	1,97	1,99	1,97	1,99	1,98	2,00	2,00
Fe^{2+}	1,33	1,34	1,32	1,35	1,33	1,38	1,33	1,36	1,31	1,38	1,31
Mn	0,04	0,05	0,04	0,04	0,04	0,05	0,04	0,04	0,04	0,05	0,04
Mg	0,86	0,85	0,91	0,93	0,88	0,83	0,90	0,83	0,89	0,83	0,90
Ca	0,76	0,78	0,74	0,75	0,79	0,77	0,76	0,78	0,76	0,75	0,74
Total	**8,00**	**8,01**	**8,01**	**8,02**	**8,01**	**8,02**	**8,02**	**8,01**	**8,00**	**8,01**	**8,00**
X_{Grs}	0,25	0,26	0,25	0,24	0,26	0,26	0,25	0,26	0,25	0,25	0,25
X_{Alm}	0,45	0,44	0,44	0,44	0,44	0,46	0,44	0,45	0,44	0,46	0,44
X_{Pyr}	0,29	0,28	0,30	0,30	0,29	0,27	0,30	0,27	0,30	0,28	0,30
X_{Sps}	0,01	0,02	0,01	0,01	0,01	0,02	0,01	0,01	0,01	0,02	0,01
X_{Mg}	0,39	0,39	0,41	0,41	0,40	0,38	0,40	0,38	0,40	0,38	0,41

CPX profiles sample 18XC1

CPX1	CP1-1	CP1-2	CP1-3	CP1-4
	Rim	Core	Core	Rim
SiO_2	45,83	45,01	45,39	44,53
TiO_2	1,31	1,32	1,35	1,52
Al_2O_3	13,18	12,97	12,67	13,58
FeO	8,07	7,96	7,98	8,28
MnO	0,03	0,05	0,00	0,05
MgO	9,02	9,13	8,83	8,47
CaO	20,78	20,55	20,66	20,56
Na_2O	1,60	1,66	1,65	1,60
Total	**99,92**	**98,77**	**98,76**	**98,74**
Si	1,71	1,70	1,71	1,68
Ti	0,04	0,04	0,04	0,04
Al	0,58	0,58	0,56	0,61
Fe^{2+}	0,25	0,25	0,25	0,26
Mn	0,00	0,00	0,00	0,00
Mg	0,50	0,51	0,50	0,48
Ca	0,83	0,83	0,84	0,83
Na	0,12	0,12	0,12	0,12
Total	**4,02**	**4,03**	**4,02**	**4,03**
X_{Mg}	0,67	0,67	0,66	0,65
Jd	12	12	12	12

CPX3	CPX3-1	CPX3-2	CPX3-3	CPX3-4	CPX3-5	CPX3-6	CPX3-7	CPX3-9	CPX3-10
	Rim	Rim			Core			Rim	Rim
SiO_2	44,58	46,08	46,42	46,02	46,08	45,81	45,88	45,40	45,77
TiO_2	1,28	1,33	1,34	1,39	1,40	1,42	1,50	1,56	1,61
Al_2O_3	13,99	12,75	12,69	12,95	12,51	12,92	13,34	13,27	13,70
FeO	10,10	8,04	8,10	8,04	8,35	7,97	7,96	8,04	7,90
MnO	0,06	0,03	0,08	0,00	0,05	0,00	0,01	0,00	0,07
MgO	8,87	8,98	9,15	9,04	9,18	8,87	9,02	8,80	8,52
CaO	18,51	20,54	20,35	20,17	20,53	20,23	20,38	20,74	20,52
Na_2O	1,46	1,81	1,64	1,68	1,56	1,72	1,89	1,50	1,65
Total	**99,08**	**99,62**	**99,95**	**99,40**	**99,81**	**99,10**	**100,14**	**99,60**	**99,88**
Si	1,68	1,72	1,73	1,72	1,72	1,72	1,71	1,70	1,70
Ti	0,04	0,04	0,04	0,04	0,04	0,04	0,04	0,04	0,05
Al	0,62	0,56	0,56	0,57	0,55	0,57	0,58	0,59	0,60
Fe^{2+}	0,32	0,25	0,25	0,25	0,26	0,25	0,25	0,25	0,25
Mn	0,00	0,00	0,00	0,00	0,00	0,00	0,00	0,00	0,00
Mg	0,50	0,50	0,51	0,50	0,51	0,50	0,50	0,49	0,47
Ca	0,75	0,82	0,81	0,81	0,82	0,81	0,81	0,83	0,82
Na	0,11	0,13	0,12	0,12	0,11	0,13	0,14	0,11	0,12
Total	**4,02**	**4,03**	**4,02**	**4,02**	**4,02**	**4,02**	**4,03**	**4,02**	**4,01**
X_{Mg}	0,61	0,67	0,67	0,67	0,66	0,66	0,67	0,66	0,66
Jd	11	13	12	12	11	13	14	11	12

CPX profiles sample 18XC6

CPX4	CP4-21	CP4-22	CP4-23	CP4-24	CP4-25	CP4-26	CP4-27	CP4-28	CP4-30
	Rim	Rim							Core
SiO_2	51,24	51,47	51,17	51,42	51,73	51,34	51,82	51,36	51,68
TiO_2	0,62	0,58	0,56	0,55	0,55	0,60	0,58	0,61	0,53
Al_2O_3	6,09	5,93	6,07	5,80	6,06	5,98	6,04	6,03	6,07
FeO	11,31	11,30	11,43	10,89	11,12	10,96	10,88	11,04	11,09
MnO	0,12	0,07	0,02	0,00	0,03	0,03	0,05	0,08	0,00
MgO	10,28	9,77	10,08	10,47	10,16	10,32	10,20	10,50	10,15
CaO	18,03	18,58	18,22	18,47	18,49	18,26	18,16	18,29	18,31
Na_2O	2,44	2,40	2,31	2,31	2,46	2,35	2,28	2,52	2,40
Total	**100,30**	**100,36**	**99,99**	**100,01**	**100,74**	**99,94**	**100,23**	**100,58**	**100,35**
Si	1,91	1,92	1,92	1,92	1,92	1,92	1,93	1,91	1,92
Ti	0,02	0,02	0,02	0,02	0,02	0,02	0,02	0,02	0,01
Al	0,27	0,26	0,27	0,26	0,27	0,26	0,26	0,26	0,27
Fe^{2+}	0,35	0,35	0,36	0,34	0,35	0,34	0,34	0,34	0,35
Mn	0,00	0,00	0,00	0,00	0,00	0,00	0,00	0,00	0,00
Mg	0,57	0,54	0,56	0,58	0,56	0,57	0,57	0,58	0,56
Ca	0,72	0,74	0,73	0,74	0,74	0,73	0,72	0,73	0,73
Na	0,18	0,17	0,17	0,17	0,18	0,17	0,16	0,18	0,17
Total	**4,02**	**4,02**	**4,02**	**4,02**	**4,02**	**4,02**	**4,01**	**4,03**	**4,02**
X_{Mg}	0,62	0,61	0,61	0,63	0,62	0,63	0,63	0,63	0,62
Jd	18	17	17	17	18	17	16	18	17

	CP4-31	CP4-33	CP4-34	CP4-35	CP4-36	CP4-37	CP4-38	CP4-39	CP4-40
	Core							Rim	Rim
SiO_2	51,39	53,04	50,87	51,24	51,06	51,67	51,32	51,11	50,93
TiO_2	0,57	0,60	0,62	0,55	0,61	0,55	0,56	0,55	0,53
Al_2O_3	6,19	9,04	6,04	6,00	6,15	6,27	5,91	5,91	5,96
FeO	10,99	8,43	10,77	11,05	10,99	11,40	11,32	10,94	11,09
MnO	0,06	0,00	0,03	0,12	0,00	0,08	0,03	0,09	0,06
MgO	10,20	8,51	10,18	10,26	10,45	10,77	10,38	10,09	10,36
CaO	17,96	17,59	18,23	18,60	17,82	18,12	18,33	18,20	18,20
Na_2O	2,38	3,46	2,34	2,40	2,52	2,62	2,57	2,24	2,45
Total	**99,91**	**100,77**	**99,28**	**100,54**	**99,81**	**101,74**	**100,61**	**99,31**	**99,78**
Si	1,92	1,93	1,91	1,91	1,91	1,90	1,91	1,92	1,91
Ti	0,02	0,02	0,02	0,02	0,02	0,02	0,02	0,02	0,02
Al	0,27	0,39	0,27	0,26	0,27	0,27	0,26	0,26	0,26
Fe^{2+}	0,34	0,26	0,34	0,34	0,34	0,35	0,35	0,34	0,35
Mn	0,00	0,00	0,00	0,00	0,00	0,00	0,00	0,00	0,00
Mg	0,57	0,46	0,57	0,57	0,58	0,59	0,58	0,57	0,58
Ca	0,72	0,69	0,74	0,74	0,71	0,71	0,73	0,73	0,73
Na	0,17	0,24	0,17	0,17	0,18	0,19	0,19	0,16	0,18
Total	**4,01**	**3,98**	**4,02**	**4,03**	**4,03**	**4,04**	**4,04**	**4,01**	**4,03**
X_{Mg}	0,62	0,64	0,63	0,62	0,63	0,63	0,62	0,62	0,62
Jd	17	24	17	17	18	19	19	16	18

CPX5	CP5-9	CP5-10	CP5-11	CP5-12	CP5-13	CP5-14	CP5-15	CP5-16	CP5-17	CP5-18	CP5-19	CP5-20
	Rim	Rim				Core	Core				Rim	Rim
SiO_2	50,95	51,05	51,11	51,43	51,71	51,21	51,47	51,29	51,22	51,07	51,30	51,86
TiO_2	0,64	0,70	0,58	0,51	0,59	0,58	0,54	0,52	0,59	0,60	0,56	0,53
Al_2O_3	6,18	6,42	6,05	6,15	6,26	6,15	6,10	5,99	5,84	5,86	5,91	5,95
FeO	11,93	11,39	10,93	11,19	10,99	11,29	11,61	10,85	11,00	10,99	11,13	11,21
MnO	0,07	0,12	0,12	0,04	0,10	0,04	0,10	0,11	0,07	0,12	0,00	0,04
MgO	9,66	10,38	10,20	9,95	10,20	10,19	10,47	10,14	9,84	10,08	10,19	10,25
CaO	17,87	18,35	18,28	17,92	18,33	17,96	18,14	18,13	17,98	18,07	18,05	18,08
Na_2O	2,30	2,40	2,41	2,23	2,61	2,43	2,37	2,47	2,56	2,42	2,21	2,77
Total	**99,79**	**100,93**	**99,78**	**99,50**	**100,94**	**100,10**	**100,99**	**99,72**	**99,22**	**99,47**	**99,48**	**100,88**
Si	1,91	1,90	1,91	1,93	1,91	1,91	1,91	1,92	1,93	1,92	1,93	1,92
Ti	0,02	0,02	0,02	0,01	0,02	0,02	0,02	0,01	0,02	0,02	0,02	0,01
Al	0,27	0,28	0,27	0,27	0,27	0,27	0,27	0,26	0,26	0,26	0,26	0,26
Fe^{2+}	0,37	0,35	0,34	0,35	0,34	0,35	0,36	0,34	0,35	0,35	0,35	0,35
Mn	0,00	0,00	0,00	0,00	0,00	0,00	0,00	0,00	0,00	0,00	0,00	0,00
Mg	0,54	0,57	0,57	0,56	0,56	0,57	0,58	0,57	0,55	0,57	0,57	0,57
Ca	0,72	0,73	0,73	0,72	0,73	0,72	0,72	0,73	0,73	0,73	0,73	0,72
Na	0,17	0,17	0,18	0,16	0,19	0,18	0,17	0,18	0,19	0,18	0,16	0,20
Total	**4,01**	**4,03**	**4,02**	**4,00**	**4,03**	**4,02**	**4,03**	**4,02**	**4,02**	**4,02**	**4,01**	**4,03**
X_{Mg}	0,59	0,62	0,62	0,61	0,62	0,62	0,62	0,62	0,61	0,62	0,62	0,62
Jd	17	17	18	16	19	18	17	18	19	18	16	20

CPX profiles sample 18XC20

CPX1	CP1-1	CP1-2	CP1-3	CP1-4	CP1-5	CP1-6	CP1-7	CP1-8
	Rim	Rim						Core
SiO_2	50,48	50,36	50,45	50,36	51,02	50,76	50,97	50,47
TiO_2	0,65	0,54	0,58	0,55	0,53	0,61	0,46	0,47
Al_2O_3	8,89	8,31	8,08	7,97	8,32	8,04	7,71	7,98
FeO	9,67	9,56	9,54	9,27	9,32	9,50	9,30	9,45
MnO	0,14	0,14	0,12	0,04	0,01	0,00	0,04	0,11
MgO	9,76	9,93	10,43	9,82	10,17	10,16	9,75	9,99
CaO	18,15	18,20	18,38	18,43	18,73	18,43	18,51	18,45
Na_2O	2,60	2,59	2,60	2,52	2,46	2,30	2,39	2,60
Total	**100,35**	**99,64**	**100,25**	**99,00**	**100,74**	**99,91**	**99,18**	**99,60**
Si	1,87	1,87	1,87	1,89	1,88	1,88	1,90	1,88
Ti	0,02	0,02	0,02	0,02	0,01	0,02	0,01	0,01
Al	0,39	0,36	0,35	0,35	0,36	0,35	0,34	0,35
Fe^{2+}	0,30	0,30	0,30	0,29	0,29	0,29	0,29	0,29
Mn	0,00	0,00	0,00	0,00	0,00	0,00	0,00	0,00
Mg	0,54	0,55	0,58	0,55	0,56	0,56	0,54	0,56
Ca	0,72	0,73	0,73	0,74	0,74	0,73	0,74	0,74
Na	0,19	0,19	0,19	0,18	0,18	0,17	0,17	0,19
Total	**4,02**	**4,02**	**4,03**	**4,01**	**4,01**	**4,01**	**4,00**	**4,02**
X_{Mg}	0,64	0,65	0,66	0,65	0,66	0,66	0,65	0,65
Jd	19	19	19	18	18	17	17	19

	CP1-9	CP1-10	CP1-11	CP1-12	CP1-13	CP1-14	CP1-15
						Rim	Rim
SiO_2	50,67	50,56	51,10	50,68	50,52	50,21	50,38
TiO_2	0,54	0,60	0,60	0,59	0,58	0,52	0,61
Al_2O_3	8,24	7,86	8,27	8,18	8,33	8,18	8,48
FeO	9,32	9,10	9,25	9,28	9,44	9,36	9,69
MnO	0,03	0,06	0,12	0,00	0,10	0,09	0,09
MgO	10,39	10,08	10,08	10,06	10,08	9,72	9,96
CaO	18,53	18,36	18,54	18,43	18,46	18,31	18,24
Na_2O	2,44	2,46	2,59	2,47	2,42	2,51	2,51
Total	**100,23**	**99,20**	**100,64**	**99,69**	**99,93**	**98,95**	**100,03**
Si	1,87	1,89	1,88	1,88	1,87	1,88	1,87
Ti	0,02	0,02	0,02	0,02	0,02	0,01	0,02
Al	0,36	0,35	0,36	0,36	0,36	0,36	0,37
Fe^{2+}	0,29	0,28	0,28	0,29	0,29	0,29	0,30
Mn	0,00	0,00	0,00	0,00	0,00	0,00	0,00
Mg	0,57	0,56	0,55	0,56	0,56	0,54	0,55
Ca	0,73	0,73	0,73	0,73	0,73	0,74	0,72
Na	0,17	0,18	0,18	0,18	0,17	0,18	0,18
Total	**4,02**	**4,01**	**4,02**	**4,01**	**4,02**	**4,01**	**4,02**
X_{Mg}	0,67	0,66	0,66	0,66	0,66	0,65	0,65
Jd	17	18	18	18	17	18	18

CPX2	CP2-1	CP2-2	CP2-3	CP2-4	CP2-5	CP2-6	CP2-7	CP2-8
	Rim	Rim						Core
SiO_2	49,77	50,35	50,93	50,26	50,27	50,45	51,00	50,89
TiO_2	0,66	0,62	0,53	0,60	0,56	0,63	0,60	0,57
Al_2O_3	9,33	8,89	8,33	8,24	8,18	8,23	8,43	8,46
FeO	9,98	9,90	9,37	9,45	9,52	9,33	8,92	9,57
MnO	0,11	0,00	0,16	0,08	0,12	0,04	0,16	0,08
MgO	9,42	9,77	9,98	9,74	9,64	10,01	9,93	9,63
CaO	18,40	18,45	18,54	18,43	18,34	18,70	18,61	18,64
Na_2O	2,75	2,69	2,72	2,36	2,48	2,49	2,56	2,33
Total	**100,47**	**100,79**	**100,62**	**99,23**	**99,18**	**100,01**	**100,28**	**100,33**
Si	1,84	1,86	1,88	1,88	1,88	1,87	1,88	1,88
Ti	0,02	0,02	0,01	0,02	0,02	0,02	0,02	0,02
Al	0,41	0,39	0,36	0,36	0,36	0,36	0,37	0,37
Fe^{2+}	0,31	0,31	0,29	0,30	0,30	0,29	0,28	0,30
Mn	0,00	0,00	0,01	0,00	0,00	0,00	0,00	0,00
Mg	0,52	0,54	0,55	0,54	0,54	0,55	0,55	0,53
Ca	0,73	0,73	0,73	0,74	0,73	0,74	0,74	0,74
Na	0,20	0,19	0,19	0,17	0,18	0,18	0,18	0,17
Total	**4,03**	**4,03**	**4,02**	**4,01**	**4,01**	**4,02**	**4,01**	**4,00**
X_{Mg}	0,63	0,64	0,66	0,65	0,64	0,66	0,66	0,64
Jd	20	19	19	17	18	18	18	17

	CP2-9	CP2-10	CP2-11	CP2-12	CP2-13	CP2-14	CP2-15
						Rim	Rim
SiO_2	50,98	51,20	50,37	50,48	50,41	50,65	50,25
TiO_2	0,63	0,59	0,50	0,62	0,57	0,68	0,60
Al_2O_3	8,33	8,43	8,40	8,52	8,47	9,01	8,73
FeO	9,46	9,07	9,16	9,24	9,26	9,60	9,81
MnO	0,08	0,16	0,05	0,01	0,08	0,17	0,12
MgO	10,23	9,93	10,20	9,83	9,36	9,82	9,54
CaO	18,46	18,40	18,34	18,20	18,50	18,71	18,32
Na_2O	2,68	2,70	2,44	2,63	2,65	2,37	2,66
Total	**100,97**	**100,48**	**99,46**	**99,70**	99,41	101,10	100,06
Si	1,87	1,88	1,87	1,88	1,88	1,86	1,87
Ti	0,02	0,02	0,01	0,02	0,02	0,02	0,02
Al	0,36	0,37	0,37	0,37	0,37	0,39	0,38
Fe^{2+}	0,29	0,28	0,29	0,29	0,29	0,29	0,30
Mn	0,00	0,00	0,00	0,00	0,00	0,01	0,00
Mg	0,56	0,54	0,57	0,54	0,52	0,54	0,53
Ca	0,73	0,73	0,73	0,72	0,74	0,74	0,73
Na	0,19	0,19	0,18	0,19	0,19	0,17	0,19
Total	**4,02**	**4,01**	**4,02**	**4,01**	**4,01**	**4,01**	**4,02**
X_{Mg}	0,66	0,66	0,66	0,65	0,64	0,65	0,63
Jd	19	19	18	19	19	17	19

CPX cores-rims sample 18XC1

	CPX2	CPX4	CPX4	CPX5	CPX5	CPX3	CPX7	CPX7
	Rim	Core	Rim	Core	Rim	Rim	Core	Rim
SiO_2	44,70	46,95	46,08	46,10	46,26	50,73	46,43	50,82
TiO_2	1,59	1,18	1,36	1,20	1,35	0,76	1,32	0,73
Al_2O_3	14,36	12,14	13,07	12,43	13,38	8,66	12,78	8,35
FeO	8,13	7,74	7,93	7,73	7,95	5,96	8,10	5,96
MnO	0,05	0,03	0,02	0,03	0,04	0,09	0,04	0,07
MgO	8,02	9,42	8,85	9,28	8,89	12,06	9,09	11,78
CaO	20,42	20,51	20,43	20,18	20,28	19,63	20,43	19,73
Na_2O	1,69	1,72	1,69	1,72	1,67	1,90	1,64	1,82
Total	**99,14**	**99,85**	**99,57**	**98,78**	**99,96**	**100,02**	**100,08**	**99,50**
Si	1,68	1,75	1,72	1,73	1,72	1,86	1,62	1,87
Ti	0,04	0,03	0,04	0,03	0,04	0,02	0,03	0,02
Al	0,64	0,53	0,57	0,55	0,59	0,37	0,53	0,36
Fe^{2+}	0,26	0,24	0,25	0,24	0,25	0,18	0,24	0,18
Mn	0,00	0,00	0,00	0,00	0,00	0,00	0,00	0,00
Mg	0,45	0,52	0,50	0,52	0,49	0,66	0,83	0,65
Ca	0,82	0,82	0,82	0,81	0,81	0,77	0,77	0,78
Na	0,12	0,12	0,13	0,13	0,12	0,13	0,11	0,13
Total	**4,02**	**4,02**	**4,03**	**4,02**	**4,01**	**4,00**	**4,00**	**3,99**
X_{Mg}	0,64	0,68	0,66	0,68	0,67	0,78	0,78	0,78
Jd	12	12	13	13	12	13	11	13

CPX cores-rims sample 18XC5

	CPX1	CPX1	CPX2	CPX2	CPX3	CPX3
	Core	Rim	Core	Rim	Core	Rim
SiO_2	50,83	50,73	51,43	50,82	50,94	50,87
TiO_2	0,74	0,76	0,59	0,73	0,75	0,70
Al_2O_3	8,35	8,66	7,78	8,35	8,13	8,44
FeO	5,75	5,96	5,58	5,96	5,67	5,89
MnO	0,01	0,09	0,01	0,07	0,02	0,05
MgO	12,17	12,06	12,30	11,78	12,12	12,10
CaO	19,84	19,63	19,92	19,73	20,07	19,93
Na_2O	1,87	1,90	1,97	1,82	1,97	1,88
Total	**99,71**	**100,02**	**99,79**	**99,50**	**99,84**	**100,07**
Si	1,86	1,86	1,88	1,87	1,87	1,86
Ti	0,02	0,02	0,02	0,02	0,02	0,02
Al	0,36	0,37	0,34	0,36	0,35	0,36
Fe^{2+}	0,18	0,18	0,17	0,18	0,17	0,18
Mn	0,00	0,00	0,00	0,00	0,00	0,00
Mg	0,67	0,66	0,67	0,65	0,66	0,66
Ca	0,78	0,77	0,78	0,78	0,79	0,78
Na	0,13	0,13	0,14	0,13	0,14	0,13
Total	**4,00**	**4,00**	**4,00**	**3,99**	**4,01**	**4,00**
X_{Mg}	0,79	0,78	0,80	0,78	0,79	0,79
Jd	13	13	14	13	14	13

CPX cores-rims sample 18XC6

	CPX1	CPX2	CPX2	CPX3	CPX3	CPX4	CPX5	CPX6
	Rim	Core	Rim	Core	Rim	Rim	Rim	Rim
SiO_2	51,44	51,68	51,24	51,87	50,66	51,13	51,32	51,30
TiO_2	0,57	0,53	0,54	0,49	0,57	0,59	0,58	0,56
Al_2O_3	5,76	5,74	5,85	5,56	5,88	6,25	6,28	5,72
FeO	11,63	11,34	11,59	11,42	11,27	11,23	11,13	11,11
MnO	0,07	0,10	0,03	0,04	0,10	0,06	0,08	0,08
MgO	9,96	9,99	9,94	10,25	9,89	10,17	10,08	10,09
CaO	18,14	18,16	18,08	18,20	18,36	18,16	18,13	18,32
Na_2O	2,38	2,35	2,44	2,38	2,39	2,42	2,46	2,43
Total	**100,13**	**100,09**	**99,90**	**100,35**	**99,28**	**100,16**	**100,18**	**99,77**
Si	1,87	1,93	1,92	1,93	1,91	1,91	1,91	1,91
Ti	0,02	0,01	0,02	0,01	0,02	0,02	0,02	0,02
Al	0,50	0,25	0,26	0,24	0,26	0,27	0,28	0,28
Fe^{2+}	0,16	0,35	0,36	0,36	0,36	0,35	0,35	0,35
Mn	0,00	0,00	0,00	0,00	0,00	0,00	0,00	0,00
Mg	0,54	0,56	0,56	0,57	0,56	0,57	0,56	0,56
Ca	0,70	0,73	0,73	0,73	0,74	0,73	0,72	0,72
Na	0,17	0,17	0,18	0,17	0,18	0,18	0,18	0,18
Total	**3,95**	**4,01**	**4,02**	**4,02**	**4,03**	**4,02**	**4,02**	**4,02**
X_{Mg}	0,77	0,61	0,60	0,62	0,61	0,62	0,78	0,62
Jd	17	17	18	17	18	18	18	18

CPX cores-rims sample 18XC10

	CPX1a	CPX1a	CPX1	CPX1	CPX2	CPX2	CPX4	CPX4
	Core	Rim	Core	Rim	Core	Rim	Core	Rim
SiO_2	51,42	50,99	50,60	50,93	50,63	50,42	50,96	51,18
TiO_2	0,60	0,72	0,59	0,54	0,60	0,72	0,65	0,63
Al_2O_3	6,34	6,68	6,43	6,31	6,39	6,58	6,46	6,45
FeO	8,22	8,36	8,16	8,43	8,33	8,87	8,54	8,33
MnO	0,07	0,11	0,08	0,11	0,08	0,06	0,01	0,07
MgO	11,83	11,98	12,10	12,18	11,90	11,84	11,94	12,21
CaO	18,45	18,54	18,78	18,72	18,71	18,47	18,46	18,40
Na_2O	2,15	2,08	2,23	2,08	2,13	2,06	2,17	2,20
Total	**99,29**	**99,68**	**99,19**	**99,53**	**99,00**	**99,17**	**99,42**	**99,61**
Si	1,91	1,89	1,89	1,89	1,89	1,89	1,90	1,90
Ti	0,02	0,02	0,02	0,02	0,02	0,02	0,02	0,02
Al	0,28	0,29	0,28	0,28	0,28	0,28	0,28	0,28
Fe^{2+}	0,26	0,26	0,25	0,25	0,26	0,26	0,27	0,27
Mn	0,00	0,00	0,00	0,00	0,00	0,00	0,00	0,00
Mg	0,66	0,66	0,67	0,67	0,66	0,66	0,66	0,66
Ca	0,73	0,74	0,75	0,75	0,75	0,75	0,74	0,74
Na	0,15	0,15	0,16	0,16	0,15	0,15	0,16	0,16
Total	**4,01**	**4,02**	**4,03**	**4,03**	**4,02**	**4,02**	**4,02**	**4,02**
X_{Mg}	0,72	0,72	0,73	0,73	0,72	0,72	0,71	0,71
Jd	15	15	16	16	15	15	16	16

	CPX5	CPX5	CXP6	CXP6	CPX7	CPX8	CPX8	CPX10
	Core	Rim	Core	Rim	Rim	Core	Rim	Rim
SiO_2	51,66	51,01	50,40	50,70	50,30	50,20	49,59	50,40
TiO_2	0,55	0,60	0,70	0,69	0,68	0,56	0,63	0,68
Al_2O_3	6,64	6,51	6,27	6,54	6,66	6,07	6,66	6,71
FeO	7,87	8,42	8,79	8,48	8,26	8,27	8,40	8,01
MnO	0,04	0,04	0,07	0,10	0,05	0,11	0,02	0,06
MgO	12,02	12,16	12,11	11,81	12,00	12,14	11,51	12,15
CaO	18,91	18,38	18,78	18,68	18,74	18,60	18,59	18,53
Na_2O	2,16	2,06	2,20	2,14	2,06	2,29	2,22	2,13
Total	**100,02**	**99,31**	**99,63**	**99,39**	**98,99**	**98,54**	**97,85**	**98,88**
Si	1,90	1,90	1,88	1,88	1,88	1,89	1,88	1,88
Ti	0,02	0,02	0,02	0,02	0,02	0,02	0,02	0,02
Al	0,29	0,29	0,28	0,28	0,29	0,27	0,30	0,30
Fe^{2+}	0,24	0,24	0,27	0,27	0,26	0,26	0,27	0,25
Mn	0,00	0,00	0,00	0,00	0,00	0,00	0,00	0,00
Mg	0,66	0,66	0,67	0,67	0,67	0,68	0,65	0,68
Ca	0,75	0,75	0,75	0,75	0,75	0,75	0,76	0,74
Na	0,15	0,15	0,16	0,16	0,15	0,17	0,16	0,15
Total	**4,01**	**4,01**	**4,04**	**4,04**	**4,00**	**4,04**	**4,03**	**4,03**
X_{Mg}	0,73	0,73	0,71	0,71	0,71	0,72	0,71	0,73
Jd	15	15	16	16	15	17	16	15

CPX cores-rims sample 18XC15

	CPX1	CPX1	CPX1	CPX2	CPX2	CPX3	CPX3	CPX4	CPX4
	Core	Rim	Rim	Core	Rim	Core	Rim	Rim	Rim
SiO_2	50,31	49,79	50,31	50,42	50,11	50,14	50,59	49,73	51,24
TiO_2	0,71	0,75	0,79	0,69	0,77	0,80	0,77	0,82	0,54
Al_2O_3	7,30	7,62	7,53	7,75	7,88	7,59	7,48	7,71	5,85
FeO	8,41	8,72	8,63	7,86	8,49	8,23	8,00	8,05	11,59
MnO	0,07	0,07	0,11	0,05	0,04	0,07	0,04	0,06	0,03
MgO	11,17	11,05	11,00	11,06	11,07	11,01	11,29	11,10	9,94
CaO	19,65	19,56	19,41	19,76	19,48	19,87	19,96	19,68	18,08
Na_2O	1,64	1,62	1,53	1,62	1,55	1,53	1,74	1,71	2,44
Total	**99,41**	**99,36**	**99,54**	**99,40**	**99,57**	**99,42**	**100,09**	**98,98**	**99,90**
Si	1,87	1,86	1,87	1,87	1,86	1,87	1,87	1,86	1,87
Ti	0,02	0,02	0,02	0,02	0,02	0,02	0,02	0,02	0,02
Al	0,32	0,34	0,33	0,34	0,35	0,33	0,33	0,34	0,33
Fe^{2+}	0,26	0,00	0,00	0,24	0,26	0,26	0,25	0,25	0,24
Mn	0,00	0,27	0,27	0,00	0,00	0,00	0,00	0,00	0,00
Mg	0,62	0,00	0,00	0,61	0,61	0,61	0,62	0,62	0,61
Ca	0,78	0,62	0,61	0,79	0,78	0,79	0,79	0,79	0,80
Na	0,12	0,12	0,11	0,12	0,11	0,11	0,12	0,12	0,10
Total	**4,00**	**4,01**	**3,99**	**4,00**	**4,00**	**4,00**	**4,01**	**4,01**	**3,99**
X_{Mg}	0,70	0,69	0,69	0,71	0,70	0,70	0,72	0,71	0,71
Jd	12	12	11	12	11	11	12	12	10

	CPX5	CPX5	CPX6	CPX6	CPX7	CPX8	CPX9	CPX9	CPX10	CPX10
	Core	Rim	Core	Rim	Core	Core	Core	Rim	Core	Rim
SiO_2	50,40	49,84	50,29	49,87	50,50	50,01	49,96	50,26	50,81	50,26
TiO_2	0,77	0,75	0,69	0,76	0,73	0,77	0,77	0,83	0,73	0,75
Al_2O_3	7,83	7,70	7,51	8,00	7,82	7,80	7,88	8,05	7,64	8,11
FeO	7,82	7,82	8,44	8,33	8,09	7,86	6,81	6,87	6,68	6,86
MnO	0,10	0,13	0,04	0,07	0,03	0,07	0,03	0,06	0,03	0,10
MgO	11,20	11,17	11,16	11,20	11,02	11,32	11,94	11,80	11,95	11,86
CaO	19,85	19,78	19,52	19,71	19,66	19,81	19,96	19,91	20,25	19,96
Na_2O	1,52	1,62	1,56	1,61	1,62	1,47	1,55	1,59	1,58	1,45
Total	**99,61**	**98,98**	**99,42**	**99,83**	**99,68**	**99,24**	**99,08**	**99,57**	**99,85**	**99,56**
Si	1,87	1,86	1,87	1,85	1,87	1,86	1,86	1,86	1,87	1,86
Ti	0,02	0,02	0,02	0,02	0,02	0,02	0,02	0,02	0,02	0,02
Al	0,34	0,34	0,33	0,35	0,34	0,34	0,35	0,35	0,33	0,35
Fe^{2+}	0,24	0,24	0,26	0,26	0,25	0,24	0,21	0,21	0,21	0,21
Mn	0,00	0,00	0,00	0,00	0,00	0,00	0,00	0,00	0,00	0,00
Mg	0,62	0,62	0,62	0,62	0,61	0,63	0,66	0,65	0,66	0,65
Ca	0,79	0,79	0,78	0,78	0,78	0,79	0,79	0,79	0,80	0,79
Na	0,11	0,12	0,11	0,12	0,12	0,11	0,11	0,11	0,11	0,10
Total	**3,99**	**4,00**	**4,00**	**4,01**	**3,99**	**4,00**	**4,01**	**4,00**	**4,00**	**4,00**
X_{Mg}	0,72	0,72	0,70	0,71	0,71	0,72	0,76	0,75	0,76	0,76
Jd	11	12	11	12	12	11	11	11	11	10

CPX cores-rims sample 18XC20

	CPX2	CPX3	CPX3	CPX4
	Rim	Rim	Rim	Rim
SiO_2	49,73	49,73	50,09	50,12
TiO_2	0,64	0,69	0,63	0,64
Al_2O_3	9,08	9,22	8,80	9,42
FeO	9,46	9,73	9,87	9,58
MnO	0,10	0,10	0,04	0,15
MgO	9,75	9,65	9,87	9,76
CaO	18,55	18,45	18,38	18,37
Na_2O	2,50	2,49	2,45	2,59
Total	**99,93**	**100,18**	**100,27**	**100,73**
Si	1,85	1,85	1,86	1,85
Ti	0,02	0,02	0,02	0,02
Al	0,40	0,40	0,38	0,41
Fe^{2+}	0,29	0,30	0,31	0,30
Mn	0,00	0,00	0,00	0,00
Mg	0,54	0,53	0,55	0,54
Ca	0,74	0,73	0,73	0,73
Na	0,18	0,18	0,18	0,18
Total	**4,00**	**4,02**	**4,02**	**4,02**
X_{Mg}	0,65	0,64	0,64	0,65
Jd	18	18	18	18

PL profiles sample 18XC1

PL1	PL1-10	PL1-11	PL1-12	PL1-13	PL1-14	PL1-15	PL1-16	PL1-17	PL1-18	PL1-19	PL1-20
	Rim	Rim								Core	Core
SiO_2	54,17	54,33	54,92	56,00	56,28	55,97	55,57	55,24	55,58	56,03	55,98
Al_2O_3	27,02	26,57	26,59	26,23	25,45	25,40	25,48	25,07	25,43	25,19	24,49
CaO	11,36	11,28	10,71	10,18	10,00	9,88	9,97	10,15	9,96	10,01	10,03
Na_2O	4,82	4,80	4,90	5,49	5,72	5,29	5,84	5,49	5,43	5,58	5,38
K_2O	0,29	0,36	0,35	0,38	0,39	0,39	0,40	0,44	0,40	0,40	0,39
Total	**97,97**	**97,53**	**97,76**	**98,57**	**98,12**	**97,27**	**97,67**	**96,86**	**97,02**	**97,65**	**96,62**
Si	2,50	2,52	2,53	2,56	2,58	2,59	2,57	2,57	2,58	2,58	2,61
Al	1,47	1,45	1,44	1,41	1,38	1,38	1,39	1,38	1,39	1,37	1,34
Ca	0,56	0,56	0,53	0,50	0,49	0,49	0,49	0,51	0,49	0,49	0,50
Na	0,43	0,43	0,44	0,49	0,51	0,47	0,52	0,50	0,49	0,50	0,49
K	0,02	0,02	0,02	0,02	0,02	0,02	0,02	0,03	0,02	0,02	0,02
Total	**4,99**	**4,98**	**4,97**	**4,99**	**4,99**	**4,97**	**5,01**	**4,99**	**4,98**	**4,99**	**4,97**
Ab	43	43	44	48	50	48	50	48	48	49	48
An	56	55	54	49	48	50	47	49	49	49	50
Or	2	2	2	2	2	2	2	3	2	2	2

PL profiles sample 18XC6

PL2	PL2-1	PL2-2	PL2-3	PL2-5	PL2-6	PL2-7	PL2-8	PL2-9	PL2-10
	Rim	Rim			Core				Rim
SiO_2	62,81	62,80	63,15	62,39	63,13	62,94	62,87	62,80	62,48
Al_2O_3	22,50	22,36	22,81	22,47	22,68	23,17	22,29	22,35	22,92
CaO	4,27	4,31	4,27	4,43	4,33	4,25	4,28	4,33	4,32
Na_2O	8,49	8,48	8,25	8,17	8,31	8,36	8,22	8,20	8,50
K_2O	0,67	0,56	0,68	0,64	0,64	0,64	0,66	0,64	0,65
Total	**99,17**	**98,80**	**99,50**	**98,42**	**99,53**	**99,65**	**98,61**	**98,54**	**99,34**
Si	2,81	2,81	2,81	2,81	2,81	2,79	2,82	2,82	2,79
Al	1,18	1,18	1,19	1,19	1,19	1,21	1,18	1,18	1,21
Ca	0,20	0,21	0,20	0,21	0,21	0,20	0,21	0,21	0,21
Na	0,74	0,74	0,71	0,71	0,72	0,72	0,71	0,71	0,74
K	0,04	0,03	0,04	0,04	0,04	0,04	0,04	0,04	0,04
Total	**4,98**	**4,98**	**4,97**	**4,97**	**4,97**	**4,97**	**4,96**	**4,96**	**4,99**
Ab	75	76	75	74	75	75	75	74	75
An	21	21	21	22	22	21	21	22	21
Or	4	3	4	4	4	4	4	4	4

PL3	PL3-1	PL3-2	PL3-3	PL3-4	PL3-5	PL3-6	PL3-7	PL3-8	PL3-9	PL3-10
	Rim	Rim			Core				Rim	Rim
SiO_2	62,09	62,80	63,29	62,85	62,91	63,74	62,92	63,76	63,65	63,10
Al_2O_3	22,63	22,52	22,29	22,51	22,66	22,73	22,72	22,53	22,88	22,43
CaO	4,04	4,25	4,32	4,20	4,23	4,19	4,19	4,33	4,19	4,21
Na_2O	8,39	8,18	8,33	8,56	8,33	8,23	8,27	8,26	8,28	**8,13**
K_2O	0,65	0,65	0,61	0,65	0,64	0,61	0,64	0,66	0,65	0,62
Total	**98,10**	**98,76**	**99,13**	**99,10**	**99,01**	**99,69**	**99,18**	**99,93**	**100,07**	**98,96**
Si	2,80	2,81	2,82	2,81	2,81	2,82	2,81	2,82	2,81	2,82
Al	1,20	1,19	1,17	1,19	1,19	1,19	1,19	1,18	1,19	1,18
Ca	0,20	0,20	0,21	0,20	0,20	0,20	0,20	0,21	0,20	0,20
Na	0,73	0,71	0,72	0,74	0,72	0,71	0,71	0,71	0,71	0,70
K	0,04	0,04	0,03	0,04	0,04	0,03	0,04	0,04	0,04	0,04
Total	**4,98**	**4,96**	**4,96**	**4,98**	**4,97**	**4,95**	**4,97**	**4,96**	**4,96**	**4,95**
Ab	76	75	75	76	75	75	75	74	75	75
An	20	21	21	21	21	21	21	22	21	21
Or	4	4	4	4	4	4	4	4	4	4

PL profiles sample 18XC15

PL1	PL1-1	PL1-2	PL1-3	PL1-4	PL1-5	PL1-6	PL1-7	PL1-8	PL1-9	PL1-10	PL1-12	PL1-13	PL1-14	PL1-15
	Rim	Rim					Core	Core					Rim	Rim
SiO_2	57,29	58,54	58,29	59,43	58,45	57,84	58,88	58,63	58,47	59,17	59,27	58,78	59,30	59,13
Al_2O_3	24,44	24,58	23,87	24,95	24,29	24,34	24,43	24,51	24,34	24,85	24,17	24,39	24,42	24,63
CaO	7,49	7,70	7,51	7,62	7,67	7,22	7,73	7,77	7,73	7,82	7,56	7,71	7,70	7,65
Na_2O	6,86	6,67	6,41	6,93	6,69	6,40	6,46	6,87	6,74	6,58	6,67	6,62	6,42	6,65
K_2O	0,30	0,28	0,29	0,32	0,28	0,57	0,36	0,23	0,25	0,29	0,28	0,28	0,29	0,31
Total	**96,85**	**98,18**	**96,99**	**99,43**	**97,60**	**96,77**	**98,17**	**98,28**	**97,83**	**99,18**	**98,24**	**98,03**	**98,38**	**98,69**
Si	2,65	2,66	2,68	2,67	2,67	2,67	2,68	2,67	2,67	2,66	2,69	2,68	2,68	2,67
Al	1,33	1,32	1,30	1,32	1,31	1,32	1,31	1,31	1,31	1,32	1,29	1,31	1,30	1,31
Ca	0,37	0,38	0,37	0,37	0,38	0,36	0,38	0,38	0,38	0,38	0,37	0,38	0,37	0,37
Na	0,61	0,59	0,57	0,60	0,59	0,57	0,57	0,61	0,60	0,57	0,59	0,58	0,56	0,58
K	0,02	0,02	0,02	0,02	0,02	0,03	0,02	0,01	0,01	0,02	0,02	0,02	0,02	0,02
Total	**5,00**	**4,97**	**4,96**	**4,98**	**4,97**	**4,97**	**4,96**	**4,98**	**4,98**	**4,96**	**4,96**	**4,97**	**4,95**	**4,97**
Ab	61	60	60	61	60	59	59	61	60	59	60	60	59	60
An	37	38	39	37	38	37	39	38	38	39	38	39	39	38
Or	2	2	2	2	2	4	2	1	1	2	2	2	2	2

PL3	PL3-1	PL3-2	PL3-3	PL3-4	PL3-5	PL3-6	PL3-7	PL3-8	PL3-9	PL3-10	PL3-11	PL3-12	PL3-13
	Rim	Rim				Core	Core					Rim	Rim
SiO_2	57,92	59,09	58,42	58,65	59,20	59,12	58,91	58,36	58,80	59,25	59,90	58,79	58,49
Al_2O_3	24,14	24,23	23,74	24,87	24,17	24,68	24,95	24,75	24,43	24,36	23,77	23,98	24,65
CaO	7,69	7,47	7,37	7,56	7,56	7,59	7,60	7,56	7,55	7,72	7,57	7,60	7,64
Na_2O	6,84	6,51	6,46	6,81	6,84	6,76	6,59	6,73	6,57	6,45	6,49	6,71	6,35
K_2O	0,25	0,29	0,29	0,28	0,30	0,29	0,27	0,30	0,28	0,28	0,30	0,28	0,27
Total	**97,29**	**97,86**	**96,54**	**98,55**	**98,47**	**98,82**	**98,59**	**98,00**	**97,84**	**98,46**	**98,31**	**97,79**	**97,80**
Si	2,66	2,69	2,70	2,66	2,68	2,67	2,66	2,66	2,68	2,68	2,71	2,69	2,67
Al	1,31	1,30	1,29	1,33	1,29	1,31	1,33	1,33	1,31	1,30	1,27	1,29	1,32
Ca	0,38	0,36	0,36	0,37	0,37	0,37	0,37	0,37	0,37	0,37	0,37	0,37	0,37
Na	0,61	0,57	0,58	0,60	0,60	0,59	0,58	0,59	0,58	0,57	0,57	0,59	0,56
K	0,01	0,02	0,02	0,02	0,02	0,02	0,02	0,02	0,02	0,02	0,02	0,02	0,02
Total	**4,99**	**4,95**	**4,95**	**4,98**	**4,97**	**4,97**	**4,96**	**4,98**	**4,96**	**4,95**	**4,94**	**4,97**	**4,95**
Ab	61	60	60	61	61	61	60	61	60	59	60	60	59
An	38	38	38	37	37	38	38	38	38	39	39	38	39
Or	1	2	2	2	2	2	2	2	2	2	2	2	2

PL profiles sample 18XC20

PL1	PL1-1	PL1-2	PL1-3	PL1-4	PL1-5	PL1-6	PL1-7	PL1-8	PL1-9	PL1-10	PL1-12	PL1-13	PL1-14	PL1-15
	Rim	Rim					Core	Core					Rim	Rim
SiO_2	57,29	58,54	58,29	59,43	58,45	57,84	58,88	58,63	58,47	59,17	59,27	58,78	59,30	59,13
Al_2O_3	24,44	24,58	23,87	24,95	24,29	24,34	24,43	24,51	24,34	24,85	24,17	24,39	24,42	24,63
CaO	7,49	7,70	7,51	7,62	7,67	7,22	7,73	7,77	7,73	7,82	7,56	7,71	7,70	7,65
Na_2O	6,86	6,67	6,41	6,93	6,69	6,40	6,46	6,87	6,74	6,58	6,67	6,62	6,42	6,65
K_2O	0,30	0,28	0,29	0,32	0,28	0,57	0,36	0,23	0,25	0,29	0,28	0,28	0,29	0,31
Total	**96,85**	**98,18**	**96,99**	**99,43**	**97,60**	**96,77**	**98,17**	**98,28**	**97,83**	**99,18**	**98,24**	**98,03**	**98,38**	**98,69**
Si	2,65	2,66	2,68	2,67	2,67	2,67	2,68	2,67	2,67	2,66	2,69	2,68	2,68	2,67
Al	1,33	1,32	1,30	1,32	1,31	1,32	1,31	1,31	1,31	1,32	1,29	1,31	1,30	1,31
Ca	0,37	0,38	0,37	0,37	0,38	0,36	0,38	0,38	0,38	0,38	0,37	0,38	0,37	0,37
Na	0,61	0,59	0,57	0,60	0,59	0,57	0,57	0,61	0,60	0,57	0,59	0,58	0,56	0,58
K	0,02	0,02	0,02	0,02	0,02	0,03	0,02	0,01	0,01	0,02	0,02	0,02	0,02	0,02
Total	**5,00**	**4,97**	**4,96**	**4,98**	**4,97**	**4,97**	**4,96**	**4,98**	**4,98**	**4,96**	**4,96**	**4,97**	**4,95**	**4,97**
Ab	61	60	60	61	60	59	59	61	60	59	60	60	59	60
An	37	38	39	37	38	37	39	38	38	39	38	39	39	38
Or	2	2	2	2	2	4	2	1	1	2	2	2	2	2

PL3	PL3-1	PL3-2	PL3-3	PL3-4	PL3-5	PL3-6	PL3-7	PL3-8	PL3-9	PL3-10	PL3-11	PL3-12	PL3-13
	Rim	Rim				Core	Core					Rim	Rim
SiO_2	57,92	59,09	58,42	58,65	59,20	59,12	58,91	58,36	58,80	59,25	59,90	58,79	58,49
Al_2O_3	24,14	24,23	23,74	24,87	24,17	24,68	24,95	24,75	24,43	24,36	23,77	23,98	24,65
CaO	7,69	7,47	7,37	7,56	7,56	7,59	7,60	7,56	7,55	7,72	7,57	7,60	7,64
Na_2O	6,84	6,51	6,46	6,81	6,84	6,76	6,59	6,73	6,57	6,45	6,49	6,71	6,35
K_2O	0,25	0,29	0,29	0,28	0,30	0,29	0,27	0,30	0,28	0,28	0,30	0,28	0,27
Total	**97,29**	**97,86**	**96,54**	**98,55**	**98,47**	**98,82**	**98,59**	**98,00**	**97,84**	**98,46**	**98,31**	**97,79**	**97,80**
Si	2,66	2,69	2,70	2,66	2,68	2,67	2,66	2,66	2,68	2,68	2,71	2,69	2,67
Al	1,31	1,30	1,29	1,33	1,29	1,31	1,33	1,33	1,31	1,30	1,27	1,29	1,32
Ca	0,38	0,36	0,36	0,37	0,37	0,37	0,37	0,37	0,37	0,37	0,37	0,37	0,37
Na	0,61	0,57	0,58	0,60	0,60	0,59	0,58	0,59	0,58	0,57	0,57	0,59	0,56
K	0,01	0,02	0,02	0,02	0,02	0,02	0,02	0,02	0,02	0,02	0,02	0,02	0,02
Total	**4,99**	**4,95**	**4,95**	**4,98**	**4,97**	**4,97**	**4,96**	**4,98**	**4,96**	**4,95**	**4,94**	**4,97**	**4,95**
Ab	61	60	60	61	61	61	60	61	60	59	60	60	59
An	38	38	38	37	37	38	38	38	38	39	39	38	39
Or	1	2	2	2	2	2	2	2	2	2	2	2	2

PL cores-rims sample 18XC1

	PL1	PL1	PL2a	PL2a	PL2b	PL2b	PL3	PL3	PL3a	PL3a	PL4	PL4
	Core	Rim	Core	Rim	Core	Rim	Core	Rim	Core	Rim	Core	Rim
SiO_2	54,31	54,00	43,00	43,35	54,83	54,77	55,41	54,99	54,81	54,18	54,44	54,77
Al_2O_3	28,74	28,55	33,27	32,81	28,17	28,28	27,15	27,09	28,38	28,52	28,53	28,31
CaO	10,49	10,49	19,73	19,46	10,24	10,38	10,22	10,56	10,23	10,56	10,59	10,13
Na_2O	5,26	4,91	0,13	0,15	5,51	5,18	5,27	5,16	5,39	5,20	5,22	5,48
K_2O	0,38	0,35	0,01	0,00	0,40	0,37	0,40	0,36	0,35	0,37	0,35	0,35
Total	**99,54**	**98,71**	**97,11**	**96,74**	**99,51**	**99,46**	**98,86**	**98,56**	**99,44**	**99,16**	**99,48**	**99,58**
Si	2,46	2,47	2,06	2,08	2,49	2,49	2,53	2,52	2,48	2,47	2,47	2,48
Al	1,54	1,54	1,88	1,86	1,51	1,51	1,46	1,46	1,52	1,53	1,53	1,51
Ca	1,53	0,51	1,01	1,00	0,50	0,50	0,50	0,52	0,50	0,51	0,51	0,49
Na	1,53	0,43	0,01	0,01	0,48	0,46	0,47	0,46	0,47	0,46	0,46	0,48
K	1,53	0,02	0,00	0,00	0,02	0,02	0,02	0,02	0,02	0,02	0,02	0,02
Total	**5,01**	**4,99**	**4,99**	**4,98**	**5,01**	**4,99**	**4,98**	**4,99**	**5,00**	**5,00**	**5,00**	**5,01**
Ab	47	45	1	1	48	46	47	46	48	46	46	48
An	51	53	99	99	49	51	51	52	50	52	52	50
Or	2	2	0	0	2	2	2	2	2	2	2	2

PL cores-rims sample 18XC10

	PL1	PL1	PL1a	PL1a	PL2	PL2	PL3	PL3	PL4	PL4
	Core	Rim	Core	Rim	Core	Rim	Core	Rim	Core	Rim
SiO_2	59,99	59,02	62,08	60,73	59,54	60,19	59,85	59,49	60,03	60,46
Al_2O_3	24,01	32,81	23,78	24,12	23,99	24,12	24,16	24,59	24,21	24,29
CaO	5,22	5,36	5,30	5,40	5,25	5,30	5,42	5,61	5,26	5,30
Na_2O	8,26	8,27	7,98	8,30	8,25	8,01	8,01	8,26	8,25	8,02
K_2O	0,46	0,43	0,49	0,43	0,50	0,46	0,49	0,41	0,48	0,48
Total	**98,33**	**97,37**	**99,93**	**99,34**	**97,81**	**98,42**	**98,26**	**98,75**	**98,48**	**98,79**
Si	2,72	2,70	2,76	2,72	2,71	2,72	2,71	2,72	2,71	2,72
Al	1,28	1,30	1,24	1,27	1,29	1,28	1,29	1,31	1,29	1,29
Ca	0,25	0,26	0,25	0,26	0,26	0,26	0,26	0,27	0,25	0,26
Na	0,73	0,73	0,69	0,72	0,73	0,70	0,70	0,72	0,72	0,70
K	0,03	0,03	0,03	0,02	0,03	0,03	0,03	0,02	0,03	0,03
Total	**5,01**	**5,03**	**4,97**	**5,01**	**5,02**	**5,00**	**5,01**	**5,03**	**5,01**	**5,00**
Ab	72	72	71	72	72	71	71	71	72	71
An	25	26	26	26	25	26	26	27	25	26
Or	3	2	3	2	3	3	3	2	3	3

	PL5	PL5	PL6	PL6	PL7	PL7	PL8	PL8
	Core	Rim	Core	Rim	Core	Rim	Core	Rim
SiO_2	61,50	61,87	60,38	61,01	61,33	60,56	61,30	60,89
Al_2O_3	24,17	24,40	24,21	24,11	23,73	24,28	24,18	24,14
CaO	5,40	5,39	5,32	5,35	5,23	5,28	5,25	5,44
Na_2O	8,21	8,32	8,17	8,22	8,22	8,44	8,08	8,07
K_2O	0,44	0,46	0,43	0,45	0,49	0,46	0,45	0,44
Total	**100,03**	**100,73**	**98,77**	**99,56**	**99,28**	**99,41**	**99,59**	**99,50**
Si	2,73	2,73	2,72	2,73	2,74	2,71	2,73	2,72
Al	1,27	1,27	1,28	1,27	1,25	1,28	1,27	1,27
Ca	0,26	0,25	0,26	0,26	0,25	0,26	0,25	0,26
Na	0,71	0,71	0,71	0,71	0,71	0,70	0,70	0,70
K	0,02	0,03	0,02	0,03	0,03	0,03	0,03	0,03
Total	**5,00**	**5,00**	**5,00**	**5,00**	**5,00**	**5,02**	**4,99**	**5,00**
Ab	72	72	72	72	72	72	72	71
An	26	26	26	26	25	25	26	26
Or	3	3	2	3	3	3	3	3

PL cores-rims sample 18XC15

	PL2	PL2	PL4	PL4
	Core	Rim	Core	Rim
SiO_2	59,23	58,80	57,92	59,02
Al_2O_3	24,54	24,40	25,62	32,81
CaO	7,52	7,61	7,94	5,36
Na_2O	6,73	6,53	6,61	8,27
K_2O	0,29	0,28	0,28	0,43
Total	**98,64**	**97,91**	**98,76**	**98,76**
Si	2,68	2,68	2,66	2,63
Al	1,31	1,31	1,33	1,37
Ca	0,36	0,37	0,38	0,39
Na	0,59	0,58	0,58	0,58
K	0,02	0,02	0,02	0,02
Total	**4,97**	**4,96**	**4,97**	**4,99**
Ab	61	60	59	59
An	38	39	39	39
Or	2	2	2	2

AMP profiles sample 18XC1

AMP1	AM1-1	AM1-2	AM1-3	AM1-4
	Rim	Core	Core	Rim
SiO_2	39,39	39,78	40,29	39,55
TiO_2	2,25	2,38	2,32	2,23
Al_2O_3	17,49	16,95	17,01	16,67
FeO	11,41	11,44	11,61	11,72
MnO	0,00	0,04	0,01	0,03
MgO	11,02	10,78	10,54	10,80
CaO	11,29	11,08	11,10	11,15
Na_2O	2,52	2,34	2,18	2,29
K_2O	1,75	1,70	1,76	1,73
Total	**97,23**	**96,51**	**96,92**	**96,24**
Si	5,92	6,02	6,08	6,01
Ti	0,25	0,27	0,26	0,25
Al	3,10	3,02	3,03	2,98
Fe^{2+}	1,43	1,45	1,46	1,49
Mn	0,00	0,00	0,00	0,00
Mg	2,47	2,43	2,37	2,45
Ca	1,82	1,80	1,79	1,81
Na	0,73	0,69	0,64	0,67
K	0,34	0,33	0,34	0,34
Total	**16,07**	**16,02**	**15,98**	**16,01**
^{IV}Al	2,08	1,98	1,92	1,99
^{VI}Al	1,02	1,05	1,11	0,99
X_{Mg}	0,63	0,63	0,62	0,62

AMP profiles sample 18XC6

AMP1	AM1-1	AM1-2	AM1-3	AM1-4	AM1-5	AM1-6	AM1-7	AM1-8	AM1-10
	Rim	Rim							Core
SiO_2	41,19	41,98	42,38	41,77	41,91	42,42	42,10	42,33	41,56
TiO_2	2,77	2,73	2,65	2,67	2,67	2,69	2,69	2,57	2,61
Al_2O_3	13,07	12,81	12,65	12,84	12,73	12,85	12,47	12,87	12,84
FeO	15,76	15,78	16,01	16,11	15,89	16,13	15,78	16,05	15,94
MnO	0,12	0,00	0,00	0,04	0,03	0,03	0,08	0,00	0,04
MgO	10,14	10,20	10,40	10,16	10,09	10,34	10,19	10,43	10,33
CaO	9,83	9,67	9,79	9,70	9,74	9,85	9,68	9,60	9,71
Na_2O	2,85	2,71	2,90	2,89	2,93	2,91	2,97	3,09	2,71
K_2O	1,23	1,17	1,18	1,22	1,20	1,17	1,18	1,17	1,12
Total	**97,12**	**97,40**	**98,11**	**97,59**	**97,49**	**98,51**	**97,30**	**98,30**	**97,12**
Si	6,15	6,23	6,25	6,20	6,24	6,23	6,27	6,22	6,18
Ti	0,31	0,30	0,29	0,30	0,30	0,30	0,30	0,28	0,29
Al	2,30	2,24	2,20	2,25	2,23	2,22	2,19	2,23	2,25
Fe^{2+}	1,97	1,96	1,97	2,00	1,98	1,98	1,97	1,97	1,98
Mn	0,02	0,00	0,00	0,01	0,00	0,00	0,01	0,00	0,01
Mg	2,26	2,26	2,29	2,25	2,24	2,26	2,26	2,29	2,29
Ca	1,57	1,54	1,55	1,54	1,55	1,55	1,54	1,51	1,55
Na	0,82	0,78	0,83	0,83	0,85	0,83	0,86	0,88	0,78
K	0,23	0,22	0,22	0,23	0,23	0,22	0,22	0,22	0,21
Total	**15,63**	**15,54**	**15,60**	**15,61**	**15,63**	**15,60**	**15,63**	**15,61**	**15,54**
^{IV}Al	1,85	1,77	1,75	1,80	1,76	1,77	1,73	1,78	1,82
^{VI}Al	0,45	0,47	0,45	0,45	0,47	0,45	0,46	0,45	0,43
X_{Mg}	0,62	0,62	0,62	0,62	0,60	0,62	0,61	0,63	0,64

	AM1-11	AM1-12	AM1-13	AM1-14	AM1-15	AM1-16	AM1-17	AM1-18	AM1-19
	Core							Rim	Rim
SiO_2	42,47	42,10	41,90	41,58	42,54	42,87	42,25	42,04	41,83
TiO_2	2,71	2,69	2,62	2,83	2,51	2,67	2,74	2,63	2,73
Al_2O_3	12,58	12,68	12,18	12,73	12,76	12,38	12,56	12,40	12,67
FeO	16,05	16,24	15,90	16,07	15,98	15,55	15,97	16,17	16,19
MnO	0,06	0,07	0,02	0,00	0,07	0,09	0,07	0,00	0,02
MgO	10,33	10,72	10,10	10,32	10,28	10,28	10,46	10,18	9,90
CaO	9,60	9,81	9,68	9,69	9,85	9,70	9,85	9,95	9,90
Na_2O	2,83	2,89	2,71	2,89	3,15	2,99	2,81	2,96	2,69
K_2O	1,17	1,18	1,19	1,25	1,23	1,22	1,22	1,22	1,24
Total	**97,89**	**98,70**	**96,44**	**97,53**	**98,59**	**97,79**	**98,09**	**97,78**	**97,37**
Si	6,26	6,17	6,29	6,17	6,27	6,34	6,23	6,25	6,24
Ti	0,30	0,30	0,30	0,32	0,28	0,30	0,30	0,29	0,31
Al	2,19	2,19	2,16	2,23	2,22	2,16	2,18	2,17	2,23
Fe^{2+}	1,98	1,99	2,00	2,00	1,97	1,92	1,97	2,01	2,02
Mn	0,01	0,01	0,00	0,00	0,01	0,01	0,01	0,00	0,00
Mg	2,27	2,34	2,26	2,28	2,26	2,27	2,30	2,26	2,20
Ca	1,52	1,54	1,56	1,54	1,55	1,54	1,56	1,59	1,58
Na	0,81	0,82	0,79	0,83	0,90	0,86	0,80	0,85	0,78
K	0,22	0,22	0,23	0,24	0,23	0,23	0,23	0,23	0,24
Total	**15,54**	**15,58**	**15,57**	**15,61**	**15,69**	**15,63**	**15,59**	**15,67**	**15,60**
^{IV}Al	1,74	1,83	1,71	1,83	1,73	1,66	1,77	1,75	1,76
^{VI}Al	0,44	0,36	0,45	0,40	0,48	0,50	0,41	0,43	0,46
X_{Mg}	0,63	0,65	0,61	0,63	0,60	0,60	0,63	0,59	0,59

AMP2	AM2-1	AM2-2	AM2-3	AM2-4	AM2-5	AM2-6	AM2-7
	Rim			Core			Rim
SiO_2	42,09	42,29	42,42	42,56	42,28	42,67	41,90
TiO_2	2,63	2,69	2,60	2,60	2,72	2,64	2,73
Al_2O_3	13,23	12,93	12,49	13,20	12,99	12,85	13,09
FeO	16,64	16,11	15,57	15,70	16,23	16,27	16,08
MnO	0,06	0,02	0,04	0,00	0,00	0,02	0,01
MgO	10,20	9,80	9,68	9,87	10,26	9,76	10,11
CaO	9,57	9,85	9,55	9,69	9,67	9,86	9,54
Na_2O	2,84	2,88	2,40	2,66	2,84	2,52	2,72
K_2O	1,21	1,15	1,25	1,22	1,21	1,23	1,21
Total	**98,63**	**97,87**	**96,24**	**97,69**	**98,33**	**98,00**	**97,69**
Si	6,16	6,27	6,37	6,29	6,21	6,31	6,20
Ti	0,29	0,30	0,29	0,29	0,30	0,29	0,30
Al	2,28	2,26	2,21	2,30	2,25	2,24	2,28
Fe^{2+}	2,04	2,00	1,95	1,94	1,99	2,01	1,99
Mn	0,01	0,00	0,01	0,00	0,00	0,00	0,00
Mg	2,22	2,17	2,17	2,17	2,25	2,15	2,23
Ca	1,50	1,57	1,54	1,53	1,52	1,56	1,51
Na	0,81	0,83	0,70	0,76	0,81	0,72	0,78
K	0,23	0,22	0,24	0,23	0,23	0,23	0,23
Total	**15,53**	**15,61**	**15,47**	**15,53**	**15,56**	**15,51**	**15,52**
^{IV}Al	1,84	1,73	1,63	1,71	1,79	1,69	1,80
^{VI}Al	0,44	0,53	0,58	0,59	0,46	0,54	0,48
X_{Mg}	0,64	0,58	0,59	0,60	0,63	0,59	0,63

AMP profiles sample 18XC20

AMP9	AM9-1	AM9-3	AM9-4	AM9-5	AM9-6	AM9-7	AM9-8	AM9-9	AM9-10
	Rim								Core
SiO_2	40,75	40,71	40,61	40,38	40,58	40,88	41,18	40,90	40,83
TiO_2	2,09	1,90	1,99	2,02	1,95	2,05	2,06	2,08	2,14
Al_2O_3	14,79	14,59	14,92	14,57	14,87	14,55	14,62	14,86	14,89
FeO	13,67	14,10	13,71	14,00	13,57	13,90	13,95	13,75	14,31
MnO	0,05	0,07	0,13	0,06	0,00	0,10	0,11	0,11	0,07
MgO	10,76	10,62	10,86	10,62	11,00	10,83	10,64	10,67	10,99
CaO	10,19	9,94	9,82	9,93	9,97	9,71	9,74	9,74	9,82
Na_2O	3,17	3,11	2,96	3,10	3,04	3,20	3,38	3,07	3,04
K_2O	1,22	1,22	1,22	1,22	1,28	1,19	1,18	1,24	1,23
Total	**96,79**	**96,34**	**96,35**	**96,07**	**96,33**	**96,59**	**96,95**	**96,47**	**97,51**
Si	6,07	6,08	6,04	6,05	6,04	6,08	6,11	6,08	6,00
Ti	0,23	0,21	0,22	0,23	0,22	0,23	0,23	0,23	0,24
Al	2,60	2,57	2,61	2,57	2,61	2,55	2,56	2,60	2,58
Fe^{2+}	1,70	1,76	1,70	1,75	1,69	1,73	1,73	1,71	1,76
Mn	0,01	0,01	0,02	0,01	0,00	0,01	0,01	0,01	0,01
Mg	2,39	2,36	2,41	2,37	2,44	2,40	2,35	2,36	2,41
Ca	1,63	1,59	1,56	1,59	1,59	1,55	1,55	1,55	1,55
Na	0,92	0,90	0,85	0,90	0,88	0,92	0,97	0,88	0,87
K	0,23	0,23	0,23	0,23	0,24	0,23	0,22	0,24	0,23
Total	**15,77**	**15,72**	**15,65**	**15,73**	**15,71**	**15,70**	**15,74**	**15,67**	**15,64**
^{IV}Al	1,93	1,92	1,96	1,95	1,96	1,92	1,89	1,92	2,00
^{VI}Al	0,67	0,65	0,65	0,63	0,65	0,63	0,67	0,68	0,59
X_{Mg}	0,65	0,66	0,70	0,66	0,69	0,68	0,65	0,67	0,70

	AM9-11	AM9-12	AM9-13	AM9-14	AM9-15	AM9-16	AM9-17	AM9-18	AM9-19	AM9-20
	Core								Rim	Rim
SiO_2	41,04	41,27	40,97	41,18	41,27	40,80	41,17	41,28	40,56	40,75
TiO_2	2,01	1,98	2,02	1,99	2,09	2,00	2,02	1,90	2,02	2,07
Al_2O_3	14,69	14,77	14,91	14,47	14,46	14,89	14,47	14,71	14,81	14,78
FeO	13,90	14,27	13,70	13,79	14,09	13,65	14,01	13,96	13,76	14,26
MnO	0,11	0,14	0,03	0,05	0,12	0,11	0,08	0,11	0,05	0,04
MgO	11,01	11,08	10,74	10,81	10,92	10,52	10,35	10,65	10,71	10,68
CaO	9,94	9,81	10,01	9,92	9,72	9,85	10,12	10,02	10,04	9,85
Na_2O	2,91	3,19	2,82	3,09	3,27	2,99	2,86	3,01	3,14	2,75
K_2O	1,23	1,26	1,22	1,26	1,29	1,16	1,22	1,22	1,29	1,27
Total	**97,04**	**98,02**	**96,48**	**96,80**	**97,30**	**96,02**	**96,52**	**96,89**	**96,49**	**96,65**
Si	6,06	6,05	6,08	6,12	6,09	6,09	6,15	6,12	6,06	6,05
Ti	0,22	0,22	0,23	0,22	0,23	0,22	0,23	0,21	0,23	0,23
Al	2,56	2,55	2,61	2,54	2,52	2,62	2,55	2,57	2,61	2,59
Fe^{2+}	1,05	1,05	1,16	1,24	1,16	1,20	1,36	1,24	1,26	1,07
Mn	0,01	0,02	0,00	0,01	0,01	0,01	0,01	0,01	0,01	0,01
Mg	2,42	2,42	2,38	2,40	2,40	2,34	2,30	2,35	2,38	2,36
Ca	1,57	1,54	1,59	1,58	1,54	1,58	1,62	1,59	1,61	1,57
Na	0,83	0,91	0,81	0,89	0,94	0,87	0,83	0,87	0,91	0,79
K	0,23	0,24	0,23	0,24	0,24	0,22	0,23	0,23	0,25	0,24
Total	**15,64**	**15,68**	**15,64**	**15,71**	**15,72**	**15,66**	**15,68**	**15,69**	**15,76**	**15,60**
^{IV}Al	1,94	1,95	1,92	1,88	1,91	1,91	1,85	1,88	1,94	1,95
^{VI}Al	0,61	0,60	0,69	0,66	0,61	0,72	0,70	0,69	0,66	0,63
X_{Mg}	0,70	0,70	0,67	0,66	0,67	0,66	0,63	0,65	0,65	0,69

AMP11	AM11-1	AM11-2	AM11-3	AM11-4	AM11-5	AM11-6	AM11-7	AM11-8
	Rim							Core
SiO_2	40,97	40,94	41,46	41,40	41,27	40,91	41,27	40,82
TiO_2	2,03	1,94	2,06	1,98	2,12	2,10	2,05	2,08
Al_2O_3	15,27	15,32	15,14	15,11	15,48	15,37	15,75	15,11
FeO	14,04	14,16	13,77	14,32	14,06	14,68	13,97	14,09
MnO	0,09	0,07	0,07	0,07	0,11	0,08	0,08	0,05
MgO	10,77	10,93	10,68	10,97	10,99	10,77	10,62	10,58
CaO	10,16	9,81	9,91	9,99	9,93	10,09	9,84	9,86
Na_2O	2,98	2,85	3,35	3,04	3,17	2,80	3,23	3,22
K_2O	1,22	1,16	1,15	1,23	1,22	1,20	1,22	1,17
Total	**97,76**	**97,25**	**97,75**	**98,17**	**98,61**	**98,18**	**98,13**	**97,35**
Si	6,02	6,00	6,10	6,04	6,00	5,97	6,03	6,04
Ti	0,22	0,21	0,23	0,22	0,23	0,23	0,23	0,23
Al	2,65	2,65	2,63	2,60	2,65	2,65	2,71	2,64
Fe^{2+}	1,15	0,93	1,27	1,08	1,05	1,02	1,15	1,21
Mn	0,01	0,01	0,01	0,01	0,01	0,01	0,01	0,01
Mg	2,36	2,39	2,34	2,39	2,38	2,34	2,31	2,34
Ca	1,60	1,54	1,56	1,56	1,55	1,58	1,54	1,56
Na	0,85	0,81	0,96	0,86	0,89	0,79	0,91	0,92
K	0,23	0,22	0,22	0,23	0,23	0,22	0,23	0,22
Total	**15,68**	**15,57**	**15,73**	**15,65**	**15,67**	**15,60**	**15,68**	**15,71**
^{IV}Al	1,98	2,00	1,90	1,96	2,00	2,03	1,97	1,96
^{VI}Al	0,67	0,65	0,72	0,64	0,66	0,62	0,74	0,68
X_{Mg}	0,67	0,72	0,65	0,69	0,69	0,70	0,67	0,66

	AM11-9	AM11-10	AM11-11	AM11-12	AM11-13	AM11-14	AM11-15
						Rim	Rim
SiO_2	41,23	41,30	41,30	41,33	40,92	41,18	41,11
TiO_2	2,05	1,99	2,00	1,94	2,01	2,08	2,09
Al_2O_3	15,22	15,66	15,18	15,39	15,46	15,34	15,64
FeO	13,78	14,54	14,17	14,21	14,14	13,96	14,27
MnO	0,10	0,06	0,04	0,05	0,04	0,09	0,11
MgO	10,65	10,74	10,58	10,47	10,93	10,85	10,75
CaO	9,93	10,08	10,10	10,02	10,08	10,09	10,04
Na_2O	2,92	3,05	2,83	3,13	3,11	3,18	3,21
K_2O	1,22	1,25	1,24	1,25	1,20	1,32	1,24
Total	**97,42**	**99,00**	**97,52**	**98,00**	**97,95**	**98,25**	**98,55**
Si	6,07	6,00	6,08	6,07	5,99	6,03	5,99
Ti	0,23	0,22	0,22	0,21	0,22	0,23	0,23
Al	2,64	2,68	2,63	2,66	2,67	2,65	2,69
Fe^{2+}	1,15	1,11	1,20	1,26	1,09	1,20	1,15
Mn	0,01	0,01	0,00	0,01	0,01	0,01	0,01
Mg	2,34	2,32	2,32	2,29	2,38	2,37	2,34
Ca	1,57	1,57	1,59	1,58	1,58	1,58	1,57
Na	0,83	0,86	0,81	0,89	0,88	0,90	0,91
K	0,23	0,23	0,23	0,23	0,22	0,25	0,23
Total	**15,63**	**15,66**	**15,63**	**15,70**	**15,69**	**15,73**	**15,71**
^{IV}Al	1,93	2,00	1,92	1,93	2,01	1,97	2,01
^{VI}Al	0,72	0,67	0,71	0,73	0,66	0,68	0,68
X_{Mg}	0,67	0,68	0,66	0,64	0,69	0,66	0,67

AMP cores-rims sample 18XC1

	AMP1a	AMP1a	AMP2	AMP2	AMP2	AMP2b	AMP2b	AMP3	AMP3	AMP4	AMP4
	Core	Rim	Core	Rim	Rim	Core	Rim	Core	Rim	Core	Rim
SiO_2	38,79	39,12	40,03	39,99	39,74	39,61	39,47	39,25	39,63	40,00	39,04
TiO_2	2,05	2,17	2,23	2,33	2,23	2,21	2,20	2,25	2,33	2,23	2,32
Al_2O_3	18,05	18,34	17,68	17,74	17,73	17,64	18,07	17,75	17,93	17,67	18,06
FeO	11,23	11,35	11,40	11,70	11,30	11,03	11,22	11,57	11,52	11,24	11,70
MnO	0,05	0,00	0,03	0,06	0,04	0,02	0,03	0,05	0,06	0,00	0,06
MgO	11,14	11,09	11,01	10,95	11,06	11,33	10,95	10,81	10,93	11,09	10,86
CaO	11,08	10,92	10,93	10,93	11,07	11,01	11,06	10,96	11,11	11,16	10,96
Na_2O	2,47	2,55	2,37	2,33	2,23	2,28	2,44	2,46	2,52	2,54	2,40
K_2O	1,69	1,71	1,71	1,73	1,79	1,66	1,57	1,61	1,62	1,66	1,64
Total	**96,62**	**97,39**	**97,47**	**97,86**	**97,26**	**96,95**	**97,14**	**96,84**	**97,79**	**97,70**	**97,13**
Si	5,75	5,75	5,88	5,85	5,85	5,82	5,82	5,82	5,82	5,88	5,76
Ti	0,23	0,24	0,25	0,26	0,25	0,24	0,24	0,25	0,26	0,25	0,26
Al	3,16	3,18	3,06	3,06	3,08	3,14	3,06	3,10	3,10	3,06	3,14
Fe^{2+}	1,06	1,05	1,15	1,12	1,13	1,14	1,03	1,17	1,20	1,25	1,08
Mn	0,01	0,00	0,00	0,01	0,01	0,00	0,00	0,01	0,01	0,00	0,01
Mg	2,46	2,43	2,41	2,39	2,43	2,41	2,49	2,39	2,39	2,43	2,39
Ca	1,76	1,72	1,72	1,71	1,75	1,75	1,74	1,74	1,75	1,76	1,73
Na	0,71	0,73	0,67	0,66	0,64	0,70	0,65	0,71	0,72	0,72	0,69
K	0,32	0,32	0,32	0,32	0,34	0,29	0,31	0,30	0,30	0,31	0,31
Total	**15,79**	**15,60**	**15,71**	**15,70**	**15,72**	**15,70**	**15,74**	**15,75**	**15,77**	**15,79**	**15,72**
^{IV}Al	2,25	2,25	2,12	2,15	2,15	2,18	2,16	2,18	2,18	2,12	2,24
^{VI}Al	0,91	0,93	0,94	0,91	0,93	0,96	0,90	0,92	0,93	0,94	0,90
X_{Mg}	0,70	0,70	0,68	0,68	0,68	0,68	0,71	0,67	0,67	0,66	0,69

AMP cores-rims sample 18XC5 – 18XC6

	18XC5		18XC6	
	AMP1	AMP1	AMP1	AMP2
	Core	Rim	Rim	Rim
SiO_2	42,90	43,00	42,00	41,83
TiO_2	1,91	2,05	2,67	2,66
Al_2O_3	15,00	15,13	13,03	13,16
FeO	8,46	8,48	15,91	16,11
MnO	0,06	0,07	0,05	0,05
MgO	14,72	14,38	10,17	10,34
CaO	10,60	10,61	9,75	9,62
Na_2O	2,86	2,89	2,84	2,86
K_2O	1,03	0,97	1,20	1,21
Total	**97,71**	**97,78**	**97,86**	**98,06**
Si	6,12	6,14	6,21	6,16
Ti	0,2	0,22	0,30	0,29
Al	2,52	2,55	2,27	2,28
Fe^{2+}	0,41	0,51	1,39	1,26
Mn	0,01	0,01	0,01	0,01
Mg	3,13	3,06	2,24	2,27
Ca	1,62	1,62	1,54	1,52
Na	0,79	0,8	0,81	0,82
K	0,19	0,18	0,23	0,23
Total	**15,6**	**15,6**	**15,59**	**15,56**
^{IV}Al	1,88	1,86	1,79	1,84
^{VI}Al	0,64	0,69	0,48	0,44
X_{Mg}	0,89	0,86	0,62	0,64

AMP cores-rims sample 18XC10

	AMP1	AMP1	AMP2	AMP3	AMP3
	Core	Rim	Rim	Core	Rim
SiO_2	42,63	42,49	42,17	41,94	41,77
TiO_2	2,29	2,67	2,50	2,49	2,62
Al_2O_3	13,46	13,51	13,25	13,48	13,41
FeO	10,51	10,69	11,03	11,22	11,28
MnO	0,09	0,08	0,03	0,03	0,04
MgO	14,03	13,61	13,49	13,55	13,29
CaO	9,84	9,72	9,77	9,74	9,80
Na_2O	3,04	3,10	3,19	3,14	3,11
K_2O	0,83	0,80	0,77	0,83	0,79
Total	**96,91**	**96,69**	**96,49**	**96,58**	**96,31**
Si	6,16	6,16	5,82	6,10	6,10
Ti	0,25	0,29	0,24	0,27	0,27
Al	2,29	2,31	3,14	2,31	2,31
Fe^{2+}	0,42	0,54	1,14	0,51	0,51
Mn	0,01	0,01	0,01	0,01	0,00
Mg	3,02	2,94	2,41	2,94	2,94
Ca	1,52	1,51	1,75	1,52	1,52
Na	0,85	0,87	0,70	0,87	0,89
K	0,15	0,15	0,29	0,15	0,15
Total	**15,53**	**15,53**	**15,74**	**15,56**	**15,57**
^{IV}Al	1,84	1,84	2,18	1,84	1,90
^{VI}Al	0,45	0,46	0,96	0,42	0,42
X_{Mg}	0,88	0,85	0,68	0,85	0,85

AMP cores-rims sample 18XC20

	AMP4	AMP6	AMP6	AMP8	AMP9	AMP10	AMP10	AMP10	AMP11
	Rim	Rim	Rim	Core	Rim	Rim	Core	Rim	Rim
SiO_2	40,66	40,40	40,44	40,91	40,58	41,34	41,46	41,16	41,01
TiO_2	1,88	1,88	1,87	2,05	2,02	2,06	2,07	2,09	1,98
Al_2O_3	15,92	15,93	16,06	14,63	15,10	15,04	14,97	15,15	15,39
FeO	14,09	14,19	14,45	14,21	14,18	13,81	14,07	14,05	14,19
MnO	0,10	0,12	0,06	0,07	0,12	0,05	0,09	0,10	0,07
MgO	10,89	10,68	11,02	10,97	10,68	10,71	10,58	10,78	10,72
CaO	10,08	9,93	9,93	9,86	10,03	9,98	9,91	9,84	10,02
Na_2O	3,05	3,08	3,04	3,24	3,06	3,01	3,06	3,03	3,10
K_2O	1,22	1,24	1,30	1,22	1,24	1,25	1,26	1,27	1,24
Total	**98,15**	**97,65**	**98,34**	**97,24**	**97,08**	**97,39**	**97,59**	**97,55**	97,90
Si	5,94	5,94	5,88	6,04	6,01	6,09	6,11	6,05	6,02
Ti	0,21	0,21	0,20	0,23	0,23	0,23	0,23	0,23	0,22
Al	2,74	2,76	2,75	2,55	2,64	2,61	2,60	2,62	2,66
Fe^{2+}	1,01	1,02	0,89	1,13	1,15	1,21	1,24	1,10	1,15
Mn	0,01	0,01	0,01	0,01	0,02	0,01	0,01	0,01	0,01
Mg	2,37	2,34	2,39	2,42	2,36	2,35	2,32	2,36	2,35
Ca	1,58	1,56	1,55	1,56	1,59	1,58	1,56	1,55	1,58
Na	0,86	0,88	0,86	0,93	0,88	0,86	0,87	0,86	0,88
K	0,23	0,23	0,24	0,23	0,23	0,24	0,24	0,24	0,23
Total	**15,67**	**15,67**	**15,65**	**15,72**	**15,70**	**15,67**	**15,67**	**15,65**	**15,69**
^{IV}Al	2,06	2,06	2,12	1,96	1,99	1,91	1,89	1,95	1,98
^{VI}Al	0,68	0,69	0,64	0,59	0,65	0,71	0,70	0,67	0,68
X_{Mg}	0,70	0,70	0,73	0,68	0,67	0,66	0,65	0,68	0,67